Comparison of Canadian and U.S. Standard Provisions for Slender Masonry Walls

by

Miguelangel Jose Bilotta

A thesis submitted in partial fulfillment of the requirements for the degree of

Master of Science

in

STRUCTURAL ENGINEERING

Department of Civil and Environmental Engineering
University of Alberta

ABSTRACT

Slender, masonry loadbearing walls made with concrete blocks are one of the most frequently used masonry structural systems in North America. They are commonly found in commercial and industrial single-storey construction, such as warehouses, and in school gymnasiums, auditoriums, and retail buildings.

Tall, masonry loadbearing walls subjected to out-of-plane (OOP) loads are often governed by flexure, as the shear demands are small compared to the flexural moments they experience. Due to their slenderness, these walls are very susceptible to second-order effects, which translate into additional moment demands caused by the presence of axial loads and the wall deflections. Research has shown that to develop rational design procedures and achieve safe and economical design, an accurate estimation of second-order effects is required.

Leading provisions in masonry design in North America, such as the ones in the U.S. and Canada, have similarities and differences that warrant investigation and require an assessment to achieve a unified design method.

This research has several goals: (1) to compare the current strength design and second-order effects provisions for OOP loadbearing masonry walls from North American standards (CSA S304-14 , TMS 402-16), with an emphasis on the provisions related with moment amplifications due to second-order moments; (2) to evaluate the influence of different parameters such as reinforcement ratio, slenderness ratio, compressive strength (f_m') and axial loading, in the flexural rigidity and effective stiffness; (3) to compare the design provisions with numerical models developed using the finite element method; and

(4) to conduct regression analyses using a data set developed using the numerical model and proposed expressions for effective stiffness suitable for code inclusion.

Overall, it is expected that this research will identify the key differences in current design standards and lead to recommendations for further harmonization between the US and Canadian codes.

ACKNOWLEDGMENTS

I would like to express my highest gratitude to my friend and supervisor, Dr. Carlos "Lobo" Cruz-Noguez. For his help when I needed it the most, and for the continuous and incredibly generous support. Your help was invaluable, Dr. Lobo.

I would also like to thank Dr. Yong Li, who guided my first steps into this adventure.

Special thanks to my friends that I met during this program: Alan Alonso, Odin Guzman, Rafael Marquez, Jiadaren Liu, Ziead Metwally, and Karren Izquierdo. You made this journey a fantastic adventure.

Endless thanks to my family and my girlfriend for their continuous support throughout my life. No words can be written to express my gratitude for your unconditional love and support.

TABLE OF CONTENTS

LIST OF TABLES

LIST OF FIGURES

LIST OF SYMBOLS AND ABBREVIATIONS

A_s	Area of Tensile Steel
ASD	Allowable Stress Design
β_d	Creep Factor
C_m	Compressive Force in the Masonry Fibre
CMU	Concrete Masonry Unit
CSA	Canadian Standards Association
TMS	The Masonry Society
d	Tensile Steel Depth of Cover
d_i	Distance from the Centroid of a Fibre to the Midpoint of the Wall
e	Axial Load Eccentricity
e_k	Kern Eccentricity
E_m	Elastic Modulus of Masonry
EI	Flexural Rigidity
EI_{eff}	Effective Flexural Rigidity
E_i	Tangent Modulus of Elasticity
FG	Fully Grouted
f'_c	Compressive Strength of Concrete
f'_m	Compressive Strength of Masonry
$f'_{m,gr}$	Grouted Compressive Strength of Masonry
$f'_{m,ug}$	Grouted Compressive Strength of Masonry
f	Design Stress

f_r	Modulus of Rupture of Concrete Block
f_s	Stress in Steel Fibre
FE	Finite Element
h	Masonry Wall Height
H	Total Height of a Masonry Wall
I_{cr}	Cracked Moment of Inertia of the Masonry Cross-Section
I_n	Nominal Moment of Inertia of the Masonry Cross-Section
I_o	Moment of Inertia of the Uncracked Effective Section of Masonry
k	Effective Length Coefficient
$[k]$	Stiffness Matrix
l	Unsupported Length of a Member
M_{cr}	Cracking Moment
M_P	Maximum Primary Bending Moment of a Member
M_T	Maximum Total Bending Moment of a Member
M_u	Total Applied Moment on a Wall
n	Number of Fibres
$N.A.$	Depth of the Neutral Axis
OOP	Out-of-Plane
RMW	Reinforced Masonry Wall
ρ	Reinforcement Ratio
P	Compressive Axial Load Placed on a Wall
P_o	Cross-Sectional Axial Load Capacity
P_{cr}	Euler (Critical) Buckling Load
PG	Partially Grouted

SEASC	Structural Engineers Association of Southern California
t	Masonry Wall Thickness
t_m	Thickness of a Mortar Joint
T	Thickness of a Wall
ULS	Ultimate Limit State
URMW	Unreinforced Masonry Wall
ε_m	Strain in the Outmost Compressive Masonry Fibre
ϕ	Curvature
σ_m	Compressive Stress of Masonry
σ_s	Stress in the Tensile Steel
$\sigma_s{}'$	Stress in the Compressive Steel
ψ	Moment Magnification Fator

1 INTRODUCTION

1.1 Background

Masonry has proven to be one of the most durable and reliable construction materials since the beginning of human civilization. The earliest masonry structures were very conservatively designed, using massive cross-sections such that their design was governed by gravity load. The design of masonry structures was greatly overhauled with the introduction of modern reinforced masonry in 1930, in which steel reinforcement was used to take the tensile stresses that masonry materials (concrete and stone) cannot. In North America, modern provisions for reinforced masonry form the basis of the Canadian Masonry Design Standard (CSA S304-14) and the Building Code Requirements and Specification for Masonry Structures (TMS 402/602).

The outstanding virtue of masonry loadbearing walls in structural applications is its capacity to resist the combined effect of eccentric axial loading and out-of-plane (OOP) bending by offering a robust axial capacity and bending stiffness. While squat walls are susceptible to shear forces, the design of tall walls is often governed by flexure, as the shear demands are usually small compared to the flexural moment. To design slender masonry elements, special attention must be given to second-order moments (i.e. additional moments caused by the presence of compressive axial load and the wall deflections due to lateral load). Determination of second-order effects heavily relies on an accurate estimation of an effective flexural stiffness. Underestimating the flexural stiffness would lead to conservative moment amplification factors, resulting in an unnecessary amplification in the design moment of the wall. North American standards' provisions for slender walls are developed based on a small set of research programs. Due to the insufficient test data, these structural members are usually overly conservative in design if the North American provisions are followed (Clayton 2020)

Research on masonry slender walls began in 1970. Yokel et al. (1970) tested sixty reinforced and unreinforced masonry walls, axially loaded using different eccentricities and slenderness ratios. The analysis established the foundations for the development of rational design methods for eccentric axially loaded masonry walls. It was observed that, due to the development of a strain gradient on the eccentrically-loaded section, they could sustain greater compressive stresses in comparison to concentrically loaded walls. The walls in this study were pin supported and had slenderness ratios ranging from 15.7 to 42.7.

In 1976, Cranston and Roberts investigated the viability of the Allowable Stress Design method (ASD) as applied to Reinforced Masonry Walls (RMW). They tested a series of 2.6 m high specimens, with slenderness ratios of 18.7, under combined axial and lateral loads. It was demonstrated that the allowable stress method, prominently used up to that point, results in uneconomical designs for RM walls. Current versions of the TMS 402-16 still offer provisions to design RMW using the ASD method while the Canadian standard decided to provide recommendations only for strength design approaches.

One of the most influential research programs in those early days was conducted by the Structural Engineers Association of Southern California (SEAOSC) and the Concrete Institute (ACI) in 1979. A total of 7, full-scale reinforced masonry walls subjected to eccentric axial loading and a uniform distributed pressure (out-of-plane) were tested. Different slenderness ratios ranging from 30 to a maximum of 48 were evaluated under pinned-pinned boundary conditions. The experimental results suggested that there was minimal evidence to provide a fixed slenderness limit. Additionally, no stability effects were appreciated when the axial loading was limited to 10% of the pure axial capacity. It was also noted the severity of second-order effects as the slenderness ratio increased, in which, in some cases, it accounted for approximately 25% of the yield moment (SEASC 1979). The findings in this experimental study formed the basis of current masonry design provisions for tall masonry walls (CSA S304-14, TMS 402-16).

As the research data increased, multiple authors recommended strength design approaches such as the Ultimate Limit State Design (ULSD), rather than the ASD method for further designs of in-plane and out-of-plane masonry elements. With the ULSD the use of taller and slender walls in North America was expanded, and a need arose for more refined methods to account for the moment demands.

Developing rational design procedures has been an endless and challenging task, as many researchers have proven (Colville 1979; Hatzinikolas et al. 1980; Hamid and Drysdale 1980; Sulwaski and Drysdale 1986). Any attempt to predict the OOP behaviour accurately in RMW appeared to be impossible if material and geometrical nonlinearity are not considered. Hatzinikolas et al. (1978) conducted an experimental program to study the geometrical nonlinearity with specimens, ranging in slenderness ratio from 13.8 to 24 and subjected to eccentric loading. The samples were tested using pinned-pinned boundary conditions. The study proposed a new method adopting the Moment Magnifier (MM) method from reinforced concrete, introducing an Effective Stiffness (EI_{eff}) concept, which attempts to predict the flexural rigidity of masonry walls based on the estimated extent of cracking in the cross-section of the specimen. The concept of effective stiffness EI_{eff} is still used in the current Canadian Standard. The TMS 402-16 committee adopted a different alternative, accepting the MM procedure, while the flexural rigidity is calculated based on the cracked modulus of inertia ($E_m I_{cr}$). Both solutions (EI_{eff} and $E_m I_{cr}$) have proven to be conservative (Liu et al. 1998; Dona et al. 2015) in predicting the flexural rigidity for RMWs.

Results from this study showed that both countries rely on the same principles of strength of materials to compute the axial and bending resistance (P-M) of masonry walls. However, provisions such as (a) maximum axial capacity, (b) maximum reinforcement ratios (c) reduction factors, and others, affect the P-M capacities considerably.

Regarding second-order effects, both North American standards offer similar methods to compute these effects. The main discrepancy between the countries is the expressions proposed to calculate the flexural rigidity of the wall. A comparison with a validated finite-element model, presented in Chapter 5, showed that the code provisions were vastly conservative in both standards for calculating moment amplifications produced by the second-order effects. For instance, amplifications factors calculated with the standards were up to 11 times higher than those produced by the numerical models.

1.2 Problem Statement

Loadbearing masonry walls are one of the most common structural systems used worldwide, however, the flexural OOP behaviour of this structure is still relatively uncertain in most circumstances. Current design standards in North America have been developed from the same studies. Although they have been updated independently, there are still many questions regarding the levels of conservatism and accuracy of the procedure proposed by the Canadian and the U.S. Committee.

Despite their proximity and the similarities between the construction materials used in the two countries, the Canadian standards for masonry design (CSA S304-14) and the Building Code Requirements and Specification for Masonry Structures (TMS 402-16 402/602) have adopted different design provisions for OOP loading. Consequently, similar structures subjected to comparable conditions, such as loading, material properties, and support type will be designed differently in Canada and the U.S. Multiple key differences are identified in both the prediction of the loadbearing capacity under flexure and the alternatives for calculating the additional moments associated with the second-order effects, especially for very tall walls.

This study aims to identify the key differences in OOP-related design provisions described in the CSA S304-14 and TMS 402-16, and assess the different methods to estimate second-order effects. The two codes will be compared to each other and also to a detailed numerical model. These results could be used to develop rational design procedures for loadbearing walls and reduce the conservatism in CSA S304-14 and TMS 402-16. Additionally, this study aims to propose a new expression to calculate the rigidity of masonry walls. These expressions could be included in future standards.

1.3 Objectives, Scope and Methods

The main objective of this study is the assessment of current design provisions from the Canadian Standard (CSA S304-14) and the U.S. Standard (TMS 402-16) for loadbearing masonry walls subjected to out-of-plane bending. To achieve this outcome, the following specific objectives must be addressed.

1. *Comparison of the strength design provisions for out-of-plane walls, recommended by the CSA S304-14 and TMS 402-16.*
    - Theoretical comparison of provisions related to the strength design of out-of-plane walls.
    - Identify and quantify the differences related to the strength design using parametric analysis based on P-M interaction diagrams.
2. *Comparison of the second-order effect related provisions for out-of-plane walls, recommended by the CSA S304-14 and TMS 402-16 .*
    - Theoretical comparison of provisions related to the second-order effects of out-of-plane walls. Comparison of the the methods to compute these effects and the effective stiffness expression recommended on each standard.
    - Identify and quantify the differences related to the effective stiffness expression proposed by each standard using parametric analyses.
3. *Evaluate the effectiveness of the provisions related to the second-order effects using a FE model.*
    - Develop and validate a finite element model for loadbearing reinforced masonry walls using experimental data.
    - Study the effect of some independent parameters in the evolution of second-order effects.
    - Compare the moment magnification effects from the FE results against those estimated by the North American standards (CSA S304-14, TMS 402-16).
4. *Develop equations to estimate the out-of-plane stiffness of reinforced masonry walls through regression analysis.*
    - Calculate an analytical effective stiffness using the strain readings from the FE results.
    - Develop a regression model using the data set obtained from the FE results.

- Measure the performance of the regression models generated and the current existing equations to calculate the effective stiffness.
- Compare the performance of the generated equations with the available alternatives.

This study is limited to the LS design and strength design methodologies prescribed in CSA S304-14 and TMS 402-16 . A set of independent parameters were selected to study their influences in the P-M resistances and establish key differences between the standards. The independent variables chosen consisted of: (a) Rebar separation, (b) Compressive strength, (c) Reduction factors, and (d) Height of the structure.

Parametric analyses regarding the second-order effects provisions were limited to studying and comparing the effective stiffness expressions proposed by each country. The following independent parameters were selected: (a) Compressive strength, (b) Reinforcement ratio, (c) Axial Load, (d) Reduction factor, and (e) Creep effects.

An investigation of the shear strength was not conducted, as the focus of this work is walls that are governed by flexure rather than shear (e.g., tall, loadbearing masonry walls). Shorter walls may be governed by shear and an assessment of both effects (flexure vs. shear) should always be conducted in the analysis of a masonry wall.

Reliability analyses, the last step before inclusion of new expressions and results in a standard, were not part of the scope of this work.

1.4 Organization of the Thesis.

This study is composed of 6 chapters.

Chapter 1 introduces the research and discusses the objectives and the scope.

In Chapter 2, the literature review is presented, including an experimental program and numerical modelling of loadbearing masonry walls.

In Chapter 3, the strength-design-related provisions from the CSA S304-14 and the TMS 402-16 are compared. Parametric studies compared the design provision using P-M interaction diagrams and quantified the influences of some independent parameters.

In Chapter 4, second-order effects related to provisions for loadbearing masonry walls are compared. Parametric studies compared the effective stiffness expressions proposed in the CSA S304-14 and TMS 402-16 , and quantified the influences of some independent parameters.

In Chapter 5, a FE model for reinforced fully and partially grouted walls is developed. The influence of multiple parameters such as slenderness ratio, compressive strength, reinforcement ratio and slenderness ratio in second-order effects of RMWs is discussed. Moment amplification factors calculated using the moment magnifier method are calculated as prescribed in CSA S304-14 and TMS 402-16 , and compared against the FE results. Three equations to estimate the effective stiffness developed using regression analysis are proposed. The performance of the regression model is compared against the available equations.

Chapter 6 summarizes the conclusions of the study and provides recommendations for future research.

2. LITERATURE REVIEW

2.1 Introduction.

Loadbearing masonry walls are a widely used structural solution to resist a combination of axial loads and OOP bending moments. In the past, these elements were built without steel reinforcement (termed as unreinforced masonry). Nowadays, current practice encourages the use of steel rebar placed and grouted into the cells of the masonry assembly (referred to as reinforced masonry). With the introduction of reinforced elements, masonry walls are a competitive alternative to other materials such as concrete and steel.

Current North American design standards (CSA S304-14, TMS 402-16) are developed mainly from the same research pool. The earliest research programs investigated the capacity of loadbearing masonry walls using the allowable stress design approach (ASD). The focus shifted rapidly to the ultimate limit strength design (ULS) approach in later programs. Using allowable stress to design masonry elements, the calculated design stresses, f, are compared to the code-prescribed maximum allowable stresses, F. The design is considered acceptable when the calculated stresses induced in the element are less than or equal to the allowable stress prescribed in the codes ($f \leq F$). Allowable stresses limits prescribed by the codes are kept within their linear range of the structure. In the new alternative (ULS), the strength of the masonry is evaluated at its ultimate failure state rather than under service loads. Design loads are factored in proportion to the degree of uncertainty using a safety factor, α. The strength of the structure is reduced by a factor, $\emptyset$, in proportion to the level of confidence in the material strength and uncertainties related to its failure mode. The design is considered acceptable when reduced resistance of the elements is greater or equal than the factored specified load ($\emptyset\ Resistance \geq\ \alpha\ Specified\ load$). The ultimate limit state of OOP masonry walls is defined by the crushing of the masonry under compression, and in more severe cases (i.e. slender wall under high axial load levels) by the instability of the structure. This method permits the structure to incursion on its non-linear range, therefore, sections designed under this method are usually more economical than the ASD.

To date, TMS 402-16 permits both the ULS and the ASD methods to compute flexural resistance. CSA S304-14 presents the ULS as the only alternative available. Although the basis of the ULS design methods is similar in both countries, the flexural and axial capacities computed by each standard are generally different. This can be attributed to multiple factors such as differences in nominal compressive strength, reduction factors, compressive width limit, axial capacity limits, ductility limits, ultimate compressive strains, nominal block dimensions, and additional provisions, which are explored in this study. The differences between the two codes in regard to the strength design method is the focus of this study.

Slenderness effects (also termed second-order effects) were identified as a major effect influencing the design of tall masonry walls in the 1980s. The influence of second-order effects can be assessed by determining the total moment experienced by the wall. This flexural moment is composed of two components: (a) primary moment and (b) secondary moment. In a conventional building, the primary moments are produced from an externally applied load such as wind load, the mass of the wall and its attachments subjected to earthquake acceleration, soil pressure, or an eccentric gravity load. The secondary moment arises from the wall out-of-plane deformation created by the primary moments and the presence of the gravity loads. Masonry walls are generally susceptible to these second-order effects due to the large deflections experienced during loading. Secondary moments have been reported to be up to 30% of the total moment for slender elements (ACI-SEASC Task Committee on Slender Walls 1982). This phenomenon leads to the development of special provisions for slender walls (defined by the CSA S304-14 and TMS 402-16 as elements with a slenderness ratio greater than 30) in North America, such as ductility limits and axial force limits.

North American design standards provided two methods to account for these slenderness effects in masonry walls: (a) $P\delta$ (load displacement method) and (b) the moment magnifier method. While the first method relies on computing second-order moment as a product of the total deflection and the gravity load, the latter proposed a single equation to magnify the primary source of moments. Both methods rely on an accurate prediction of the flexural rigidity (EI). Experimental results demonstrated that loading conditions, tensile bond strength, and the type of the wall must be taken into account to compute accurate prediction of slenderness effects (Hatzinikolas et al. 1978). As calculating the flexural rigidity is a fundamental aspect of computing second-order effects, multiple authors have attempted to propose equations based on regression analysis developed on the basis of experimental and analytical data (Liu et al. 1998, Liu and Dawe 2003, Mohsin 2005). However, estimating the flexural stiffness for reinforced masonry walls has proven to be rather complex, as it requires accounting for phenomena such as tensile cracking, plastic strain, and nonlinear degradation (Pettit 2019).

This chapter presents a review of available literature related to the experimental, analytical and numerical research program of loadbearing masonry walls. Techniques implemented for numerical analysis are discussed, and proposed equations to estimate the flexural rigidity of masonry walls are presented.

2.2 Experimental Programs and Behaviour of Masonry Walls.

Experimental programs of loadbearing masonry walls began in the 1970s. Yokel and Dikkers (1971) tested 192 brick and concrete block specimens under eccentric axial load, out of which 28 were reinforced concrete masonry walls, 13 solid concrete masonry walls, and 48 unreinforced specimens. The specimens were 1.2 m and 0.6 wide and up to 6 m high. Free rotation at the top of the wallettes was allowed while it was restricted on the base. The same program includes experimental testing of prisms. The prism test result suggested that the flexural-compressive strength increases with a gradual increase of the strain gradient. Interaction diagrams curves with axial compressive strength and flexural capacity were presented. The results suggested an increase in the accuracy of the interaction diagrams if the effect of the strain gradients is considered. Computing second-order effects with the moment magnifier method drove conservative predictions compared to the experimental results. The same year, Yokel (1971) proposed a differential equation for deflections of walls with prismatic cross-sections assuming an elastic material without tensile strength. The exact solution of this equation was used to derive an expression to calculate an equivalent critical load P_{cr} given in equation 2.1

$$P_{cr} = \frac{0.64\pi^2 Ebu_i^3}{h^2} \tag{2.1}$$

Where, E is the modulus of elasticity, u_i is the eccentricity, and h is the height of the wall.

The beam-column concept was explored by Chen and Atsuta (1973) to investigate the behaviour of loadbearing walls. The study developed axial strength curves for multiple materials. It was concluded that the tensile strength of plain concrete or masonry walls is a significant parameter influencing the strength of the walls, which was previously neglected.

Cranston and Robert (1976) investigated the validity of using the British Standard (CP 111-1970) to predict the behaviour of reinforced masonry walls. A total of 38 eccentrically loaded concrete block walls were tested. It was shown that the method described in the British Standard based on the working stress method tends to produce conservative results when compared to experimental results. Based on the test results, stress-eccentricity-rotation curves were plotted, which captured the behaviour of the structure satisfactorily. The study concluded that limit state design procedures outperformed working stress procedures to design reinforced masonry walls.

A few years later, a comprehensive testing program consisting of 68 concrete masonry walls was developed (Hatzinikolas et al. 1978). All the specimens were tested under pinned-pinned conditions and variable eccentricities to evaluate structures under single and double curvature. Slenderness ratios ranging from 12 to 22 were evaluated. The flexural rigidity of the walls was analyzed as a function of the cracking of the cross-section. An increase in the capacity of the specimen was found when tested under double curvature compared to single curvature experiments. Results also indicate a reduction of the axial capacity due to the presence of the joint reinforcement. The author proposed the moment magnifier method to evaluate the slenderness effects of reinforced masonry walls, which are still used today. Evaluating the second-order effects from the experimental results and comparing them against those calculated by the moment magnifier method suggested that loading conditions, tensile bond strength, and type of wall (reinforced or unreinforced) must be taken into account if accurate predictions are expected.

Until 1982, most experimental programs focused on short masonry walls, in which P-Delta effects were not significant. Nevertheless, the demand for taller structures grew in the early 1980s with economic stability and the construction of warehouses and commercial buildings. The American Concrete Institute (ACI) and Structural Engineers Association of Southern California (SEASC 1982) developed an experimental program to study fully grouted reinforced masonry walls subjected to out-of-plane bending and eccentric axial loading. They tested 9 walls, 1.2 m wide and 7.5 m high. Different slenderness ratios were evaluated: 30.6, 38.8, and 52.6. All walls were subjected to a combination of eccentric gravity load and uniformly distributed lateral pressure. The eccentric axial load was applied through a pulley system using a drum of water. Once the peak axial load was reached, a uniform distributed pressure was applied to one side of the walls using an airbag (Fig. 2.1). The maximum applied axial load was 15.3 kN, which represents 24% of the full section stress (P_u/A_n) for the walls with a block thickness of 246 mm, as the average compressive strength of the masonry (f'_m) was reported to be 18.7 MPa.

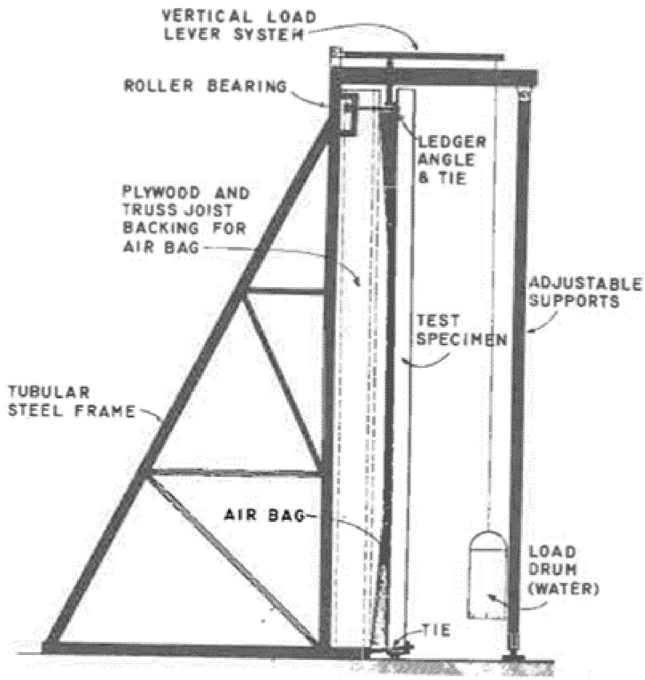

Figure 2.1 – Side Elevation of Test Setup (ACI-SEASC Task Committee on Slender Walls)

Once the desired axial load was reached, the lateral uniform pressure was monotonically increased. Due to safety proposes, the lateral load was stopped when it was judged that the masonry would reach its crushing strain. Although it was reported that from the 9 panels, only 2 reached the crushing of the masonry, yielding of the rebar was achieved in all the cases before the loading was stopped. The maximum mid-span displacement was reported to be approximately 415 mm (Fig. 2.2). Second-order effects were described to be more prominent in the thinner specimens (143 mm), accounting for about 20% of the total moment when the reinforcement began to yield. Results from this test formed the basis of current design provisions in North America, such as maximum and minimum reinforcement clauses, axial load limits, and midspan deflection limits.

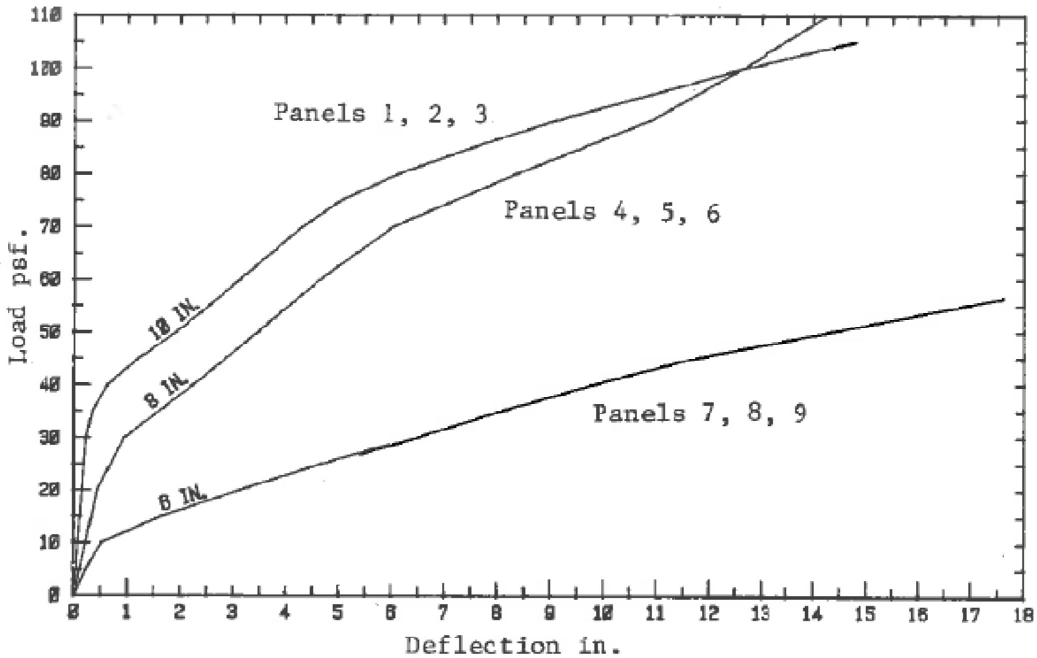

Figure 2.2 – Push-Over Curves (ACI-SEASC Task Committee on Slender Walls)

The studies referenced above showed that moment amplification due to slenderness effects were important for the design of tall walls. Maksoud and Drysdale (1993b) explored the possibility of using a moment magnification factor to design slender masonry walls. It was found that geometrical and material nonlinearity were important parameters for their response. Additionally, high compressive stresses in the cross-section were found to influence the ultimate response of the walls due to the effect of stiffness degradation. Further parametric analyses demonstrated rapid stiffness degradation in slender walls compared to stocky specimens. These effects were attributed to the coupling action of the geometrical and material non-linearity. Attempts to predict flexural stiffness based on an elastic tangent or secant modulus of the masonry material were reported to be unconservative.

The MM method became popular in North America due to its simplicity. However, the method largely depends on an accurate calculation of the flexural stiffness. Therefore, further research focused on evaluating the flexural rigidity of reinforced masonry walls. Liu and Dawe (2001) tested 36 reinforced masonry walls subjected to a combination of axial loading and lateral loads through a 4-point bending method. Strain recorders were provided in the tension and compression faces of each specimen. A flexural rigidity was obtained using the strain readings, and it was compared against the results computed using the expression proposed by the Canadian Standard. It was concluded that the standard produced unconservative results for structures under low axial levels, but as the loading is increased, the expression becomes conservative.

Mohsin (2005) conducted an experimental program to evaluate the flexural rigidity of masonry walls when considering rotational stiffness at the base. The study consisted of 8 reinforced masonry walls tested under eccentric axial loading. All the walls were 1.2 m wide with 200 cm nominal thickness blocks. Two slenderness ratios were evaluated: 29 and 34. The rotational stiffness was simulated using a steel shape at the base for which flexural rigidity was equivalent to commonly used foundations for loadbearing masonry walls. Experimental results show that as the rotational stiffness increased, the axial and flexural capacity were enhanced, while the second-order effects were reduced. An analytical flexural stiffness was calculated and compared against the CSA S304-04 expression. It was found that the effective stiffness calculated using the S304-04 expression produced conservative results for structures with and without base rigidity. The difference was more pronounced whenever a rotation stiffness was present. The study proposed an effective stiffness equation based on non-linear regression analysis, which considered the effect of the base rigidity and slenderness ratio.

Further studies assessed the capacity of the American standard (TMS 402-08) of estimating the flexural rigidity of masonry walls. Popehn et al. (2009) tested 4 unreinforced walls under eccentric axial loading. The walls were 0.8 m wide and 3.5 m high. The specimens were tested under simply supported conditions. Results indicated that moment amplification factors calculated as per the TMS 402-08 were up to 1.85 greater than those obtained in the experiment.

Isfeld et al. (2018) investigated the effect of base support conditions on the deflected shape of partially grouted walls subjected to eccentric axial loading and an OOP line load. Three panels were tested under simply supported conditions and what was referred to as pinned-fixed boundary conditions. The specimens were 1.2 m wide and 2.4 m high with a slenderness ratio of 12. The three walls were each tested with both the pinned-fixed and pinned-pinned boundary conditions. The axial load was applied through two actuators in displacement control up to a maximum of 250 kN, while the OOP line load was applied at mid-height by using a box beam connected to steel cables (Fig. 2.3). Experimental displacement profiles were compared with calculations based on the CSA S304-14. The authors concluded that the current standard is overly conservative, resulting in displacement 26 times greater than the experimental. The researchers also proposed that the design of slender walls should be re-examined.

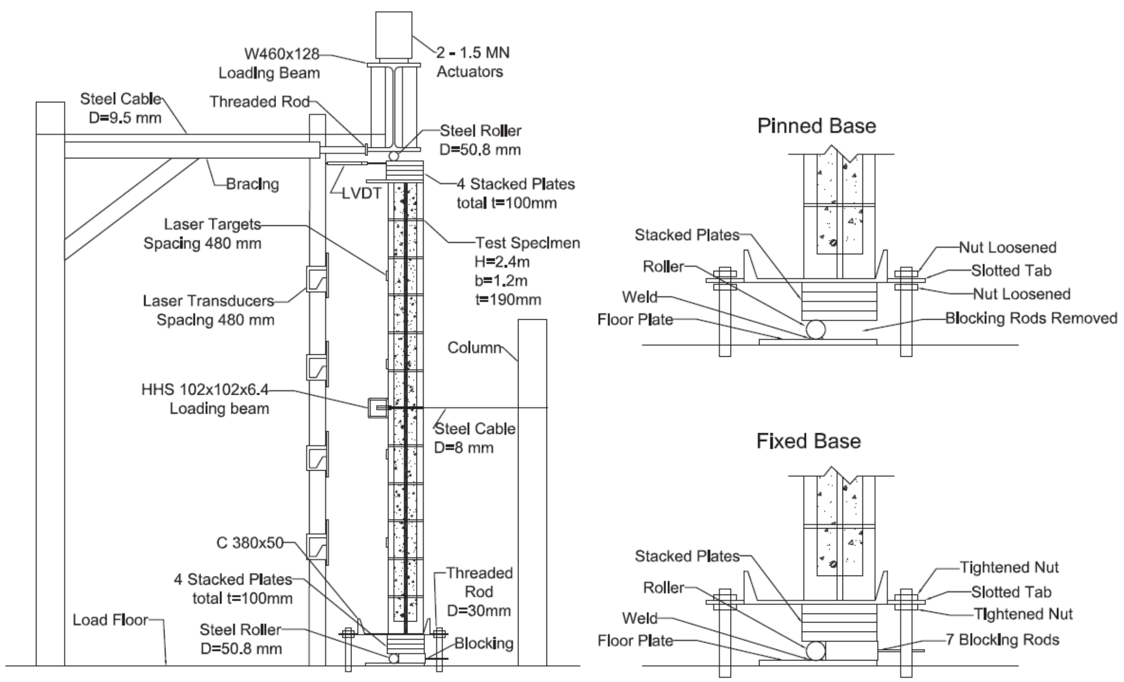

Figure 2.3 – Test set-up (Isfeld et al. 2019)

More recent studies were conducted by Pettit (2019) at the University of Alberta. A full-scale test of four identical partially-grouted reinforced masonry wallettes was developed. All the specimens were subjected to a combination of out-of-plane bending and 250 kN of axial loading. The specimens were 1.2 m wide, 12-course (2.4 m) high, and standard 20 cm nominal thickness blocks were used. A control specimen was evaluated under pin end conditions, while the other featured an active, reactive support to simulate the base rigidity as Mohsin (2005). It was shown that the lateral load capacity of walls with base rigidity is up to 92.7% higher than equivalent structures under pinned conditions.

Although the experimental studies have grown in both quality and quantity in the past years, there are still many challenges regarding understanding the rather complex behaviour of reinforced and unreinforced masonry walls. This assumption is reflected in current North American design standards. Despite the Canadian (CSA S304-14) and the American (TMS 402-16) standards having been developed based on the same research pool, each committee mandates different provisions to compute the flexural and axial resistances of masonry walls. It is evident from the experimental data that second-order effects are a critical aspect in the design of slender masonry walls subjected to OOP bending. However, the above studies have proven that current methods specified in both the American and the Canadian standards to compute second-order moments produced moment amplifications up to 2 times higher than the experimental results.

2.3 Numerical and Finite Element Modelling.

It is clear from the literature above that experimental testing has formed the foundations of our current knowledge of the behaviour of reinforced and unreinforced masonry walls. However, physical testing programs are often limited by economic and practical constraints. The development of comprehensive experimental programs is expensive and time-consuming, as they might require building full-scale masonry walls and mechanisms to simulate loading conditions on which these elements are often subjected. Finite element analysis has arisen as an excellent alternative to overcome this constraint by providing accurate and cost-efficient predictions of the behaviour of the masonry, which are validated based on previous experimental results. Numerical models can be used to investigate complex phenomena such as stiffness degradation, buckling analysis, earthquake simulations of full-scale masonry, which might not be feasible for an experimental evaluation.

In a broad manner, numerical modelling using the finite element method (FEM) in a structural engineering context could be divided into macro and micro modelling. In the macro modelling approach (Fig. 2.4a), a homogeneous behaviour of masonry with no distinction between units and mortar is assumed. The masonry is modelled as a series of continuum elements. These models are an effective alternative to analyze the global behaviour of reinforced masonry walls, but are unable to capture detailed failure modes.

Micro modelling is more computationally expensive, however, it is usually adopted when the local behaviour of the masonry walls is of interest. In a detailed micro-model (Fig. 2.4b), the masonry cross-section is modelled as a continuum element, and the unit-mortar interfaces as a discontinuum element. Micro-models can provide accurate and precise results but are limited to simulating relatively small members due to their computational intensity.

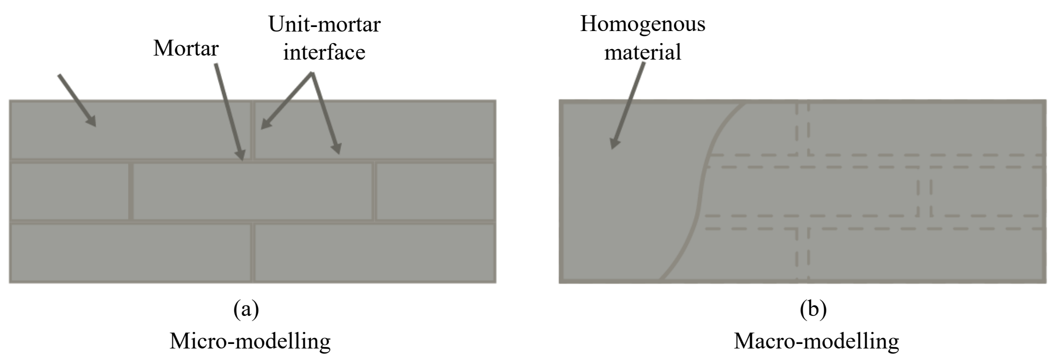

Figure 2.4 - Finite Element Approaches (Adapted from Kurdo et al. 2017)

2.3.1 Micro modelling

Early FE micro-models were introduced by Page (1978) for walls made with masonry bricks subjected to in-plane loading. The author used an 8-node plane stress continuous element assuming isotropic elastic properties to describe the masonry unit. Nonlinear linkage elements were used to model the mortar joints. The stiffness matrix was derived based on relative displacement vectors in the normal and shear direction. The equilibrium of the element is shown in 2.2. Unfortunately, the failure criteria was not defined and the ultimate load could not be captured.

$$\{F\} = [k]\{w\} \tag{2.2}$$

Where,

The force vector: $\{F\} = \{F_s\ F_n\}$

The stiffness matrix $[k]$= $[k_s\ 0\ 0\ k_n]$

The displacement vector $\{w\}$= $\{w_s(top) - w_s(bottom)\ w_n(top) - w_s(bottom)\}$,

Ali et al. (1986) created a nonlinear FE micro-model for brick wall subjected to in-plane loading which implemented a local failure criterion for both the joint and brick elements. The model was developed using 2D plane stress elements. The stress-strain relationship of the brick and the joint elements were adopted from several experimental studies. Three failure criteria were defined: (a) fracture of the mortar under tension-compression or tension-tension state of stress, (b) crushing of the brick under compressive stresses, and (c) bond failure at the interface of the joint and brick elements. The authors utilized a FE mesh consisting of four noded quadrilateral elements. The results of the numerical model of the brick wall subjected to in-plane loads were compared against experimental studies and showed a decent agreement.

A more rigorous FE model was developed by Sayed-Ahmed and Shrive (1994) of 7-course high masonry wallettes. The interaction between blocks and mortar joint was simulated using a 3D continuous FE model. Geometrical and material nonlinearity was considered using an 8-node shell element. Elasto-plastic behaviour of mortar and masonry was assumed. The solution algorithm is based on an iterative process using arc-length method. Comparison with experimental results obtained in 7-course high wallettes under concentrated load shows a decent correlation. Different from previous research, this model was able to capture the failure of the specimens based on the appearances of cracks and instability effects.

Lofti and Shing (1994) developed a micro FE model of unreinforced masonry walls. The mortar joints were modelled using interface elements, while the masonry assemblage with a smeared crack approach. It was found that the model was able to predict the shear behaviour of the mortar joints accurately. Cracking initiation and propagation under the tension and shear state of stress were also included through the material constitutive relationship. Using an interface element was reported to be an efficient approach in predicting the loadbearing capacity of masonry walls and identifying local failure modes in the masonry elements.

Yi and Shrive (2001) developed a 3-D FE micro model for unreinforced masonry walls. The authors attempted to model masonry units, mortar joints, and grouted cores separately. The mortar joints and masonry block were described using iso-parametric shell elements. Solid elements were used for the grouted cores. Cracking propagation was modelled with a smeared crack approach. The non-linear behaviour was traced using an iterative process. It was reported that the numerical model was able to capture failure modes related to the progressive cracking propagation, web-splitting and crushing of mortar joints. Verification of the numerical evaluation showed a moderate agreement with the previous experiments.

2.3.2 Macro Modelling

A macro-modelling approach for slender masonry walls with cavity was attempted by Wang et al. (1997). The model was created using beam-column elements available in the commercial software ABAQUS. The masonry element was treated as a homogenous single unit. A predefined concrete material from ABAQUS was implemented. This material had the ability to capture tensile cracking with a linear tension softening branch. The compressive behaviour of the element was defined using results from prism testing, while the tensile properties were defined based on the bond strength between the block and the mortar joint. A Newton-Raphson iterative procedure was used with load control protocol until the peak load was reached. For the post-peak behaviour, the analysis was shifted into a modified risk algorithm to capture the softening of the structure. According to the authors, the model was able to predict the masonry behaviour accurately when it was compared against experimental results.

A homogenous masonry element was proposed by Lopez et al. (1999) to account for the anisotropic nature of the material. The main feature of this model was that it could predict cracking in all directions with greater computational efficiency than other micro-models. The theory of mapped spaces was used to transform the anisotropic behaviour of the masonry into an isotropic space based on a modified Mohr-Coulomb criterion. The authors suggested that the proposed approach considerably reduced the computational effort required for mesh generation. The model was validated using previous experimental programs, and it was reported to have an excellent correlation with the results. Although the model was reported to be unable to identify the fracture mechanism of the masonry, this publication formed the basis of practical modelling approaches for large scale masonry structures, which are impractical for micro-model approaches.

Another homogenization technique to model masonry elements was proposed by Ma et al. (2001). The authors introduced a representative volume element (RVE), which intends to capture the equivalent elastic properties, strength, and failure patterns of a masonry assembly. This approach was used to simulate the masonry unit and joint materials as a whole. An equivalent stress-strain relationship for the RVE was proposed based on constitutive relationships of masonry units and mortar. The numerical model defined three modes of failure: (a) tensile failure of the mortar, (b) combined shear failure of the brick and mortar and (c) crushing failure of the brick. Although this technique was reported to be an excellent alternative for masonry walls subjected to in-plane bending, unfortunately, it was not recommended for OOP behaviour. It was shown that for intensively variable stress-strain fields, the homogenization technique was not applicable.

Liu and Dawe (2003,b) investigated the flexural behaviour of loadbearing reinforced masonry walls using a FE macro-model. The authors idealized the masonry walls as 2-node, 4 degrees of freedom (DOF) beam-column elements. Material and geometrical nonlinearity were accounted for through a moment-curvature analysis of the cross-section (Fig. 2.5). The stresses at each fibre of the cross-section were calculated with the stress-strain relationship given in equation 2.3. An iterative process was selected to apply gradual increments in the loading combined with a reduced stiffness matrix. For every load increment, the moment-curvature relationship was traced, the material failure was checked to compare the total bending moment with the maximum flexural capacity. The maximum axial load was obtained using eigenvalue analysis. Parametric analyses demonstrate an excellent correlation with the experimental data (Fig. 2.6). This publication demonstrated the effectiveness of developing simplified versions of numerical models based on moment-curvature relationships for RMWs. The same FE model was later used to assess the design method proposed by the CSA S304-14 to quantify second-order moments in RMWs.

$$\sigma_m = 1.067 f'_m \left[\frac{2\varepsilon_c}{0.002} - \left(\frac{\varepsilon_c}{0.002}\right)^2\right] \tag{2.3}$$

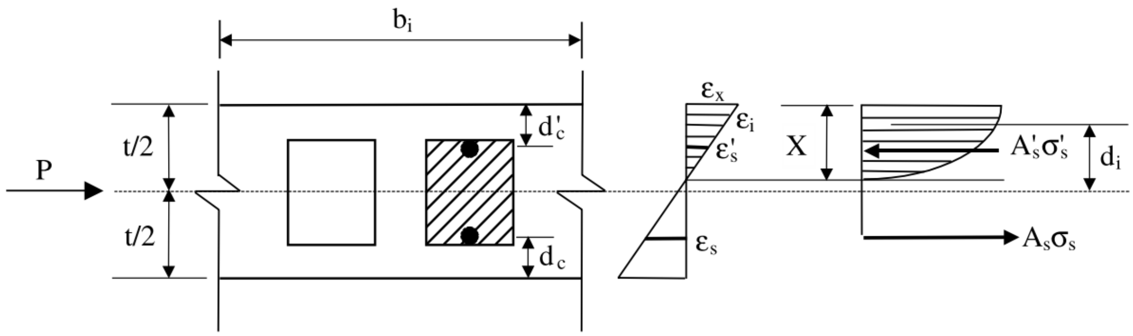

Figure 2.5 - Cross-section evaluation (Liu and Dawe 2003)

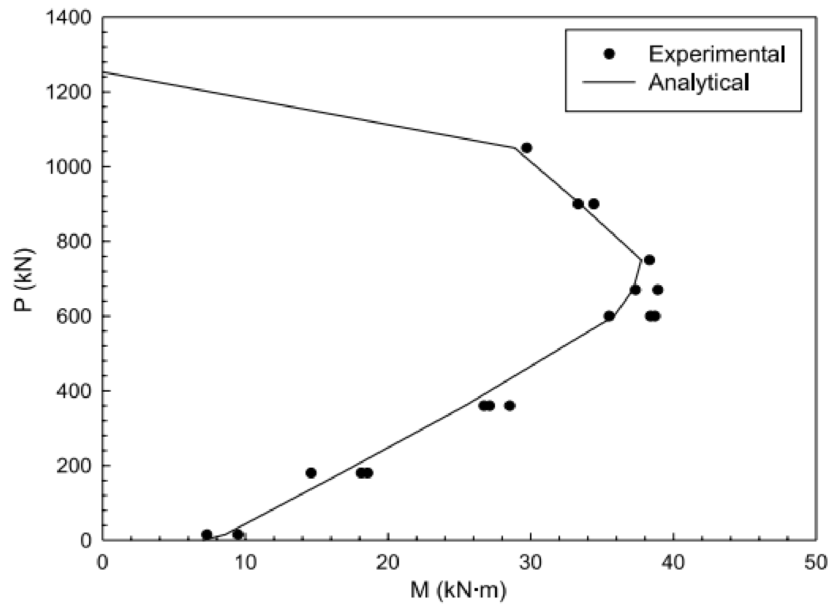

Figure 2.6 – Comparison of results for single-layer reinforced walls with two No. 10 reinforcing bars and h/t = 8.6 under combined axial and lateral loading (Liu and Dawe 2003)

Dona et al. (2018) developed two cantilevers fibre-based models of reinforced masonry walls using the Open-source software framework (OpenSees). The model accounts for spread of plasticity through a force-based element available in the OpenSees Library (NonlinearBeamColumn). Geometrical nonlinearity is considered by implementing a geometric corotational transformation. The homogenized masonry behaviour was modelled using *Concrete02*, which is based on the Kent-Scott Park Model curve. The failure criterion was based on reaching the maximum masonry strain. Parametric studies demonstrated almost a perfect correlation between experimental results and the numerical evaluation (Fig 2.7). This study showed the effectiveness of fibre-based sections to evaluate the flexural behaviour of RMWs.

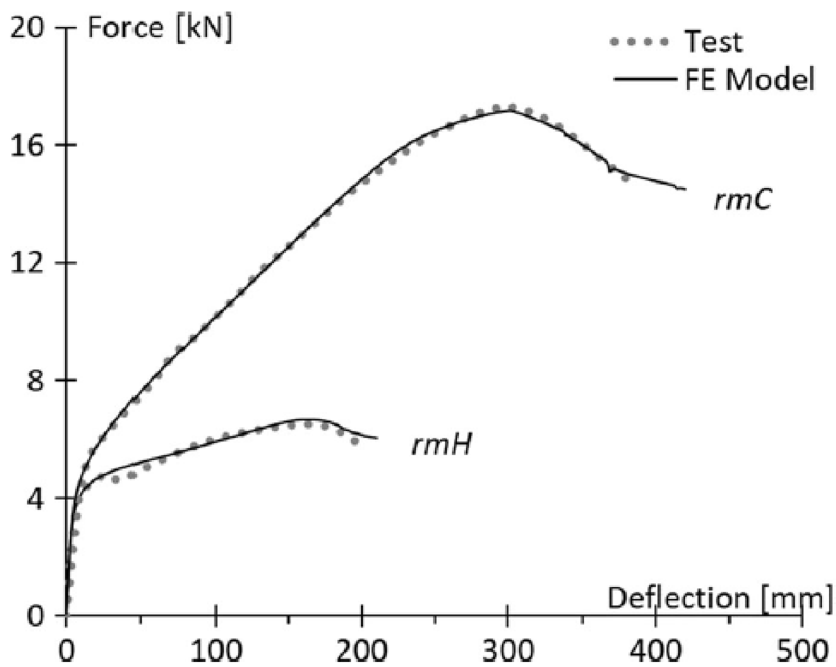

Figure 2.7 – Model Validation. Push-Over Curves (Dona et al 2018)

Pettit (2019) presented a mechanic-based model to predict the behaviour of loadbearing walls under pinned-pinned conditions, including the presence of base rigidity. Material and geometrical nonlinearity was accounted for through a fibre-section approach. The model is based on the differential equation governing the displacement of elastic beam-column under axial load and distributed lateral load. Moment curvature analyses were used to calculate the stress-strain relationship from the masonry cross-section. A maximum crushing strain of 0.003 was defined, and the instability of the structure was analyzed using eigen value analysis. The analysis model process is described in Fig. 2.8. Load displacement response of previous experimental analysis showed a good agreement with the numerical evaluation response. Further applications of the model, such as development of interaction diagrams assuming slenderness effects, are presented.

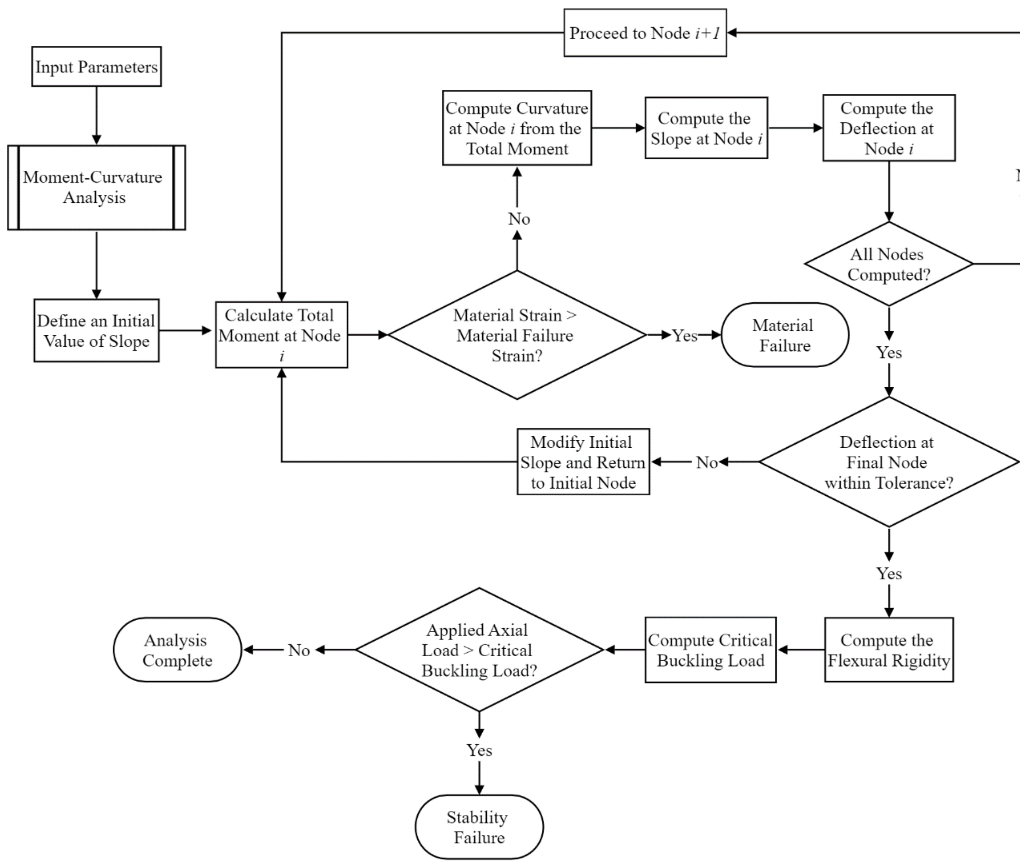

Figure 2.8– Analysis model Process (Clayton 2019)

2.4 Flexural Rigidity review

The earliest expressions to calculate out-of-plane rigidity of masonry walls were presented by Yokel (1971a; 1971b). The authors proposed an equation to estimate the rigidity of a wall as a function of the stress level and cracking of the cross-section subjected to vertical and transverse loading. For structures under eccentric loading, an approximation expression is suggested for unreinforced masonry (Eq. 2.4) and another for reinforced masonry (Eq. 2.5)

$$EI = \frac{E_i I_n}{2.5} \tag{2.4}$$

$$EI = \frac{E_i I_n}{3.5} \tag{2.5}$$

Where, E_i is the tangent modulus of elasticity and I_n the gross moment of inertia of the uncracked section.

A different alternative is suggested for walls susceptible to excessive cracking (Eq. 2.6):

$$EI = E_i I_n \left(0.2 + \frac{P}{P_o}\right) \leq 0.7 E_i I_n \tag{2.6}$$

In which P_o is the wall's axial load capacity, and P is the applied compressive load. Factors such as slenderness ratio and load eccentricity were not considered in Eq 2.5. The factor $(0.2 + \frac{P}{P_o})$ intends to include the cracking effects in the cross-section.

Hatzinikolas et al. (1978) realized that the cracked inertia of loadbearing masonry walls is influenced by the mortar penetration, mortar overhand and even the type of masonry unit. Consequently, the authors suggested performing experimental testing to determine an accurate flexural stiffness. Based on the available concrete standard, it was suggested to incorporate factors relating the effects of loading eccentricity to calculate the flexural rigidity. The research was concluded by proposing an expression to estimate the stiffness of the wall (Eq. 2.7).

$$EI = E_m I_o \left[0.5 - \frac{e}{t}\right] \geq 0.1 E_m I_o \tag{2.7}$$

Where, E_m is the modulus of elasticity of the masonry. I_o is the gross moment of inertia, e is the load eccentricity and t is the thickness of the block.

In 1995 an experimental program was conducted by Aridru and Dawe (1995) to investigate the flexural rigidity of the masonry walls exclusively. Multiple parameters were studied, such as reinforcement ratio, loading eccentricity and slenderness ratio.

Reinforced and unreinforced partially grouted walls were tested. The authors concluded that the measurement of the strain at the surface was a reasonable strategy to estimate the flexural rigidity. Additionally, it was suggested that the bending moment and the flexural stiffness could be exponentially related.

Aboud et al. (1995) defined an upper and lower bound flexural rigidity based on the moment-curvature relationship. An expression to calculate the flexural stiffness as a function of the out-of-plane deflection and the term Effective Flexural stiffness was introduced, accounting for possible variations of modulus of elasticity and the moment of inertia, as given in 2.8.

$$EI_{eff} = EI_g^f R + EI_{cr}(I - R) \tag{2.8}$$

EI_{cr} is the cracked stiffness and R is a function of the moment ratio. EI_g^f is a modified sectional stiffness given by:

$$EI_g^f = \frac{\beta M_{cr} L^2}{\Delta_{cr} I_g^f} \tag{2.9}$$

Where β is a proposed factor to related the effect of the loading condition and the boundary conditions, M_{cr} is the cracking moment, L is the structure's span, Δ_{cr} is the cracking displacement, and I_g^f is a modified gross inertia considering an uncracked section.

A comprehensive experimental program was conducted by Liu et al. (1998) of 72 full-scale concrete masonry walls under eccentric axial loading, with the purpose of calculating the flexural stiffness. An experimental moment-curvature was developed from the strain readings to calculate the Effective Stiffness of the sections, as given below:

$$EI = \frac{M}{\phi} \tag{2.11}$$

$$\phi = \frac{\varepsilon_1 - \varepsilon_2}{t} \tag{2.12}$$

In which ε_1 is the strain at the tension face of the masonry and ε_2 is the strain at the compression face.

A reduction of the flexural stiffness was reported whenever the axial loading was increased. The same modulus of elasticity was obtained throughout the linear phase of the stress-strain relationship. At higher loads, the flexural rigidity was reduced due to the non-linear evolution of the masonry material and the development of cracking. Two equations were proposed based on the experimental results.

$$EI_{eff} = 0.7E_m I_o \quad for \quad 0 \leq \frac{e}{t} \leq 0.18 \tag{2.13}$$

$$EI_{eff} = 2.7E_m I_o e^{-7.5\left(\frac{e}{t}\right)} \geq E_m I_{cr} \quad for \quad \frac{e}{t} > 0.18 \tag{2.14}$$

Where, E_m is the modulus of elasticity, I_{cr} is the cracked moment of inertia, I_o is the gross inertia, and e is the loading eccentricity.

Liu and Dawe (2003) studied the flexural rigidity of reinforced masonry walls using a numerical model. The influences of multiple parameters in the rigidity of the walls were investigated: reinforcement ratio, load eccentricity, end eccentricity and slenderness ratio. Comparison of the numerical results with the flexural rigidity calculated using the Canadian standard showed that provisions underestimate the wall stiffness under a broad range of conditions (Fig. 2.9 and Fig. 2.10).

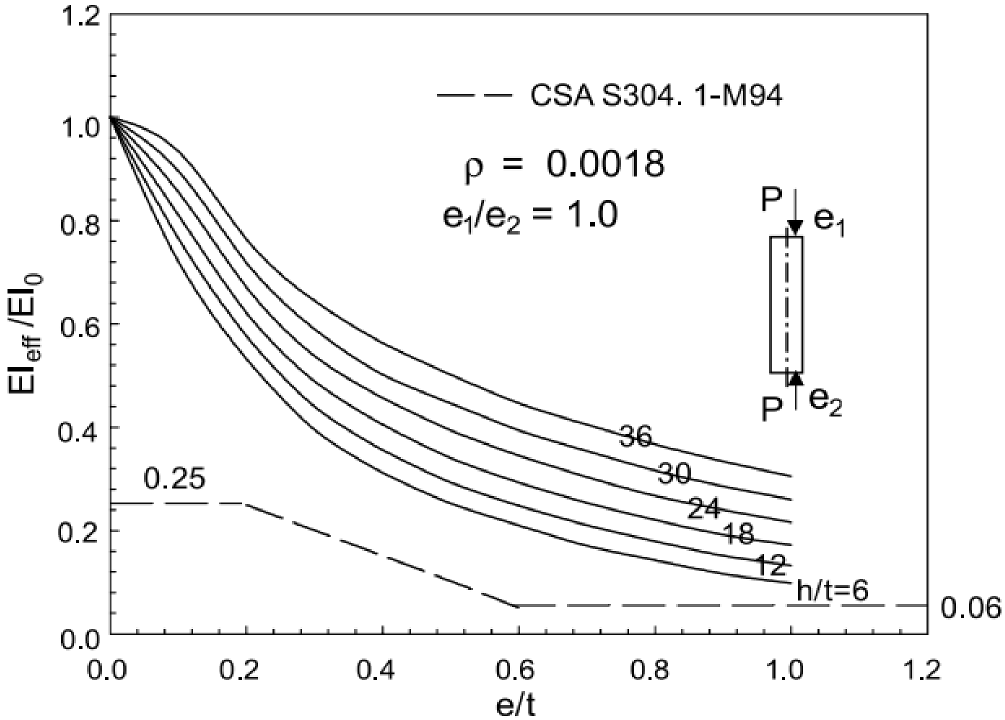

Figure 2.9– EI_{eff}/EI_o versus e/t. Eccentric Axial Loading (Liu and Dawe 2003)

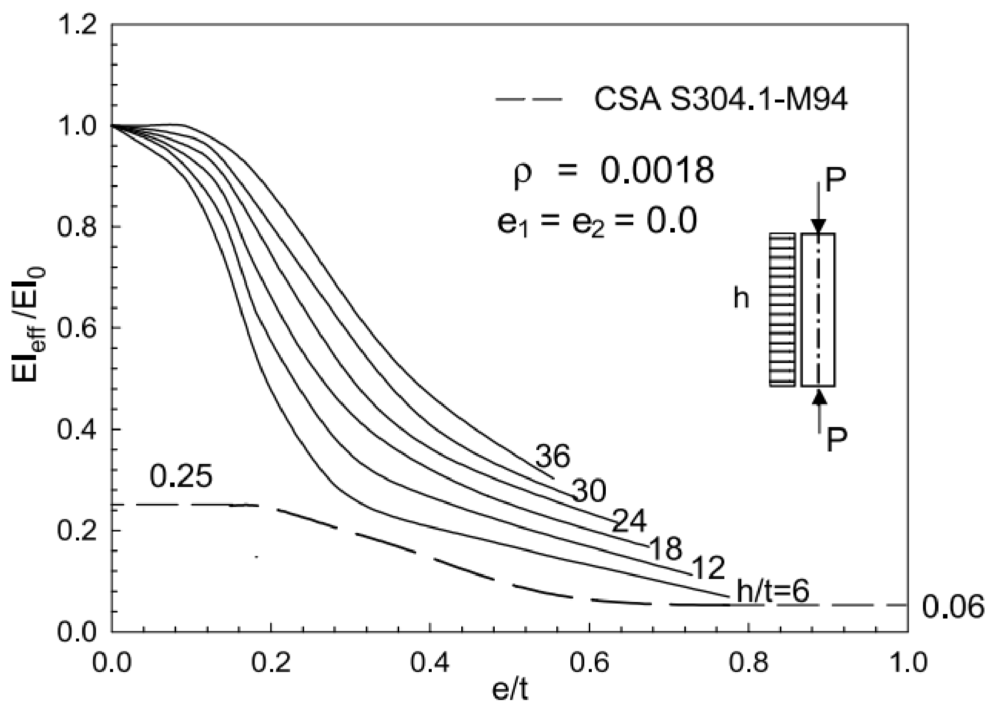

Figure 2.10– EI_{eff}/EI_o versus e/t. Eccentric concentric Loading (Liu and Dawe 2003)

Based on the numerical results, a regression analysis was performed, and the following equation as a lower and upper bound approximation were defined:

$$\frac{EI_{eff}}{EI_o} = 0.8 - 1.95\left(1 - 0.01\frac{h}{t}\right)\left(\frac{e}{t}\right) \quad for \quad 0 \leq \frac{e}{t} \leq 0.4 \tag{2.15}$$

$$\frac{EI_{eff}}{EI_o} = 0.022\left(1.00 + 0.35\frac{h}{t}\right) \quad for \quad \frac{e}{t} > 0.4 \tag{2.16}$$

Mohsin (2003) used a numerical model to develop a data set of flexural stiffness values for 300 wall specimens. The key parameter from this study was identifying the influences of based rigidity on the OOP stiffness of reinforced masonry walls. A non-linear regression analysis was performed to obtain an expression for flexural rigidity, considering the effect of base rigidity and slenderness ratio.

$$\frac{EI_{eff}}{EI_o} = \left[\left\{5 + 0.32\left(\frac{h}{t}\right) - 0.0039\left(\frac{h}{t}\right)^2\right\}\left\{0.0158e^{-0.0158\left(\frac{e}{t}\right)}\right\}\{5 + 2.9r - 12r^2\}\right] \tag{2.17}$$

For $e/t < 0.33$ & $h/t \leq 42$ & $r \leq 0.26$.

$$\frac{EI_{eff}}{EI_o} = \left[\left\{0.01 + 0.12\left(\frac{h}{t}\right) - 0.00094\left(\frac{h}{t}\right)^2\right\}\left\{0.0787e^{-0.0787\left(\frac{e}{t}\right)}\right\}\{3 + 1.836r - 12r^2\}\right] \tag{2.18}$$

For $0.33 \leq e/t < 0.42$ & $30 \leq h/t \leq 42$ & $0 \leq r \leq 0.26$.

$$\frac{EI_{eff}}{EI_o} = \left[\left\{1 - 0.05\left(\frac{h}{t}\right) - 0.000892\left(\frac{h}{t}\right)^2\right\}\left\{1.7024e^{-0.0133\left(\frac{e}{t}\right)}\right\}\{1 + 2.2r - 12r^2\}\right] \quad (2.19)$$

For $0.33 \leq e/t < 0.42$ & $30 \leq h/t \leq 36$ & $0 \leq r \leq 0.051$.

3. STRENGTH DESIGN COMPARISON

3.1 Loadbearing Reinforced Masonry Walls under axial load and Out of Plane Bending

Masonry buildings rely on the inherent compressive strength, lateral strength, and stiffness of masonry walls to transfer gravitational and lateral loads to the foundations and to guarantee the stability of the structures. Masonry walls resist eccentric or concentric axial loading, out-of-plane loads normal to the surface, and in-plane loads (Drysdale 2005). Walls subjected to the combined effect of axial compressive forces and out-of-plane (OOP) bending moment (Fig. 3.1) are termed loadbearing walls and are the subject of this study. Generally, the design of loadbearing walls against lateral loads relies on simple principles of mechanics, such as strain compatibility and internal force equilibrium, as the length of a wall is typically much larger than its thickness and Bernoulli theory is applicable. However, the inclusion of the axial loading in the system makes the analysis and design more complex.

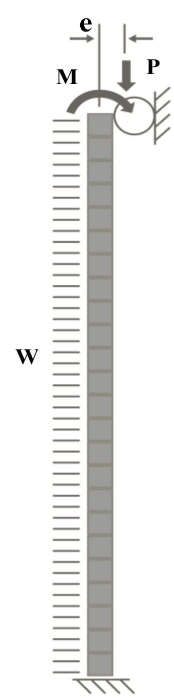

Figure 3.1 – Loadbearing OOP wall loading condition. Eccentric axial loading.

Masonry walls can be constructed either as fully grouted (Fig. 3.2a) or partially grouted (Fig. 3.2b) walls. In fully grouted (FG) walls grout is poured on every cell. FG walls could be used for several reasons. For instance, FG walls are cost-effective when the longitudinal reinforcement is placed close enough that not pouring grout in every cell becomes impractical, or when it is required to increase the gross area to resist high axial forces. FG walls may be required when the combination of gravity and lateral load require a deeper compressive block in the masonry to balance the tension forces in the steel reinforcement. It may also be done to satisfy seismic detailing requirements.

On the other hand, partially grouted (PG) walls, where only cells with rebars are grouted, are a cost-effective option for most designs. This style of construction reduces the cost and the weight of the structural elements if the loads on the building are relatively low. In PG walls, the compressive block fits within the flange of the masonry units and it is enough to balance the tension in the steel reinforcement.

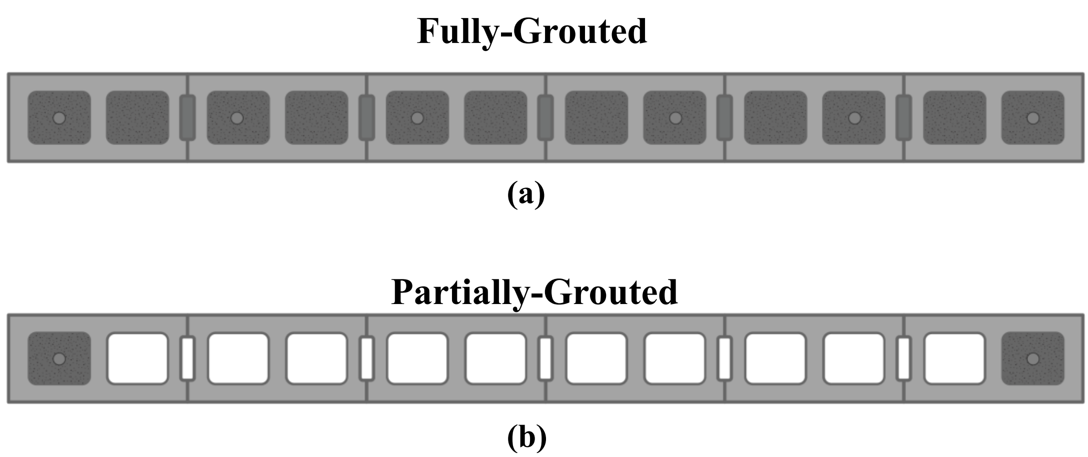

Figure 3.2 – Masonry section. (a) Fully grouted wall (b) Partially grouted

3.2 Comparison of strength design provisions.

This section compares the key design provisions from the CSA S304-14 and TMS 402-16 related to the strength design of out-plane reinforced masonry walls. First, the provisions are compared in terms of the code equations and underlying principles, and later parametric studies are used to quantify the differences numerically. In this chapter, Canadian related equations are named under C-3.X (e.g. C-3.1) while the American related as U.S-3.X (e.g.. U.S-3.1). Expressions that are common in both standards are named as 3.X (e.g. 3.1).

3.2.1 Masonry Assembly Compressive Strength (f'_m).

The compressive strength of the masonry refers to the ability of a masonry assembly to withstand compressive loads. The CSA S304-14 and the TMS 402-16 allow the determination of the compressive strength of the masonry by testing prisms or using tabulated values. Most designers prefer to use the tables due to their simplicity of use, while prism testing is rarely conducted. The tabulated values of the masonry compressive strength assembly from the CSA S304-14 and the TMS 402-16 are shown in Table 3.1 and Table 3.2, respectively.

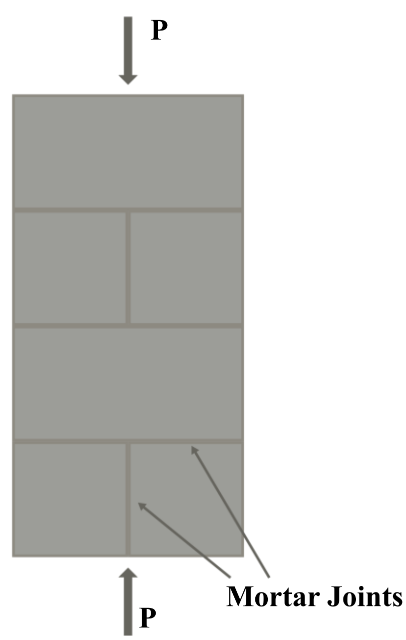

Figure 3.3 – Masonry Assembly

Table 3.1 – Specified compressive strength normal to the bed joint, $\boldsymbol{f'_m}$, for concrete block masonry, MPa, Adapted from Table 4

Specified compressive strength of unit (average net area)*, MPA	**Type S Mortar**		**Type N mortar**	
	Ungrouted hollow units	**Solid units or grouted hollow units**	**Ungrouted hollow units**	**Solid units or grouted hollow units**
30 or more **	17.5	13.5	12	9
20	13	10	10	7.5
15	10	7.5	8	6
10	6.5	5	6	4.5

*Linear interpolation may be used ** For concrete block units with a specified compressive strength greater than 30 MPa, Clause 5.1.2 may be used to determine an f'_m that could exceed the values given in this table.

Table 3.2 – Compressive Strength of Masonry Based on the Compressive Strength of Concrete Masonry Units and Type of Mortar Used in Construction, Adapted from TMS 402-16 602-16 Table 2

Net area compressive strength of concrete masonry, psi (MPa)[1]	Net area compressive strength of ASTM C90 concrete masonry units, psi (MPa)	
	Type M or S mortar	Type N mortar
1,750 (12.07)	-	2,000 (13.79)
2,000 (13.79)	2,000 (13.79)	2,650 (18.27)
2,250 (15.51)	2,600 (17.93)	3,400 (23.44)
2,500 (17.24)	3,250 (22.41)	4,350 (28.96)
2,750 (18.96)	3,900 (26.89)	-
3,000 (20.69)	4,500 (31.03)	-

[1]For units of less than 4in. (102 mm) nominal height, use 85% of the values listed.

As seen on the tables above, both countries define two types of mortar used in construction. Type "S" mortar is implemented for structural purposes while type "N" is mostly used in non-structural elements. Canada specifies the compressive strength of the block units, whereas in the US, the compressive strength of the masonry assembly.

CSA S304-14 makes a distinction between the compressive strength of ungrouted hollow units $f'_{m,ug}$, and grouted hollow units or solid elements $f'_{m,gr}$, while TMS 402-16 does not make such distinction and a unique value of f'_m is used throughout the design.

Using interpolation, TMS masonry strength values are approximately 15% higher than their counterparts in for the same block strength. The implications of the different interpretations are discussed in this work for both the strength design and calculations of the second-order effects.

3.2.2 Modular Block Dimensions and Net Area Definition.

Minor differences are appreciable in the dimensions of the typical block used in Canada and the United States. Overall, the Canadian blocks are slightly smaller than in the U.S. Table 3.3, and Table 3.4 show the equivalent block used in each country with its respective dimensions. Nominal height and length are 10 mm higher than the actual values in the CSA S304-14 to account for the mortar joint, which is approximately 10mm thick. Fig. 3.4 shows a typical masonry block with two hollow cells.

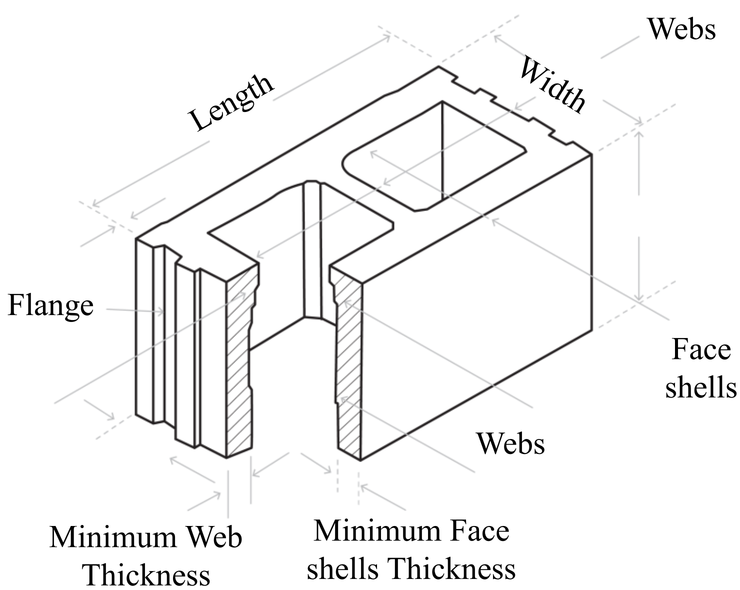

Figure 3.4 – Nominal block dimension definitions

Table 3.3 – Canadian Modular Blocks dimensions.

Block Nominal Width Canada, mm (in)	Equivalent U.S Block Nominal Width, mm (in)	Actual Width, mm (in)	Minimum Faceshell Thickness, mm (in)	Minimum Web Thickness, mm (in)
100 (3.94)	101.6 (4)	90 (3.54)	20 (0.78)	20 (0.78)
150 (5.90)	152.4 (6)	140 (5.51)	29 (1.14)	25 (0.98)
200 (7.87)*	203.2 (8)	190 (7.48)	30 (1.18)	25 (0.98)
250 (9.84)	254 (10)	240 (9.44)	35 (1.38)	28 (1.10)
300 (11.81)	304.8 (12)	290 (11.41)	35 (1.38)	30 (1.18)

*Most commonly used.

Table 3.4 – United States Modular Blocks dimensions.

Block Nominal Width U.S, mm (in)	Equivalent Canadian Block Nominal Width (mm)	Actual Width (mm)	Minimum Faceshell Thickness (mm)	Minimum Web Thickness (mm)
101.6 (4)	100 (3.93)	92.1 (3.62)	19.1 (0.75)	19.1 (0.75)
152.4 (6)	150 (5.90)	142.9 (5.62)	25.4 (1)	19.1 (0.75)
203.2 (8)	200* (7.87)	190 (7.48)	31.8 (1.25)	19.1 (0.75)
254 (10)	250 (9.84)	240 (9.44)	31.8 (1.25)	19.1 (0.75)
304.8 (12)	300 (11.81)	290 (11.41)	31.8 (1.25)	19.1 (0.75)

*Most commonly used.

The CSA S304-14 specifies the use of an "effective cross-sectional area" to determine the strength of the walls using hollow masonry blocks. Similarly, the TMS 402-16 uses the term "net cross-sectional area". Although each standard provides a slightly different term for this concept, the physical interpretation is the same.

Net cross-sectional area (A_n) or effective cross-sectional area (A_e) refers to the total area of masonry, including the area of the voids filled with grout, but excluding the webs of ungrouted cells. To illustrate this, Fig. 3.5 shows the net cross-sectional area for a PG and FG cases.

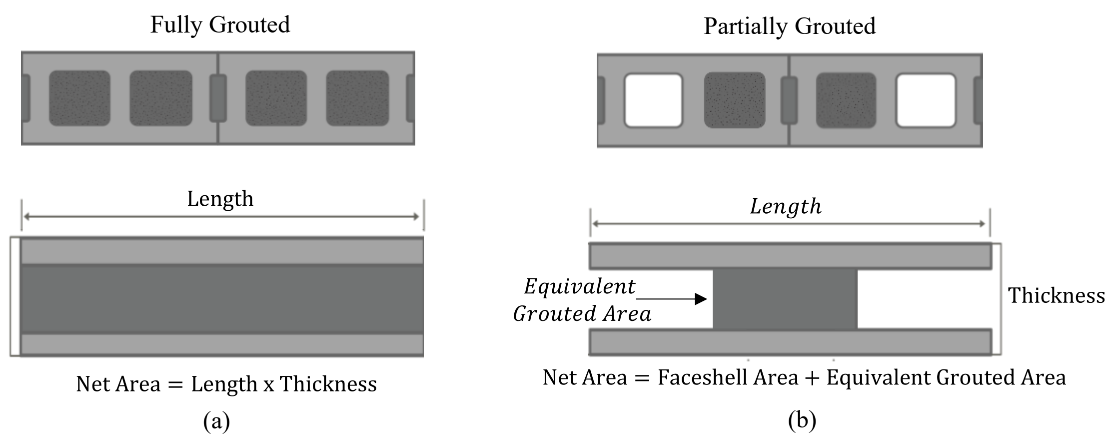

Figure 3.5 - Net Area and Effective Area (a) Fully grouted section (b) Partially Grouted Section

For a fully grouted section, the net area becomes the gross area of the cross section essentially. However, for a partially grouted section, the area is the summation of the total area of the face shells and the equivalent grouted area (excluding webs of ungrouted cells).

3.2.3 Slenderness Definition

This section compares the slenderness definition adopted by each standard. Depending on the slenderness ratio of the structure, each standard requires particular provisions to satisfy the design. These requirements are discussed in section 3.2.4. The limitations in the wall capacity as a function of the slenderness ratio are described in section 3.2.5.

The CSA S304-14 describes 3 types of walls based on their slenderness ratio. For all the type, the slenderness ratio ($\frac{kh}{t}$) depends on the effective length factor *k*, the wall length *h*, and the width of the block *t*. Table 3.5 shows the slenderness definition per CSA S304-14

Table 3.5 – CSA S304-14 Slenderness definition

Clauses	Equations	Comment
10.7.3.3.1	$\frac{Kh}{t} < \left(10 - 3.5\left(\frac{e1}{e2}\right)\right)$ (C-3.1) Where, $e1$ is the smaller virtual eccentricity occurring at the top or bottom of a vertical member at lateral support and $e2$ the largest virtual eccentricity.	Non-slender wall. Second-Order effects negligible
10.7.3.3.2	$\left(10 - 3.5\left(\frac{e1}{e2}\right)\right) < \frac{Kh}{t} \leq 30$ (C-3.2)	Slender Walls. Calculate Second-Order Effect
10.7.3.3.3	$\frac{Kh}{t} \geq 30$ (C-3.3)	Slender Walls. Calculate Second-Order Effect + Extra provisions

TMS 402-16 proposed a different definition for the slenderness limit. TMS 402-16 defines the slenderness ratio as the ratio between the structure height *h*, and the radius of gyration *r*, ($\frac{h}{r}$). Two simple definitions are provided, if h/r < 99, the wall should not be considered as a slender structure, and if h/r ≥ 99, then the wall is considered as a slender and more strict provisions and details must be used. Table 3.6 summarizes the slenderness definition per TMS 402-16

Table 3.6 – TMS 402-16 slenderness definition

Clauses	**Equations**	**Comment**
9.3.5.4.2	$\frac{h}{r} < 99$ (U.S.- 3.1)	Non-slender wall.
9.3.5.4.2	$\frac{h}{r} \geq 99$ (U.S.- 3.2)	Slender Walls.

Although TMS 402-16 uses the radius of gyration to define the slenderness ratio instead of the block thickness as the CSA S304-14, numerically, both expressions are relatively similar for a pinned-pinned condition (*k = 1)*. For solid rectangular sections, the radius of gyration is approximately 0.3t (Eq. 3-1).

$$r = \sqrt{\frac{I}{A}} = \sqrt{\frac{\frac{bh^3}{12}}{bh}} = \frac{h}{\sqrt{12}} \sim 0.3h = 0.3t \qquad 3\text{-}1$$

The A23.3 standard to design concrete structure allows assuming the radius of gyration of for solid rectangular cross-section as $0.3t$.

Substituting this approximation in the TMS 402-16 expression,

$$\frac{h}{0.3t} = 99\,; \frac{h}{t} \sim 30$$

Consequently, in most cases, the slenderness definition adopted to design a wall is relatively similar in the US and Canada. Only for some partially grouted specimens with widely spaced reinforcement, the approximation proposed by the A23.3 might not be necessarily accurate. The approximation is based on rectangular sections (which for masonry walls implies fully grouted sections). Partially grouted walls do not have a solid rectangular cross-section. In a wall in which the bars are widely spaced, the 0.3t approximation becomes less accurate.

3.2.4 Reduction Factors

The limit states design approach used by both standards requires that the design strength (factored resistance) be greater than the required strength (factored loads). Design strength refers to the reduced value of the actual resistance of a material or cross-section affected by safety factors or reduction factors. Required strength is the total load multiplied by a certain safety factor. These factored loads are specified in other regulatory documents for both countries, the NBCC and ASCE 7 for Canadians and US design, respectively.

Each country has different load combinations to calculate the required strength, although the philosophy to amplify the loads is similar (for instance, greater amplification factors are used for live loads than for dead load).

The design strength is computed following different approaches. CSA S304-14 applies reduction factors to the material strength to calculate factored resistance, while in the TMS 402-16 the factors are applied to the nominal resistance based on the expected mode of failure. Table 3.7 summarizes the reduction factor applied by both standards.

Table 3.7 – Reduction Factors

Standard	Reduction factor	Comments
CSA S304-14	Masonry Strength: $\emptyset_m = 0.6$ Steel Strength: $\emptyset_s = 0.85$ OOP wall stiffness: $\emptyset_e = 0.75$	Material strength reduction factors
TMS 402-16	Flexural Capacity: $\emptyset = 0.9$ Axial capacity: $\emptyset = 0.9$	Nominal Strength reduction Factor

As shown in Table 3.7, CSA S304-14 mandates a reduction to the material strength by a factor depending on the type of material. To compute the compressive stress of the masonry, C_m, the material strength has to be reduced by 40%, while the tensile capacity provided by the steel reinforcement by 10%. Additionally, the standard requires to affect the OOP stiffness calculation by a 25% reduction which is used to compute second-order effects (this is the focus of a major discussion in Chapter 4). On the other hand, TMS 402-16 does not reduce the strength of the material but rather decided to affect the nominal capacity by a single factor for flexural ($M_r = \emptyset M_n$) and axial ($P_r = \emptyset P_n$) behavioral response. The wall stiffness remains unaffected.

3.2.5 Provisions related to the flexural capacity (P-M interaction development)

The strength of a wall against the applied axial load and the bending moment in loadbearing walls is typically represented as a P-M interaction diagram (Fig 3.6). The P-M interaction line is a visual representation of the possible combinations of moments and axial loading that are equal to the strength of the wall. Combinations of axial load and moment that are outside the region enclosed by the line are unsafe, and those that fall inside are safe.

To create a P-M interaction diagram, one strategy is to vary the depth of the neutral axis in a cross-section. For each value of the neutral axis c, the forces in the materials, such as the compression in the masonry C_m, and the tension in the reinforcement T_s, are computed. Equilibrium must be satisfied. The net force P_r represents the amount of axial load that the cross-section can resist (Eq. 3.1). The moment caused by the forces C_m, T_s, and P_r, is the moment resistance of the wall

$$C_m = T_s + P_r \tag{3.1}$$

For ultimate limit state design, the axial load resistance, P_r, corresponds with the equivalent applied load, such that $P_f = P_r$.

TMS 402-16 and CSA S304-14 provide limitation for the maximum allowed P_r in the element. The limitations are further discussed in section 3.2.5.2.

To calculate the compressive forces, C_m, carried by the masonry, its nonlinear stress-strain relationship should be simplified into a well-defined shape that provides a reasonable estimate of the magnitude when the strain reaches its ultimate value, which is defined differently by each standard. As prescribed in CSA S304-14 (Clause 11.2.1.6) and TMS 402-16 (Clause 9.3.2), both committees allow the use of an equivalent stress block approach to determine the compressive strength of masonry elements. The equivalent stress block assumptions at ultimate conditions are shown in Fig 3.6.

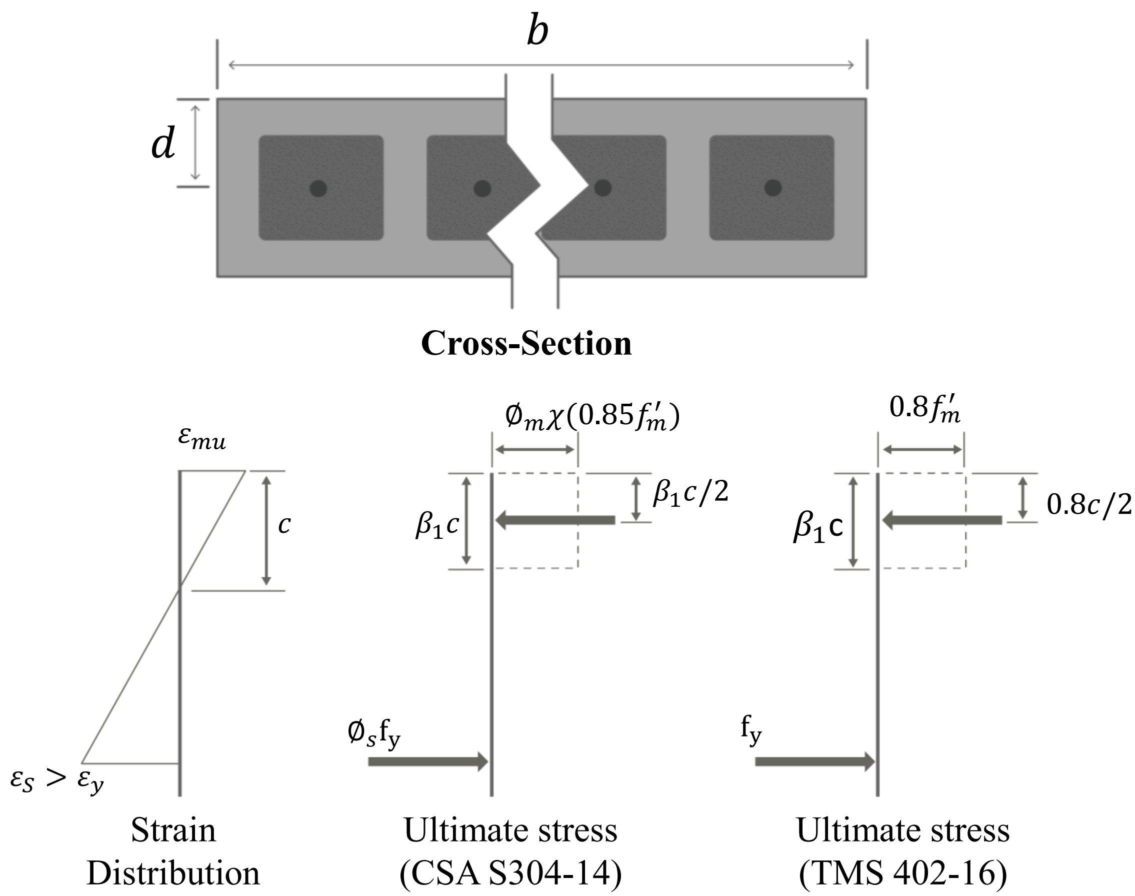

Figure 3.6 – Equivalent Stress Block assumptions.

Table 3.8 shows the equation proposed by each standard to calculate the compressive strength of the masonry based on the equivalent stress block approach.

Table 3.8 – Masonry Compressive Strength

Standard	**Masonry Compressive Strength C_m**
CSA S304-14	$C_m = \phi_m \chi (0.85 f'_m) b \beta_1 c$ C-3.4
TMS 402-16	$C_m = (0.80 f'_m) b \beta_1 c$ U.S.- 3.3

In terms of the crushing strain of the masonry materials, each standard recommends a different value. CSA S304-14 allows reaching a maximum strain of 0.003, whereas the TMS 402-16 sets a limit of 0.0025.

CSA S304-14 adopts a coefficient of 0.85 for the equivalent compressive block during the force equilibrium ($0.85\ f'_m$), versus 0.80 suggested by the TMS 402-16 committee. At ultimate conditions, this represents a 5% difference in the compressive strength of the masonry if the equations are directly compared. Although the smaller size of the U.S. compressive block would seem to be the conservative option, the Canadian committee provides a material reduction factor to the masonry strength $\emptyset_m$ of 0.65, which is ultimately translated to a reduction of the compressive strength of the masonry of 35%.

Additionally, the Canadian standard includes a factor, χ, which is used to account for the direction of compressive stress in a masonry member relative to the direction used in the determination of f'_m, nevertheless, for the design of OOP walls this factor is taken as 1.

The variability in the f'_m relative to the position of the neutral axis in the determination of the flexural strength is also to be noted. CSA S304-14 allows using different values of f'_m depending on where the neutral axis is located with respect to the block faceshell and grouted cell. If the compressive zone is placed at the faceshell, designers have the option to select the compressive strength of an ungrouted prism ($f'_{m_{ug}}$), which is typically greater than the effective f_m of the grouted masonry ($f'_{m_{gr}}$). TMS 402-16 does not establish a similar condition, and the use of a constant f'_m is encouraged throughout the design.

The tensile forced T_s carried by the steel reinforcement in Eq -3.1 at yield is calculated as shown in Table 3.9.

Table 3.9 – Tensile Strength Equations

Standard	Tensile strength T_s
CSA S304-14	$T_s = \emptyset_s A_s F_y$ C-3.5
TMS 402-16	$T_s = A_s F_y$ U.S.- 3.4

Similar triangles can again be used with the strain distribution to determine the reinforcing steel strain, ε_s, which may be expressed as

$$\varepsilon_s = \frac{\varepsilon_{mu}(d - c)}{c} \qquad 3.2$$

The elastic force in the reinforcement could then be determined by substituting the stress f_s forf_y in Eq 3.2

$$f_s = \varepsilon_s E_s \qquad 3.3$$

As noted in Table 3.9, both standards rely on the same approach to calculate the tensile force carried by the steel reinforcement. CSA S304-14 mandates to include the material reduction factor $\emptyset_s = 0.9$, whereas TMS 402-16, as commented before, does not require to reduce the material strength but instead reduces the nominal capacities.

The flexural capacity of the cross-section can be calculated by solving the resulting internal moment about its depth, d. Most conventional walls in North America are built using a single layer of reinforcement located at the centre of the cell ($d = t/2$), which coincides with the line of action arising from concentric loads. Therefore, the moment resistance under this condition can be directly calculated using the compressive strength of the masonry as shown in Eq - 3.4. The moment equilibrium can be calculated about any point of the cross-section, as long it involves the interaction between the three forces on equilibrium (P_r, T_s, C_m). TMS 402-16 mandate to use the nominal capacity factor $\emptyset = 0.9$ to reduce by 10% the moment resistance ($M_r = \emptyset M_n$). On the other hand, CSA S304-

14 does not applies any equivalent factor to the nominal capacity ($M_r = M_n$), as the material strength are already affected by $\emptyset_m$ and by $\emptyset_s$.

$$M_n = C_m\left(\frac{t}{2} - \frac{\beta_1 c}{2}\right) \tag{3.4}$$

Figure 3.7 and 3.8 illustrate a generic P-M interaction diagram for a PG cross-section developed using the CSA S304-14 and the TMS 402-16 . These curves are calculated for a 4 meters high wall, reinforced with 10M bars spaced at 1200 mm using a nominal compressive strength of 15MPa (Canadian values). No reduction factors are applied. Factored axial load resistances (P_r) are plotted in the vertical axis, while its corresponding factored moment resistance (M_r) along the horizontal axis. The area surrounded by the solid line represents the allowed combination of factor axial loads and moments. These diagrams are developed following the mechanics described above, and there are not affected by any additional provisions (i.e. Axial loading limits). In the following sections, the additional requirements to consider when developing the interaction curves as mandated by the CSA S304-14 and TMS 402-16 are explained. For each provision (i.e. axial loading capacity limit) it is shown the same interaction diagrams developed above, but affected by its respective requirements. The curves are only affected by one provision at a time. At the end of the theoretical comparison, interaction curves affected by all the provisions are shown.

The following points of interest are depicted in Fig. 3.7 and 3.8

- Point A (Pure axial compression) = Largest axial compressive load. All the fibres of the sections are under full compression.
- Point B (Compression with minor bending) = The section starts to experience bending forces. All the fibres are under compressive strains.
- Point C (Steel develops tensile strain) = Tensile strain is developed in the rebar fibres. The tensile strength of the masonry is neglected.

- Point D (Balance point) = Masonry reaches its crushing strain, and the tensile reinforcement achieves the yielding strain simultaneously. Failure of the masonry occurs at the same time as the steel yields
- Point E (Tension Controlled resistances) = The yielding strain of the reinforcement will be exceeded before the masonry reaches its crushing strain.
- Point F (Pure Bending point) = The section is under pure bending (P = 0). The tensile strain in the rebar exceeds the yield strain.

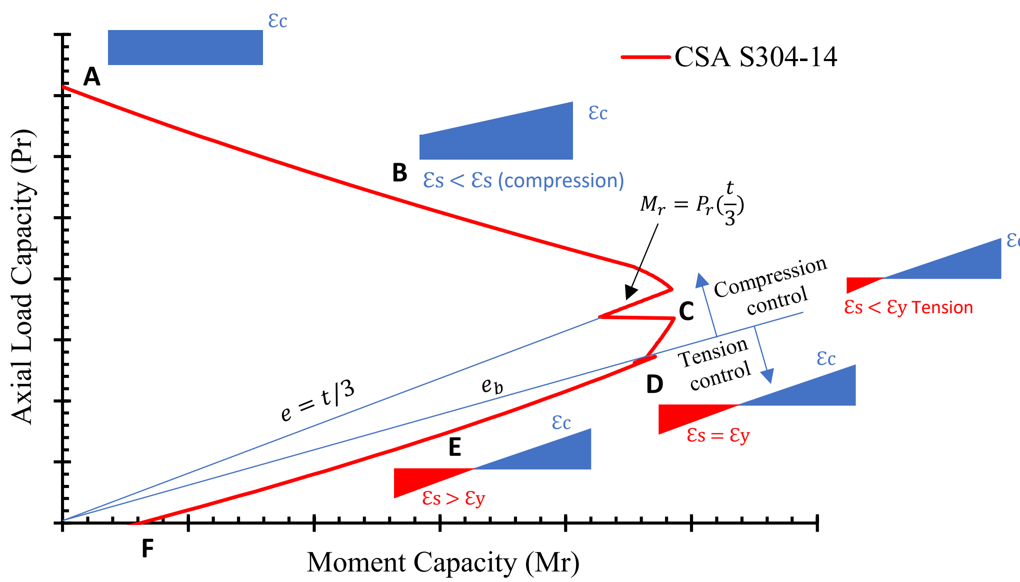

Figure 3.7 – Typical P-M interaction diagram for reinforced masonry wall as per CSA S304-14

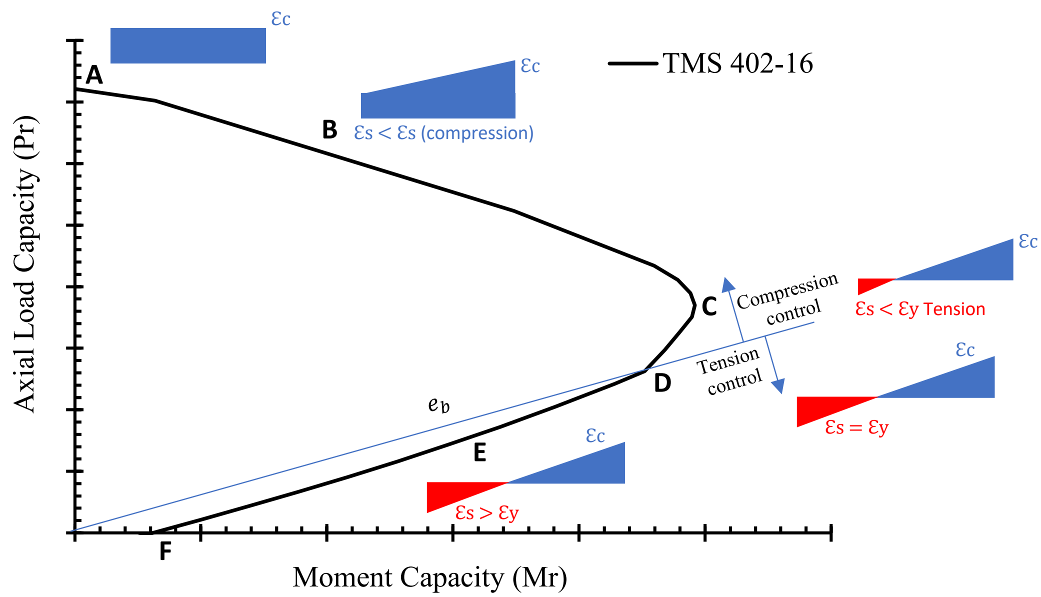

Figure 3.8 – Typical P-M interaction diagram for reinforced masonry wall as per TMS 402-16

Figure 3.7 and 3.8, it is important to notice the distinction between the compression-controlled (between point A to E) and tension-controlled region (between point E to F). Summarizing, in compression-controlled regions, P-M resistances are mainly governed by the magnitude of the compressive strength of the masonry. On the contrary, in tension-controlled regions of the interaction diagram, the response is primarily controlled by the tensile strength of the reinforcement. Both zones are described in greater detail below.

Between point A up to point C, the section is considered entirely in compression, as not tensile strains are yet developed $(c > d)$. If the neutral axis depth crosses the centroid of the reinforcement, *d*, it will not be subjected to tensile stresses. To compute P-M resistances under this region, both the CSA S304-14and TMS 402-16 neglect the contribution of the steel reinforcement. Essentially, the masonry wall can effectively be considered as an unreinforced specimen for its design since the reinforcement is no longer being relied upon to carry tensile stresses. P-M resistances in this region are purely governed by the compressive strength of the masonry. An area of discontinuity in the CSA S304-14 curve appears due to restriction of the standard for Unreinforced Masonry Walls (UMWs). CSA S304-14 limits the virtual eccentricity of the section (M_r/P_r) to a maximum of t/3 for UMWs. This limit intends to impede instability effects due to excessive cracking propagation. Therefore, applying this restriction is a requirement even for RMWs if the steel is not yet activated in tension, as the section is effectively an unreinforced specimen up to this point. Before the steel is activated, the moment resistances should not exceed $P_r\left(\frac{t}{3}\right)$. No discontinuity is seen on the TMS 402-16 402 curves, as the committee does not offer a similar provision.

At point C, tensile strains are developed on the reinforcement fibres. The section is no longer considered under a state of pure compression. Both standards assumed no tensile strength of the masonry, therefore, flexural stresses are carried entirely by the steel reinforcement. Since the maximum tensile strain of the rebar has not yet been reached ($\varepsilon_s < \varepsilon_y; F_s = \varepsilon_s E_s$), the flexural capacity is still mainly dependable on the masonry compressive strength magnitude rather than the yield strength of the reinforcement. Failure of the wall will be reached before the yielding of the rebars is achieved.

At point D, the rebars reach their yield strain, and the P-M resistances are computed using the rebar yield strength, f_y. For design purposes, no strain hardening of the reinforcement should be considered. The value of the yield strength should be used as a maximum induced stress on the rebars. For instance, for a specimen reinforced with rebars which yield strength is 400 MPa, from point D to F, the P-M capacities are computed using a maximum value of 400 MPa, independently of its strain levels. Therefore, under this area the response is primarily controlled by the yield strength of the reinforcement and to a lesser extent by the masonry compressive strength of the masonry, as it is used to compute the depth of the equivalent masonry compression block.

3.2.5.1 Axial Compressive Force Limit (Pr)

Both standards present similar approaches to calculate the maximum resistance axial forces. This is calculated based on the net area (grouted and ungrouted) of the masonry and the compressive strength (f'_m). Table 3.10 shows the equation used on each standard.

The P-M interaction curves presented in section 3.2.5 affected by their respective axial limit are illustrated in Fig 3.9 and 3.10. On each figure, the axial loading limit for both non-slender ($\frac{kh}{t} < 30$) and slender ($\frac{kh}{t} > 30$) walls are shown. The height of the structure was not modified for the axial limit calculations.

Table 3.10 – Axial Compressive Force Clauses

Standard	Clauses	Equations	Comments
CSA S304-14	10.4.1, 10.4.7.4.6.4	**For** $\frac{kh}{t} < 30$ $Pr(max) = 0.80(0.85\phi_m f'_m A_e)$ (C-3.7) **For** $\frac{kh}{t} > 30$ $P_r(max) = 0.1\phi_m f'_m A_e$ (C-3.8)	CSA S304-14 mandates two expressions based on slenderness limits.
TMS 402-16	9.3.4.1.1	**For** $\frac{h}{r} < 99$ $Pr(max) = 0.80(0.80f'_m A_n)\left(1 - \left(\frac{h}{140r}\right)^2\right)$ (U.S.- 3.6) **For** $\frac{h}{r} \geq 99$ $Pr(max) = 0.80(0.80f'_m A_n)\left(\left(\frac{70r}{h}\right)^2\right)$ (U.S.- 3.7) $P_r(max) = 0.05f'_m A_n$ (U.S.- 3.8)	TMS 402-16 provides two equations that consider the slenderness ratio. Additionally, for cases where $\frac{h}{r} \geq 99$ shall not exceed 5% of the gross axial capacity

Comparing Fig. 3.7 and 3.8 (P-M curves unaffected by any provision) with Fig 3.9 and Fig. 3.10 (P-M curves affected by the axial limit provisions), it is shown that the North American standards do not allow to achieve a pure axial compressive limit state for reinforced masonry walls. Axial capacities are capped, and this limit seems to be more restrictive for higher slenderness ratios.

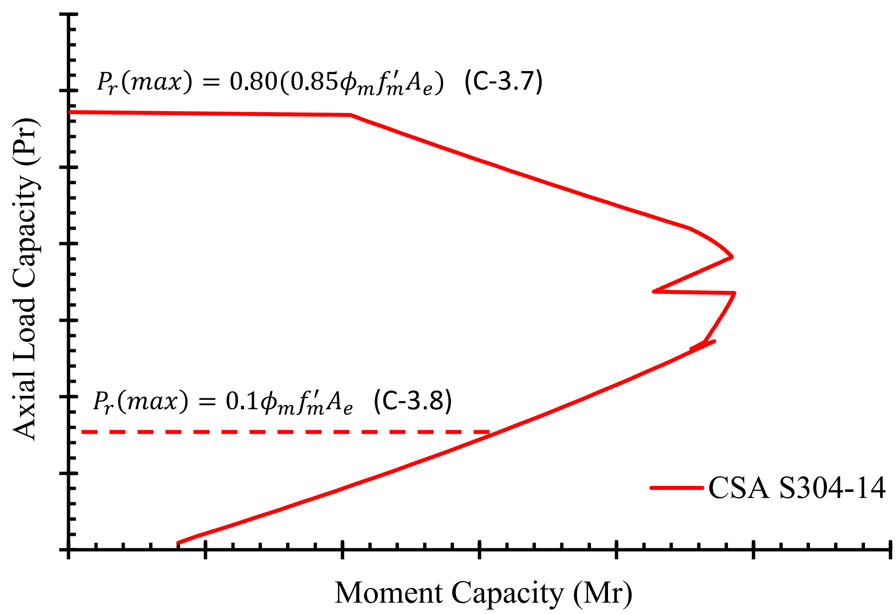

Figure 3.9 – P-M interaction diagram for reinforced masonry wall as per CSA S304-14 . Affected by axial compressive limit.

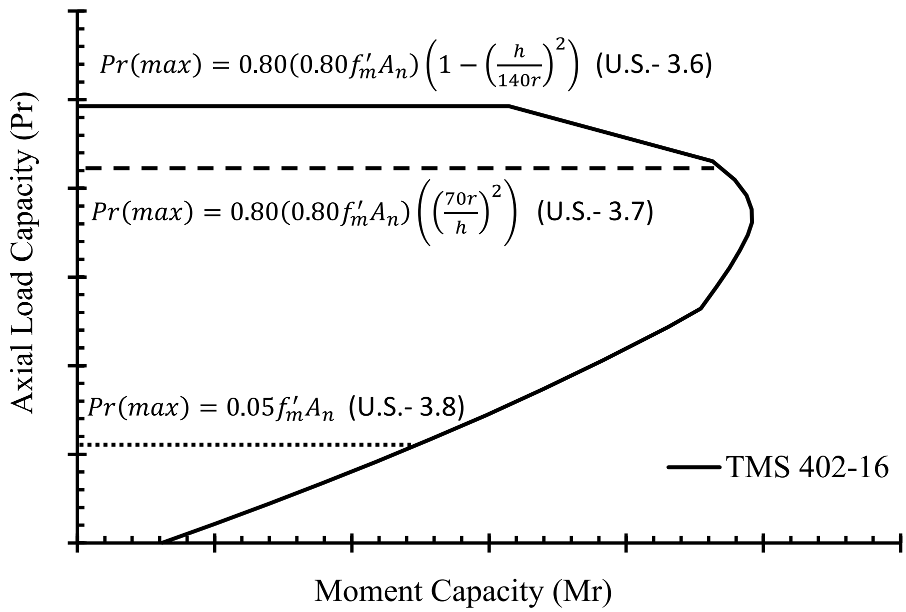

Figure 3.10 – P-M interaction diagram for reinforced masonry wall as per TMS 402-16 . Affected by axial compressive limit.

Table 3.10 shows that the TMS 402-16 expressions proposed two equations that are a function of the height and radius of gyration. For structures with a slenderness ratio of less than 99, the expression is affected by the factor $\left(1 - \left(\frac{h}{140r}\right)^2\right)$. Instability effects in structures with $\frac{h}{r} < 99$ under typical axial loads are not expected, as the mode of failure is expected to be controlled by material failure, such as the crushing of the masonry blocks in compression and yielding of the reinforcement. For the same height-to-thickness ratio, CSA S304-14 recommends an equation independent of the h/t ratio. Thus, for a given cross-section, the axial limit will be the same while the slenderness ratio does not exceed the threshold value of 30.

Walls with a higher slenderness ratio are expected to be more susceptible to instability effects. For these cases, the TMS 402-16 proposes a more rigorous factor $\left(\left(\frac{70r}{h}\right)^2\right)$ to calculate the axial limit, as shown in Fig. 3.9. Although the same height was used to compute this limit, using U.S.-3.6 led to a lower capacity. Additionally, the standard requires that the compressive forces do not exceed 5% of the total axial capacity (U.S.-3.7).

The Canadian committee mandates a single additional restriction for slender walls. This restriction ensures that the applied axial compression load in the wall must not exceed 10% of the gross capacity based on the compressive strength of the masonry unit (C-3.8).

3.2.5.2 Effective Compressive Width Limit.

When a wall is subjected to an external bending moment, it is resisted by an internal couple is created in the steel and masonry materials. Tensile stresses are generated in the steel reinforcement, and compressive stresses are created in the masonry materials. If the steel bars are widely spaced, the compressive stresses tend to appear near the locations of the steel bars, so that the compressive stress can more efficiently balance the tensile stress (Fig. 3.11-a.1). If the steel bars are closely spaced, the distribution of compressive stresses are mostly uniform along the width of the wall (Fig. 3.11-b.1). The difference between the two distributions of compressive stress is known as shear lag.

To capture the effects of shear lag, the standards introduced the concept of effective width (b_{eff}). This is the maximum width of masonry in which compression is permitted to occur to balance the tension in the steel reinforcement and preserve the coupling of the two actions (Fig. 3.11-a.2)

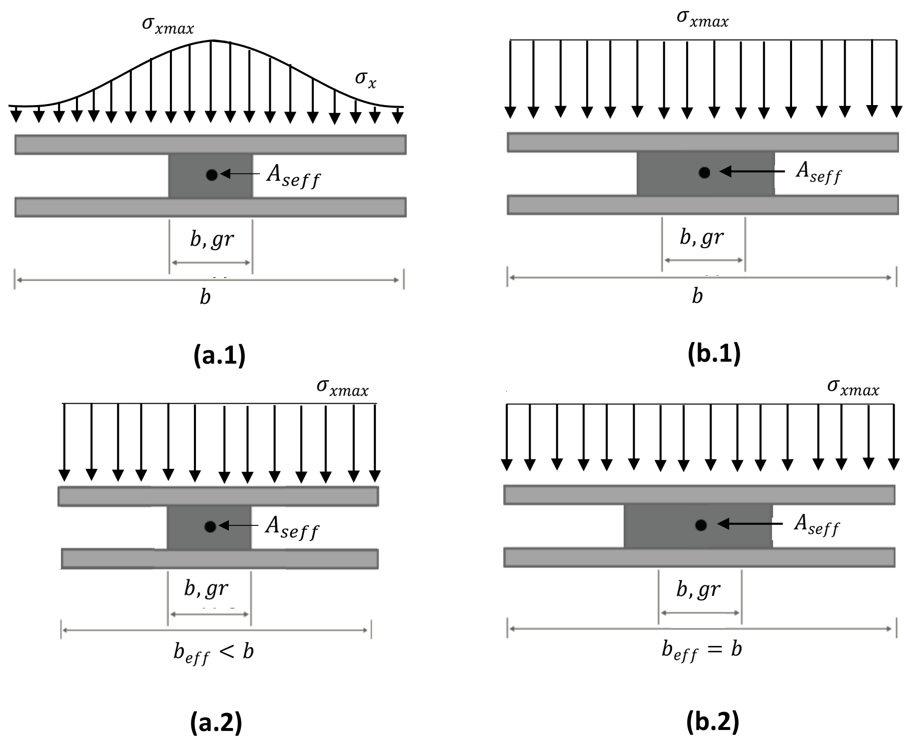

Figure 3.11 – Shear Lag Effect in RMWs. (a.1) Widely Spaced reinforcement stress distribution. (a.2) Standard simplification. (b.1) Closely spaced reinforcement stress distribution. (b.2) Standard simplification

The effective width limit is only applicable for combinations of axial load and moment on which the steel is assumed to carry tensile stresses. It does not apply for load combinations in which the steel is not in tension.

CSA S304-14 limits the effective compression zone to a minimum of

- 4 times the wall thickness
- the spacing between bars.

While TMS 402-16 allows the designers to set the compression zone width to the minimum of:

- 6 times the wall thickness,
- the spacing between rebars,

- or 72 inches (1828.8 mm).

Table 3.11 summarizes the effective compressive width limit imposed by the North American standards.

Table 3.11 – Effective Compressive Width equations.

Standard	Compressive Width Limit
CSA S304-14	$b_{eff} = min\ (4t, rebar\ spacing)$ C-3.6
TMS 402-16	$b_{eff} = min\ (6t, rebar\ spacing, 72\ inches)$ U.S.- 3.5

Theoretically, the CSA S304-14 offers a more conservative provision, where for some circumstances, the effective width used could be 40% lower than a design developed using the TMS 402-16 approach. For instance, for a rebar spacing of 1400 mm (or 55 inches), and block size thickness of 190 mm (or 7.48 inches), the b_{eff} calculated using U.S.- 3.5 is governed by the 6t limit, and the total width to assume in the design is 1140 mm (or 44 inches). For the same conditions, the b_{eff} computed using CSA S304-14 is governed by the 4t limit, which results in a maximum width of 740 mm (or 29 inches). Additionally, the limit mandated by CSA S304-14 could be triggered for a lower rebar spacing compared to TMS 402-16 (6t vs 4t). Such reduction translates into a decrement of both the flexural and axial capacity of OOP walls.

The effect of this provision is graphically shown in Fig. 3.12 and Fig. 3.13. The P-M interaction curves developed in section 3.2.5, are affected by their respective reductions due to the compressive width limits (dashed curve). On each figure, the P-M resistances neglecting this limit (solid curve) are also presented.

In both diagrams, the P-M capacities decreased due to the reduction of the effective width used to compute the resistances once the steel starts to develop tensile strains.

Additionally, it appears that due to the stricter limit proposed by , the P-M capacities are reduced by a greater proportion than that of the TMS 402-16 curves.

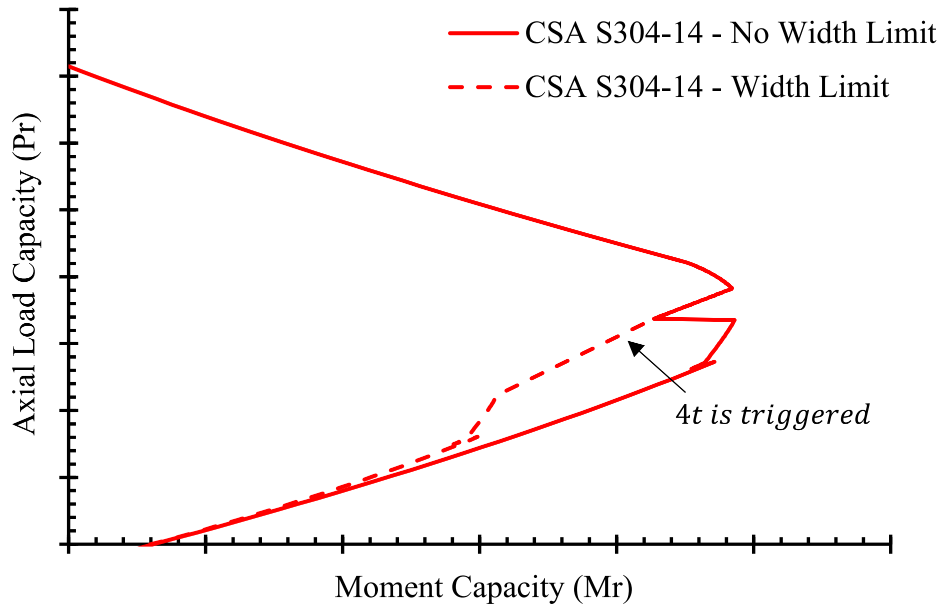

Figure 3.12 – P-M interaction diagram for reinforced masonry wall as per CSA S304-14. Affected by effective compressive width limit.

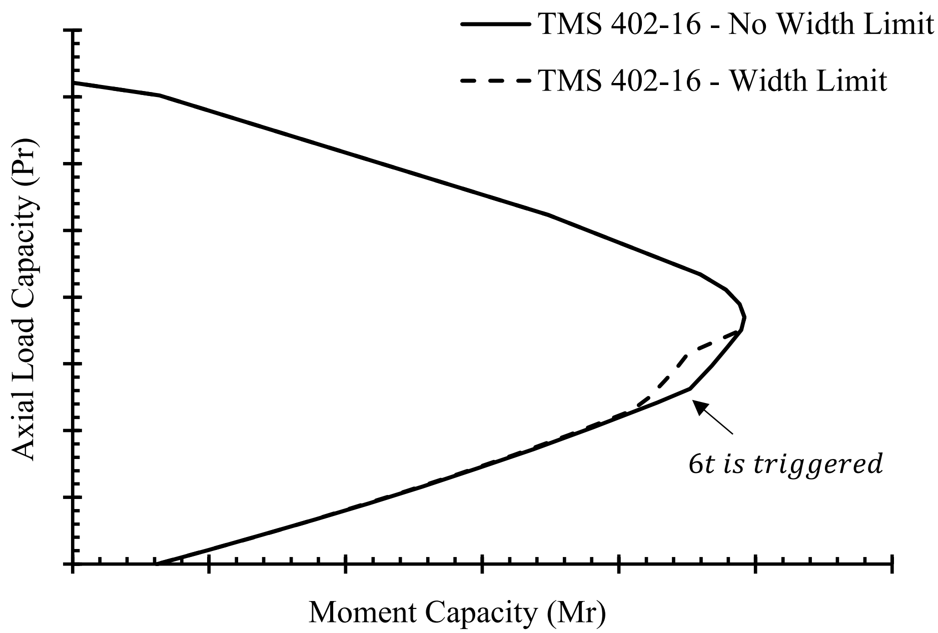

Figure 3.13 – P-M interaction diagram for reinforced masonry wall as per TMS 402-16 . Affected by effective compressive width limit.

3.2.5.3 Maximum axial load capacity related to ductility

TMS 402-16 provides a maximum flexural reinforcement provision (Cl. 9.3.3.2) which has the purpose of maintaining an adequate ductility level by specifying a minimum strain in the flexural reinforcement ($1.5\varepsilon_y$) under an axial load combination based on $D + 0.75L + 0.525Q_e$. This requirement is expressed in terms of a maximum reinforcement ratio, ρ_{max}, above which the wall will not meet this ductility requirement. By limiting the amount of steel in the wall, the capacity of the wall is effectively reduced.

For fully grouted members with only concentrated tension reinforcement, the maximum reinforcement is given by:

$$\rho_{max} = \frac{As}{bd} = \frac{0.64f'm\left(\frac{\varepsilon_{mu}}{\varepsilon_{mu} + \alpha\varepsilon_y}\right) - \frac{P}{d_v}}{f_y} \qquad \text{(U.S.- 3.8)}$$

The α parameter in U.S.- 3.8 is specified as follows:

- 3.0 for reinforced shear walls (Intermediate seismic detail required)
- 4.0 for reinforced shear walls (Special seismic detail required)
- 1.5 for all other cases.

If there is concentrated compression reinforcement with an area equal to the concentrated tension reinforcement, A_y, the maximum reinforcement is (TMS 402-16):

$$\rho_{max} = \frac{As}{bd} = \frac{0.64 f'_m \left(\frac{\varepsilon_{mu}}{\varepsilon_{mu} + \alpha\varepsilon_y}\right) - \frac{P}{bd}}{f_y} \qquad \text{(U.S.- 3.9)}$$

For partially grouted sections where the neutral axis lies in the flanges, the maximum reinforcement is determined as a fully grouted member with tension reinforcement only (U.S.- 3.9). If the neutral axis is located at the web, the maximum reinforcement is determined as:

$$\rho_{max} = \frac{As}{bd} = \frac{0.64 f'_m \left(\frac{\varepsilon_{mu}}{\varepsilon_{mu} + \alpha\varepsilon_y}\right)\left(\frac{b_w}{b}\right) + 0.80 f'_m\, t_{fs}\left(\frac{(b - b_w)}{bd}\right) - \frac{P}{bd}}{f_y} \qquad \text{(U.S.- 3.10)}$$

While CSA S304-14 does not have a ductility limitation for non-slender walls (kh/t < 30), for walls with $\frac{kh}{t} \geq 30$ the tension steel is required to yield before the crushing strain of the masonry is reached. To achieve this objective, Cl 10.7.4.6 and 10.7.4.6.5 present an equation derived based on a steel yield strain of 0.002 and a yield strength of 400 MPa.

$$\frac{c}{d} \leq \frac{600}{600 + f_y} \qquad \text{(C-3.9)}$$

Where, c is the depth of the neutral axis, d is the distance from the masonry fibre of maximum strain to the centroid of the steel rebar, and f_y the yield strength of the steel reinforcement.

To illustrate the differences between the two codes, Table 3.12 compares the c/d ratio required by each standard based on the strain profile for typical yield strength of 400 MPa. Larger *c/d* ratios imply deeper compressive blocks that are able to balance more steel reinforcement in tension. More reinforcement allowed in the cross-section is generally indicative of more capacity.

Additionally, The P-M interaction curves presented in section 3.2.5 affected by their respective ductility limits are illustrated in Fig. 3.14 and Fig. 3.15. On each figure, the TMS 402-16 and the CSA S304-14 limit are shown. No other provisions are applied to the figures (i.e. Axial limit or compressive width limit)

Table 3.12 – Comparison of maximum reinforcement provisions.

$CSA\ S304-14$ $\varepsilon_{mu} = 0.003$	$TMS\ 402-16$ $\varepsilon_{mu} = 0.0025$	$\frac{CSA}{TMS}$
$\frac{c}{d} = \frac{600}{600+f_y} = 0.6$	$\frac{c}{d} = \frac{\varepsilon_{mu}}{\varepsilon_{mu}+1.5\varepsilon_y} = 0.45$	1.32

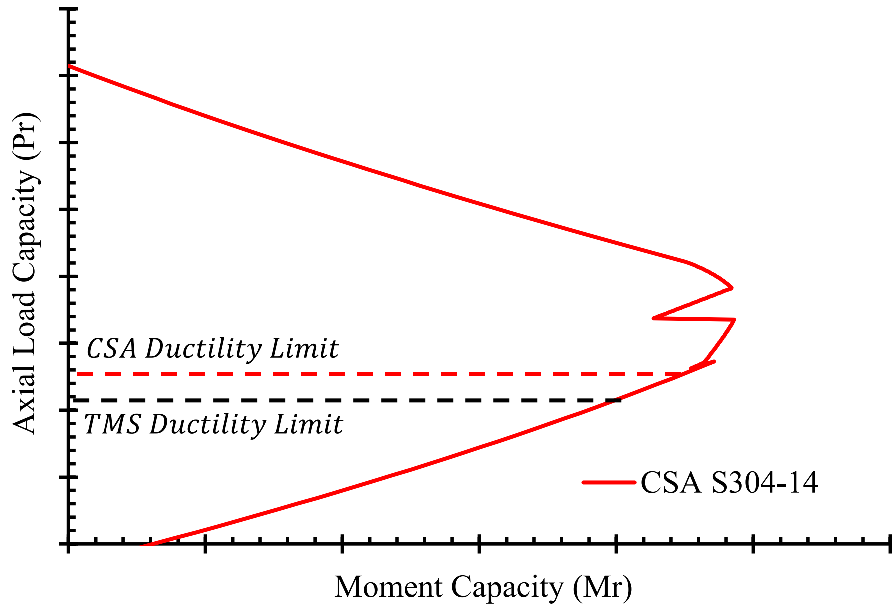

Figure 3.14 – P-M interaction diagram for reinforced masonry wall as per CSA S304-14. Affected by ductility related limits.

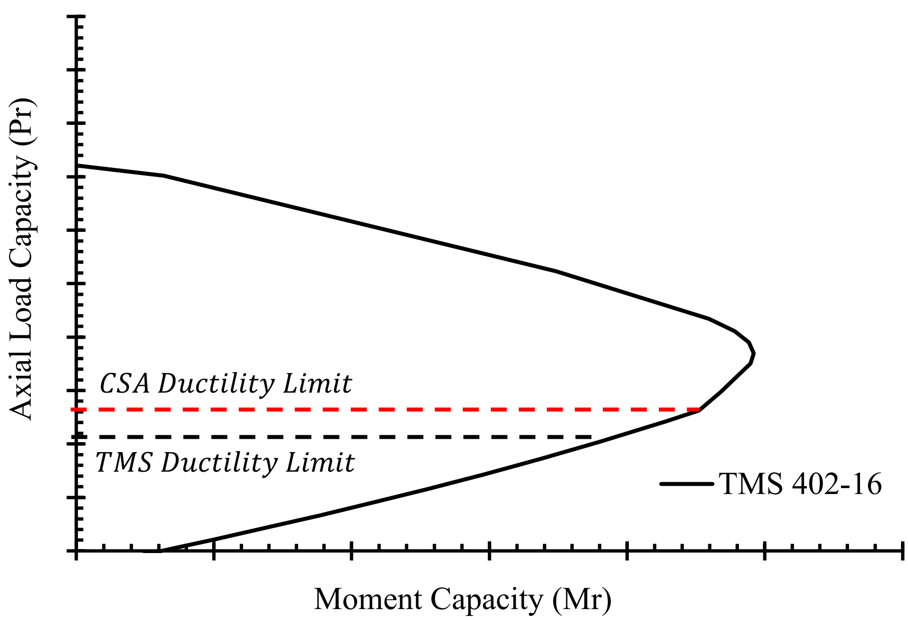

Figure 3.15 – P-M interaction diagram for reinforced masonry wall as per TMS 402-16. Affected by ductility related limits.

From Fig. 3.14,3.15 and Table 3.12, it seems that higher axial load is allowed by the Canadian committee when both standards require satisfying ductility limits. However, such limitations are only required for structures with height-to-thickness ratios greater than 30 by the CSA S304-14, whereas the TMS 402-16 mandates this provision for all values of slenderness. Additionally, it is essential to consider that ρ_{max} mandated by the TMS 402-16, shall be satisfied for a loading combination of $D + 0.75L + 0.525Q_e$, while the CSA S304-14 equivalent provisions should be verified for all the ULS load combinations as per the NBCC. Thus, the ductility limits provision mandated by the CSA S304-14 is typically revised for higher loads than the TMS 402-16 (e.g. 1.5D + 1.5L vs D+0.75L+052Q_e). This might be translated into more robust designs in Canada to satisfy this provision.

3.2.5.4 P-M interaction diagrams summary

This section shows a sample of a typical moment interaction diagram designed as per the CSA S304-14 (Fig. 3.16) and TMS 402-16 (Fig. 3.17). The discussed provisions are included in these P-M curves.

The following references points are depicted in Fig. 3.16

- Point C-1 = Maximum axial load capacity as per Clause 10.4.1 (Section 3.2.5.1)
- Point C-2 = Steel develops tensile strain. Effective compressive width limit is triggered.
- Point C-3 = Ductility limit as per Clause 10.7.4.6 (Section 3.2.5.3)
- Point C-4 = Maximum axial load capacity for slender walls (Section 3.2.5.1)

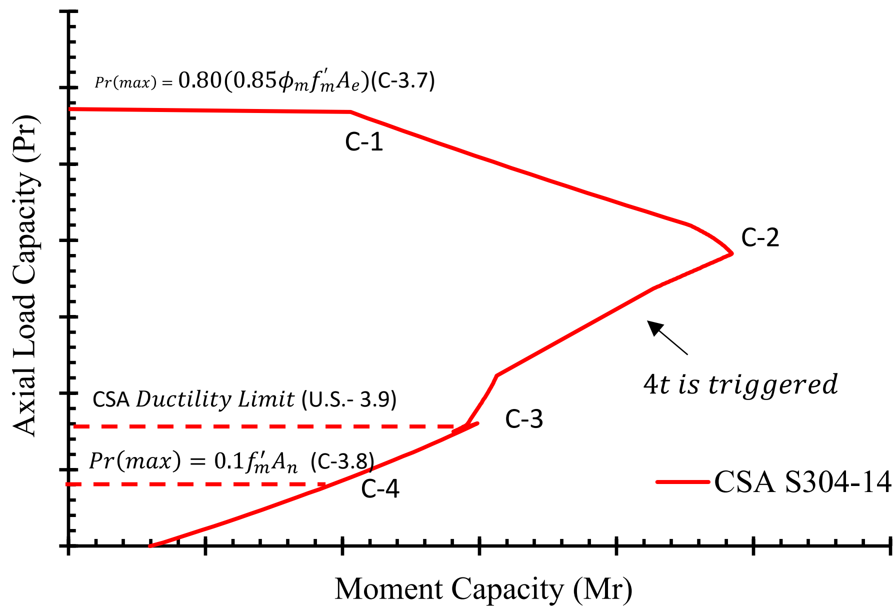

Figure 3.16 – Typical P-M interaction diagram as per CSA S304-14

The following reference points are depicted in Fig. 3.17.

- Point US-1 = Maximum axial load capacity as per Clause 9.3.4.11 (Section 3.2.5.1)
- Point US-2 = Steel develops tensile strain. Effective compressive width limit is triggered.
- Point US-3 = Steel reaches yield strain.
- Point US-4 = Ductility limit as per Clause 9.3.3.2. (Section 3.2.5.3)
- Point US-5 = Maximum axial load capacity for slender walls (Section 3.2.5.1)

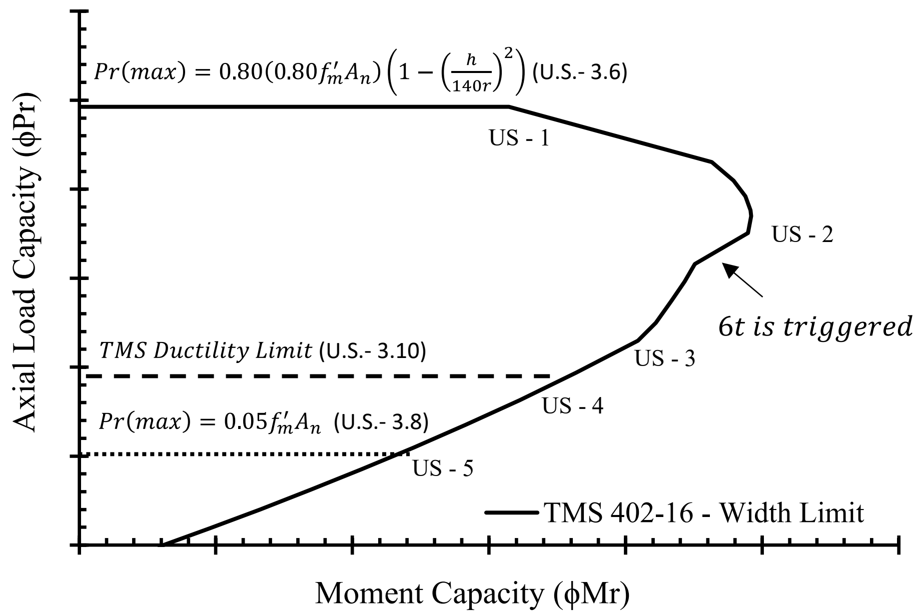

Figure 3.17 – Typical P-M interaction Diagram as per TMS 402-16

3.3 Parametric Studies

To quantify the differences between the Canadian standard (CSA S304-14) and the American standard (TMS 402-16) in a systematic way, parametric studies were conducted to evaluate the impact of isolated parameters on the capacity of fully and partially grouted walls loaded with axial compressive forces and out of plane bending. The capacity of the walls is represented by axial-moment (P-M) interaction diagrams. Throughout the discussion, P-M curves computed using the CSA S304-14 are presented in red and those using TMS 402-16 in black. A standardized wall width of 1.0 m was selected and magnitudes are presented as kN/m or kNm/m for axial loads and moment, respectively. The parameters of this study are classified as fixed, independent, and dependent, which are described as follows.

3.3.1 Fixed parameters

The fixed parameters were not changed in the study and were constant for all the P-M diagrams. For a direct comparison between both standards, the same block sizes, rebar size, and steel yield strength were used unless specified otherwise. The values of the fixed parameters above were set to those used for typical wall construction in Canada. All the calculations are done for a 1-metre width of wall. The fixed parameters are summarized in Table 3.13.

Table 3.13 – Fixed parameters summary.

Parameter	Value
Block thickness	190 mm (7.48 in)
Yield Strength of Steel*	400 MPa (58 ksi)
Rebar Size (10M)*	11.3 mm (0.44 in) diameter
Height of the Wall**	4 m (157.48 in)

* Canadian value used for consistency. **Independent parameter for section 3.3.4.4

3.3.2 Independent parameters

The independent parameters were varied to investigate their effects on the dependent parameters. The study had four independent parameters consisting of the rebar spacing, the compressive strength of the masonry, the material and strength reduction factors, and the height of the wall.

Variation of the rebar separation would trigger the maximum effective width provision described on each standard. This parameter is selected to study the effect of this provision in reducing the capacity of the walls.

In section 3.2.1, it was commented that nominal compressive strength values used in the

United States are consistently higher than those in Canada for the same block strength. The compressive strength is selected as an independent parameter to evaluate the implication of the differences in nominal compressive strength, and to compare the sensitivity of each standard from the variation of this parameter.

The nature of reduction factors mandated by each standard is different. While CSA S304-14 provides reduces the capacities of the material (i.e. $\emptyset_m$ for masonry, $\emptyset_s$ for steel) TMS 402-16 specifies a strength reduction factor to affect nominal capacities. The reduction factor is selected as an independent parameter to study the implications of the different approaches in the P-M resistances.

Variation of the height of the wall would impact the axial capacity of the walls. Additionally, it would trigger requirements related to the design of slender walls. Therefore, this parameter is selected to understand its effect on the axial loading capacities of OOP walls.

3.3.3 Dependent parameters

The dependent parameter is the strength of out-of-plane loadbearing masonry walls in terms of the flexural and axial capacity. The strength of the walls is evaluated using P-M interaction diagrams.

3.3.4 Effects of Independent Parameters on the Strength of the Walls

3.3.4.1 Effect of rebar spacing.

The spacing between the rebar leads to two design scenarios. First, both standards limit the maximum allowed width of the compression zone, b_{eff}, as described in section 3.2.5.2. Increasing the rebar spacing could trigger this limitation. Second, increasing the rebar spacing would often decrease the grouted area per meter assumed during the design. Less grouted area reduces the flexural and axial resistance of the walls.

To study these effects, 4 P-M interaction diagrams of walls, 4 meters high reinforced with 10 M rebars, 20 cm blocks with a nominal strength of 15 MPa are shown in Fig. 3.18. Table 3.14 summarizes the parameters used in Fig. 3.18.

The rebar spacing is increased by 400 mm in each scenario, starting from 200 mm (for a spacing equal to 200 mm, the wall is fully grouted) up to 1400 mm. This rebar arrangement is selected to trigger the effective compressive width limitation in both standards. Table 3.13 shows the respective b_{eff} mandated by each standard for the rebar arrangements used in the diagrams. The effective compression width for a 20 cm block is triggered for the rebar spacing of 1000 mm and 1400 for CSA S304-14 and TMS 402-16 provisions, respectively. The solid red and black lines represent the P-M interaction curves considering the compressive width limitation, while the dashed lines are the equivalent curves assuming that no such limit exists. In all the graphs, the maximum axial compressive load related to the ductility limits in the TMS 402-16 standard is also shown.

Table 3.14 – Effective Compressive width for a nominal block thickness of 200 mm

Rebar Spacing (mm)	Block thickness multiplier (mm)		b_{eff} (mm)		b_{eff} per meter (mm/m)	
	CSA S304-14 (4t)	TMS 402-16 (6t)	CSA S304-14	TMS 402-16	CSA S304-14	TMS 402-16
200	760	1200	200	200	1000	1000
600	760	1200	600	600	1000	1000
1000*	760	1200	760	1000	760	1000
1400**	760	1200	760	1200	542.9	857.1

*CSA S304-14 provision is triggered **TMS 402-16 provision is triggered

Table 3.15 – Summary parameters used in Fig. 3.18.

Parameters	CSA S304-14	TMS 402-16
Wall Height (m)	4	4
Compressive Strength of The Masonry (f'_m)	$f'_{m_{ug}} = 10\ MPa$ $f'_{m_{gr}} = 7.5\ MPa$	$f'_{m_{ug}} = 10\ MPa$ $f'_{m_{gr}} = 10\ MPa$
Block Thickness (mm)	190	190
Rebar Size (Canadian Nomination	10M	10M
Rebar Separation (mm)*	200, 600, 1000, 1400	400, 800, 1200, 1400
Reduction Factors (∅)	$\emptyset_m = 1\ ,\emptyset_s = 1$	$\emptyset = 1$

*Variable Parameter

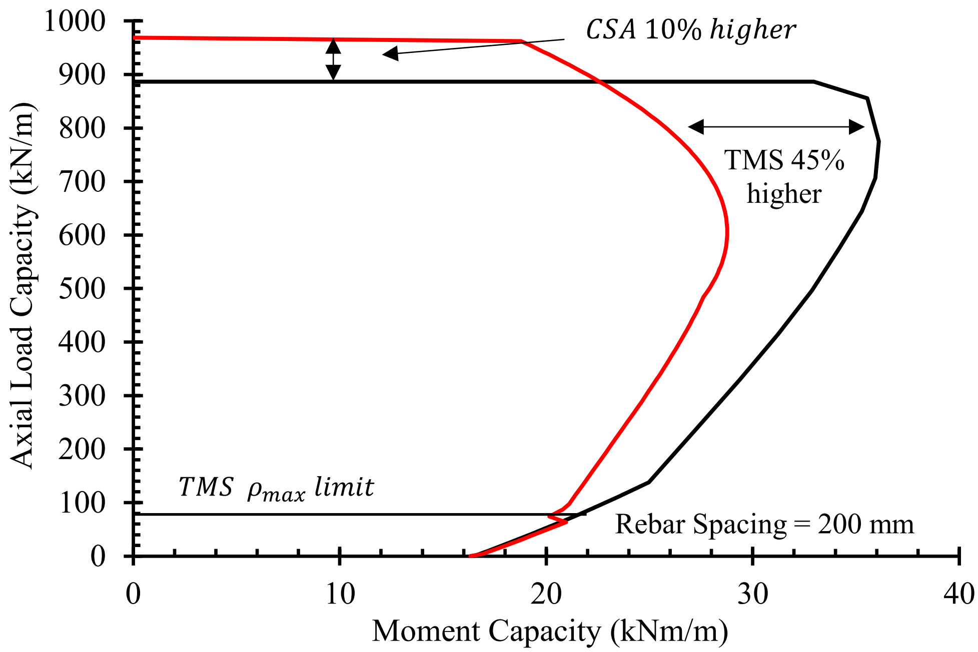

Figure 3.18 – Effect of rebar spacing. Rebar spacing of 200 mm (Fully grouted)

In Fig. 3.18, the compression-controlled region moment resistances (i.e. 800 kN/m) computed using the TMS 402-16 are shown to be up to 45% greater than the corresponding CSA S304-14 values. This dissimilarity is attributed to the differences in grouted compressive strength ($f'_{m_{gr}}$) utilized by each standard. As discussed in section 3.2.1, CSA S304-14 prescribes a grouted and ungrouted compressive strength, while TMS 402-16 does not make such distinction. Between 150 kN/m and 1000 kN/m of axial loading, the neutral axis lies on the grouted core. Therefore, CSA S304-14 P-M resistances in this range are computed using a f'_m value of 7.5 MPa. The TMS 402-16 curve is developed using a compressive strength of 10MPa for all the axial loading levels.

From an axial load range of 0 kN/m up to approximately 150 kN/m the response of both curves are almost identical. At this range, the response is primarily controlled by the tension reinforcement, and to a lesser extent by the masonry compressive strength. At this range of loads, the neutral axis lies on the faces hell of the block, and both the CSA S304-14 and TMS 402-16 resistances are calculated using the same f'_m and f'_y values of 10 MPa and 400 MPa, respectively.

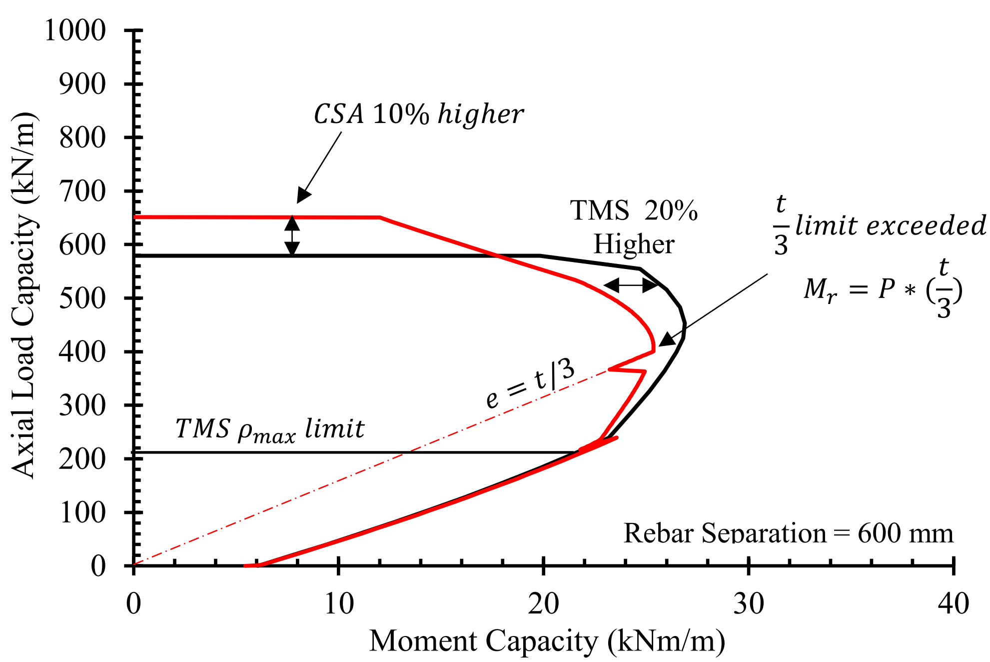

Figure 3.19 – Effect of rebar spacing. Rebar spacing of 600 mm (Partially grouted)

At a rebar spacing of 600 mm (Fig. 3.19) the wall becomes partially grouted. The differences in the compression-controlled region (i.e. 500 kN/m) decrease considerably in contrast to the fully grouted wall of Fig 3.10. In this region, the moment resistances computed using TMS 402-16 provisions are up to 20% greater than of CSA S304-14 (15% less than the fully grouted wall). This can be attributed to the reduction of the grouted area per meter assumed during the design, compared to the wall with 200 mm spacing. For a rebar spacing of 600 mm, the grouted area per meter is 41,958 mm^2/m, whereas for a spacing of 200 mm (fully grouted section) is 126,000 mm^2/m. Compatibility and equilibrium in the cross-section show that the neutral axis lies on the grouted core only between 700 kN/m and 425 kN/m in Fig 3.10: therefore, CSA S304-14 resistances are computed using smaller values of f'_m (7.5 MPa). Not only a lower f'_m is used for a smaller range of axial loading, but the contribution of the grouted area in the strength of the wall is reduced considerably. At 400 kN/m of axial, an area of discontinuity in the CSA S304-14 curve appears due to the restriction of the standard for unreinforced masonry elements. The Canadian committee limits the virtual eccentricity of the section

(M_r/P_r) to a maximum of t/3 for UMWs. Moreover, because less grouted area is involved in the design, the tension-controlled region is extended. At much higher axial loads the response is dominated by the yield strength of the steel. The steel is activated sooner as less masonry area is used during the force equilibrium. The P-M resistances are almost identical up to 250 kN/m. More importantly, both curves are computed using an effective width of 1 meter as no compressive width limit is yet active in any of the standards.

Additionally, the maximum axial capacity due to the ductility limit mandated by the TMS 402-16 is increased by approximately 100 kN/m in contrast to the curve with a rebar separation of 200mm. Less masonry area is assumed in the design with a rebar spacing of 600 mm. Thus, the yield strain is achieved at higher axial loads.

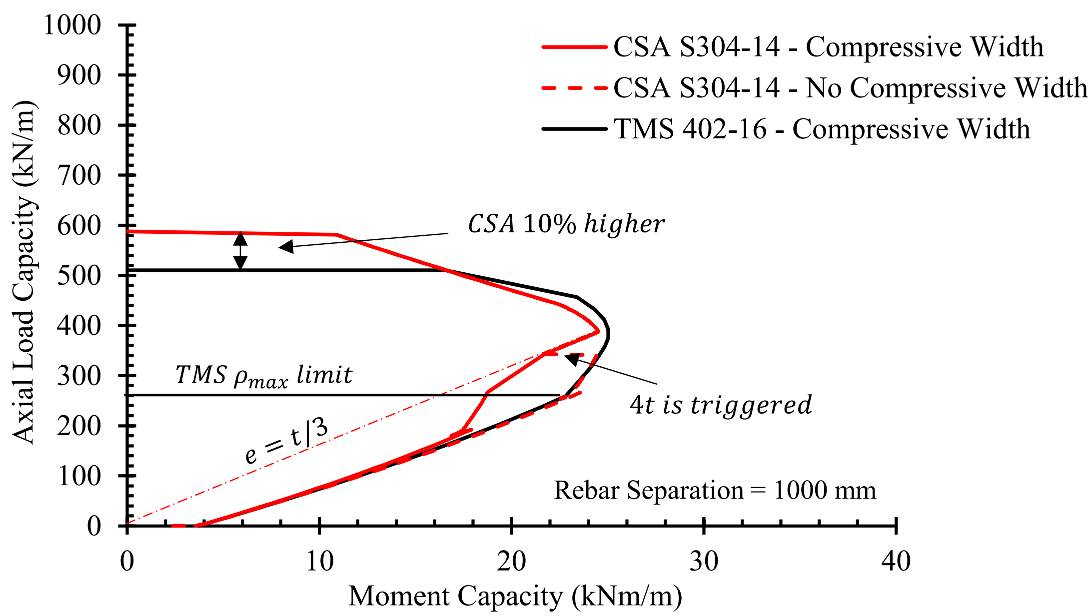

Figure 3.20 – Effect of rebar spacing. Rebar spacing of 1000 mm (Partially grouted)

For a rebar spacing of 1000 mm (Fig. 3.20), the grouted area is reduced considerably to 25200 mm^2/m. Both interaction curves are similar between 400 kN/m to 500 kN/m of axial loading. After 400 kN/m the flexural capacity of the CSA S304-14 curve is limited to a maximum of $P * (\frac{t}{3})$ up to 350 kN/m axial loading (and the section is considered unreinforced). If the loads increase, the steel reinforcement becomes active in tension and the CSA S304-14 compressive width limit is triggered. The TMS 402-16 interaction diagram is not affected by this limit, as the 6t bound is not yet exceeded. The solid red line in Fig 3.12 represents the P-M curve of the wall affected by the compressive width limit, while the dashed red line corresponds to a case in which the limit is not applied. The reduction of the capacity of the section in the CSA S304-14 calculations compared to those of TMS 402-16 between the range of 200 kN/m and 350 kN/m is noticeable. After 350 kN/m the CSA S304-14 P-M resistance is calculated using a compressive width of 760 mm/m (240 mm/m less than with 600 mm of rebar spacing).

The axial load limit related to the ductility effects increased by approximately 70 kN/m in contrast to the trial with a rebar spacing of 600 mm.

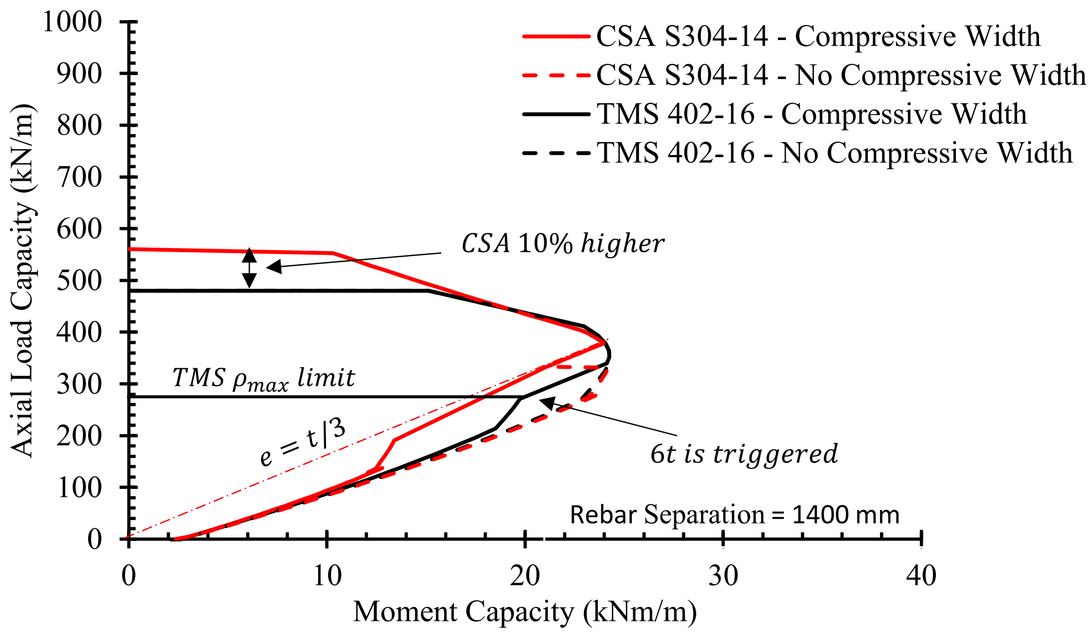

Figure 3.21 – Effect of rebar spacing. Rebar spacing of 1400 mm (Partially grouted)

At the highest spacing studied (1400 mm, Fig. 3.21) the influence of the grouted core area on the strength of the wall is less significant. At this spacing, the grouted area is reduced considerably. Therefore, both P-M curves are identical in the compression-controlled zone up to 400 kN/m of axial loading, where the discontinuity due to the URM limit imposed by the CSA S304-14 appears. At 330 kN/m of axial load, the reinforcement starts carrying tensile stresses, and the compressive width limits are triggered in both standards. The reduction in the capacity of the section is more pronounced in the CSA S304-14 curve than its counterpart, as illustrated in the bottom right portion of Fig 3.20. This difference can be attributed to the effective compressive width used by each standard for the development of these curves. CSA S304-14 restricted the maximum compressive width to 542 mm/m, whereas TMS 402-16 uses 857 mm/m for its design. The moment capacity for purely flexural dominated response (i.e. low axial load levels) do not change significantly. Although lower compressive width will result in greater depth of the equivalent compressive blocks, *c,* this region is predominantly dominated by the tension strength of the rebars. P-M curves developed neglecting the compressive width limitations would result in two perfectly aligned curves as shown by the dashed lines in Fig. 3.21.

An additional figure is presented in this section to demonstrate the reduction of the capacity of the section due to the decrease in the grouted area. Fig. 3.22 shows the P-M interaction diagrams of two walls with two reinforcement arrangements: 10M bars separated at 400 mm and 20M bars spaced every 1200 mm. Both arrangements represent the same reinforcement area per meter of wall (250 mm^2/m). Assuming that only the cells that contain rebars are filled with grout, at higher rebar spacing, less masonry area is considered during the design of the wall with the rebar spaced every 1200 mm.

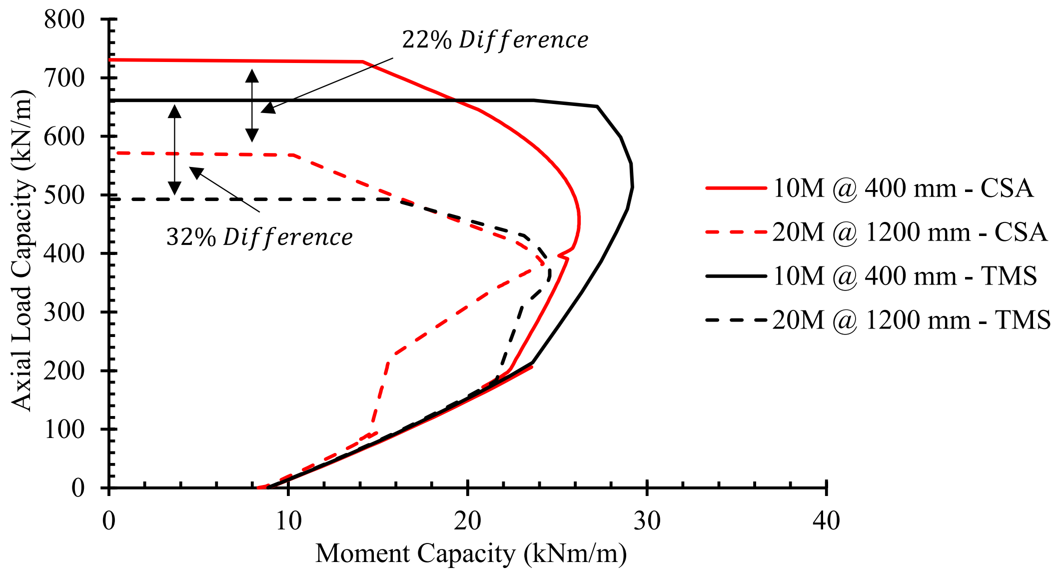

Figure 3.22 – Equivalent reinforcement area, different rebar spacing as per CSA S304-14.

From Fig. 3.22 the reduction in the strength of the walls in the compression-controlled region is noticeable. A section with the rebars separated every 400 mm is designed assuming a total masonry area (grouted + ungrouted) of 131200 mm^2/m. For 1200 mm of rebar spacing, the total area of the masonry is 92000 mm^2/m. As in compression-controlled regions, the response is dominated by the compressive strength of the masonry, so less grouted area results in smaller P-M resistances. The axial cap of the CSA S304-14 diagram with a spacing of 1200 mm of is 560 kN/m versus 720 kN/m for the 400 mm spacing version, representing roughly a 22% reduction in capacity compared to the wall with the lower rebar separation. The maximum allowed axial forces from the TMS 402-16 curves decreased 32% (From 660 kN/m to 550 kN/m). Under medium axial load levels (between 350 kN/m and 100 kN/m) the compressive width limit is triggered in both standards, reducing the flexural capacity by a great margin. As commented before, the reduction due to this limitation is more pronounced in the CSA S304-14 diagrams than in the TMS 402-16 version. At lower axial load levels, the resistances of all the curves presented in Fig 3.21 start to align with each other in the tension-controlled domain.

3.3.4.2 *Effect of the Compressive Strength of the Masonry*

As mentioned in section 3.2.1, the nominal compressive strength values specified in the TMS 402-16 402 are consistently higher than those prescribed in the CSA S304-14 for the same block strength.

The Canadian standard makes a distinction between ungrouted and grouted compressive strength. Depending on the neutral axis location during the compatibility analysis and the desired level of detail in the calculations, designers can opt for either grouted or ungrouted strength values. For instance, for a 15 MPa nominal block strength, if the neutral axis lies beyond the faceshell and within the grouted core, the strength of the masonry is taken as 7.5 MPa (Table 3.16). The American standard does not make such distinction, and a consistent value of 13.29 MPa is used for a 15 MPa block strength, independently of the neutral axis location.

Table 3.16 – Equivalent Compressive Strength Values

Nominal Block Strength (MPa)	CSA S304-14 f_m' (MPa)		TMS 402-16
	$f_{m_{ug}}'$	$f_{m_{gr}}'$	f_m' (MPa)
15	10	7.5	13.29
20	13	10	16.31

To study the effect of the differences in masonry compressive strength, P-M interaction diagrams of fully grouted walls, 4 meters high, reinforced with 10M bars spaced at 200 mm (i.e. effective width is 1 meter) were developed for 15MPa and 20MPa nominal strength blocks using each the respective properties of each standard. No strength reduction factors are applied.

The geometrical and material properties are summarized in Table 3.17. The blue circles in the P-M curves represent the inflection point where the steel is activated in tension, and the response is no longer controlled entirely by the compressive strength of the masonry.

Table 3.17 – Summary parameters used in Fig. 3.23

Parameters	**CSA S304-14**	**TMS 402-16**
Wall Height (m)	4	4
Compressive Strength of The Masonry (f'_m)*	<u>15 MPa Nominal</u> $f'_{m_{ug}} = 10\ MPa$ $f'_{m_{gr}} = 7.5\ MPa$ <u>20 MPa Nominal</u> $f'_{m_{ug}} = 13\ MPa$ $f'_{m_{gr}} = 10\ MPa$	<u>15 MPa Nominal</u> $f'_{m_{ug}} = 13.29\ MPa$ $f'_{m_{gr}} = 13.29\ MPa$ <u>20 MPa Nominal</u> $f'_{m_{ug}} = 16.31\ MPa$ $f'_{m_{gr}} = 16.31\ MPa$
Block Thickness (mm)	190	190
Rebar Size (Canadian Nomination)	10M	10M
Rebar Separation (mm)	200	200
Reduction Factors ($\emptyset$)	$\emptyset_m = 1.0$, $\emptyset_s = 1.0$	$\emptyset = 1.0$

*Variable Parameter

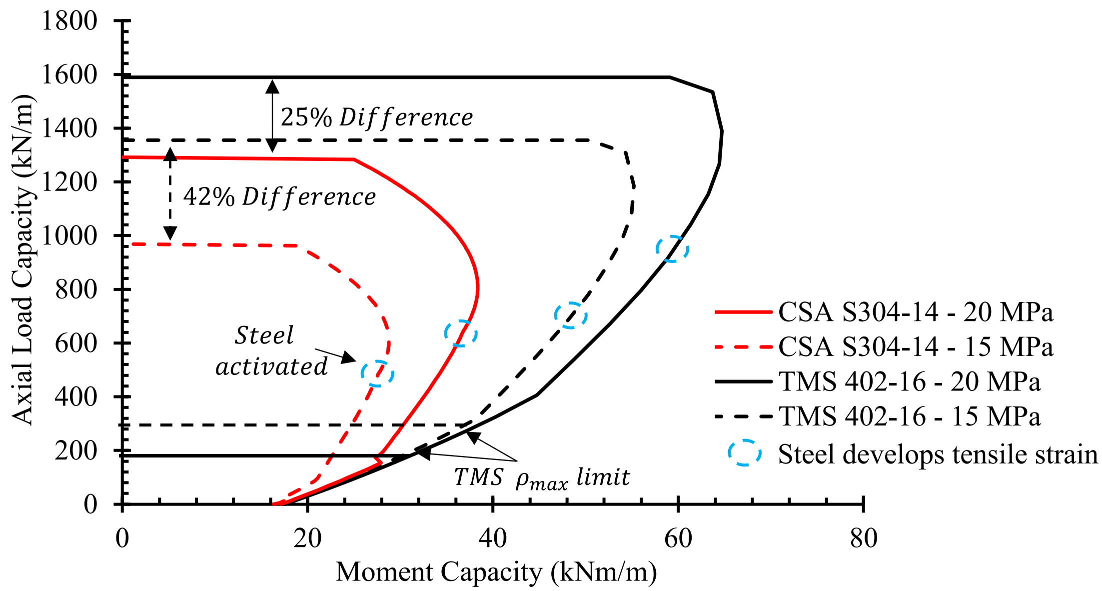

Figure 3.23 – Variation of the Compressive Strength f'_m.

From Fig. 3.23 seems that the masonry compressive strength significantly impacts the response in the tension- and compression-controlled regions. These dissimilarities seem to be more pronounced for the 15 MPa block than the 20 MPa block, as the differences in the masonry strength values are higher for 15 MPa blocks. For instance, the grouted compressive strength ($f'_{m_{gr}}$) prescribed in TMS 402-16 strength for a 15MPa block is 4.26 MPa higher than that of the CSA S304-14, while for a 20 MPa is 3.31 MPa.

In the tension-controlled region, the response is primarily dominated by the tension in the steel rebar and to a lesser extent by the compressive strength of the masonry, thus the influence of the masonry compressive strength is reduced. At pure bending (P = 0 kN/m), this influence is negligible: the ratio of the moment resistance from the TMS 402-16 over the CSA S304-14 $\left(\frac{M_{r(US)}}{M_{r(CN)}}\right)$ for a nominal strength of 15MPa and 20 MPa is 1.15 and 1.03, respectively.

For the compression-controlled region, the differences are more pronounced as the compressive strength of the masonry governs the response. Up to the blue circles highlighted with a blue dashed circle, P-M resistances are computed entirely using the masonry strength, as no tensile strains are yet developed. However, due to the higher compressive stresses allowed by TMS 402-16, in Fig. 3.23, the maximum axial capacity of TMS 402-16 designs are 42% and 25% higher for the 15 MPa and 20 MPa blocks, respectively, in comparison to those calculated with the CSA S304-14 code. The point where the maximum bending moment occurs in each diagram is also an interesting reference for this study. The maximum bending moments from the TMS 402-16 curves are 61% and 50% higher for the 15 MPa and 20 MPa blocks, respectively, compared to those calculated using the CSA S304-14 magnitudes code.

The axial capacity limits governed by the ductility limits imposed by TMS 402-16, are also affected due to the increment of compressive strength. The axial limit in the 15 MPa curve is approximately 60 kN/m higher than that of the 20 MPa diagram. Using higher compressive strength would require less axial force to reach the yield strain of the rebar due to the force equilibrium.

3.3.4.3 Effects of reduction factors $\emptyset$.

The principle of mechanics used to calculate the P-M resistances of masonry walls are relatively similar in both countries. However, each standard specifies reduction factors to decrease the resistance of the walls. These factors intend to account for uncertainties in materials or possible design and construction errors. As discussed in section 3.2.4, CSA S304-14 mandates material reduction factors that intends to affect the strength of the masonry ($\emptyset_e = 0.6$) and the steel ($\emptyset_s = 0.85$) independently, while TMS 402-16 opt to decrease the nominal resistances of the P-M interaction curves using a single factor ($\emptyset = 0.9$).

To evaluate the effects of these factors in the strength of the wall, P-M interaction diagrams of walls, 4 meters high reinforced with 10M rebars, 20 cm blocks with a nominal strength of 15 MPa are developed. Fig. 3.24 represents a fully grouted section with rebar spaced at 200 mm, while Fig. 3.25 shows a partially grouted wall with the rebar spacing set to 1400 mm. For each wall, the P-M curve with its nominal capacity (no reduction factors) and the alternative with the reduction factors applied are shown. Canadian blocks dimensions and material properties were used (Table 3.18.)

Table 3.18 – Summary parameters used in Fig. 3.24 and 3.25.

Parameters	CSA S304-14	TMS 402-16
Wall Height (m)	4	4
Compressive Strength of The Masonry (f'_m) (Canadian Values)	15 MPa Nominal $f'_{m_{ug}} = 10\ MPa$ $f'_{m_{gr}} = 7.5\ MPa$	15 MPa Nominal $f'_{m_{ug}} = 10\ MPa$ $f'_{m_{gr}} = 10\ MPa$
Block Thickness (mm)	190	190
Rebar Size (Canadian Nomination)	10M	10M
Rebar Separation (mm)	200 (Figure 3.24) 1400 (Figure 3.25)	200 1400
Reduction Factors (∅)*	$\emptyset_m = 1\ , \emptyset_s = 1$	$\emptyset = 1$

*Variable parameter

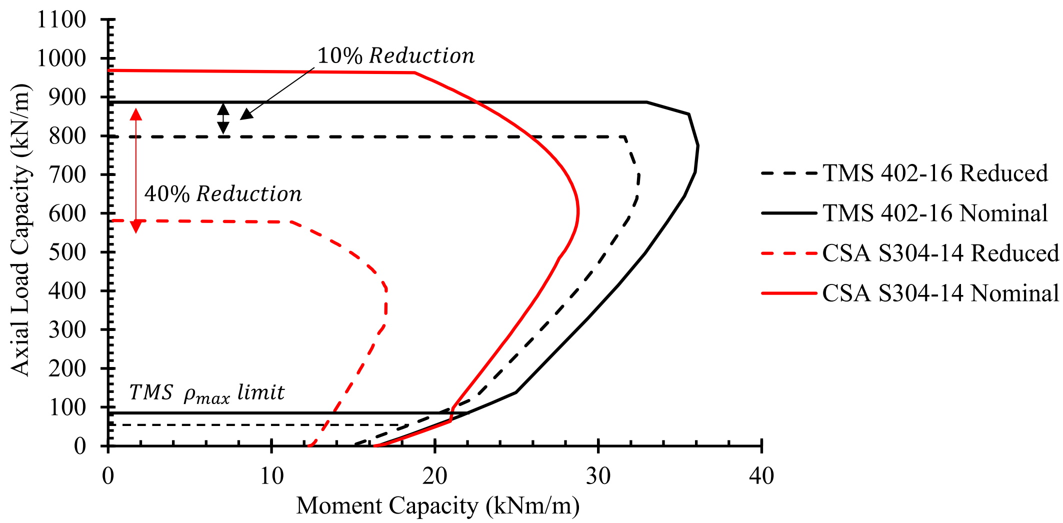

Figure 3.24 – Reduced vs Nominal P-M interaction diagrams. 200 mm rebar spacing.

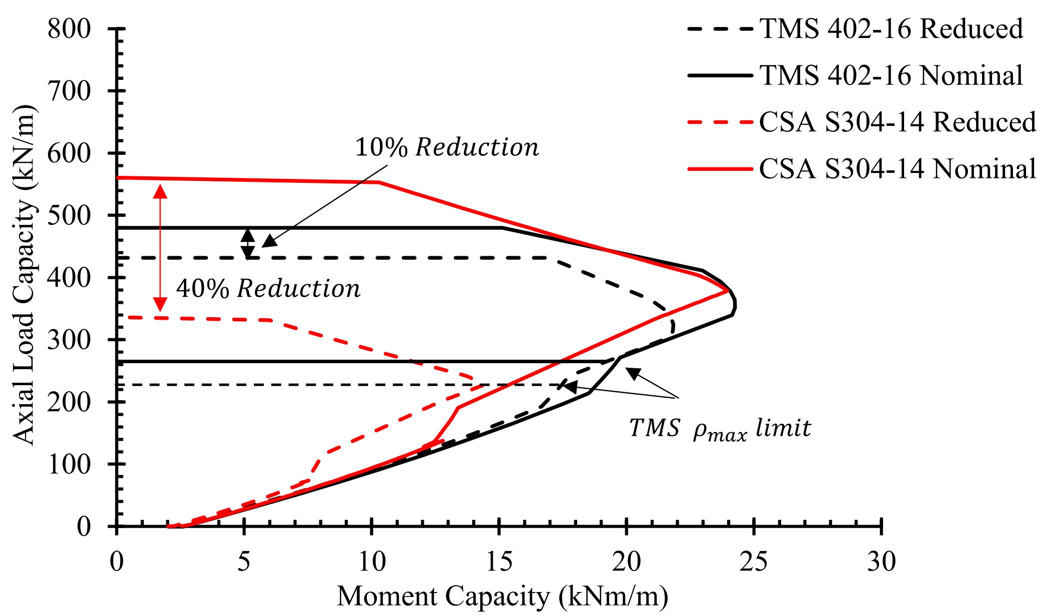

Figure 3.25 – Reduced vs Nominal P-M interaction diagrams. 1400 mm rebar spacing.

As depicted in the above figures and previous analyses, the nominal CSA S304-14 and TMS 402-16 resistances are quite similar. However, the differences become significant when overlaying P-M interaction curves affected by reduction factors and those with nominal capacities. CSA S304-14 reduced resistances are noticeably different from the nominal capacities. In the TMS 402-16 curves, although are also influenced by its reduction factors, the reduction seems to be less pronounced than that of CSA S304-14.

For the fully grouted wall shown in Fig. 3.24, the influence of the reduction factors in the compression controlled region is more prominent than in flexural dominated regions (i.e. at low axial loads). It is important to note that between 900 kN/m and 120 kN/m nominal capacities computed using the TMS 402-16 are greater than those calculated with the CSA S304-14. On this range, TMS 402-16 flexural and axial resistances are computed using a stronger compressive strength than that of CSA S304-14 (10 MPa versus 7.5 MPa), as explained in sections 3.2.1 and 3.3.4.1. The pure axial response (M = 0) is an excellent reference to assess the effect of this independent variable in the strength of the wall.

The CSA S304-14 axial cap is decreased by 40%, whereas the TMS 402-16 by 10% due to reduction factors. Interestingly, CSA S304-14 nominal axial caps were 5% greater than that of the TMS 402-16, however, when both curves are affected by the reduction factor the TMS 402-16 resistances at pure axial response become 25% higher than the Canadians values. This difference is attributed to the notably lower material resistances factor $\emptyset_m$= 0.6 used by the CSA S304-14 compared to the behaviour-based factor proposed in the TMS ($\emptyset$ = 0.9). While TMS 402-16 402 directly reduces the axial capacity ($\emptyset P_r$), the expression proposed by CSA S304-14 to compute the maximum compressive force is proportional to the strength of the masonry, which is affected by $\emptyset_m$. Axial capacities from the ductility limits are also affected by the reduction factors. This limit decreased by approximately 10%.

For all the other P-M resistance combinations, the CSA S304-14 magnitudes are calculated using the 60% of the masonry compressive resistance. Before the steel reinforcement develops tensile strains, the Canadian curves are only affected by the decrease in the strength of the masonry. In the tension-controlled response (i.e. at low axial loads) the nominal P-M resistances are identical from 0 kN/m to 100 kN/m of axial load. However, when the $\emptyset$ factors are used in the design, the CSA S304-14 moment resistance is approximately 18% less than the TMS 402-16 at pure bending (P = 0). While the American standard decreases the nominal flexural capacity by 10%, the CSA S304-14 resistance is being affected by a reduction of the strength of the masonry and steel simultaneously. Although this region is mainly governed by the tension in the steel (decreased by $\emptyset_s = 0.85$), to a lesser extent is affected by the compressive strength of the masonry, as it is used to compute the depth of the equivalent compression block. As explained before in section 3.3.4.1, the smaller the neutral axis depth, the lower the moment resistance.

In the partially grouted section from Fig. 3.25, the compression-controlled region from the nominal P-M curves is identical between 480 kN/m to 400 kN/m. However, the decrement of the P-M capacities in the compression-controlled region seems to be as impactful as for the fully grouted wall. Maximum axial capacities decrease at the same proportion as in Fig 3.13. CSA S304-14 maximum axial resistances are outperformed by the TMS 402-16 when the reduced curves are compared. Different from the fully grouted wall, the tension-controlled region is less affected by the reduction factors. For a rebar spacing of 1400 mm the masonry area is reduced considerably, therefore, the influences of the reduction of the masonry strength due to the $\emptyset_m$ factor is not quite impactful. Although not readily noticeable in Fig. 3.25, the TMS 402-16 moment resistance is 3% greater than the CSA S304-14 magnitudes at pure bending. This discrepancy can be attributed to multiple reasons. Partially, it is due to the lower b_{eff} value (4t vs 6t) used by the CSA S304-14 standard to compute P-M resistances once the effective compressive width limit is triggered. As commented repeatedly (section 3.2.5.1, 3.3.4.2), TMS 402-16 prescribes higher compressive width dimensions than the Canadian standard. This, combined with the reduction of compressive strength of the masonry due to the factor, increases the depth of the equivalent compression block used during the force equilibrium. Therefore, the moment arm in the internal equilibrium is reduced, and consequently, lower moment resistances are computed.

3.3.4.4 Effect of the Variation of the Height of the Wall.

The previous P-M interaction diagrams were developed assuming a constant height of 4 meters. To evaluate the effect of increasing the wall height on the strength of the wall, P-M interaction curves for a 20 cm – 15MPa masonry wall reinforced with 10M bars spaced at 400 mm are shown in **.** Three wall heights were used, 4 meters ($\frac{h}{t} = 21.05$), 5 meters ($\frac{h}{t} = 26.31$) and 6 meters ($\frac{h}{t} = 31.57$). These slenderness ratios were intentionally selected to investigate the effect on slender and non-slenderness walls. The ductility limits mandated by each standard are included in the P-M curves. It is important to note that moment amplifications due to second-order effects are not included in this analysis. These effects are extensively studied in the next chapter. This section only investigates the strength of the wall in terms of P-M interaction curves.

Table 3.19 – Summary parameters used in Fig. 3.26

Parameters	CSA S304-14	TMS 402-16
Wall Height (m)*	3.8, 4.75, 5.7	3.8, 4.75, 5.7
Compressive Strength of The Masonry (f'_m) (Canadian Base Values)	15 MPa Nominal $f'_{m_{ug}} = 10\ MPa$ $f'_{m_{gr}} = 7.5\ MPa$	15 MPa Nominal $f'_{m_{ug}} = 10\ MPa$ $f'_{m_{gr}} = 10\ MPa$
Block Thickness (mm)	190	190
Rebar Size (Canadian Nomination)	15M	15M
Rebar Separation (mm)	400	400
Reduction Factors ($\emptyset$)	$\emptyset_m = 1.0$, $\emptyset_s = 1.0$	$\emptyset = 1.0$

*Variable parameter

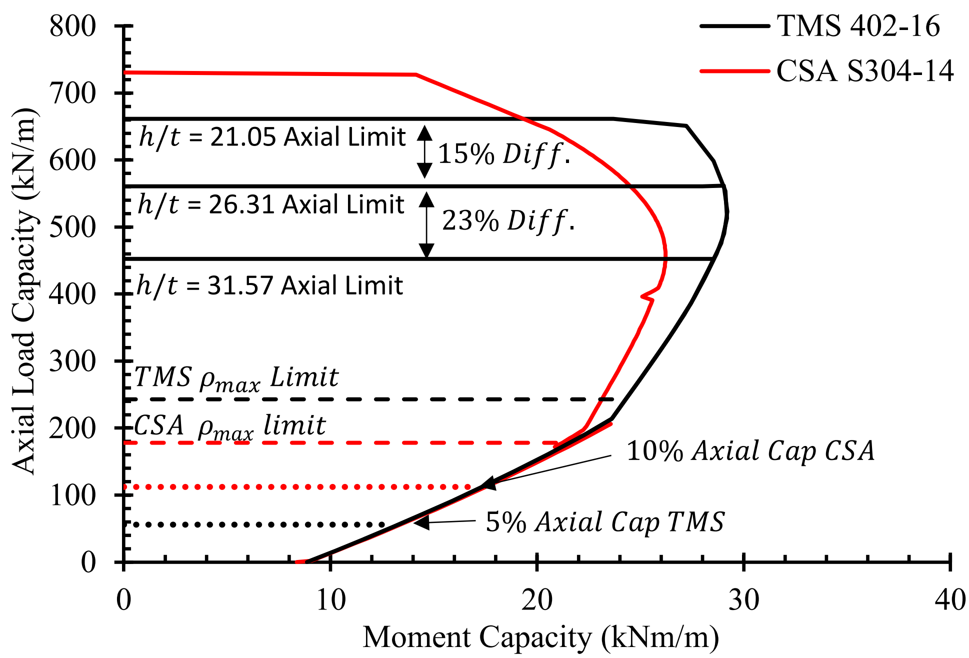

Figure 3.26 – Effect of the height variation in P-M interaction curves.

As shown in Fig. 3.26, the axial cap resistances in the TMS 402-16 curves progressively decrease as a function of the slenderness ratio. Increasing the height from 4 meter to 5 meters decreased the axial cap by 15%, whereas from 5 meters to 6 meters, the resistance decreased by 23%. As discussed in section 3.2.5.2, the TMS 402-16 standards prescribed two equations to compute the maximum allowed axial forces in the section as a function of the height of the structure and the thickness of the block. Slender members ($h/t \geq 30$) are susceptible to instability effects, therefore, the equation proposed by the standards (U.S.- 3.21) to calculate the axial cap for this type of wall becomes stricter.

The variation of the height of the structure does not affect P-M interaction curves developed using the CSA S304-14 as it does for those derived with the TMS 402-16. The expression mandated by the S304-14 to calculate the axial cap limit (C-3.7) does not depend on the slenderness of the structure, except when kh/t exceeds 30. In this case, the CSA S304-14 axial caps are limited by clause 10.7.4.6, which required that the yielding of the rebar is achieved before the crushing of the masonry (CSA S304-14 $\rho_{max}\ limit$

in Fig. 3.26). It is essential to note that the ρ_{max} limit mandated by the CSA S304-14 ought to be satisfied for all the ultimate limit state load combinations applicable.

In TMS 402-16, the maximum reinforcement requirement must be satisfied for any wall, independently of its slenderness ratio. The 402-16 equivalent provision is verified only under $D + 0.75L + 0.525Q_e$. Typical factored axial loads computed using the load combinations described in the NBCC are greater than those computed using $D + 0.75L + 0.525Q_e$.

Both standards imposed an additional restriction of the axial capacity for slender members. CSA S304-14 mandates that the applied compressive load in the wall should not exceed $0.1\phi_m f'_m A_e$. Due to these provisions, the maximum axial load for the CSA S304-14 curve is reduced by 65% compared to the capacity restricted by the ρ_{max}. P-M American curves are affected by a similar provision, however, the axial load is limited to a 5% of the maximum axial capacity $f'_m A_e$.

Consequently, it is clear the pronounced decrement of the axial capacity in Fig 3.26. The maximum compressive load decreased from 220 kN/m to 60 kN/m, which represents a reduction of 114%. It is important to remember that no reduction factors are applied to these curves. If the CSA S304-14 expression would have been influenced by the reduction factor $\emptyset_m$, the maximum axial capacity would have risen to 65 kN/m, which is almost equivalent to the TMS 402-16 magnitude. These limits often govern the design of slender masonry walls in both Canada and the United States.

3.4 Summary

The findings of the theoretical and numerical comparison of the flexural capacity, axial capacity from the North American standards are summarized in Table 3.20.

Table 3.20 – Comparison of the parameters investigated. Flexural and Axial Capacity.

Parameter	Validation	Comments
Rebar Spacing and Compressive Width Limits	Medium	• Increasing the rebar spacing implies less grouted area if only the grouted is poured in cells with rebars. Therefore, the capacity of the masonry is reduced considerably, especially in compression-controlled zones. • At higher spacing, the difference in the P-M resistances between standards decreases in the tension-controlled regions. • The compressive width limit suggested by the CSA S304-14 is triggered earlier than the TMS 402-16 . For 200 mm concrete blocks, the compressive width will be limited at 800 mm spacing, while the TMS 402-16 provision is triggered at 1200 mm. • Not only the compressive width limit from the CSA S304-14 is triggered earlier, but it is stricter.
Different f'_m values prescribed in each standard	High	• Masonry compressive strength values specified in the TMS 402-16 are significantly higher than those prescribed by the CSA S304-14 for the same block strength. • Compression controlled regions are the most affected by the different f'_m values. Tension controlled regions are affected by a minor margin. • The dissimilarities are more prominent for the 15 MPa block than the 20 MPa block.

Reduction Factors $\emptyset$	**High**	• The Canadian committee introduces strength reduction factors for the compressive strength of the masonry ($\emptyset_m$) and the yield strength of the rebar ($\emptyset_s$). However, the TMS 402-16 mandated a unique behaviour-based factor of 0.9. • Reduction factors imposed by the CSA S304-14 are more severe than those proposed by the TMS 402-16 . • The comparison of the nominal P-M interaction curves shows an excellent correlation in the overall capacity of the wall.
Variation of the Wall's Height	Low	• Variation of the height will only affect the maximum allowed axial force. • Increasing the height from 4m to 5m decreased the axial cap by 15%, whereas from 5 meters to 6 meters, the capacity was reduced 20%, due to the more strict provisions for walls with with $\frac{h}{t} \geq 30$ • The P-M interaction curves from the CSA S304-14 are only affected if the slenderness ratio is greater or equal to 30. The clause 10.7.4.6 is triggered, and the walls are required to achieve yielding in the rebars before the ultimate strain of the masonry. Any gradual increment of the height will not affect this provision.
Maximum reinforcement		• A maximum reinforcement limit is mandated by the CSA S304-14 for slenderness ratios greater or equal to 30, whereas for the TMS 402-16 is required for any slenderness ratio. • The maximum reinforcement provisions from both standards are very strict. Although in theory, the TMS 402-16 prescribe a more severe restriction ($1.5\varepsilon_y$) than the CSA S304-14 (ε_y). The reduction factor $\emptyset_m$ from the CSA S304-14 decreases the compressive strength

	capacity considerably, and consequently yielding is achieved at lower axial forces than the TMS 402-16 .

4. SECOND-ORDER EFFECTS COMPARISON.

4.1 Introduction

In essence, as the slenderness ratio (defined by the CSA S304-14 as kh/t , and by the TMS 402-16 as h/t) increases, the axial capacity decreases due to the potential for instability effects as illustrated in Fig. 4.1

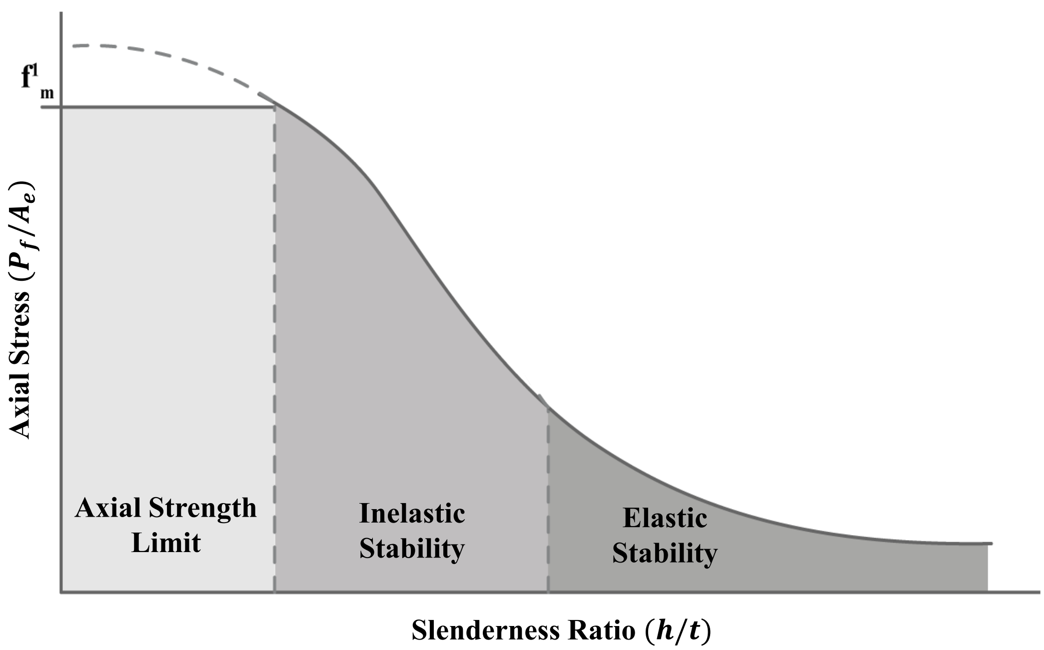

Figure 4.1 - Effect of slenderness in the axial capacity of masonry walls.

For most severe cases (i.e. very slender walls), this decrement in the axial compressive capacity can be associated with buckling. However, neither the CSA S304-14 nor the TMS 402-16 considers such failure mode explicitly for the design of masonry walls. Slenderness effects in RMWs subjected to weak axis bending are accounted for by calculating moment amplifications arising from the deflection of the structure.

Masonry walls subjected to out-of-plane bending could be discretized in two types of flexural moments: (a) primary moment, M_p, and (b) secondary moments, M_s. The primary moments originate from the loads applied to the wall, such as eccentric axial loads, wind, soil pressure or applied moments. Second-order moments arise as a consequence of the deflections due to the primary sources of moments. An axial eccentricity is created, which ultimately increases the bending moment experienced by the element. Therefore, the resulting factored moment, M_t, is then composed of both the primary and second-order moments (Fig. 4.2).

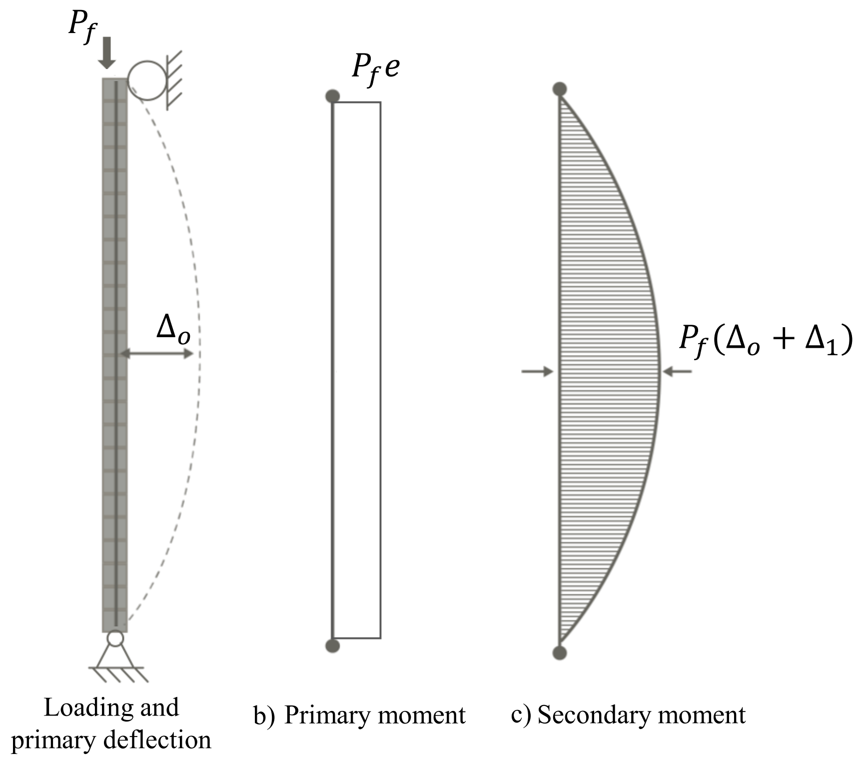

Figure 4.2 – Bending moment in masonry walls.

Both the CSA S304-14 and the TMS 402-16 provide two alternatives to compute the total factored moment, M_t, accounting for slenderness effects: (a) the P-Delta method ($P\delta$) and the Moment Magnifier Method (MM). These methods require using the effective stiffness, EI_{eff}, of the wall to calculate the moment amplification effects. Each standard specifies its approach to estimating the flexural rigidity of the elements.

The moment magnifier method was introduced in the 2013 edition of the TMS 402-16 . As it is relatively new, the preferred choice is to use the P-Delta method in the U.S. In

Canada, the most common method is the moment magnifier due to its simplicity. Both approaches are explained in detail in section 4.3.

This chapter compares the design methods proposed in CSA S304-14 and TMS 402-16 to calculate second-order effects in RMWs subjected to OOP bending moment. The provisions are presented, and key differences are identified. Parametric analyses quantify the influences of independent parameters (i.e. axial load, compressive strength of the masonry, reinforcement ratio, and strength reduction factor) in the rigidity of the walls calculated using the standards procedures.

4.2 Effective Stiffness Calculation

This section describes and compares the procedure proposed by each standard to calculate the stiffness of the masonry walls against OOP bending. The rigidity of the walls is calculated as the product of the modulus of elasticity (E_m) defined by the CSA S304-14 as $850f'_m$ and the TMS 402-16 as $900f'_m$ and the moment of inertia of the section. Nevertheless, the nonlinear stress-strain nature of the masonry, cracking propagation and yielding of the steel reinforcement make it impossible to determine a moment of inertia value. The gross moment of inertia (I_o) is only applicable if a linear-elastic behaviour is expected. Therefore, an effective stiffness (EI_{eff}) concept is introduced to adequately describe the moment-curvature relationship and compute deformations using linear elastic methods. Although both standards rely on calculating the rigidity to anticipate the second-order effects, each country offers a different alternative to calculate the effective stiffness.

4.2.1 TMS 402-16

TMS 402-16 offers two expressions to compute the effective stiffness, which depends on whether the acting moment (M_u) exceeds the cracking moment (M_{cr}). The equations are presented as follow:

$$EI_{eff} = E_m 0.75 I_n \ when\ M_u < M_{cr} \qquad \text{U.S. - 4.1}$$

$$EI_{eff} = E_m I_{cr} \; when \; M_u \geq M_{cr} \qquad \text{U.S. - 4.2}$$

Where E_m is the modulus of elasticity computed as $900f'_m$, I_n is moment of inertia of the uncracked section, and I_{cr} the cracked moment of inertia.

The cracking moment is calculated using the following expression (U.S. - 4.3), which depends on the modulus of rupture of the block (f_r), the section modulus block (S), and the applied axial force.

$$M_{cr} = \left(f_r + \frac{P}{A_g}\right)S \qquad \text{U.S. - 4.3}$$

The standard assumes that if the cracking moment is not exceeded, the wall is still on its linear-elastic range, and the gross inertia properties could be used to compute deflections and second-order effects. For cracked elements, cracked properties should be used instead.

The American committee proposed an equation to calculate the cracked moment of inertia, I_{cr} (U.S.-4.4). This equation accounts for the nonlinear nature of the masonry and the effect of the axial loading in the rigidity of the element.

$$I_{cr} = n\left(A_s + \frac{P_u T_{sp}}{f_y 2_d}\right)(d - c)^2 + \frac{bc^3}{3} \qquad \text{U.S. - 4.4}$$

Where A_s is the reinforcement area, P_u is the axial load, T_{sp} the thickness of the block, f_y is the steel yield strength, b is the compressive width and c is the neutral axis depth calculated as:

$$c = \frac{A_s fy + P_u}{0.64 f'_m \, b} \qquad \text{U.S. - 4.5}$$

According to clause 11.3.5.5.5 in TMS 402-16 , the procedure described above only applies if the neutral axis is located within the face shell. For other cases, the rigidity should be calculated by a "comprehensive" analysis.

4.2.2 CSA S304-14

The Canadian committee proposed an equation to calculate the effective stiffness based on a combination of the cracked and uncracked sections properties as displayed in C - 4.1.

$$(EI)_{eff} = E_m[0.25I_o - (0.25I_o - I_{cr})]\left(\frac{(e - e_k)}{(2e_k)}\right) \qquad \text{C - 4.1}$$

Where, E_m is the modulus of elasticity computed as $850f'_m$, I_o is the moment of inertia of the uncracked section, I_{cr} is the cracked moment of inertia, e is the virtual eccentricity computed as $\left(\frac{M_{fp}}{P_f}\right)$, e_k is the kern eccentricity determined as the section modulus, S_e, divided by the cross-sectional area , $A_{e.}$

The maximum and minimum limits of the effective stiffness are given in C-4.2. The value of $(EI)_{eff}$ must be between E_mI_{cr} and 2 $0.25E_mI_o$.

$$E_mI_{cr} < (EI)_{eff} \leq 0.25E_mI_o \qquad \text{C - 4.2}$$

CSA S304-14 permits the determination of the effective stiffness by alternate methods that shall account for the influence of the axial loading, variable moment of inertia and nonlinear stress-strain distribution.

The CSA S304-14 does not provide an equation to calculate the I_{cr}, but current design practices in Canada rely on calculating the I_{cr} using a linear stress distribution and a transformed section defined C - 4.3.

$$I_{cr} = \frac{b(kd)^3}{12} + \frac{b(kd)(kd)^2}{2} \qquad \text{C - 4.3}$$

Where for single reinforced masonry,

$$kd = d(\sqrt{2n(\rho) + n(\rho)} - n(\rho)\ , \qquad \rho = \frac{A_s}{bd} \qquad \text{C - 4.4}$$

Alternatively, the neutral axis (*kd*) can be calculated using transformed section analysis.

4.2.2.1 Rigidity Coefficient

The Canadian standard requires that the effective stiffness (EI_{eff}) must be affected by the rigidity coefficient (Eq. C - 4.5) from Clause 10.7.4.2.2. This clause mandates the application of a reduction factor $\emptyset_e = 0.75$, which intends to account for the effects of variability of materials on the deflections and buckling calculations, to the theoretical value of the flexural stiffness. Additionally, the rigidity coefficient includes the effect of the long-term deflections of the masonry by introducing a creep factor (through dividing the flexural stiffness by a quantity $1 + 0.5\beta_d$).

$$EI_{eff} = \frac{\phi_e EI_{eff}}{1 + 0.5\beta_d} \qquad \text{C - 4.5}$$

Where β_d is the ratio of factored dead load moment to total factored moment.

4.2.3 Comparison Discussion.

- The TMS 402-16 offers two alternatives that depend on whether the cracking moment calculated using U.S. - 4.3 is exceeded or not. In contrast, the CSA S304-14 provides an equation with an upper and lower bound limit.
- The TMS 402-16 provides an equation to compute the cracked moment of inertia(U.S.-4.4). This expression intends to consider the axial load and non-linear nature of the masonry. CSA S304-14 does not offer an alternative to calculate this parameter. However, as commented in section 4.2.2, cracked inertia is commonly

calculated assuming a linear stress distribution and a transform section approach without considering the axial loading effects.

- Although the TMS 402-16 does not provide an upper bound limit explicitly, uncracked cases should be computed using 75% of the gross moment of Inertia (U.S.-4.2). If this is compared against the upper bound limit provided by the CSA S304-14 ($0.25E_mI_o$), the American values will always be 200% higher than that of the Canadian.
- The CSA S304-14 introduces a rigidity coefficient which mandates to affect the effective stiffness by a reduction factor of $\emptyset_e = 0.75$ and the inclusion of creep effects. The TMS 402-16 does not offer any equivalent provisions, nor is it required to affect the stiffness by a reduction factor or creep effects.

4.3 Methods to calculate moment magnifications due to second-order effects.

4.3.1 Load Displacement Method ($\boldsymbol{P\delta}$)

The load-displacement method intends to allow the direct calculations of the secondary moment based on the deflected shape of the wall, as these moments are produced by the eccentricity created from the total deflection.

Figure 4.3 illustrates the case for a simply supported wall subjected to a uniform distributed pressure and concentric axial load. The primary moment due to the uniform pressure W can be approximated using a parabolic shape. The deflection at mid-height of the wall due to this moment is defined as Δ_o. This deflection can be calculated either from principles of mechanics using beam theory or any other method as it arises from the known pressure W. Due to the primary deflection, there is now an eccentricity created with the top applied load, which defines our first source of secondary moment, M_s, as $P_f\Delta_o$ (Fig. 4.3a). However, a secondary deflection, Δ_1, is introduced from the second-order moment originated by the initial deformation Δ_o. Consequently, the total deformation of the system accounting for primary and secondary sources of moments is

$\Delta_o + \Delta_1$ as indicated in Fig. 4.3b. Although both standards rely on the same assumption and derivation of equation 4-1, each country defines different alternatives to compute the deflections induced in the system.

The total factored moment can then be expressed as:

$$M_t = M_p + M_s$$
$$M_t = M_p + P_f(\Delta_o + \Delta_1) \tag{4.1}$$

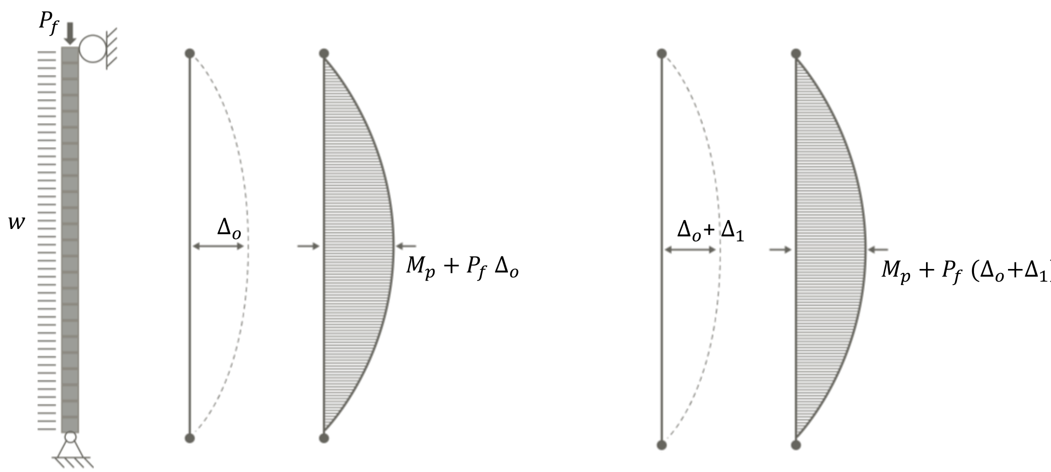

a) Primary moment: Uniform pressure + $P_f\Delta_o$ b) Total Moment = Primary + Secondary

Figure 4.3 – Load Displacement method for simply supported conditions.

4.3.1.1 TMS 402-16

The load-displacement method proposed in the TMS 402-16 , relies on the same principle explained in section 4.3.1. The standard mandates determining the total moment at mid-height of the wall using U.S. - 4.6.

$$Mu = \frac{W_u h^2}{8} + \frac{P_u e_u}{2} + (P_{uw} + P_u)\delta_u \qquad \text{U.S. - 4.6}$$

Where W_u is the factored uniform lateral load, P_u is the applied axial load, e_u is the axial loading eccentricity, P_w is the self-weight of the structure at mid-height, and δ_u is the mid-span deflection.

This method is only allowed by the American standard when:

$$\frac{P_u}{A_g} \leq 0.20\ f'_m \qquad \text{U.S. - 4.7}$$

The American committee offers two expressions to compute the ultimate deflection, δ_u, based on the cracking moment of the walls (U.S. - 4.8, and U.S. - 4.9). These equations are given for simply supported conditions. For other support conditions, moments and deflections shall be calculated using established principles of mechanics.

For $M_u < M_{cr}$

$$\delta_u = \frac{5M_u h^2}{48E_m I_n} \qquad \text{U.S. - 4.8}$$

For $M_u \geq\ M_{cr}$

$$\delta_u = \frac{5M_u h^2}{48E_m I_n} + \frac{5(M_u - M_{cr})h^2}{48E_m I_{cr}} \qquad \text{U.S. - 4.9}$$

Where M_u is the factored moment, M_{cr} is the cracking moment calculated using U.S. - 4.3, E_m is the modulus of elasticity of the masonry and I_{cr} is the cracked moment of inertia.

4.3.1.2 CSA S304-14

The CSA S304-14 mandates two equations to calculate the total moment of the structure using the load-displacement method depending on the slenderness ratio. CSA S304-14 permits to neglect the influences of the self-weight for structures with a height-to-thickness ratio lower than 30 (C - 4.6).

For $\frac{kh}{t} < 30$

$$M_t = M_p + P_f \Delta_f \qquad \text{C - 4.6}$$

Where M_p is the primary moment due to the lateral loading and eccentric axial force, P_f is the factored axial load, and Δ_f is the deflection at mid-span including second-order effects $(\Delta_o + \Delta_1)$.

CSA S304-14 does not mandate an expression to calculate the primary and secondary deflections. However, Canadian designers usually opt to compute these magnitudes based on an iterative approach. For the simple support condition in Fig 4.3, the primary deflection, Δ_0, can be calculated as:

$$\Delta_0 = \frac{5W_u h^4}{384EI_{eff}} \qquad \text{C - 4.7}$$

Where W_u is the factored uniform lateral load, h is the height of the structure, and EI_{eff} is the effective stiffness affected by the rigidity coefficient from section 4.2.2.1.

The secondary deflection, Δ_1, can be calculated as:

$$\Delta_1 = \frac{5P_f(\Delta_o + \Delta_1)h^2}{48EI_{eff}} \qquad \text{C - 4.8}$$

Where P_f is the applied axial load, h is the height of the structure.

As indicated in C - 4.8, this creates an iterative process since the secondary moment, $P_f(\Delta_o + \Delta_1)$, is used to determine secondary deflections.

For walls with slenderness ratios greater than 30, CSA S304-14 prescribes in clause 10.7.4.6.6 that the total factored moment, M_t, shall be determined at the mid-height of the wall and shall be calculated as:

For $\frac{kh}{t} \geq 30$

$$M_t = \frac{W_u h^2}{8} + \frac{P_{ft} e}{2} + (P_{fw} + P_{ft}) \Delta_f \quad \text{C - 4.9}$$

Where W_u is the factored uniform lateral load, P_{ft} is the factored axial load, $e_u$is the axial loading eccentricity, P_{fw} is the factored weight of wall tributary at mid-height of the structure, and Δ_f is the mid-span deflection, including the second-order effects.

Equation C - 4.9 is adapted from the Uniform Building Code (NBCC), which is based on the loading conditions of a wall under a uniform distributed pressure and eccentric gravity load.

4.3.1.2.1 Comparison discussion

- For $\frac{kh}{t} < 30$, the Canadian standard does not specify any means to calculate the primary moment or deflection. It also does not require to include the self-weight of the structure in the calculations (C - 4.6). Hence, the load-displacement method could be implemented for any loading condition as long as the primary moment,M_p, is correctly calculated. For the same slenderness ratio, TMS 402-16 mandates the inclusion of the self-weight of the walls in the calculations (U.S. - 4.6). For $\frac{kh}{t} \geq 30$, both the CSA S304-14 and TMS 402-16 expressions are derived for simply supported conditions, in which maximum bending moment and deflections occur nearly at mid-height. For different boundary conditions, deflection and primary moment need to be calculated using principles of mechanics or other methods.
- TMS 402-16 recommends expressions to calculate deflections based on beam theory and the cracking moment for simply supported conditions (U.S. - 4.3 and U.S. - 4.4). No equation is mandated by the CSA S304-14, but it is required that the method selected consider additional deflections due to second-order effects. Common design practices in Canada relies on an iterative method to obtain Δ_f (C - 4.7).

- TMS 402-16 restricts the use of the load-displacement method for certain axial stress levels ($\frac{P_u}{A_g} \leq 0.20\ f'_m$). Canada permits to compute second-order effects with this method regardless of the conditions.

4.3.2 Moment Magnifier Method

The moment magnifier approach is a method developed originally for slender reinforced concrete structures and later adapted for masonry elements. This method offers a simplified approach to compute the total moment of the structure, M_t, by amplifying the primary moment using an amplification factor instead of calculating the second-order moments as the product of the gravity load and the maximum displacement of the structures. The MM equation is given by:

$$M_t = M_p * Amplification\ factor \qquad 4.2$$

A simply supported wall loaded with an eccentric axial load, P_f, is used to illustrate the development of the MM. This case is shown in Fig. 4.4. The total deflected shape and the secondary moment diagram are assumed to be defined using a half-sine function, where Δ_0 is the deflection due to the primary sources of moment (i.e. lateral pressure) and Δ_1 the deflection from secondary moments. Therefore, the total deflection at mid height, Δ_t, is then $\Delta_t = \Delta_0 + \Delta_1$ (Fig. 4.4a) and the secondary moment, M_s, $M_s = P_f(\Delta_0 + \Delta_1)$ (Fig 4.4.b).

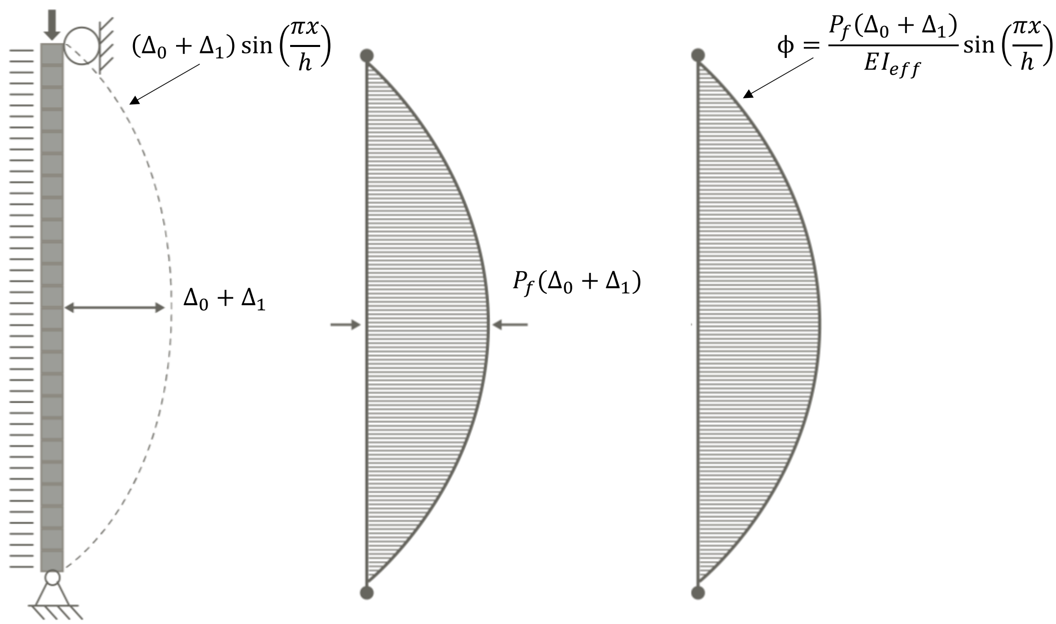

Figure 4.4 – Moment Magnifier derivation.

Knowing that the curvature of the section is defined by $\emptyset = M_t/EI$, and using the same sinusoidal shape assumption as before, the curvature profile can be then defined as $\frac{P_f(\Delta_o+\Delta_1)}{EI_{eff}} sin\, sin\, \left(\frac{\pi x}{h}\right)$. The secondary deflection at mid-height, Δ_1, can be then calculated using the moment-area method, where the area of the half-curvature (from the top to mid-span) in Fig. 4.4c, is calculated as:

$$A = \int_0^{\frac{h}{2}} \frac{P_f(\Delta_o + \Delta_1)}{(EI)_{eff}} sin\, sin\, \left(\frac{\pi x}{h}\right) dx = \frac{P_f(\Delta_o + \Delta_1)h}{\pi(EI)_{eff}} \qquad 4.3$$

Calculating the centroid of this half-area, *A*,

$$\underline{x} = \frac{Q}{A} = \frac{\int_0^{\frac{h}{2}} \frac{P_f(\Delta_o + \Delta_1)}{(EI)_{eff}} sin\, sin\, \left(\frac{\pi x}{h}\right)\, x\, dx}{\int_0^{\frac{h}{2}} \frac{P_f(\Delta_o + \Delta_1)}{(EI)_{eff}} sin\, sin\, \left(\frac{\pi x}{h}\right)\, dx} = \frac{h}{\pi} \qquad 4.4$$

The deflection at mid-height can be computed as,

$$\Delta_1 = A\left(\frac{h}{\pi}\right)$$

$$\Delta_1 = \frac{P_f(\Delta_o + \Delta_1)h}{\pi(EI)_{eff}}\left(\frac{h}{\pi}\right) = \frac{P_f h^2}{\pi^2 EI}(\Delta_o + \Delta_1) \qquad 4.5$$

Recognizing that the Euler buckling load, P_{cr}, is defined as

$$P_{cr} = \frac{\pi^2 EI}{h_w^2} \qquad 4.6$$

Then Eq 4.6 becomes

$$\Delta_1 = (\Delta_o + \Delta_1)\left(\frac{P_f}{P_{cr}}\right) \qquad 4.7$$

Re-arranging,

$$\Delta_1 = \Delta_o \frac{P_f/P_{cr}}{1 - P_f/P_{cr}}$$

Since the total deflection is the sum of Δ_o and Δ_1, it can be expressed in terms of Δ_o as,

$$\Delta_t = \Delta_0 + \Delta_1$$

$$\Delta_t = \Delta_0 + \Delta_o \frac{P_f/P_{cr}}{1 - P_f/P_{cr}}$$

$$\Delta_t = \frac{\Delta_0\left(1-\left(\frac{P_f}{P_{cr}}\right)+\left(\frac{P_f}{P_{cr}}\right)\right)}{1-P_f/P_{cr}}$$

$$\Delta_t = \frac{\Delta_0}{1-\frac{P_f}{P_{cr}}} \qquad 4.8$$

Knowing that the total moment, M_t, can be computed as the summation of the primary source of moment $M_P = P_f e$ and the product of the axial loading, P_f, and the total deflection, Δ_t,.

$$M_t = P_f e + P_f \Delta_t$$

$$= P_f e + \frac{P_f \Delta_o}{1-\frac{P_f}{P_{cr}}} \qquad 4.9$$

Where for a rectangular moment diagram Δ_o can be calculated as,

$$\Delta_o = \frac{P_f e h_w^2}{8EI} \qquad 4.10$$

Substituting this back into the total factored moment yields:

$$M_t = P_f e + P_f\left[\frac{P_f e h^2}{8EI_{eff}\left(1-\frac{P_f}{P_{cr}}\right)}\right]$$

$$M_t = P_f e\left[\left(1+\frac{0.23\left(\frac{P_f}{P_{cr}}\right)}{1-\left(\frac{P_f}{P_{cr}}\right)}\right)\right] \qquad 4.11$$

The term $0.23(P_f/P_{cr})$ is a function of the shape of the primary moment diagram ($P_f e$). For a parabolic moment diagram, such as that caused by uniform lateral pressure (i.e, wind load) this term becomes nearly zero. Therefore, the total moment , M_t, is computed as follows:

$$M_t = M_p\left(\frac{1}{1-\frac{P_f}{P_{cr}}}\right) \qquad 4.12$$

4.3.2.1 TMS 402-16

The magnified moment according to the TMS 402-16 is calculated as:

$$M_t = \Psi M_u \qquad \text{U.S.-4.7}$$

Where M_u is the factored moment from the first-order analysis. The moment magnification factor Ψ is calculated using:

$$\Psi = \frac{1}{1-\frac{P_u}{P_e}} \qquad \text{U.S.-4.8}$$

Where, P_u is the applied axial load and P_e the critical buckling load calculated as

$$P_e = \frac{\pi^2 E_m I_{eff}}{h^2} \qquad \text{U.S.-4.9}$$

Where E_m is the modulus of elasticity of the masonry, I_{eff} is the stiffness of the wall, and h is the height of the structure.

4.3.2.2 CSA S304-14

The expression 4.12 is derived for symmetric single curvature situations. For cases of unequal end eccentricities, $e_1$and e_2, the CSA S304-14 propose an equivalent moment factor, C_m. Thus, the CSA S304-14 expression is given by C - 4.10.

$$M_t = M_p \left(\frac{C_m}{1 - \frac{P_f}{P_{cr}}} \right) \quad \text{C - 4.10}$$

Where M_p is the factored moment from the first-order analysis. P_f is the applied axial load and P_{cr} is the euler buckling load, and the C_m is calculated as:

$$C_m = 0.6 + \frac{0.4M_1}{M_2} \geq 0.4 \quad \text{C - 4.11}$$

Where M_1 is the smaller factored end moment taken as a negative for double curvature and M_2 is the larger end moment always taken positive. The ratio $\frac{M_1}{M_2}$ may be taken as 1.0 if both end eccentricities are less than 0.1t or when lateral loads contribute more than 50% of the primary moments.

The Euler buckling load,P_{cr}, is modified to include the rigidity coefficient as indicated in C - 4.12

$$P_{cr} = \frac{\pi^2 EI_{eff}}{kh^2} \quad \text{C - 4.12}$$

4.3.2.3 Comparison discussion

The moment magnifier equations recommended by both committees are essentially the same. Only minor differences are identified, such as the C_m factor and the effective length factor (k). C_m Relates the moment diagram to an equivalent uniform moment distribution. The American committee does not require such factor as in most cases, the applied lateral load consists of uniform pressure, leading to a C_m value of 1. For cases with largely concentrated end moments this factor could introduce a significant deviation between the standards.

The effective length factor, k, proposed by the CSA S304-14 could introduce some deviation if different boundary conditions are assumed. The CSA S304-14 allows designers to take advantage of the boundary conditions, which is typically done by Canadian designers for non-slender structures. However, for very slender structures, a common practice is to design the element assuming a pinned-pinned condition ($k = 1$), ignoring any attribute from the base rigidity. Only for this case, the terms kh in CSA S304-14 and h in TMS 402-16 are equivalent.

4.3.3 Parametric Studies.

This section investigates the influences of some independent parameters in the effective stiffness formulation provided by each standard through parametric analyses. This section only evaluates and compares the procedure described in the CSA S304-14 and TMS 402-16 to compute the effective stiffness. Thus, the effectiveness of their formulations is not assessed. The parameters in this study are classified as fixed, dependent and independent, which are described as follows.

4.3.3.1 Fixed parameters

The fixed parameters were not changed in this study and were constant for all the OOP walls. The thickness, mild steel properties, length and rebar spacing were the fixed parameters of this study. The thickness of the walls was set to 190 mm, which represents a 20 cm nominal block commonly used in Canada. Canadian mild steel properties were used with a yield strength of 400 MPa and a Young's modulus of 200GPa. The length of the wall was set to 1000 mm, as the analyses were done for equivalent 1m sections. Two rebar spacing were selected. For fully grouted walls the spacing was set to 200 mm, which represents a rebar per cell. For partially grouted trials the rebar spacing was set to 800 mm.

4.3.3.2 Dependent parameters

The dependent parameter of the study consisted of the OOP stiffness of reinforced masonry walls using the effective stiffness formulations as per the CSA S304-14 and

TMS 402-16. This parameter is studied under different values of the independent parameters

4.3.3.3 Independent parameters

The independent parameters were varied to investigate their isolated effect on the dependent parameter. This study had four independent variables consisting of the compressive axial loading, reinforcement ratio, compressive strength (f'_m), the reduction factor ($\emptyset_e$), and the creep factor (β_d).

The axial loading was selected as an independent variable to evaluate its effect on enhancing the flexural stiffness and quantify the differences between the standards as this parameter is increased. Five reinforcement ratios were investigated in this study, consisting of 0.5, 1, 1.5, and 2.5. The increment was set to 0.5 to evaluate the influence of this parameter in the effective stiffness calculation and establish a comparison between the standards based on a gradual increment of the reinforcement area. The effect of the reduction factor $\emptyset_e$ described in section 4.2.2.1 and mandated by the CSA S304-14 was quantified and compared against the TMS 402-16 alternatives to compute the stiffness of the wall, and the CSA S304-14 curve neglecting this factor. Four compressive strength levels were selected for this study, 7.5 MPa, 10 MPa, 15 MPa, 20 MPa, and 25 MPa to study the sensitivity of both expressions against the increment of this parameter and quantify the differences under multiple levels of compressive strengths.

4.3.3.4 Effects of the Independent Parameters on the Effective Stiffness.

4.3.3.4.1 Effect of Axial Loading ($\boldsymbol{P_f}$)

This section investigates the effects of axial loading in the effective stiffness formulation. It should be expected that higher compressive forces reduce the curvature of the section subjected to bending stress, enhancing the stiffness of the element.

To study this effect, Fig. 4.5 and 4.6 shows the influence of the axial loading (P) in the flexural stiffness ($E_m I_{eff}$) calculated as per the North American standards for a fully (Fig. 4.5) and a partially grouted (Fig. 4.6) trial. The material and geometrical properties are summarized in Table 4.1. The axial load (P_u), was normalized by a 10% of the nominal axial capacity of a fully grouted trial with a 20 cm blocks with a nominal strength of 15 MPa ($0.1f'_m A_e$). The effective stiffness ($E_m I_{eff}$) was normalized by the gross moment of inertia of the fully grouted section described above times the modulus of elasticity ($E_m I_o$).

Table 4.1 – Summary of properties. Effect of Axial Load.

Parameters	**CSA S304-14**	**TMS 402-16**
Compressive Strength of The Masonry (f'_m)	$f'_m = 15\ MPa$	$f'_m = 15\ MPa$
Modulus of Elasticity	$850f'_m$	$900f'_m$
Block Thickness (mm)	190	190
Rebar Size (Canadian Nomination)	10M	10M
Rebar Separation (mm)	Fig. 4.5 200 Fig. 4.6 800	Fig. 4.5 200 Fig. 4.6 800
Reduction Factors ($\emptyset_e$)	$\emptyset_e = 1$	$-$
Creep Factor (β_d)	$\beta_d = 0$**	$-$

** A value of 0 is used to neglect the influences of this factor.

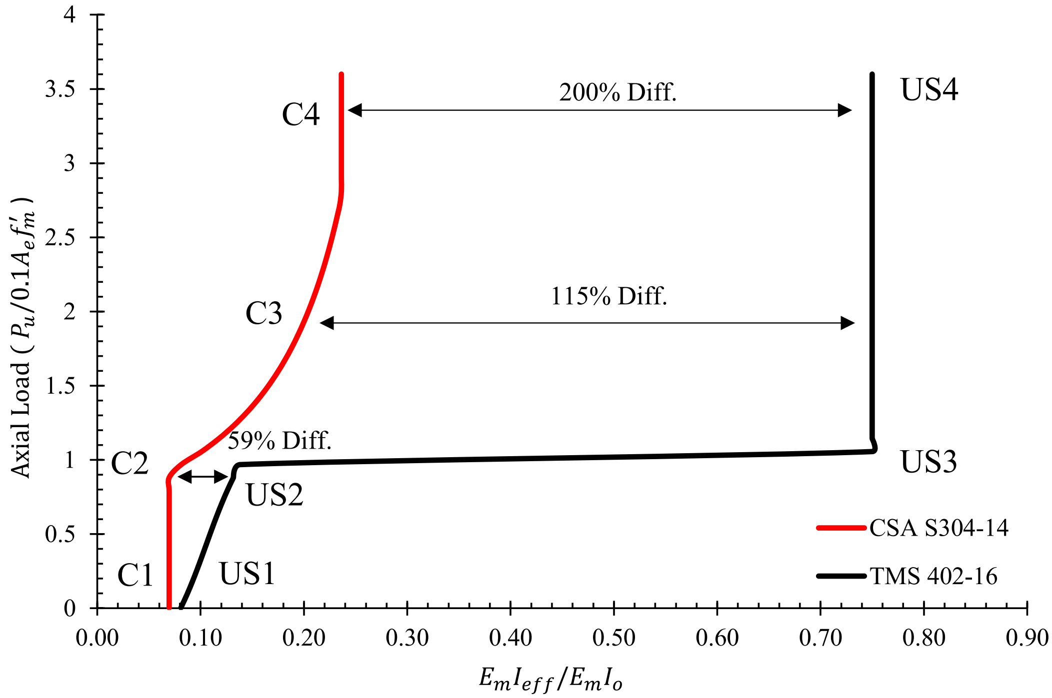

Figure 4.5 - Effect of the Axial Loading in the Effective Stiffness Fully Grouted.

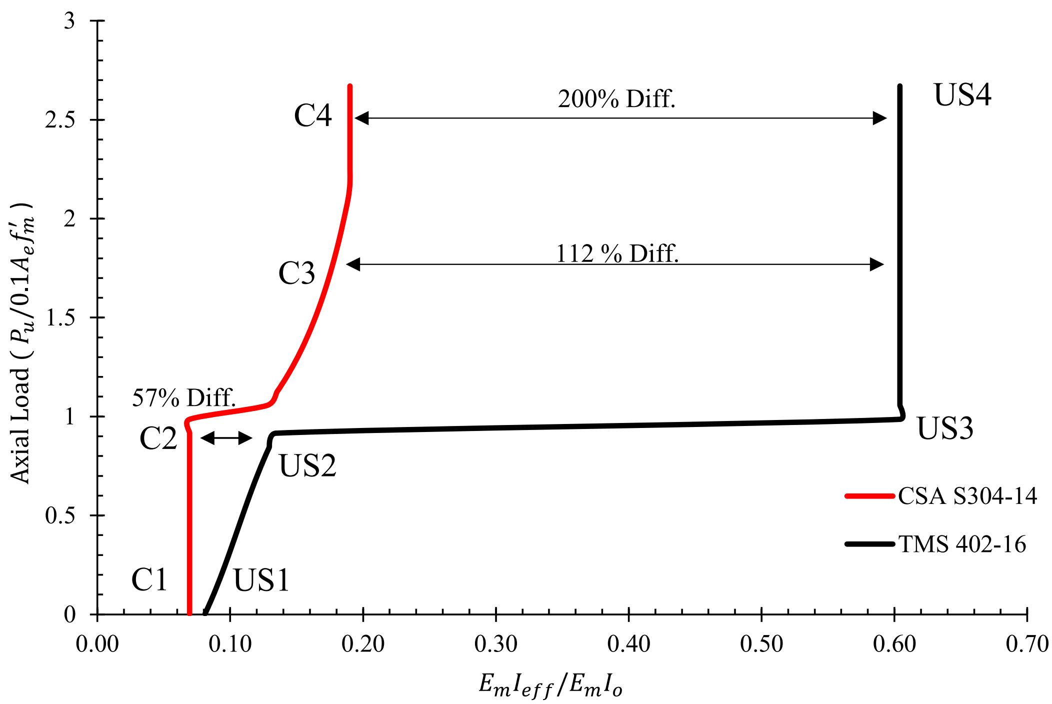

Figure 4.6 – Effect of the Axial Loading on the Effective Stiffness. Partially Grouted.

For partially and fully grouted walls, the behaviour is consistent. The description and comparison below are valid for both cases. The CSA S304-14 and TMS 402-16 procedures are discussed first, and a comparison is established at the end of this section.

As seen in Fig 4.5 and 4.6, the influences of the axial loading on the Canadian formulation can be summarized in 3 phases. From point C1 to C2 the lower bound limit of C - 4.2 ($E_m I_{cr}$) is used to compute the stiffness of the wall. Low axial loading levels produces high virtual eccentricities ($e = M_f / P_u$). When the virtual eccentricity is 3 times higher than the kern eccentricity (e_k), the masonry section is considered cracked. In these cases the stiffness is calculated using $E_m I_{cr}$, and as I_{cr} $(\mathrm{C}-\ 4.3)$ depends only on the material properties and the geometry, it will remain constant throughout any axial load level that leads to $e > 3_{ek}$. For any case where $e < 3_{ek}$ (From point C2 to C4 on Fig. 4.5 and 4.6), the effective stiffness is computed using C - 4.1, which considers the influence of the axial loading based on the virtual eccentricity, e. At this range, higher axial loads will lead to a gradual increment of the $(EI)_{eff}$. Finally, at lower levels of eccentricity (i.e. High axial load), the structure is considered uncracked, and the upper limit is used instead ($0.25 E_m I_o$). If the axial load is applied concentrically, an accidental eccentricity equivalent to 10% of the thickness of the block should be assumed.

In contrast to the CSA S304-14, the TMS 402-16 offers two alternatives to compute the rigidity of the element based on a simple condition. In cases in which the applied moment exceeds the cracking moment (M_{cr}) computed using U.S. - 4.3, the cracked moment of inertia should be used to compute the stiffness ($E_m I_{cr}$ $\mathrm{U.S.}-4.2$). For the other case ($M_u \geq M_{cr}$) the TMS 402-16 allows using 75% of the gross inertia ($E_m 0.75 I_n$, $\mathrm{U.S.}-4.1$) to compute the rigidity of masonry walls. It is important to note that the equation provided by the TMS 402-16 to calculate the cracking moment explicitly considers the axial loading. This relationship is illustrated in Fig. 4.7, where the cracking moment increases almost linearly relative to the applied axial load. Thus, the higher the axial loading, the bigger is the moment required to exceed the cracking moment.

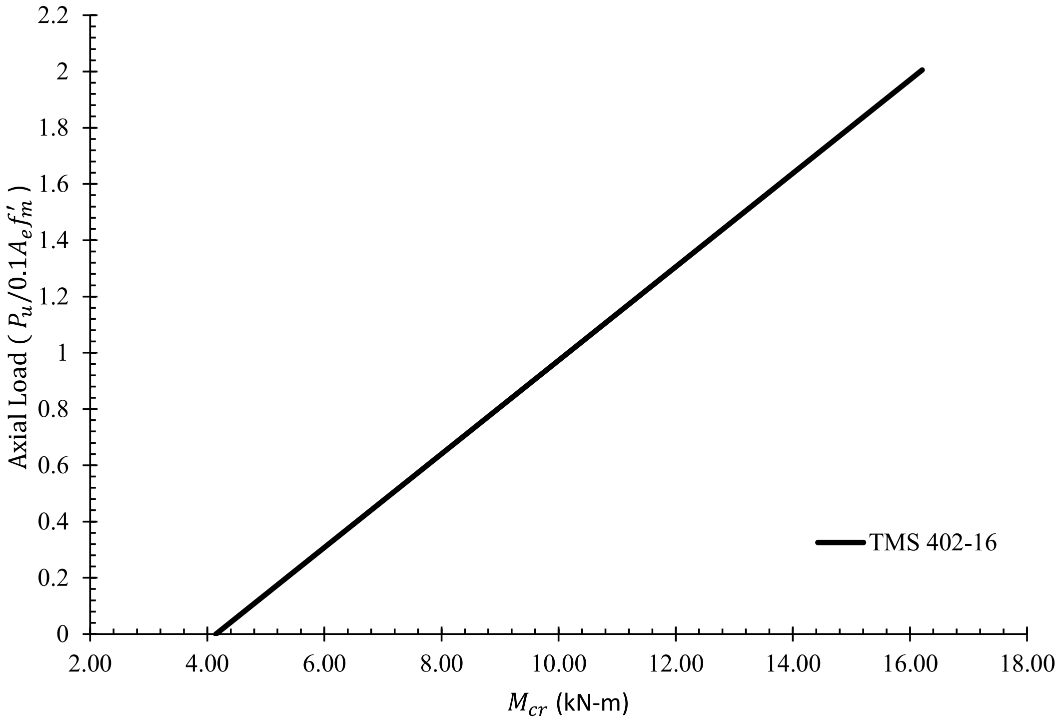

Figure 4.7 – Axial loading versus cracked moment of inertia. TMS 402-16 .

By evaluating Fig. 4.5 and 4.6, the relationship between the axial loading and the stiffness of the wall calculated using TMS 402-16 procedure can be seen. From point US1 to US2, the stiffness of the wall is computed using the cracked moment of inertia ($E_m I_{cr}$). As noted before, the proposed equation in the TMS 402-16 explicitly considers the interaction of the axial loading. Higher compressive forces in the element enhance the OOP rigidity of the wall. In uncracked cases where the acting moment does not exceed the cracking moment (From point US3 to US4), the stiffness of the wall is not affected by any variation of the axial loading, as in this range where it is calculated using the gross moment of inertia.

To quantify and compare the influence of the axial loading in both standards, three points in Fig. 4.5 and 4.6 were selected. The first point is C2. Up to this position, the rigidity of the wall is computed using the cracked moment of inertia in both standards. While the CSA S304-14 curve is constant through all this range (From C1 to C2), the TMS 402-16 counterpart is being enhanced by the compressive forces, which results in differences of up to 59%. After C2, although the effective stiffness from the CSA S304-14 is calculated using C - 4.1, which considers the effect of the axial loading, the influence of this parameter seems to be more notorious in the American expression. Up to US2 the wall is considered cracked according to the TMS 402-16 ($EI_{eff} = E_m I_{cr}$), at this point values calculated using the TMS 402-16 standards are 114% higher compared to the CSA S304-14 . Finally, at axial loading ranges where the wall is considered uncracked by both standards (After C3 in the CSA S304-14 and after US3 in the TMS 402-16 curve), the TMS 402-16 stiffness value will always be 200% higher than the CSA S304-14 . Both committees rely on the gross moment of inertia at this range, nonetheless, while the TMS 402-16 allows using 75% ($EI_{eff} = E_m 0.75 I_O$) of the inertia, the CSA S304-14 is limited to a maximum of 25% ($EI_{eff} = E_m 0.25 I_O$)

4.3.3.4.2 Reduction Factor $\emptyset_e$

One of the major differences between the standards is the adoption of a reduction factor $\emptyset_e$ in Canada. The CSA S304-14 mandates to apply a reduction factor equal to $\emptyset_e = 0.75$ to account for the variability of materials on the deflections and buckling calculations. This factor translates directly to a reduction of stiffness by 25%. The American committee does not mandate any equivalent factor. Although concrete design provisions in the United States recommend a similar decrease to account for uncertainties in the stiffness of the wall, TMS 402-16 does not include it for masonry elements. According to the commentary version of the TMS 402-16, the committee considers unnecessary the additional conservatism that this factor would bring to the stiffness computation. It could be argued that the TMS 402-16 implicitly introduces a reduction factor for uncracked masonry sections as the gross moment of inertia is reduced by 25% (U.S. - 4.1). However, it is essential to note that the $\emptyset_e$ factor is mandated by the CSA S304-14 in both uncracked and cracked cases.

Figure 4.8 shows the influences of this parameter on the stiffness of the wall. The parametric analysis in section 4.3.3.4.1 was repeated but it was added a CSA S304-14 curve affected by the reduction factor, which is represented using a dashed red line.

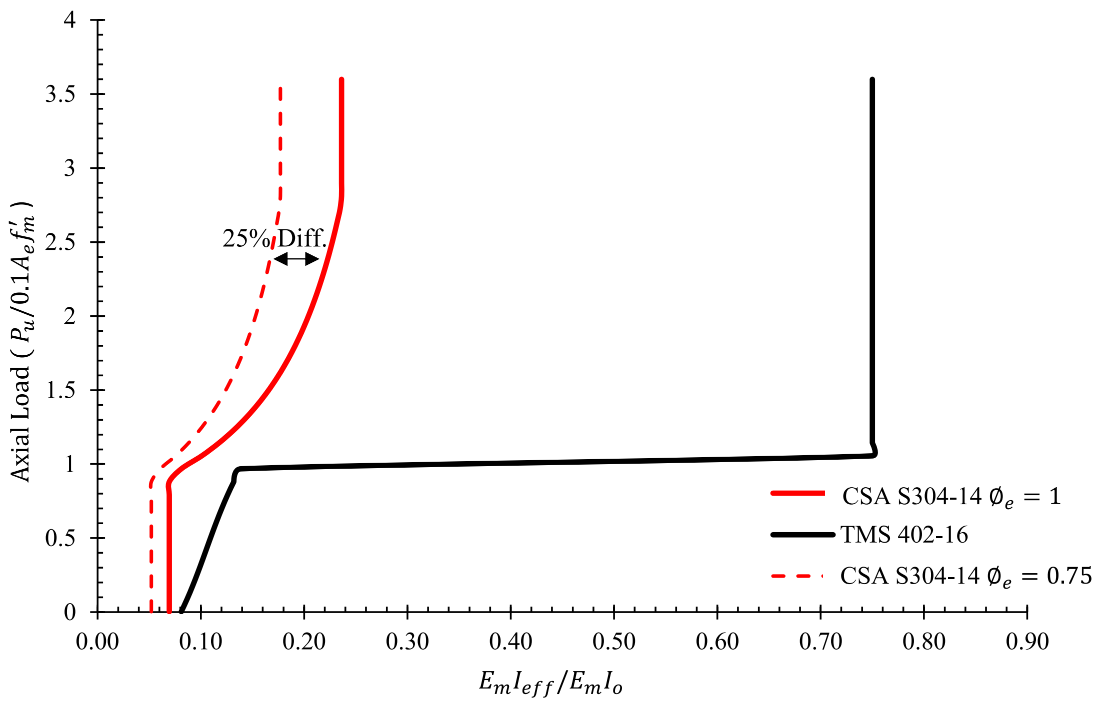

Figure 4.8 – Effect of the reduction factor $\emptyset_e$

As seen in Fig 4.8, the stiffness of the wall in both the cracked and uncracked cases is reduced by 25% if the CSA S304-14 calculations are affected by the $\emptyset_e$ factor. Thus, the percentage of difference between both standards increases by the same amount as the reduction. The necessity of this additional conservatism is not evaluated by the parametric analysis presented in this section. However, an apparent decrease can be seen in the stiffness of the wall that ultimately increases the amplification of the primary moment. These results are not yet compared with experimental or analytical data. Parametric analysis in chapter 5 quantifies the consequences of applying the reduction factor $\emptyset_e$ compared with finite element models.

4.3.3.4.3 Effect of creep factor ($\boldsymbol{\beta_d}$)

In section 4.2.2.1 the rigidity coefficient mandated by the CSA S304-14 was introduced. This coefficient considers the effect of additional deformations produced by long-term exposure to persistent mechanical stresses (creep effects) using the creep factor (β_d). The TMS 402-16 does not mandate a comparable provision, and the creep effects are not considered in the stiffness calculation.

The CSA S304-14 calculate this factor as the ratio between the factored dead load moment, which is the moment produced by the eccentric axial load from the dead load combination ($P_f e$), and the total factored moment ($\beta_d = \frac{M_{dead}}{M_{total}}$) Thus, a creep factor of 0 would indicate that the primary moment is only induced by the lateral loading, while a factor of 1 is only possible if the only source of the primary moment is due to the axial eccentricity loading.

Table 4.2 shows the variation of the flexural stiffness due to the addition of the creep effects in the CSA S304-14 equation. As a reference for this study, an accidental eccentricity of 10% of the block thickness is selected to calculate the moment due to dead load ($M_d = P_{fd} e$). The axial loading was increased by a ratio of 10 kN. The same wall properties as section 4.3.3.4.1 were adopted for the analysis.

Table 4.2 - Influence of the creep factor β_d from the CSA S304-14

EI_{eff}/EI_o $Control$ No Creep Included *	Axial Dead Load (kN/m)	Creep Factor (β_d)	EI_{eff}/EI_o Creep Included *	Decrement (%)
0.15	5.00	0.01	0.15	0.63
0.15	10.00	0.01	0.14	1.27
0.15	15.00	0.02	0.14	1.90
0.15	20.00	0.03	0.14	2.53
0.15	25.00	0.03	0.14	3.17
0.15	30.00	0.04	0.14	3.80
0.15	35.00	0.04	0.15	4.43
0.17	40.00	0.05	0.16	5.07
0.18	45.00	0.06	0.17	5.70
0.19	50.00	0.06	0.18	6.33
0.20	55.00	0.07	0.19	6.97
0.21	60.00	0.08	0.20	7.60
0.22	65.00	0.08	0.20	8.23
0.22	70.00	0.09	0.20	8.87
0.23	75.00	0.10	0.21	9.50
0.23	80.00	0.10	0.21	10.13
0.23	85.00	0.11	0.21	10.77
0.24	90.00	0.11	0.21	11.40
0.24	95.00	0.12	0.21	12.03
0.24	100.00	0.13	0.21	12.67
0.24	105.00	0.13	0.21	13.30

*Values normalized as section 4.3.3.4.1

As seen in Table 4.2, the additional deformations originated by the creep effects are accounted for in the CSA S304-14 by imposing a reduction of the effective stiffness as the creep factor increases. For the reference selected in this study, low axial loads (i.e. 5-20 kN/m) represent a reduction of the EI_{eff} by approximately 3%, while higher compressive forces could lead to a decrease of up to 13%. It is important to notice that the eccentricity selected for this analysis represents the smallest axial eccentricity for a 20cm nominal block (accidental eccentricity). Greater loading eccentricities could lead to higher moments produced by the dead load and consequently higher creep factors. For structures loaded with only eccentric axial load, the reduction is quite significant. This case results on a β_d a factor of 1, which is translated to a reduction of the EI_{eff} of 50%.

4.3.3.4.4 Effect of the Compressive strength f'_m and modulus of elasticity (E_m)

Although there are differences in the commonly used prism compressive stress (f'_m) values between countries (section 3.2.1), all the parametric studies in this section were done using identical values. This analysis studies the influence of the variation of the compressive strength in the formulations proposed by the CSA S304-14 and TMS 402-16 to compute the OOP stiffness of masonry walls.

This document presents only one of the multiple cases, as the behaviour is consistent in all the circumstances evaluated. Fig 4.9 shows the variation of the compressive strength vs the normalized effective stiffness ($E_m I_{eff}/E_m I_o$). The stiffness is normalized as in section 4.3.3.4.1. The material properties are summarized in Table 4.3. No axial loading is considered for comparison purposes. Therefore, any differences between the standards can only be attributed to the independent variable studied in this section.

Table 4.3 - Summary of properties. Effect of Compressive Strength

Parameters	CSA S304-14	TMS 402-16
Modulus of Elasticity	$850f'_m$	$900f'_m$
Block Thickness (mm)	190	190
Rebar Size (Canadian Nomination)	10M	10M
Rebar Separation (mm)	200	200
Reduction Factors ($\emptyset_e$)	$\emptyset_e = 1$	$-$
Creep Factor (β_d)	$\beta_d = 0$**	$-$

** A value of 0 is used to neglect the influences of this factor.

As shown in Fig 4.9, both formulations are influenced by the compressive strength of the masonry assembly. Higher compressive strength leads to stiffer walls. However, the TMS 402-16 expression seems to be more sensitive to the variation of this parameter. As despite in the figure, for a compressive strength value of 10 MPa the EI_{eff} calculated using the American procedure is approximately 8% greater than that of the Canadian, while for a compressive strength of 20 MPa, the TMS 402-16 is 20% higher than of the CSA S304-14 .

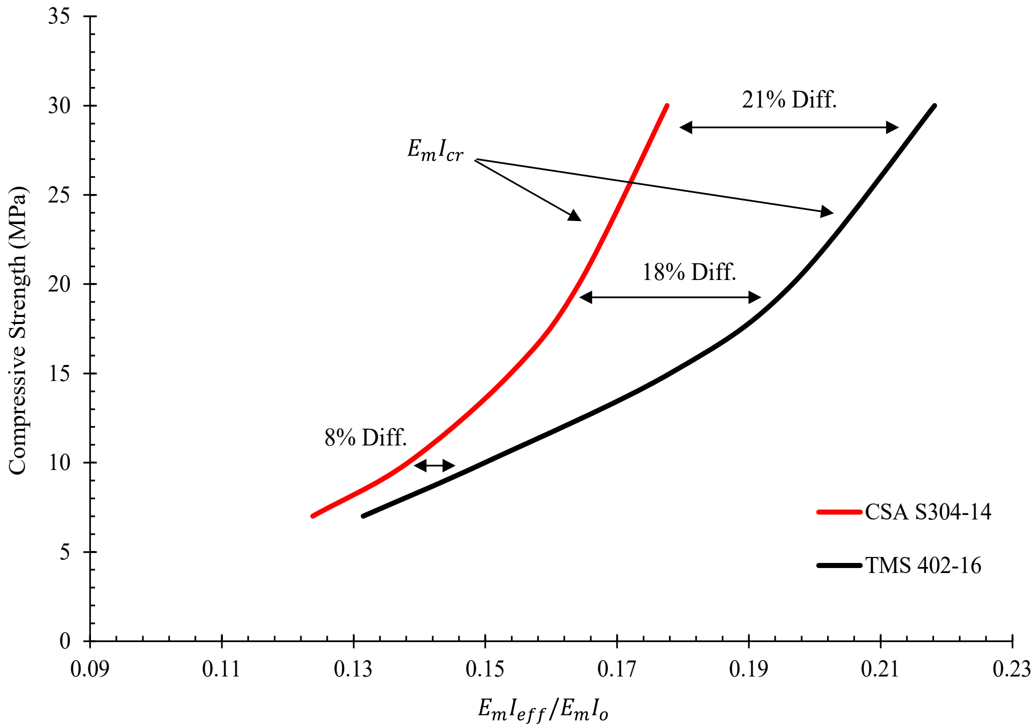

Figure 4.9 – Effect of the compressive strength.

It could be expected that the increment of the effective stiffness could be attributed entirely to the E_m as it is a function of the f'_m (i.e. $E_m = 850f'_m$ in the CSA S304-14). Higher compressive strength will lead to a larger E_m, but it will also lead to a smaller cracked moment of inertia. Although each standard has a different formulation for I_{cr}, this parameter is proportional to the modular ratio ($n = \frac{E_s}{E_m}$). Increasing E_m decreases the modular ratio and the cracked moment of inertia (I_{cr}). This is shown in Fig 4.10, where the variation of the compressive strength versus the normalized cracked moment of inertia is depicted.

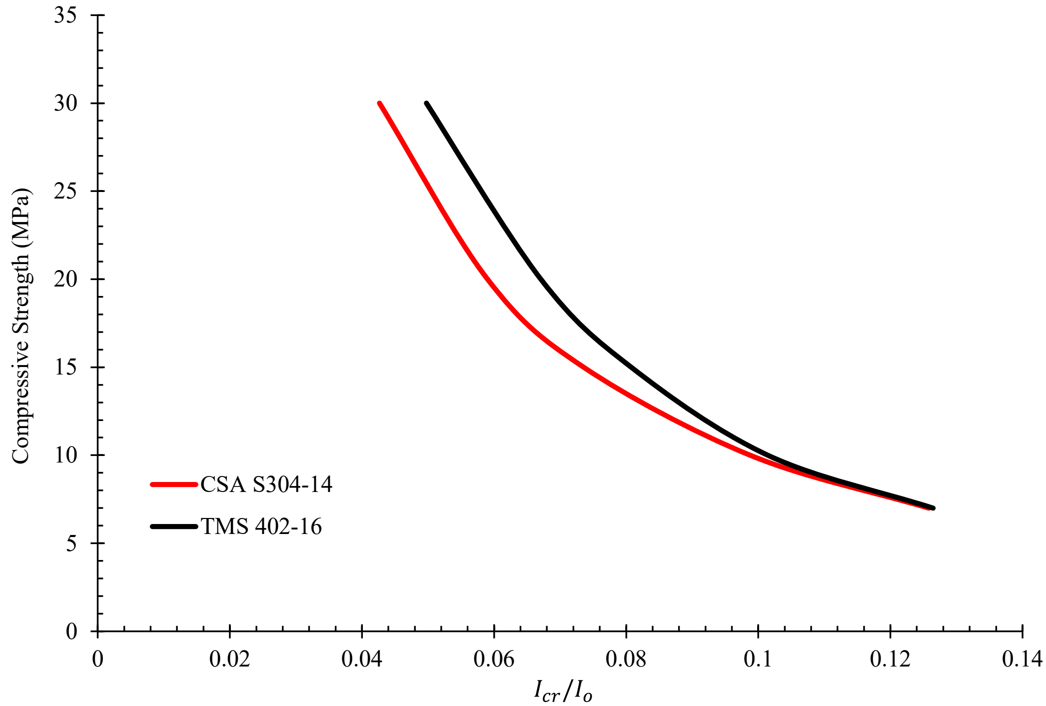

Figure 4.10 – Variation of the cracked moment of inertia.

However, the influence of the modulus of elasticity is negligible when the section is considered cracked. To demonstrate this assumption, the TMS 402-16 equations to compute the flexural stiffness is used. Neglecting the term $\frac{bc^3}{3}$ (Which is typically smaller) and the axial loading in the I_{cr} expression from the TMS 402-16 , leads to a modified version of equation U.S. - 4.4, as shown below:

$$I_{cr} = n(A_s)(d-c)^2 \qquad \text{U.S. - 4.12}$$

Thus, when calculating the $E_m I_{cr}$ the equation will take the following form:

$$E_m I_{cr} = E_s(A_s)(d-c)^2 \qquad \text{U.S. - 4.13}$$

The modified expression no longer considers the E_m and the only variable affected by a variation of the f'_m is the compressive depth (c). Increasing the compressive strength of the masonry decreases the compressive depth length, thus enhancing effective stiffness. Fig. 4.11 illustrates the evolution of the compressive depth versus the f'_m as per the CSA S304-14 and TMS 402-16 . This figure illustrates that higher compressive strength leads to a smaller neutral axis depth, as a smaller masonry area is needed for the internal equilibrium of forces. For typical f'_m values (5-25 MPa) a variation of 10 MPa in the compressive strength could lead to about 10-15% of increment in the stiffness of the wall.

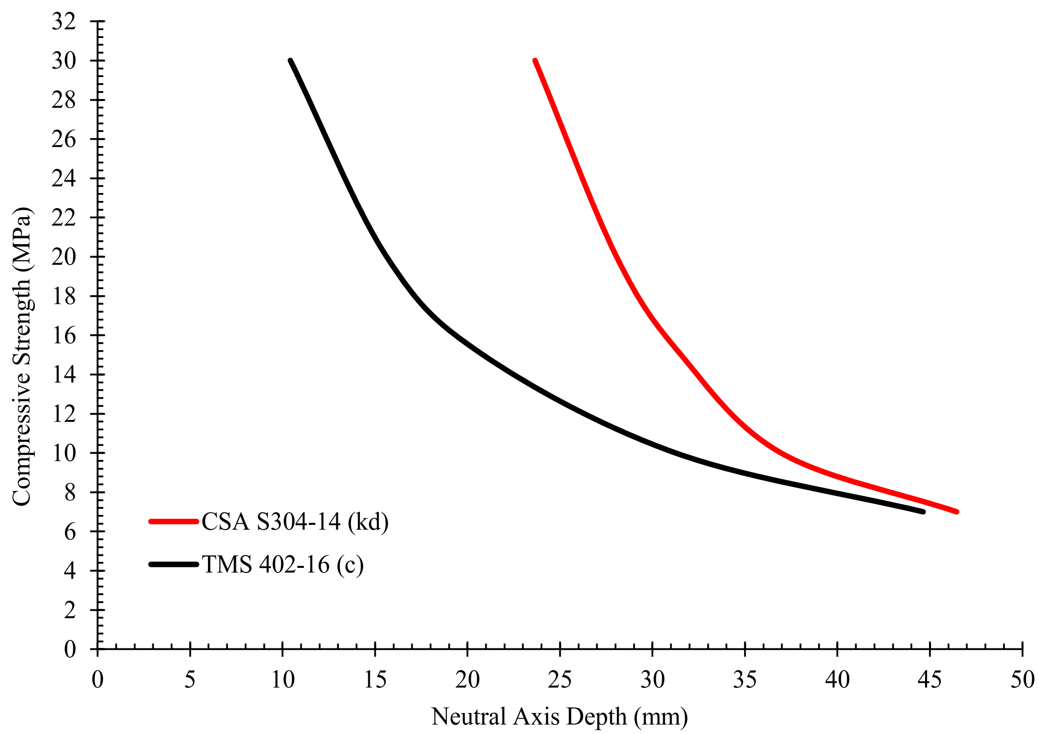

Figure 4.11 – Neutral Axis Depth Evolution.

4.3.3.4.5 Effect of the Reinforcement Ratio

In this section, the influences of the variation of the reinforcement ratio in the OOP stiffness of reinforced masonry walls is evaluated. It is expected that increasing the area of steel enhances the stiffness of the element. Mechanically, the more steel the section has, the bigger is the transformed area section. Thus, the section is able to resist higher tensile forces, which ultimately increases the cracked moment of inertia of the cross-section.

To evaluate this assumption, Fig. 4.12 shows the variation of the normalized effective stiffness calculated as per the TMS 402-16 and the CSA S304-14 versus the reinforcement ratio. The same normalization used in section 4.3.3.4.1 was used. The materials and geometry properties are summarized in Table 4.4. No axial loading is assumed for comparison purposes, as the intention is to evaluate the isolated effect of the reinforcement area.

Table 4.4 – Summary of properties in Fig. 4.11.

Parameters	CSA S304-14	TMS 402-16
Compressive Strength of The Masonry (f'_m)	$f'_m = 15\ MPa$	$f'_m = 15\ MPa$
Modulus of Elasticity	$850f'_m$	$900f'_m$
Block Thickness (mm)	190	190
Reduction Factors ($\emptyset_e$)	$\emptyset_e = 1$	−
Creep Factor (β_d)	$\beta_d = 0$**	−

** A value of 0 is used to neglect the influences of this factor.

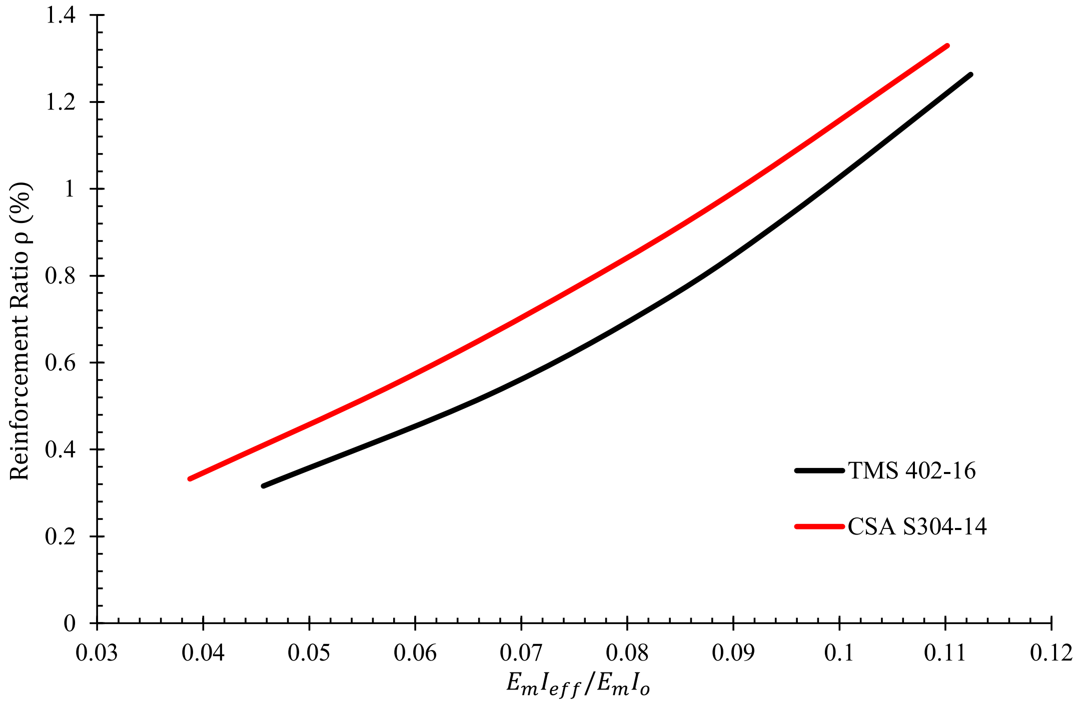

Figure 4.12 – Effect of the Variation of the Reinforcement Ratio.

This analysis is valid for both the fully and partially grouted sections. From Fig. 4.12, it seems that the OOP rigidity of the wallets is enhanced due to the increment of the area of steel. In both expressions, the rate of increment seems to be proportional. Doubling the reinforcement ratio (from 0.5% to 1.0%) increases the stiffness of the wallets by approximately 60%. However, under the parameters shown in Table 4.4, the expression to calculate the cracked moment of inertia from TMS 402-16 is not applicable for reinforcement ratios greater than 1.8%, as the neutral axis calculated using U.S. - 4.4 lies beyond the face shell of the element. It is expected that for axially loaded members, the relative difference between the standards increases considerably.

4.4 Summary

A mapped summary of the influences of the independent parameters in the flexural stiffness compute using the North American equations is presented in Table 4.5

Table 4.5 – Comparison of the parameters investigated. Second-Order Effects.

Parameter	Influence	Comments
Variation of the Axial Loading	**High**	• The CSA S304-14 does not account for the axial loading in the cracked moment of inertia (I_{cr}) while the TMS 402-16 does it. As the axial load is increased, the difference between both standards becomes more pronounced. Flexural stiffness calculated according to the CSA S304-14 are more conservative in all the conditions. • For cracked walls, the TMS 402-16 was demonstrated to be up to 59% higher than that of the CSA S304-14. For uncracked cases, the American stiffness is 3 times greater than that of the CSA S304-14 .
Variation of the Reinforcement Ratio	Low	• As the reinforcement ratio increases, the effective stiffness according to both standards is enhanced by similar proportions. • Doubling the reinforcement ratio (from 0.5% to 1.0%) has proven to enhance the flexural stiffness by approximately 60% • The TMS 402-16 expression to calculate the depth of the neutral axis is only applicable for reinforcement ratios lower than 1.5%, under the compressive strength evaluated.
Variation of the f'_m.	Low	• Although increasing the compressive strength of the masonry decreased the cracked moment of inertia (I_{cr}), due to the effect of the modular ratio. Increasing the f'_m enhance the effective stiffness. • The TMS 402-16 expression is more sensitive to a variation of the compressive strength. Thus, at higher values, the

		differences between the standard increases. ● Between 10 MPa and 25 MPa the increment is more pronounced (About 25%). After 25 MPa the increment is negligible.
Reduction Factor $\emptyset_e$	**High**	● The Canadian Committee proposed a reduction factor $\emptyset_e$ which decreased by 25% the EI_{eff} directly. The TMS 402-16 committee finds such factors unnecessary. ● Applying this factor to the CSA S304-14 calculation results in a decrease of 25% in all the axial loading ranges.
Creep factor β_d	Low **- High**	● The TMS 402-16 does not consider the effect of the creep in the calculations of the effective stiffness. However, the CSA S304-14 accounts for it through a creep factor β_d. ● Depending on the loading condition, the effect of the creep factor can be negligible. Nevertheless, if the source of the primary moment is mainly due to the eccentric axial loading, the creep factor could reduce the flexural stiffness by up to 50%

5. FINITE ELEMENT MODEL FOR FLEXURAL RIGIDITY EVALUATION

5.1 Introduction.

In Chapter 4, the methods to calculate second-order effects according to the North American standards (i.e. CSA S304-14, TMS 402-16) were introduced. It was found that both committees offer two alternatives to calculate the moment amplifications, (a) P-Delta method and (b) Moment Magnifier Method. Although minor differences were identified in the adoption of the MM according to each standard (i.e. c_m and k factors). the most significant discrepancy between both countries relates to the expressions used to calculate the effective stiffness in RMWs. To assess the accuracy of the effective stiffness equations in both codes, in the absence of an experimental data set, numerical analysis validated based on previous experimental programs (e.g., SEASC and Mohsin 2003) are a viable alternative.

In this chapter, a fibre-based model for reinforced fully and partially grouted masonry walls subjected to out-of-plane bending and concentric axial load is developed using the Open System for Earthquake Engineering Simulation (OpenSEES) software package. Material and geometrical nonlinearity are included. The numerical model is validated using experimental programs of fully and partially grouted walls (SEASC 1987, Mohsin 2003).

This study selected four independent parameters to evaluate their isolated effects on the second-order effects in RMWs. These parameters consisted of masonry compressive strength (f'_m), slenderness ratio$(\frac{h}{t})$, reinforcement ratio(ρ) and axial loading (P). Analytical moment amplification factors were calculated and compared with CSA S304-14 and TMS 402-16. The data set created consisted of 1535 fully grouted walls and 403 partially grouted trials.

Using the strain information obtained with the model, three expressions for the effective stiffness were developed and compared against the design provisions from TMS 402-16 and CSA S304-14. These equations were derived using multilinear regression analysis.

5.2 Finite Element Model

A fibre-based model was created using the Open System for Earthquake Engineering Simulation (OpenSEES) platform. OpenSEES was developed within the Network for Earthquake Engineering Simulation (NEES) and serves as an object-oriented, open-source software framework dedicated to finite element modelling and analysis. This tool is extensively used in the research community due to its efficacy and accuracy in predicting complex structural behaviours. Although the source code of OpenSEES is written in C++, allowing users to create new classes, materials, elements, etc. The numerical model is created using TCL scripts language that includes the structural model geometry, section, analysis type, recorders and solvers.

This software has proven to be an excellent tool that accurately predicts the behaviour of masonry walls subjected to in-plane and OOP loads using a fibre-section approach. (Dona et al 2018, Entz 2018, Alonso et al. 2019).

5.2.1 Fibre Modelling Approach

The fibre model sectional approach is a widely used technique in finite element analysis due to its ability to produce excellent predictions using fewer computational resources than continuous models. In this approach, the sectional stress-strain state of the elements is obtained through integrating the uniaxial stress-strain response of individual fibres in which the section is divided (Casarotti and Rui 2006). Structural members are represented by a series of elements with finite length and an assigned cross-section. The OpenSEES framework provides a library with multiple elements and classes. Two elements are typically adopted to model nonlinear structures (i.e., Force-based elements and displacement-based elements). These elements allow the incorporation of the spread of plasticity along the member length and the interaction between the axial forces and transverse deformation of the section. Thus, using enough elements permits the reproduction of plastic hinges along the entire length of the member without using localized plasticity elements as other modelling techniques. (Casarotti and Rui 2006).

The fibre section adopted in this study is illustrated in Fig. 5.1. The cross-section is composed of masonry fibres, and a lumped rebar fibre located at the centre of the cross-section to simulate the total area of steel in a masonry wall. The material constitutive relationships are explained in section 5.2.2, while the element formulation used is detailed in section 5.2.3.

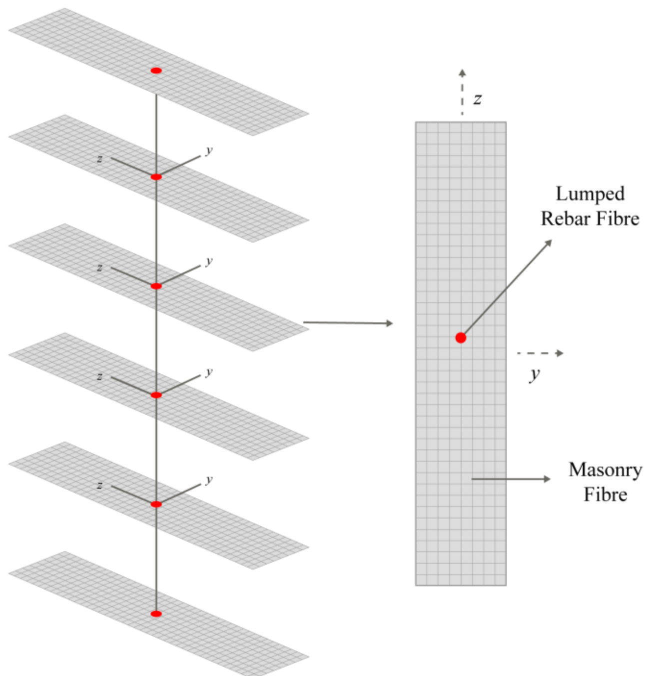

Figure 5.1 – Fibre Section model. (Bilotta et al 2021)

5.2.2 Material Properties.

5.2.2.1 Masonry

Uniaxial stress-strain laws material from the OpenSEES library were implemented. The homogenous behaviour of the fully-grouted masonry was recreated using "*Concrete02*" based on the Kent-Scott-Park model. A parabolic stress-strain relationship is assumed up to the maximum compressive stress of the masonry, followed by a linear softening branch stopping at the maximum crushing strain. The material also assumes a linearly tensile strength increment, followed by a linear tension softening branch to failure.

The model proposed by Priestley and Elder (1983) to evaluate the homogenous behaviour of the masonry assemblage was adopted in this study to calculate the ultimate and crushing stress of the masonry fibres, the maximum compressive strength is assumed to happen at a strain of 0.002 (Drysdale and Hamid 2005) (Fig. 5.2). This material model has demonstrated excellent results on fully and partially grouted specimens (Mohsin 2003, Clayton 2020). The model also presents an excellent correlation with the "Concrete02" parabolic stress-strain distribution and can be expressed as:

$$\begin{aligned} &\sigma_m = \{ f'_m \left[\frac{2\epsilon}{0.002} - \left(\frac{\epsilon}{0.002}\right)^2\right] && \epsilon \\ &\leq 0.002 \; f'_m[1 - Z(\epsilon - 0.002)] && 0.002 < \epsilon \\ &\leq \; \epsilon_{2ou} \qquad 0.2 f'_m && \epsilon > \epsilon_{2ou} \end{aligned} \tag{5.1}$$

Where:

$$Z = \frac{0.5}{\left(\frac{3 + 0.29 f'_m}{145 f'_m - 1000}\right) - 0.002} \tag{5.2}$$

$f'_m, \epsilon, \sigma_{mt}$ *and* E_m are the grouted masonry strength, grouted masonry strain, grouted masonry tensile stress and modulus of elasticity of the masonry. The maximum tensile strength of the masonry was assumed to be 0.65 MPa, linear elastic until cracking and with a linear tension softening.

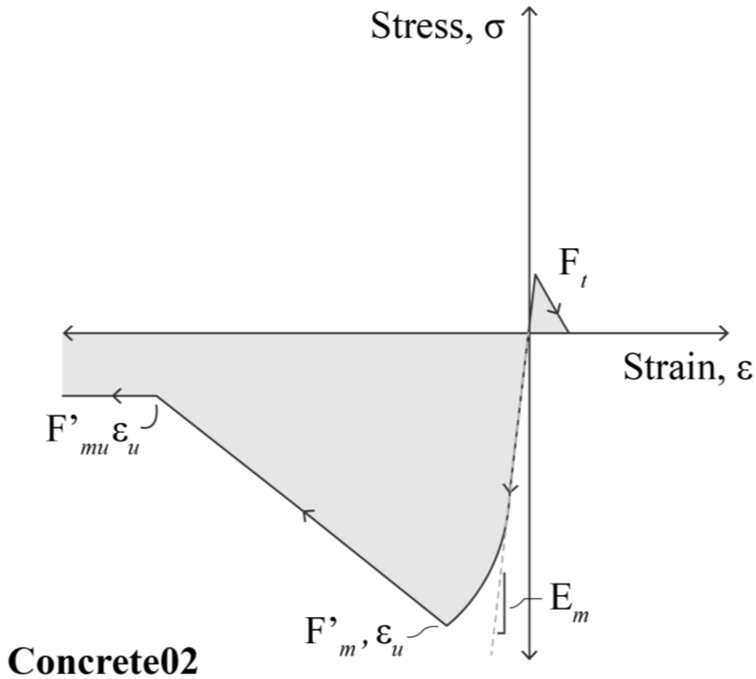

Figure 5.2 – Behaviour of Masonry under Compression according to Priestley and Elder model and *Concrete02.*

5.2.2.2 Steel reinforcement

OpenSEES *"Steel02"* a uniaxial material model with isotropic strain hardening based on the Giuffre-Menegotto-Pinto model, was used to simulate the longitudinal reinforcement. From the available models in the library, *Steel02* demonstrated to have the best equilibrium between convergence and correlation rates during the parametric analysis of this chapter, therefore, it was selected from all the other steel models available. Fig. 5.3 illustrates the stress-strain relationship of "*Steel02.*"

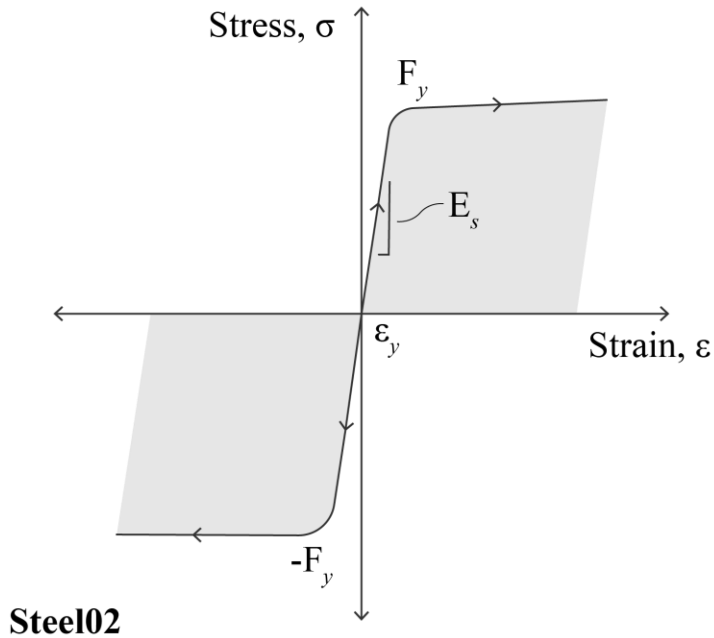

Figure 5.3 – Steel 02 Material Model.

5.2.3 Element Formulation

5.2.3.1 Beam-Column Element

For nonlinear analysis using a fibre section approach, a number of elements are available in the OpenSEES framework, including elastic, inelastic, nonlinear, displacement-based and force-based elements. For this study, the "nonlinearBeamColumn" element was implemented. This element is based on a non-iterative or iterative force formulation, which considers the spread of plasticity along the element (OpenSEES)

Forces-based elements rely on the availability of an exact equilibrium solution within the basic system of a beam-column element. Thus, equilibrium between the elements and sections should be exact in the range of constitutive nonlinearity. The section forces are determined from the basic forces by interpolation. Principles of virtual forces are used to formulate the compatibility between the section and the elements deformations (Fig. 5.4)

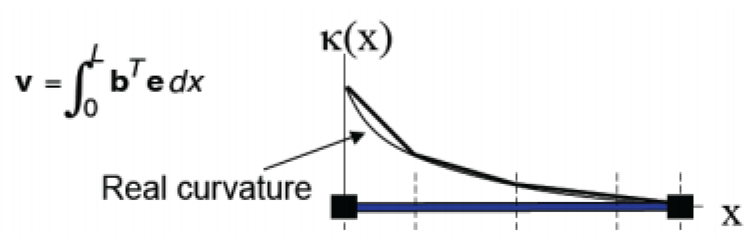

Figure 5.4 - Principle of virtual forces (Terzic 2011)

5.2.4 Failure Modes

Two failure modes are defined in the model:

1. Crushing of the masonry fibre: Triggered when the strain in the masonry exceeds the specified crushing strain in compression based on the Priestley and Elder
2. Rupture of the reinforcement: Triggered when the tensile strain exceeds the specified rupture strain based on the Giuffre-Menegotto-Pinto model

5.3 Validation.

To evaluate the performance of the model, two experimental programs with different loading scenarios were used. The first campaign corresponds to the experimental results of slender masonry walls from the ACI-SEASC Task Committee on Slender Walls (SEASC 1982), which have formed the basis of current design standards in Canada and the United States. The second is the experimental program conducted by Mohsin in 2003 at the University of Alberta.

5.3.1 Experimental program 1. Fully-grouted walls subjected to a monotonic uniform lateral pressure and eccentrically axial load (SEASC 1982)

5.3.1.1 Experimental Setup

The experimental program consisted of 9 reinforced masonry panels subjected to a uniform lateral pressure and an eccentric axial load. All panels were 1.2m wide, but with different block thicknesses (Table 5.1). The boundary conditions for all the specimens were pinned-pinned. Multiple slenderness ratios were evaluated, starting from 30 up to

53 (Table 5.1). The eccentric axial load was applied through a pulley system using a drum of water, and it was held constant during the lateral loading application.

Once the axial load reached the peak value, a uniform lateral pressure was applied monotonically using an airbag along with the wall height and width. The displacement at mid-span was read as rapidly as possible and recorded manually. Due to safety concerns, the lateral load was stopped when it was judged that the crushing strain of the masonry would be near to occur. From the nine panels tested, only 2 reached the crushing of the masonry. Different thicknesses of concrete masonry units were used: 6 in (143 mm), 8 in (194 mm), and 10 in (246 mm). Fig. 5.5 and Fig. 5.6 depicts the test setup and specimen details.

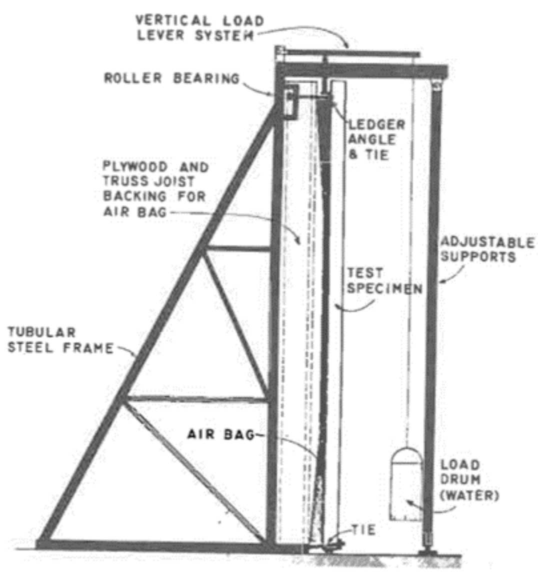

Figure 5.5 – SEASC Experimental Setup (SEASC 1982)

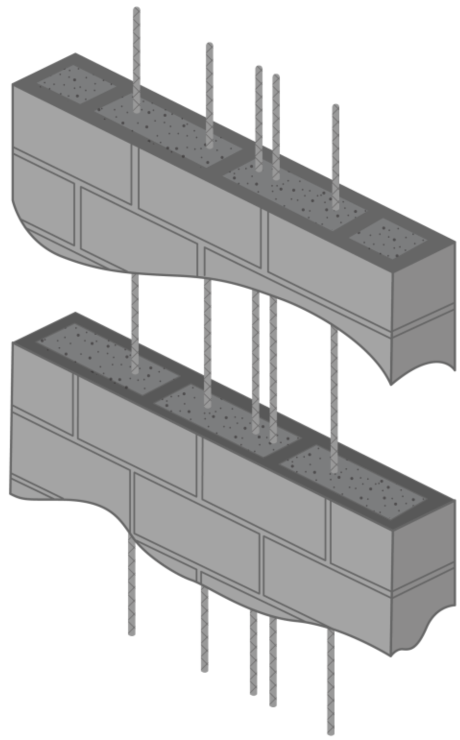

Figure 5.6 – SEASC Specimen detail (SEASC 1982)

Table 5.1 - Masonry Wall Panel Summary (SEASC 1982)

Panel	Block Thickness (mm)	Axial Load (kN/m)	Eccentricity (mm)	h/t	Failure Mode
1	246	4.67	198.5	30.6	Stopped Test
2	246	15.3	198.5	30.6	Stopped Test
3	246	15.3	198.5	30.6	Stopped Test
4	194	15.3	97.07	38.8	Stopped Test
5	194	15.3	97.07	38.8	Stopped Test
6	194	5.7	97.07	38.8	Stopped Test
7	143	5.7	71.57	52.6	Crushing
8	143	5.7	71.57	52.6	Crushing
9	143	5.7	71.57	52.6	Stopped Test

5.3.1.2 Material properties

Material properties of the walls are shown in Table 5.2 and Table 5.3, respectively. The compressive strength and the modulus of elasticity of the masonry were calculated on-site through prism testing.

Table 5.2 – Masonry Material Properties (SEASC 1982)

Masonry Unit Thickness (mm)	Compressive Strength (MPa)	Modulus of Elasticity (MPa)
246	17.0	14,962
194	17.9	11,859
143	22.0	10,963

All the panels were reinforced with five #4 bars, Grade 60 steel (Fig. 5.6). The steel rebar properties are shown in Table 5.3. The distance from the outer face of the wall to the centerline of the steel was measured after pouring the grout into the masonry cells. Table 5.4 shows the rebar positioning summary.

Table 5.3 – Rebar Material Properties (SEASC 1982)

Yield Strength (MPa)	Ultimate Strength (MPa)	Elastic Modulus (MPa)
483	758	197,190

Table 5.4 – Placement of Steel reinforcement (SEASC 1982)

Panel	Thickness (mm)	Distance "d" from Outer Face of Wall to Centerline of Steel (mm)					
		Bar 1	Bar 2	Bar 3	Bar 4	Bar 5	Ave. d
1	246	131.8	131.8	125.4	128.5	125.4	128.5
2		106.4	106.4	119.1	106.4	119.1	111.5
3		133.3	130.3	133.3	133.3	136.6	133.3
4	194	105.6	105.6	105.6	107.6	98.5	104.1
5		119.3	111.7	109.2	111.7	98.5	112.7
6		83.8	83.8	81.2	81.2	78.7	81.7
7	143	71.8	74.9	81.0	81.0	81.0	77.9
8		55.3	56.8	56.3	54.8	61.2	56.8
9		76.2	80.0	75.9	75.9	77.9	77.2

5.3.1.3 Loading Protocol

The eccentric axial loading was applied using a load control integrator and held constant during the analysis. The loading eccentricity effect was simulated by applying an equivalent moment at the top of the structure. The self-weight was modelled as a uniform distributed load equivalent to the weight of each specimen according to its block thickness. Displacement control was used to apply the distributed lateral load that simulates the effects of the airbag. For the validation, the lumped rebar approach was used. The lumped rebar was placed at the average "d" location specified in Table 5.4.

5.3.1.4 Validation.

Graphs illustrating the uniform distributed lateral pressure as a function of the midspan deflection for all the panels are shown from Fig. 5.6 to 5.15.

Panel 3,4,5, and 6 showed a satisfactory correspondence before the yielding of the reinforcement. After the yielding point, the strain hardening effects were not accurately captured by the numerical evaluation. One possible explanation is that the bilinear stress-strain behaviour assumption used for the steel material did not accurately capture the strain hardening effect of the rebar. Additionally, it is possible that the rebar position provided in the report was not measured correctly, and the average distance was used. This is very frequently observed even in supervised construction. Incorrect rebar positioning can be translated into an increment or decrement of the moment arm of the cross-section, which can significantly impact the behaviour at post-yielding.

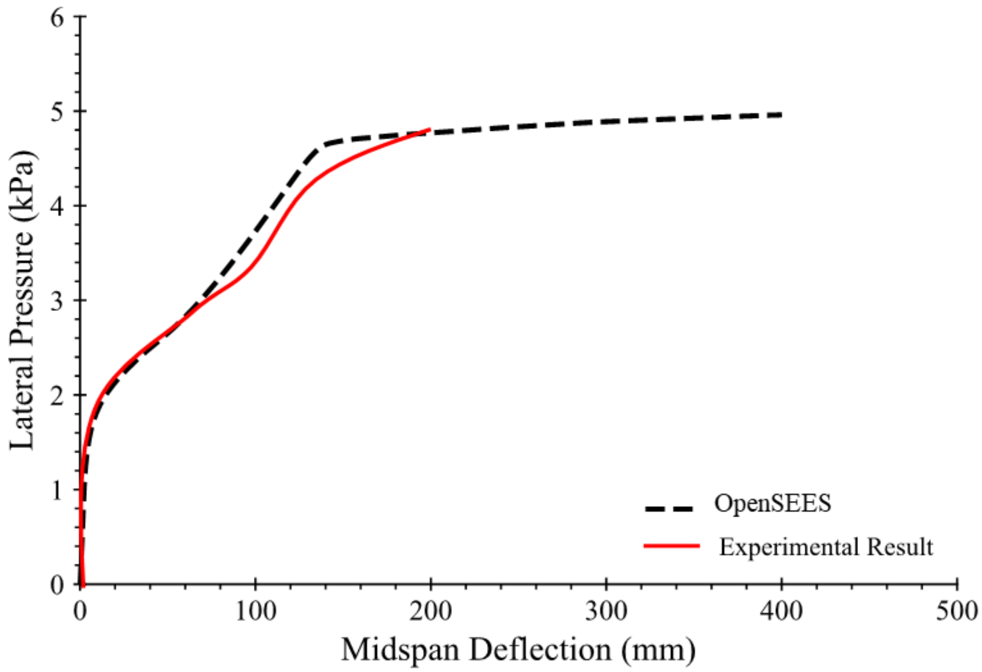

Figure 5.7 – Comparison of analytical model prediction to results of SEASC experiment panel 1

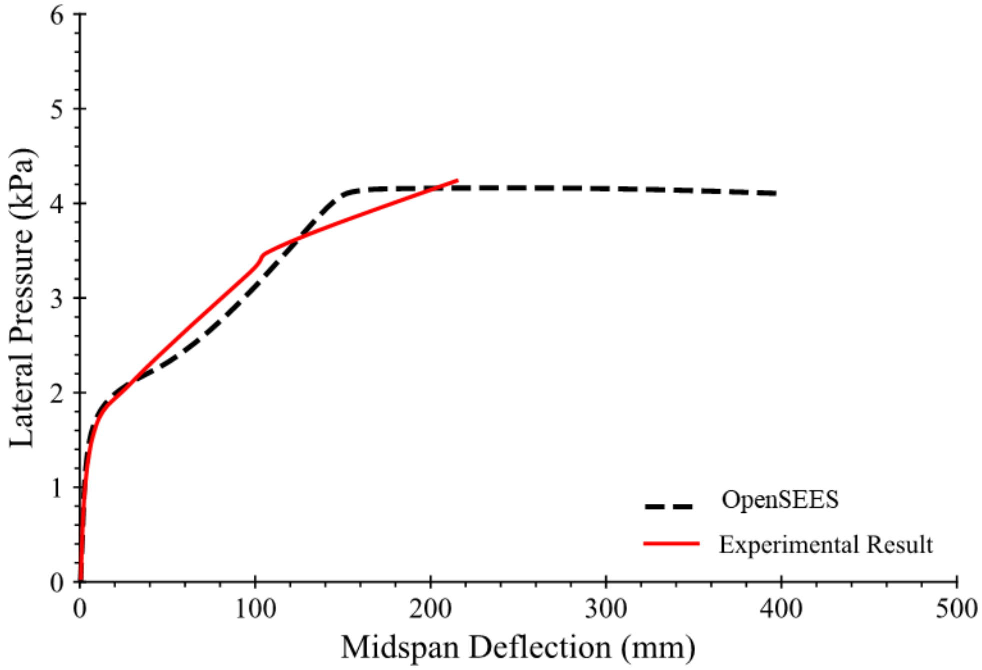

Figure 5.8 – Comparison of analytical model prediction to results of SEASC experiment panel 2

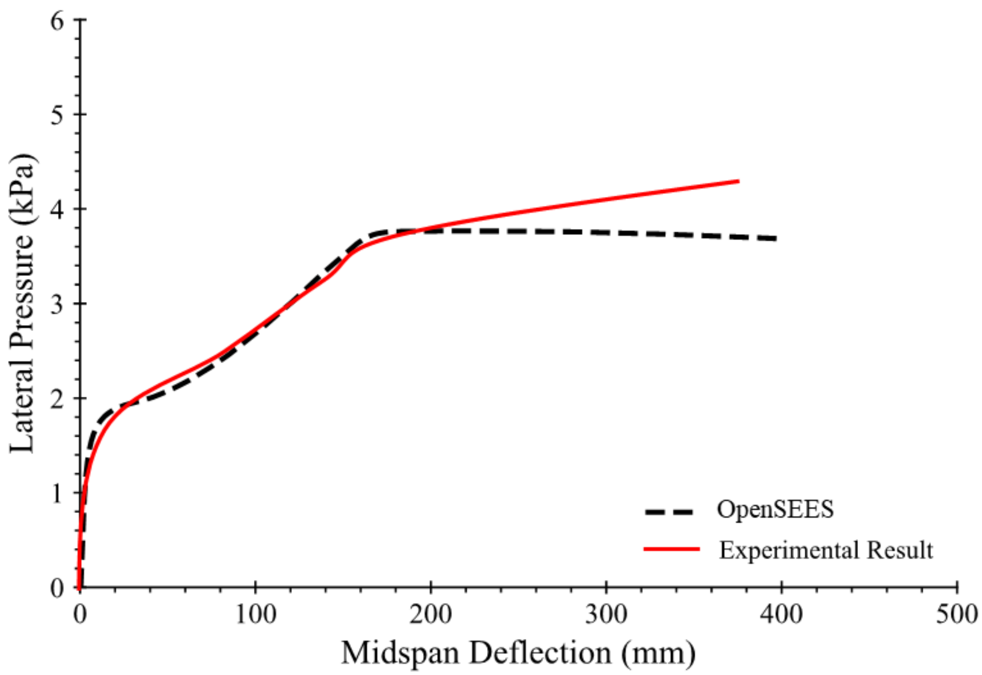

Figure 5.9– Comparison of analytical model prediction to results of SEASC experiment panel 3

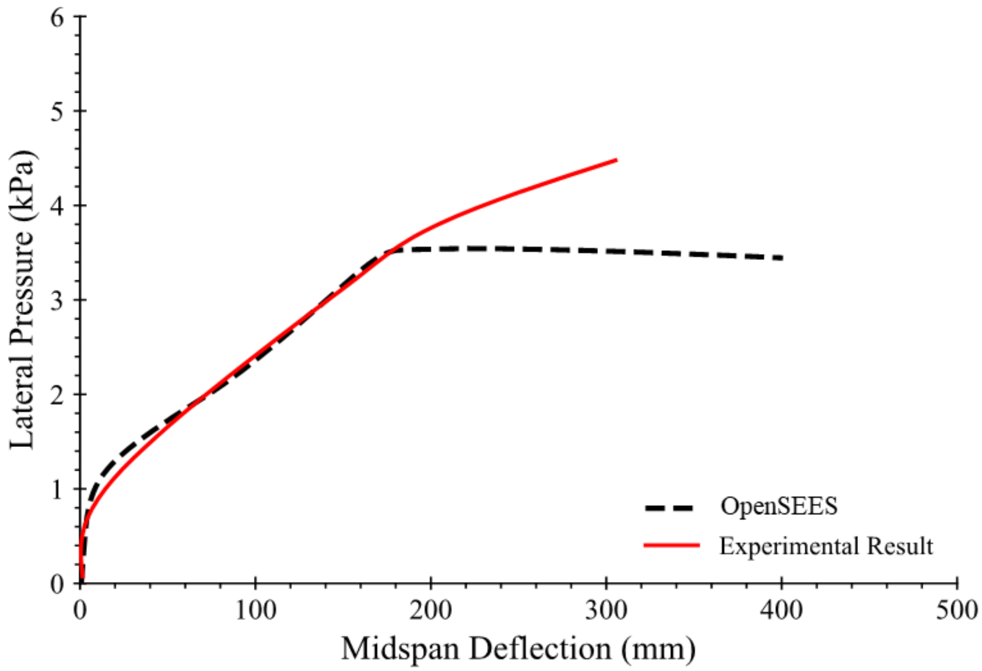

Figure 5.10– Comparison of analytical model prediction to results of SEASC experiment panel 4

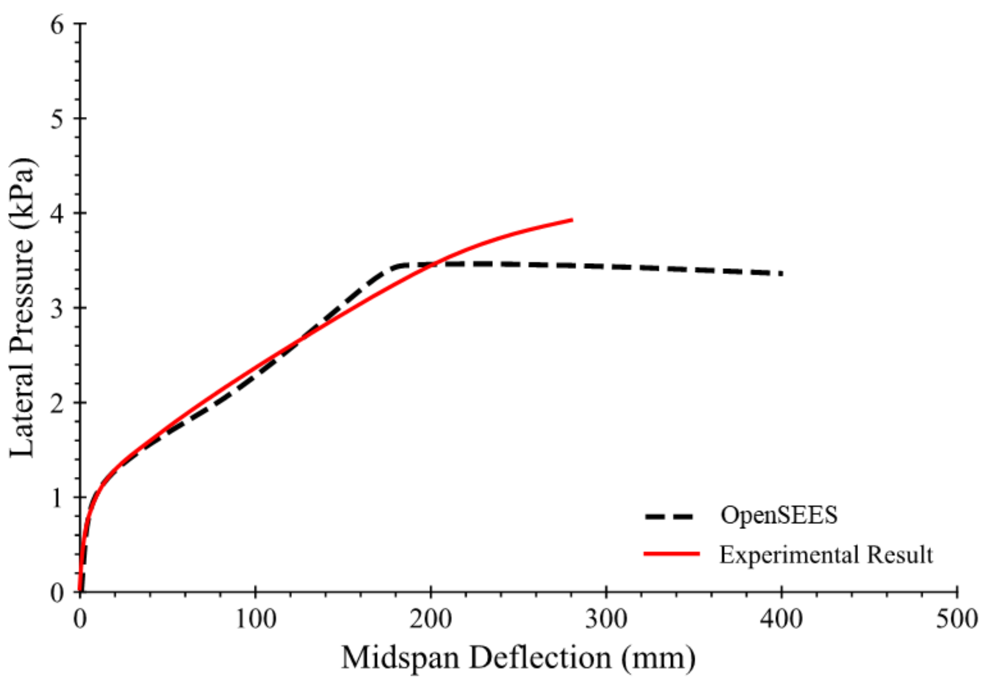

Figure 5.11– Comparison of analytical model prediction to results of SEASC experiment panel 5

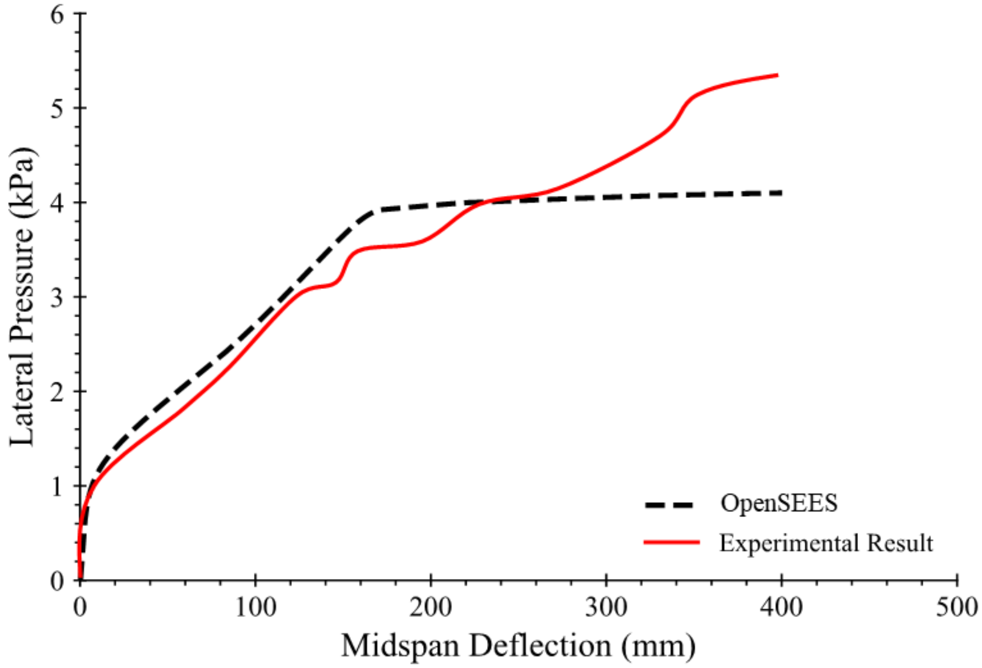

Figure 5.12– Comparison of analytical model prediction to results of SEASC experiment panel 6

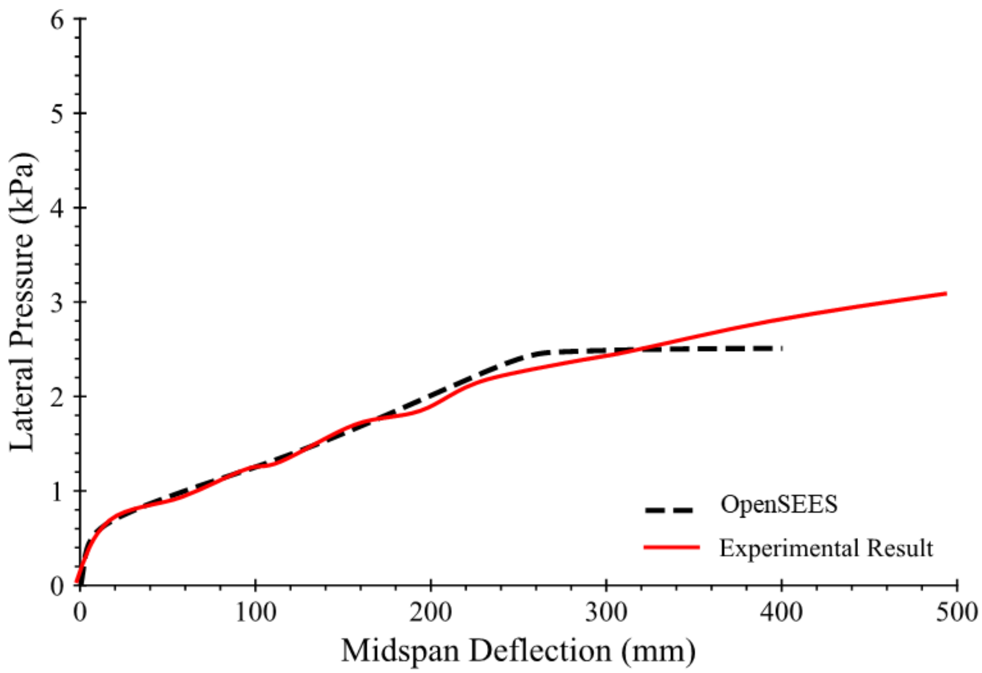

Figure 5.13– Comparison of analytical model prediction to results of SEASC experiment panel 7

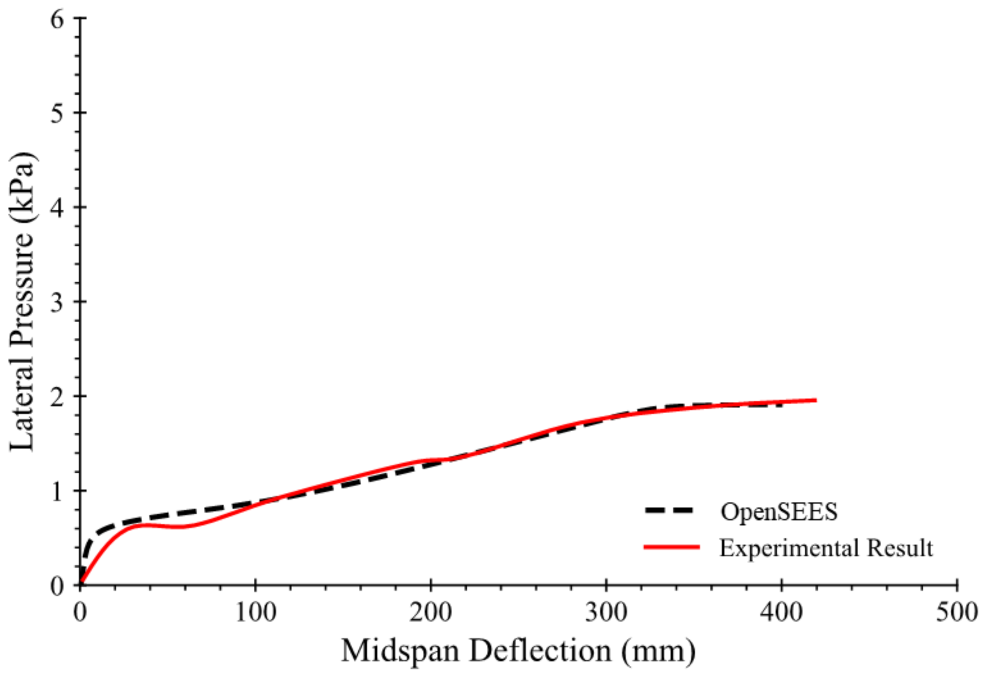

Figure 5.14 – Comparison of analytical model prediction to results of SEASC experiment panel 8

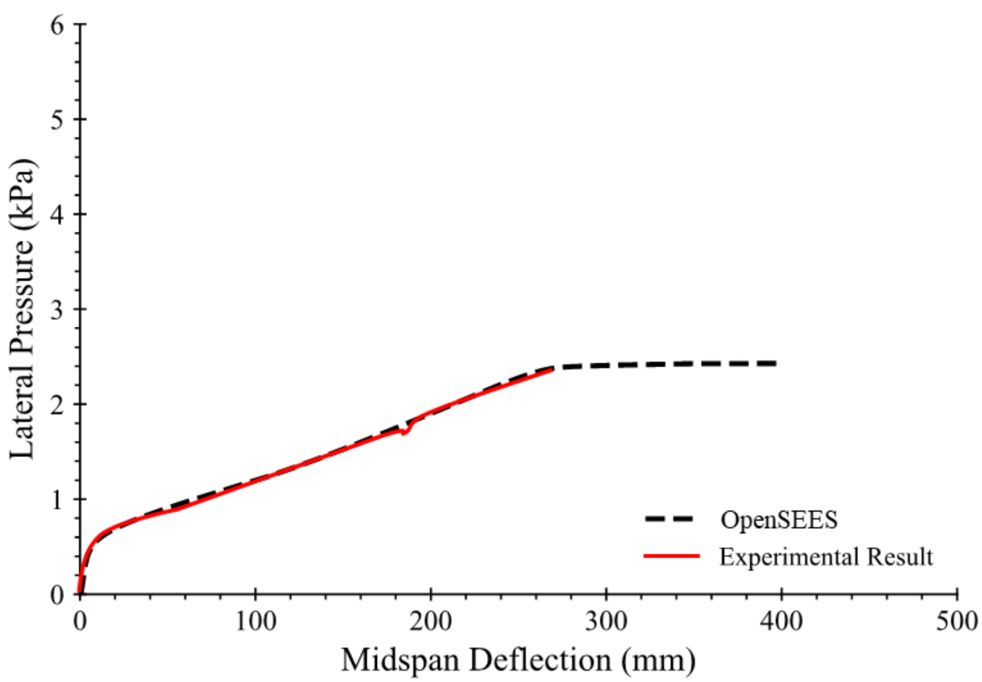

Figure 5.15 – Comparison of analytical model prediction to results of SEASC experiment panel 9.

5.3.2 Experimental program 2. Slender partially-grouted walls subjected to monotonic increasing eccentric axial load (Mohsin 2003).

5.3.2.1 Experimental description and Setup

Eight partially-grouted walls were tested under an eccentric axial load using different support conditions. The experimental program was developed to study the influences of base rigidity in slender masonry walls. The eccentric axial loading was monotonically increased up to the failure point. From the eight specimens, two panels were tested under pinned conditions in both ends. Table 5.5 summarizes the specimens used for the model validation. Figure 5.16 illustrates the experimental setup.

Table 5.5 – Test Specimen Summary (Mohsin 2003)

Specimen	Block Thickness (mm)	h/t
W3	190.10	28.6
W8	190.10	33.9

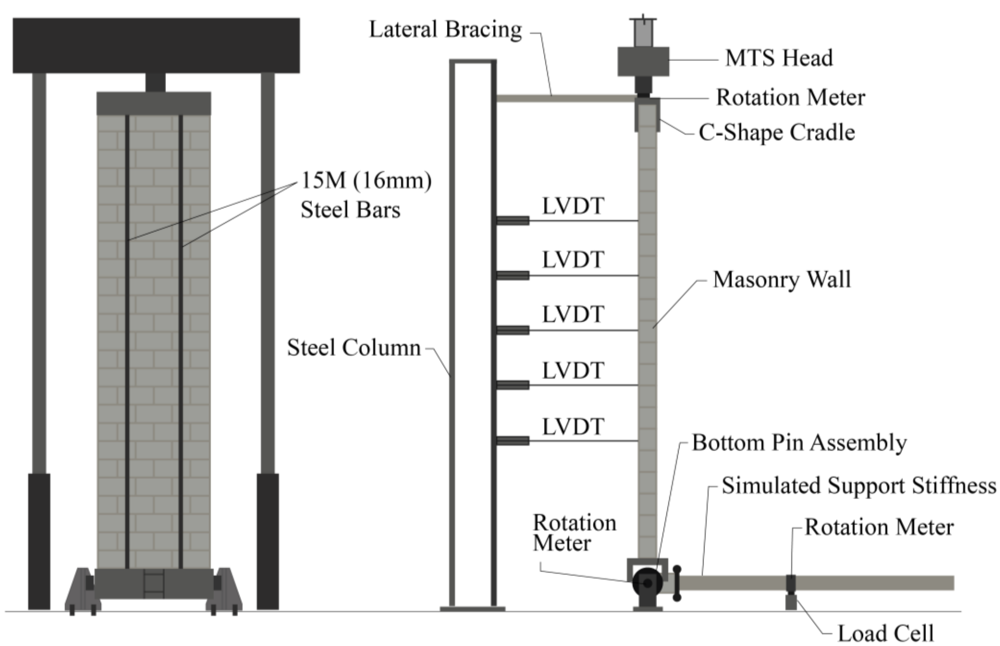

Figure 5.16 –Experimental Setup (Mohsin 2003)

5.3.2.2 Masonry Assemblage

All the specimens had an identical cross-section (Fig. 5.17). Two 15M reinforcing steel bars grade 60 with a nominal yield strength of 400 MPa were used. The compressive strength of the masonry and modulus of elasticity were determined through the testing of hollow and grouted prisms. The material properties of the walls are shown in Table 5.6 and Table **5.7**.

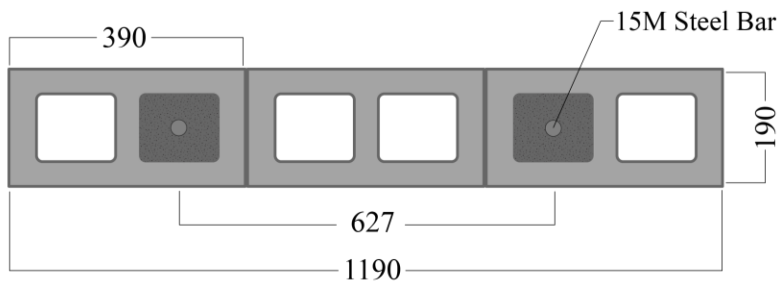

Figure 5.17 – Specimens Cross-Section (Mohsin 2003)

Table 5.6 – Masonry Material Properties (Mohsin 2003)

Prism Type	Compressive Strength (MPa)	Modulus of Elasticity (MPa)
Hollow	14.6	14,335
Grouted	10.2	7,379

Table 5.7 – Reinforcing Steel Properties (Mohsin 2003)

Yield Strength (MPa)	Ultimate Strength (MPa)	Elastic Modulus (MPa)
423	568	215,000

5.3.2.3 Numerical Evaluation Loading Protocol

The eccentric axial loading was applied using a displacement control protocol integrator until material failure or convergence issues were obtained. The loading eccentricity effect was simulated by simultaneously applying an equivalent moment at the top of the structure with the axial load (the axial load and the bending moment increase at the same ratio). The self-weight was modelled as a uniform distributed load equivalent to the weight of each specimen based on the thickness of the block.

The fibre section was created using the lumped bar approach. The masonry block webs were neglected. Only the face shells and an equivalent grouted cell were modelled, as shown in Fig. 5.18. An effective compressive strength ($f'_{m,eff}$) value was used for both the face shells and the grouted core.

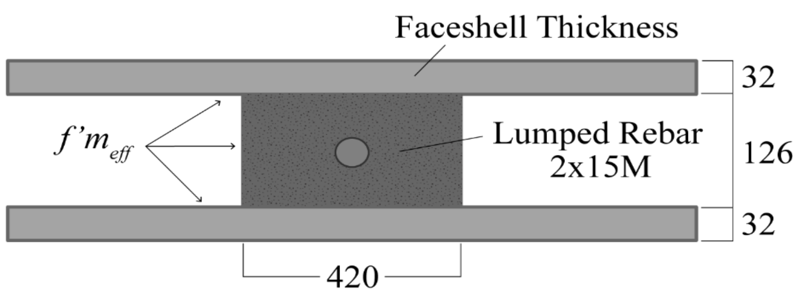

Figure 5.18 – Fibre Section. Mohsin 2003 experimental program.

5.3.2.4 Validation.

Figures 5.19 and 5.20 present the force-deflection curve for panel W3 and W8, respectively from Mohsin (2003) experimental program. An excellent correlation was found between the numerical evaluation and the experimental data in both panels during the elastic response. The peak eccentric axial load was captured accurately in both cases. The largest discrepancy appears after the peak load is reached. After the peak load, the stiffness degradation from the numerical evaluation is more significant than the experimental data.

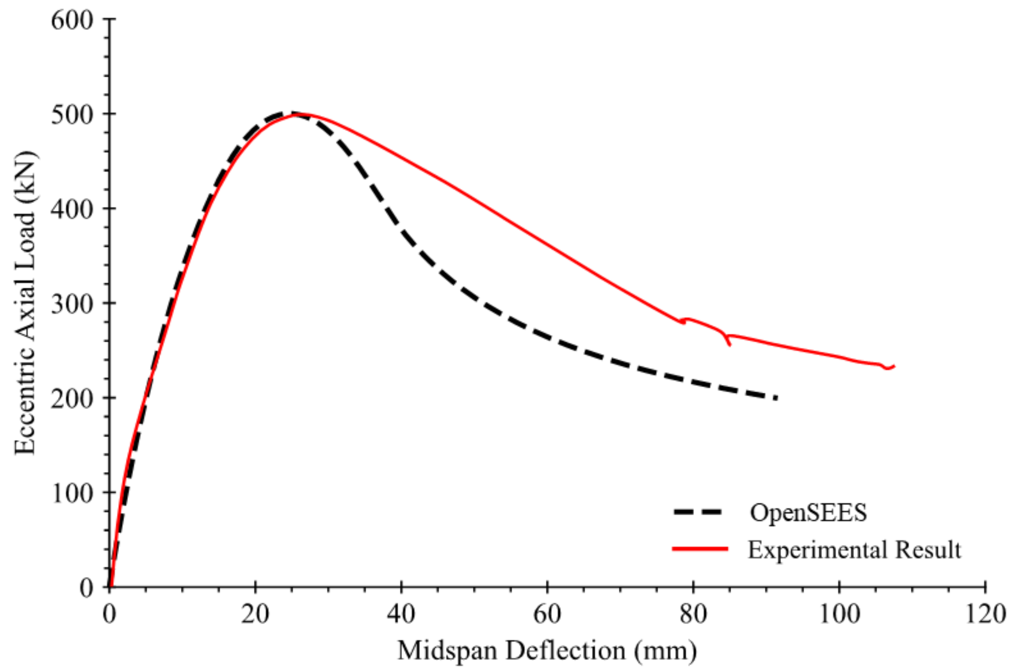

Figure 5.19 – Experimental and numerical force-deflection curves. Mohsin Panel W3.

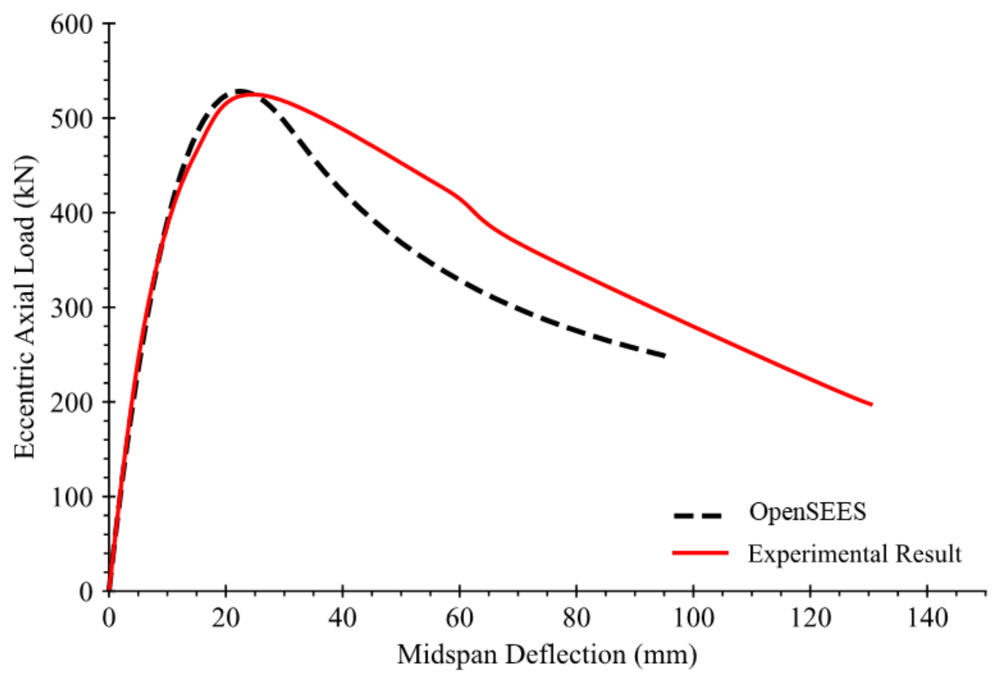

Figure 5.20– Experimental and numerical force-deflection curves. Mohsin Panel W8.

5.4 Parametric Studies.

The fibre model described above was used to evaluate the out-of-plane behaviour of fully grouted RMWS subjected to concentrically axial load and uniformly distributed lateral pressure under pinned conditions (Fig. 5.21). Multiple simulations were held. Fully and partially grouted walls were studied. The parameters of this study are classified as fixed, independent, and dependent.

Additionally, this section evaluates the effectiveness of the moment magnifier method proposed in the North American Standards (i.e. CSA S304-14, TMS 402-16). The evaluation is held by comparing the amplification effects calculated using the existing equations from the standards against the numerical evaluation.

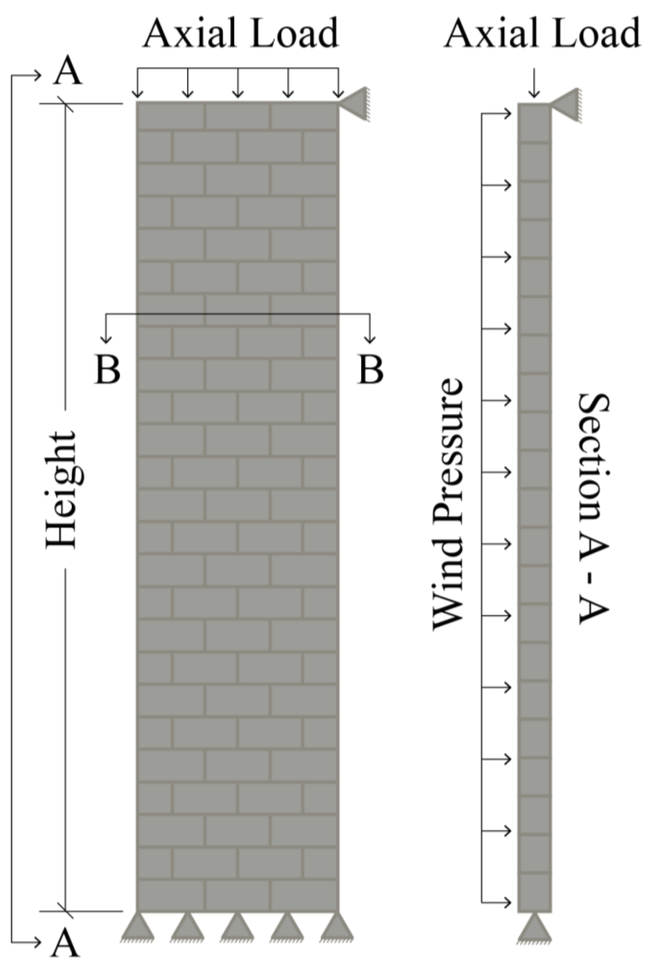

Figure 5.21 – Parametric Analysis Model.

5.4.1 Analysis description and Loading Protocol

The concentric axial load was applied at the top node using a load control integrator and was held constant throughout the analysis. The self-weight was later applied as a uniform load distributed along the height of the structure equivalent to the weight, also using a load control integrator.

For the uniform distributed pressure, a third load pattern with *"element load"* type was applied to each element through a displacement control integrator. The control node was set to the middle node (Midspan). The displacement increased monotonically, and consequently, the equivalent distributed load rose at the same rate.

Fully grouted elements were modelled as a rectangular cross-section, as explained in section 5.3.1.1. For partially grouted trials, a rebar spacing of 627 mm was assumed, with only grouted poured of cells with reinforcement (Mohsin 2005, Clayton 2019).

As the lumped rebar approach was validated (sections 5.3.1 and 5.3.2), all the numerical evaluation used an equivalent steel fibre placed at the center of the cross-section. For fully grouted trials, an equivalent rectangular section was used to model the homogenized behaviour of the masonry and grout as described by Priestly and Elder. For partially grouted trials a simplified equivalent section as shown in section 5.3.2.2

All the data points were obtained using a consistent criterion. The max crushing strain of the masonry was set to 0.003, as the CSA S304-14 recommends. The values were obtained at the maximum applied moment due to the lateral pressure (i.e. ultimate load). If a maximum applied moment was not achieved before the crushing strain of the masonry, the values at crushing were used. Any simulation that did not achieve a convergence before reaching the crushing strain of the masonry was discarded.

5.4.2 Fixed Parameters

These types of parameters were not changed throughout the study and were constant for all the walls modelled. The thickness of the block, the yield strength and modulus of elasticity of the steel, the boundary conditions, and the grouted cell arrangements were the fixed parameters of this study.

A thickness of the block of 190 mm was selected, which is equivalent to a 20 MPa nominal block thickness used in Canada. The typical yield strength of the reinforcement in Canada is 400 MPa, while in the United States 416 MPa (60 ksi). For consistency, a yield strength of 400 MPa with a modulus of elasticity of 200 GPa was selected. All the walls were investigated under pinned-pinned conditions.

The fixed parameters are summarized in Table 5.8.

Table 5.8 – Fixed Parameters Summary.

Parameter	Value
f_y (MPa)	400
Steel Modulus of Elasticity (GPa)	200
Block Thickness (mm)	190
Wall Width (mm)	1200
Number of Grouted Cells	6/6 For Fully Grouted 2/6 For Partially Grouted

5.4.3 Dependent Parameter

The dependent parameter of this study consisted of the OOP stiffness of the reinforced masonry walls. This parameter is investigated using the ratio between the primary source of moment induced in the system and the total moment accounting for geometrical nonlinearities (M1/Mt) at the ultimate load.

5.4.4 Independent Parameter

The independent parameters were varied to investigate their effects on the dependent parameter. This study had four independent parameters consisting of the compressive strength of the masonry (f'_m), the reinforcement ratio (ρ), the slenderness ratio (*h/t*), and the axial load (*P*).

Table 5.9 and 5.10 summarize the variation of the parameters used per simulation for the fully grouted and partially grouted trials, respectively.

Table 5.9 – Model simulation Matrix for Fully-grouted trials

Parameter	Range	Variation per simulation	Total Variations
Axial load (kN/m)	5-105	5 kN/m	21
Slenderness ratio (h/t)	20-60	10	5
Steel reinforcement ratio ρ (%)	0.52 – 2.63	0.52	5
f'_m (MPa)	10-30	10	3

Table 5.10 – Model simulation matrix for partially-grouted trials

Parameter	Range	Variation per simulation	Total Variations
Axial load (kN/m)	5-100	10 kN/m	11
Slenderness ratio (h/t)	20-60	10	5
Steel reinforcement ratio ρ (%)	0.175 – 0.52	0.175	3
f'_m (MPa)	10-30	10	3

The axial loading was selected as an independent parameter to investigate both its effects on the flexural stiffness of the cross-sections and the overall stability of the element. The variation range was chosen based on discussions with practicing engineers in Alberta. Typical axial loads for loadbearing masonry walls in Canada range between 50 kN/m and 70 kN/m. In this study, it was expected to develop a regression analysis for fully grouted elements. Therefore, a more extensive data set was created for fully grouted trials.

Multiple slenderness levels were selected to compare the evolution of the second-order effects as the slenderness ratio increases. With a constant block thickness throughout the simulations, the wall height was increased by 1.9m per step. The minimum ratio selected (i.e. 20) corresponds to a relatively short wall on which second-order effects might not be significant. The maximum height is 11.4m (i.e. h/t = 60), representing a very tall wall where the second-order effects are expected to govern the design.

Three levels of compressive strength of the masonry were adopted. Low (10 MPa), medium (20 MPa) and high compressive strength levels (30 MPa). This parameter was selected to understand the evolution of the flexural stiffness under different levels of compressive strength. For this study, nominal masonry capacities were used.

For the fully grouted walls, the minimum reinforcement ratio ρ selected (i.e. 0.52%) for the analysis is equivalent to 10M(11.3 mm) rebars spaced every 200 mm. The maximum ρ (i.e. 2.63%) represents a highly reinforced structure with 25M bars every 200 mm. Although this amount of steel might not be feasible for some solutions, future standard versions might start accepting higher reinforcement ratios with more relaxed provisions. For the partially grouted trials, the reinforcement ratio was selected based on a rebar spacing of 600 mm. Thus, the minimum ratio studied (0.25%) represents a reinforcement arrangement of 10M bars every 600 mm, while the highest is equivalent to 20M bars every 600 mm.

From the total of 1575 fully grouted simulations, 42 were discarded due to convergence issues. From the 495 partially grouted trials, the total number of valid simulations were 403.

5.4.5 Effects of the Independent Parameters.

To evaluate the effect of the independent parameters in the second-order effects of RMWs, M1/Mt versus Axial Load graphs were developed. M1 in the graph refers to the maximum applied moment due to the lateral pressure, while MT is the total moment in the element, which includes the primary and secondary moments. M1/Mt refers then to the inverse of the moment magnification factor. This is the factor the primary moment must be multiplied by to obtain the moment capacity or design moment of the wall. Thus, the smallest the ratio M1/Mt is, the larger the second-order effects are. These figures are presented for all the reinforcement ratios and compressive strength levels studied (From Fig. 5.22 to 5.29).

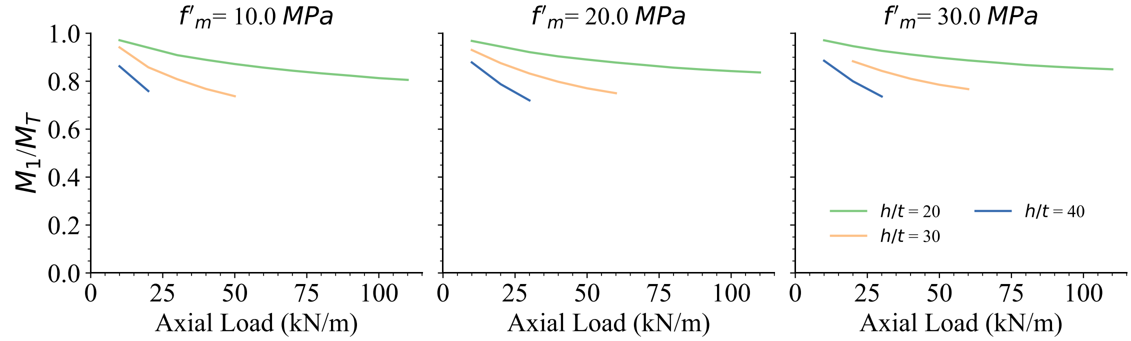

Figure 5.22 – M1/Mt vs Axial Load. Partially grouted $\rho = 0.175\%$

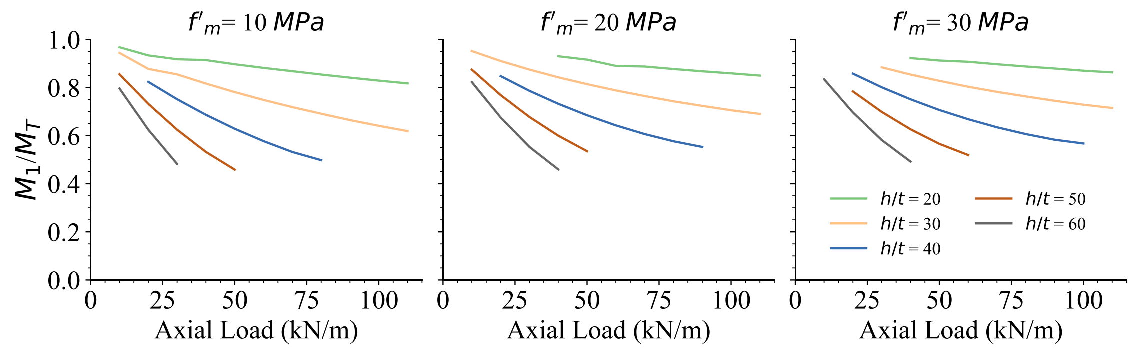

Figure 5.23 – M1/Mt vs Axial Load. Partially grouted $\rho = 0.35\%$

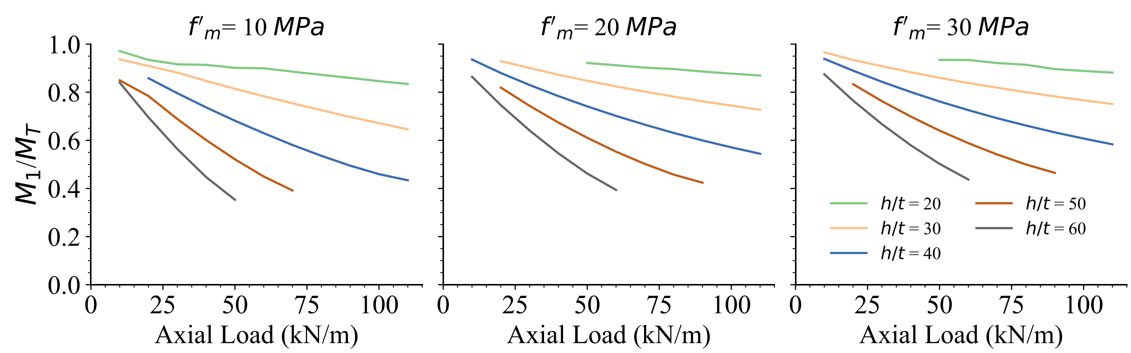

Figure 5.24 – M1/Mt vs Axial Load. Partially grouted $\rho = 0.52\%$

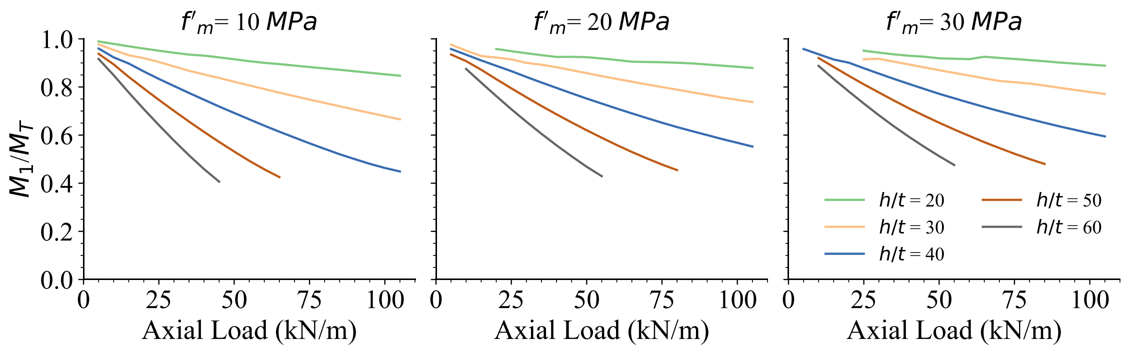

Figure 5.25 – M1/Mt vs Axial Load. Fully grouted $\rho = 0.52\%$

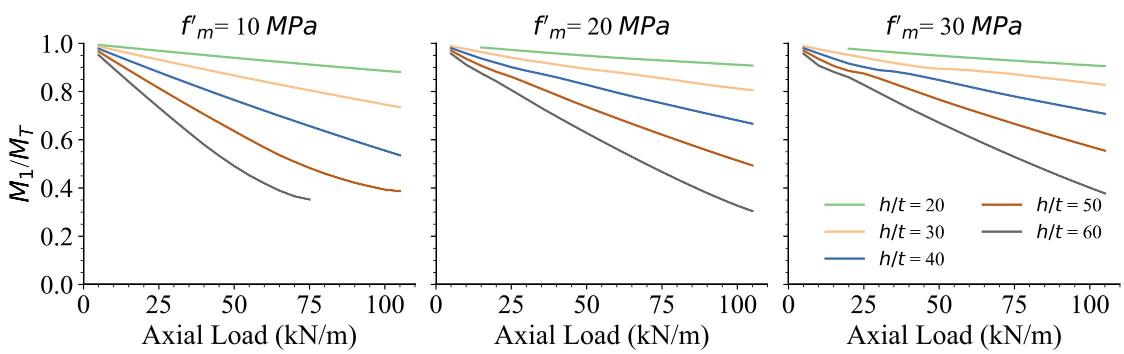

Figure 5.26 – M1/Mt vs Axial Load. Fully grouted $\rho = 1.01\%$

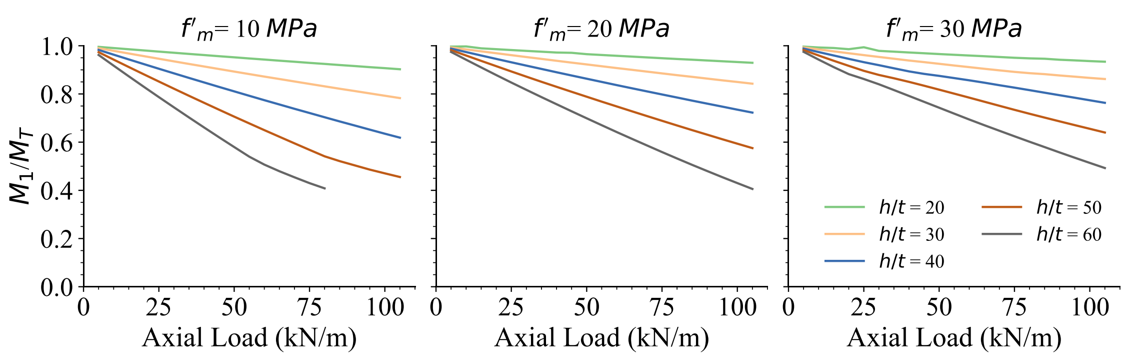

Figure 5.27 – M1/Mt vs Axial Load. Fully grouted $\rho = 1.57\%$

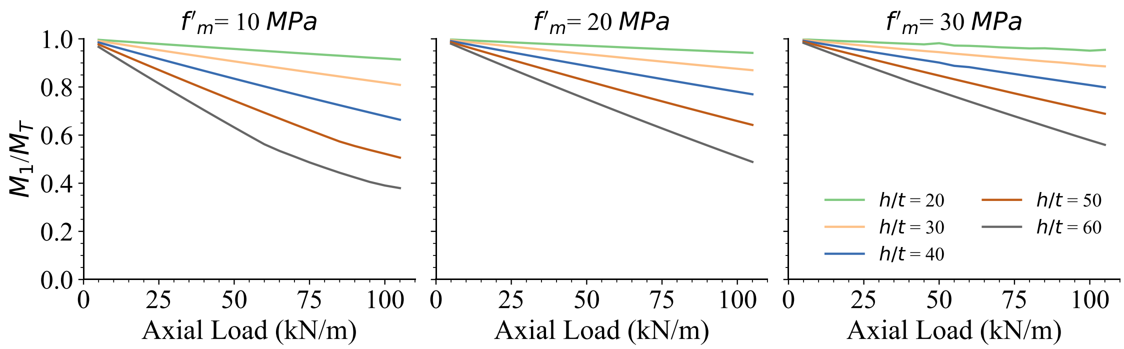

Figure 5.28 – M1/Mt vs Axial Load. Fully grouted $\rho = 2.1\%$

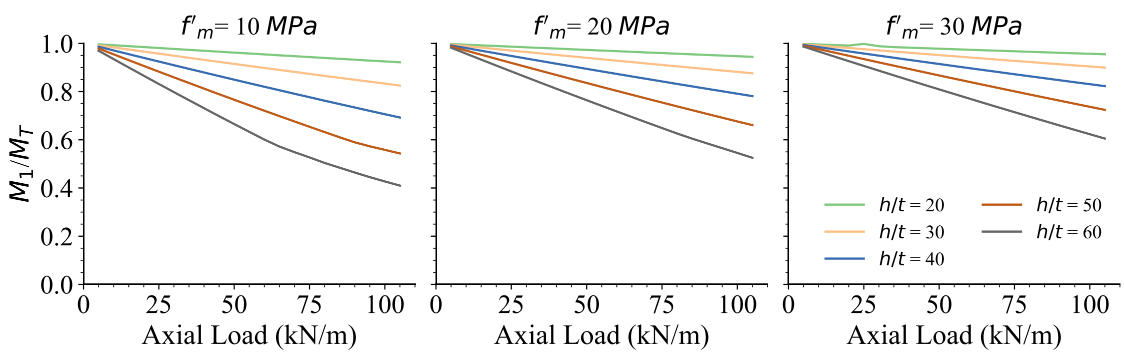

Figure 5.29 – M1/Mt vs Axial Load. Fully grouted $\rho = 2.6\%$

5.4.5.1 Effect of the Axial Load

As illustrated in the above figures, the second-order effects are influenced by the axial loading induced in the structural system. The axial load has a significant role in both the flexural stiffness of the cross-section and the instability effects induced in the global system. As commented before (Section 4.3.3.4.1), increasing compressive axial forces is known to decrease the curvature of the cross-section and hence enhance the flexural rigidity (EI) of the cross-section. However, it simultaneously increases the geometrical nonlinearity induced in the system due to the second-order effects leading to a decrease in the global stiffness *(k)*.

To illustrate this phenomenon, Fig 5.30 and Fig 31 are presented. Fig 5.30 illustrates the normalized total lateral load ($\sigma_h h/f'_m t$) versus the normalized mid-span deflection (Δ/t) for a fully grouted specimen with a slenderness ratio of 40, subjected to concentric axial loads of 40, 60, 80 and 100 kN/m. Fig. 5.31 shows the evolution of the total, the primary and the second-order moment for the same wall under a 100 kN/m of axial load.

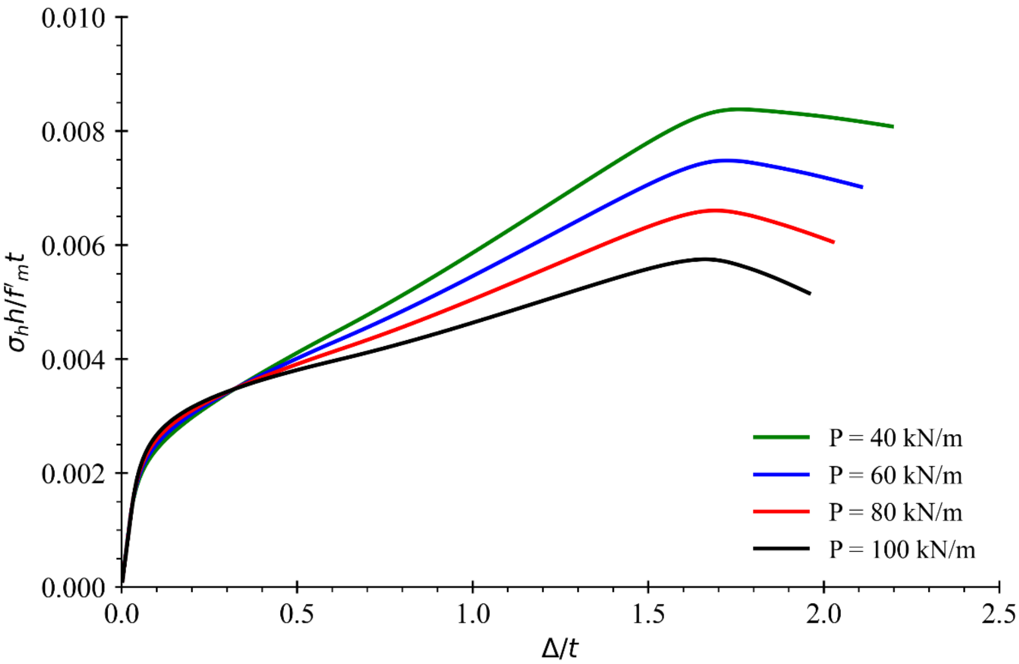

Figure 5.30– Normalized Lateral pressure versus normalized mid-span deflection. $\rho =$ 1%. Variable Axial Load.

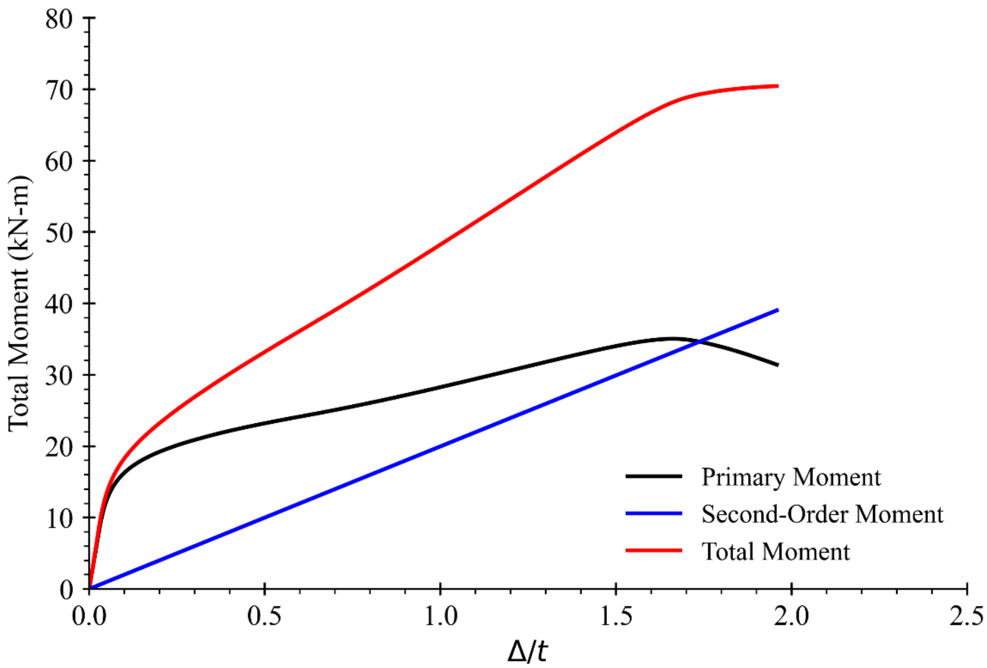

Figure 5.31 – Total, primary, and second-order moment evolution versus normalized mid-span deflection. $\rho = 1\%$. P = 100 kN/m.

In Fig. 5.31, the decrease in the applied pressure due to the higher axial forces is shown. Between 0.1 to 0.4 Δ/t, the enhancement of the flexural rigidity due to the compressive forces is evident. A greater later pressure is required to achieve the same deformation for walls with higher axial loads. However, as the applied pressure rises, geometrical nonlinearities become predominant, leading to a lower capacity at ultimate load. The reduction in the lateral load capacity indicates that the proportion of first-order moments from the total moment decreases. This behaviour is clearly shown in Fig. 5.30. At low deformation levels, the total moment is mainly due to the lateral applied pressure. Since the structure keeps deforming, the second-order moment grows gradually, while the increment rate of the primary moment starts to decline. An inflection point is eventually reached at approximately 1.7Δ/t where the proportion of second-order effects becomes dominant, and the primary source of moments drops.

It is essential to notice that the axial load also modifies the mode of failure on which the ultimate load is reached. At low axial load levels (e.g. 5 kN/m to 35 kN/m), the material failure governs the ultimate load. Due to the strain hardening of the steel, the lateral applied load kept rising to the maximum crushing strain 0.003 was reached. The ultimate load is no longer achieved at the crushing strain for higher axial load levels (e.g. 40 kN/m to 105 kN/m). The second-order effects become more predominant, and the ultimate condition depends on the stability effects rather than the material behaviour.

For all the conditions evaluated in this study, the critical buckling load was never reached. However, as the instability condition is amplified due to the axial loading, higher forces would produce pronounce instability effects in the M1/Mt ratio. Although the structure did not buckle under the applied axial load, the system reached an instability condition, where a small pressure translated into a rapid increment of the deformation. Thus, it becomes difficult to develop significant bending stresses in the section at ultimate load. This effect is more notorious in partially grouted elements as their gross inertia is lower than fully grouted sections. Revision of the data showed that the axial loading drastically shifted the failure mode in some partially grouted trials.

5.4.5.2 Effect of the Slenderness Ratio

As the slenderness ratio increases, the structure becomes more susceptible to moment amplifications due to second-order effects. However, it is essential to point out that the slenderness ratio does not modify the flexural rigidity (EI) of the cross-section but decreases the global stiffness matrix (k) due to the geometrical nonlinearities. This can be shown by comparing two walls with identical cross-sections subjected to the same axial load levels. For instance, in Fig. 5.25 a wall with a compressive strength of 10 MPa under an axial load of 50 kN/m and a height-to-thickness ratio of 40, has an M1/Mt ratio of 0.72, while the same section for a slenderness ratio of 50 the M1/Mt is 0.49. This represents an increment of 47% of the second-order moment from increasing the height of the structure by 1.9 meters.

Additionally, the slenderness ratio modifies the failure condition on which the ultimate load is reached. For smaller ratios (e.g. 20), the second-order effects might not be significant, therefore, the failure is usually governed by crushing of the masonry even under high axial forces. For higher ratios, the ultimate load is reached due to instability.

Partially grouted elements seem to be more susceptible to slenderness effects as the gross inertia is smaller than fully grouted trials. Instability effects were presented under any axial load level for the partially grouted trials with $\rho = 0.175\%$ and slenderness ratio greater than 40.

5.4.5.3 Effects of the Reinforcement Ratio.

From Fig 5.22 to 5.29 it seems that structures with higher reinforcement ratios are less susceptible to slenderness effects. Based on transformed section principles, the area of steel is transformed into equivalent masonry area through the modular ratio (n). Thus, the more steel in the section, the greater the cracked moment of inertia.

Additionally, it should be noticed that increasing the reinforcement area sacrifices the ductility of the walls. For heavily reinforced walls, the second-order effects are less significant, and the ultimate load is mainly achieved at the crushing strain of the masonry, while the rebars do not reach the yielding strain. In lower reinforcement ratios, the yielding of the rebar is achieved, and the stiffness of the section is affected by the yield strain developed. The more ductility the system experiment, the higher the stiffness degradation at ultimate load will be.

5.4.5.4 Effect of the Compressive Strength

The modulus of elasticity of the masonry rises whenever the compressive strength is increased. Consequently, higher f'_m will often translate in a clear enhancement of the stiffness if the ultimate load is achieved when the structure is still in its linear range or in moderate ductility levels. However, if the strength of the masonry increases, less masonry area would be needed to equilibrate the tension forces from the steel in the internal equilibrium. The neutral axis (c) is then reduced, and by compatibility analysis, more strain could be developed in the steel reinforcement. For instance, at reinforcement ratios greater than 1.5, the yield strain of the rebar was achieved only under compressive strength levels of 20 and 30 MPa. In cases where a high yield strain is developed, the stiffness is degraded due to the ductility effects.

5.4.6 Comparison and Evaluation of the Second-order Effects Calculated using the North American Standards.

In section 5.4.5 it was discussed the effect of the independent parameters in the second-order effects of RMWs. This section compares the moment amplification factor obtained by the Canadian standard (CSA S304-14) and the American standard (TMS 402-16) against the results from the numerical evaluation. The methods are evaluated using the same simulations presented in section 5.4.5. The influence of the independent parameters on the percentage of error produced in the MM method is discussed.

These factors are calculated using the moment magnifier method as described in section 4.3.2. For all the data sets created in this section, the effective length *(k)* and the cm factors mandated by the CSA S304-14, are taken as 1. Thus, the conditions used to calculate all the amplification factors are identical. The expression used in this section is given by equation 5.1.

$$Amplification\ factor = \left(\frac{1}{1 - \frac{P_f}{P_{cr}}}\right) \qquad 5.1$$

Where P_f is the applied axial load and P_{cr} is the critical buckling load assuming a *k* factor equal to 1.

Two sets of graphs are shown per each reinforcement ratio, set "A" and set "B".

Set "A" corresponds to contour plots that illustrate the percentage of error between the moment magnification factor calculated by each standard and the numerical analysis. A constant scale is used for all the groups to facilitate the comparison under different reinforcement ratios. The contour is generated using cubic interpolation between the available values. The blank spaces in set "A" represent points where the critical buckling load is exceeded according to the standards, and consequently, an amplification factor cannot be calculated. This set of graphs can be used as an estimation to determine at which range of value the moment amplifications calculated are within an acceptable margin of error.

Set "B" shows the ratio of M1/MT versus the axial load, similarly to section 5.4.5. M1/Mt refers then to the inverse of the amplification factors calculated using equation 5.1. CSA S304-14 expression neglecting the reduction factor φ_e is also included to evaluate the consequences of reducing by 25% the cracked moment of inertia. As commented in section 4.2.1, the equations to calculate the effective stiffness proposed by the TMS 402-16 are only valid if the neutral axis (U.S. 4-1) is within the face shells. If the neutral axis is beyond the face shell, the standards mandate to compute the stiffness using any method rooted in strength of materials and equilibrium. For those cases, in this study, the effective stiffness was calculated using the following equations (5.2 and 5.3), which are derived based on transformed section analysis of cracked sections. This approach considers the axial loading in both the calculation of the depth of the neutral axis and the cracked moment of inertia.

$$c = \frac{-n(A_s + \frac{P}{(f_s)}) + \sqrt{\left(n\left(A_s + \frac{P}{f_s}\right)\right)^2 + 2ndb_{eff}\left(A_s + \frac{P}{f_s}\right)}}{b_{eff}} \qquad 5.2$$

$$I_{cr} = n\left(A_s + \frac{P_u}{f_s}\right)(d-c)^2 + \frac{bc^3}{3} \qquad 5.3$$

Where P is the applied axial load, n is the modular ratio, A_s is the area of steel, b_{eff} is the effective width, and f_s is the stress in the steel calculated by Hooke's Law and should not exceed the yield strength.

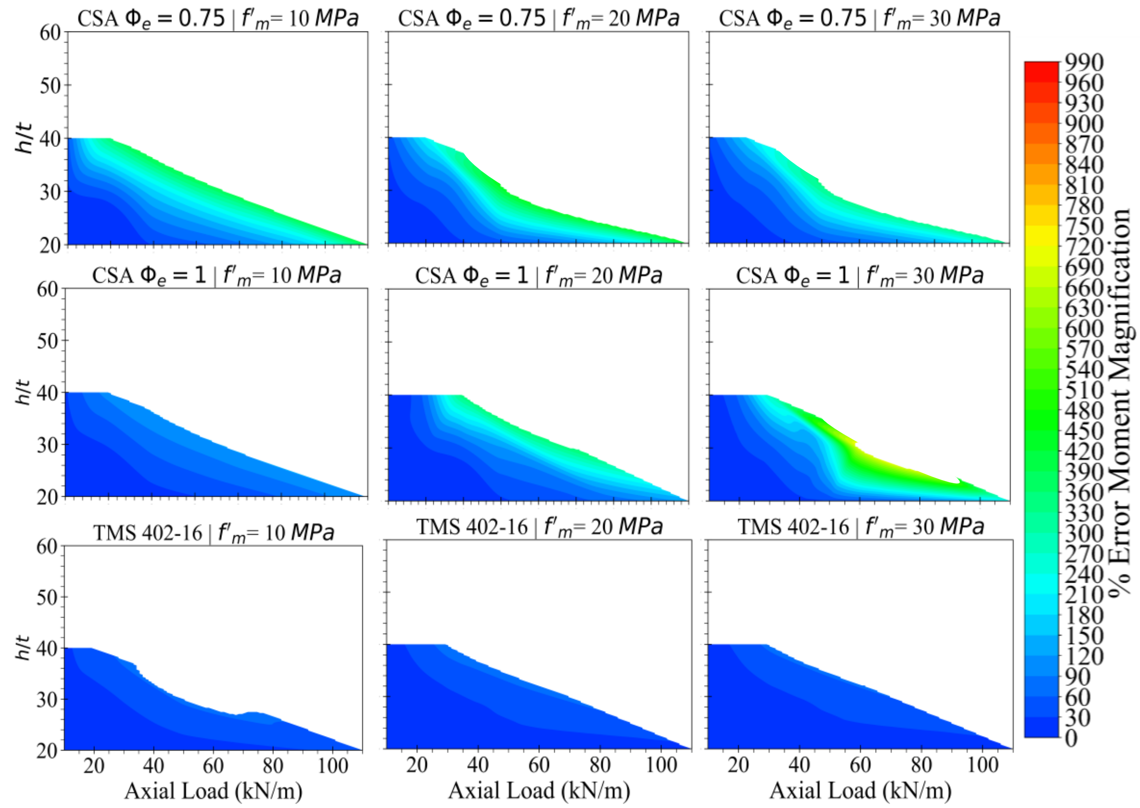

Figure 5.32 – Set A. Percentage of error in Moment Magnification factors. Partially ρ=0.175%

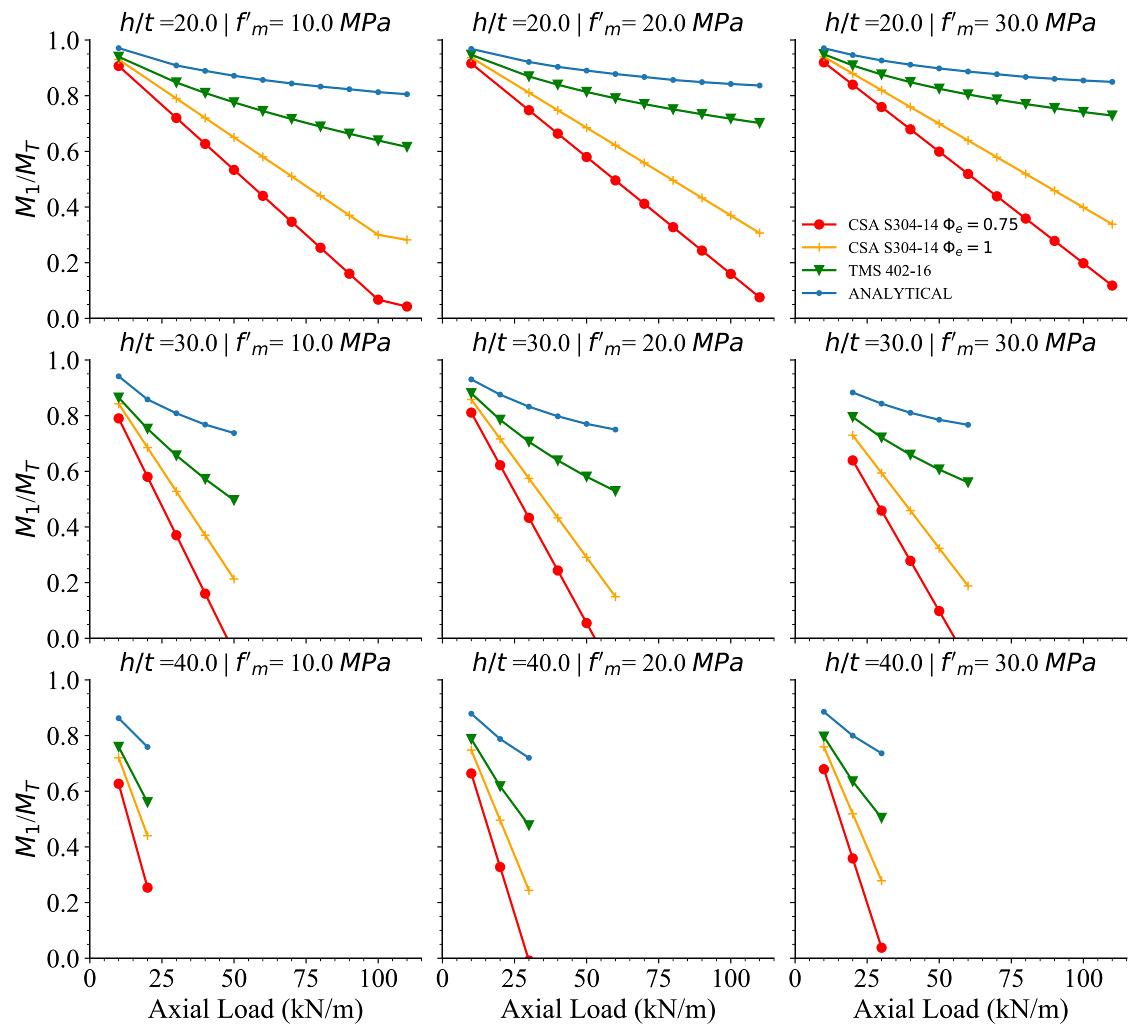

Figure 5.33 – Set B. M1/Mt vs Axial Load. Partially grouted ρ=0.175%

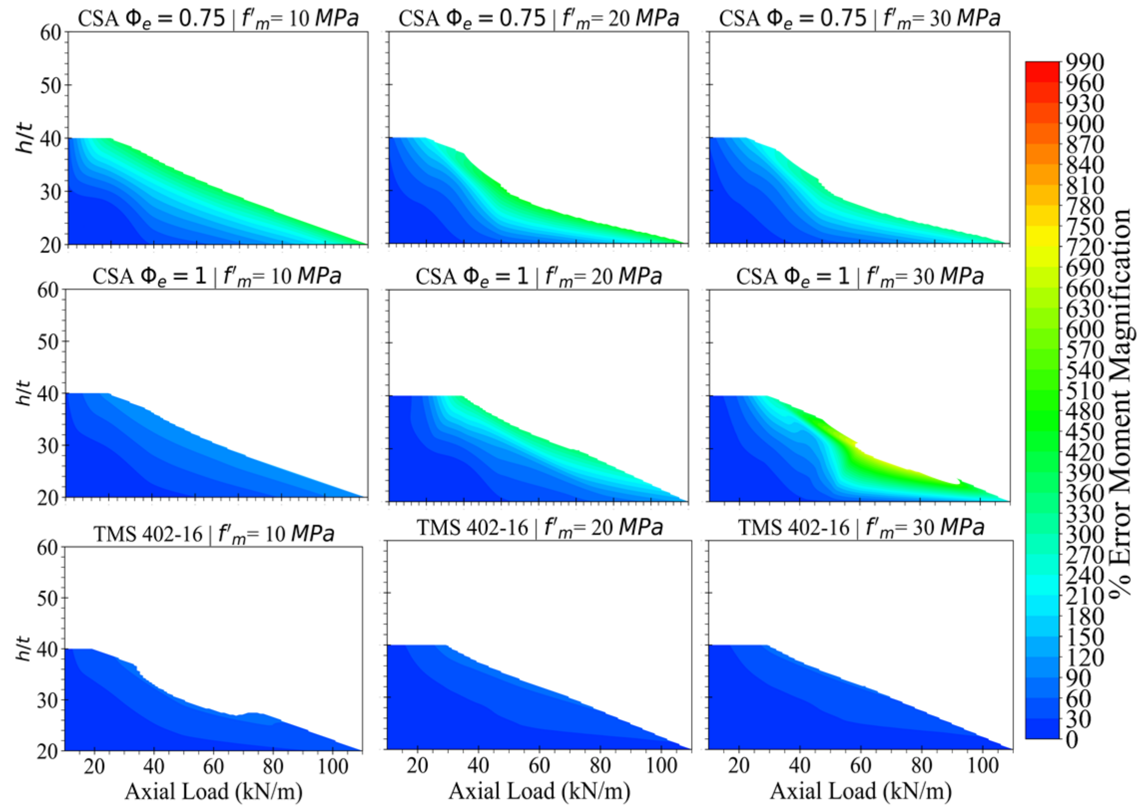

Figure 5.34 – Set A. Percentage of error in Moment Magnification factors. Partially ρ=0.35%

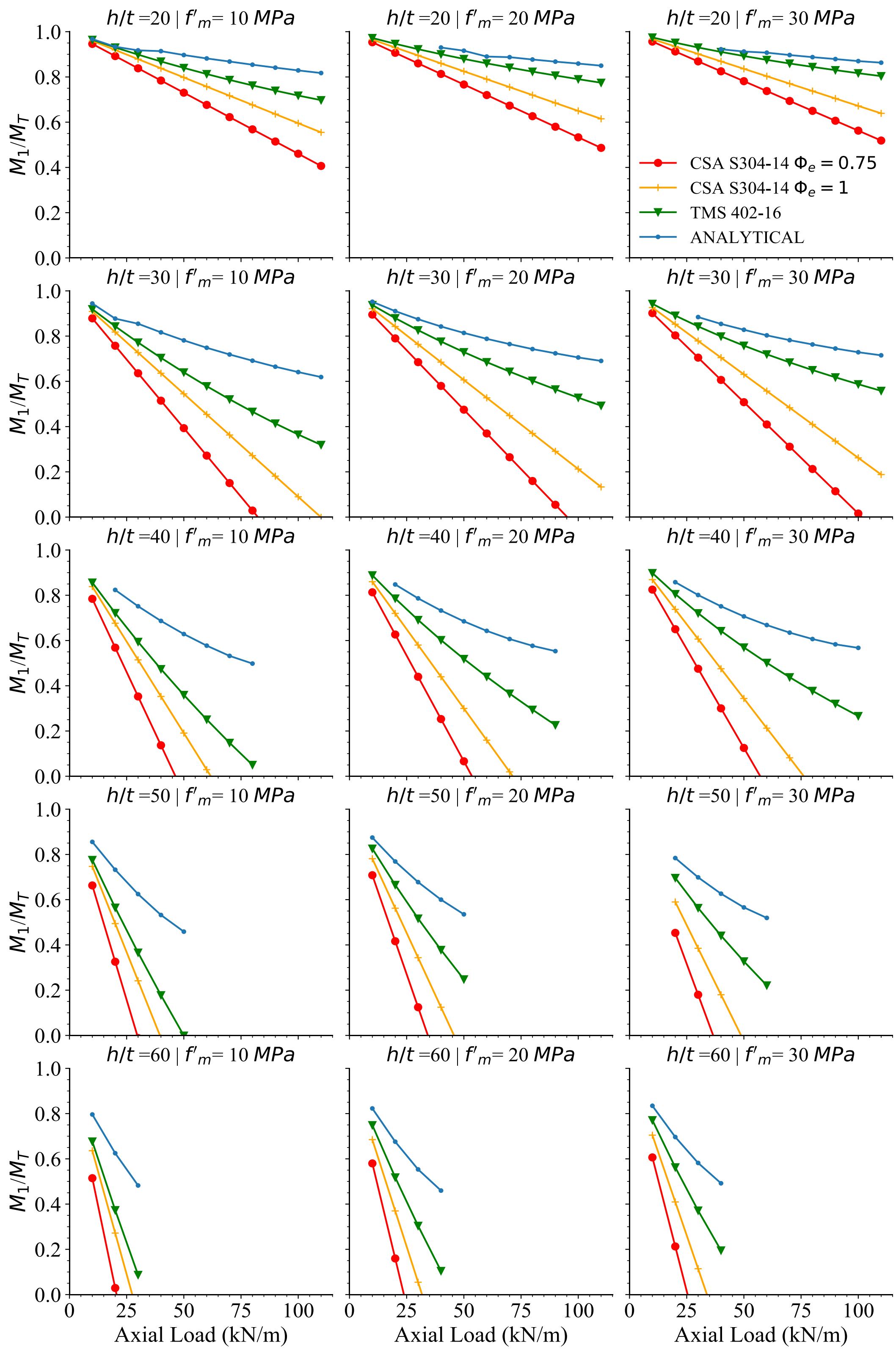

Figure 5.35 – Set B. M1/Mt vs Axial Load. Partially grouted ρ=0.35%

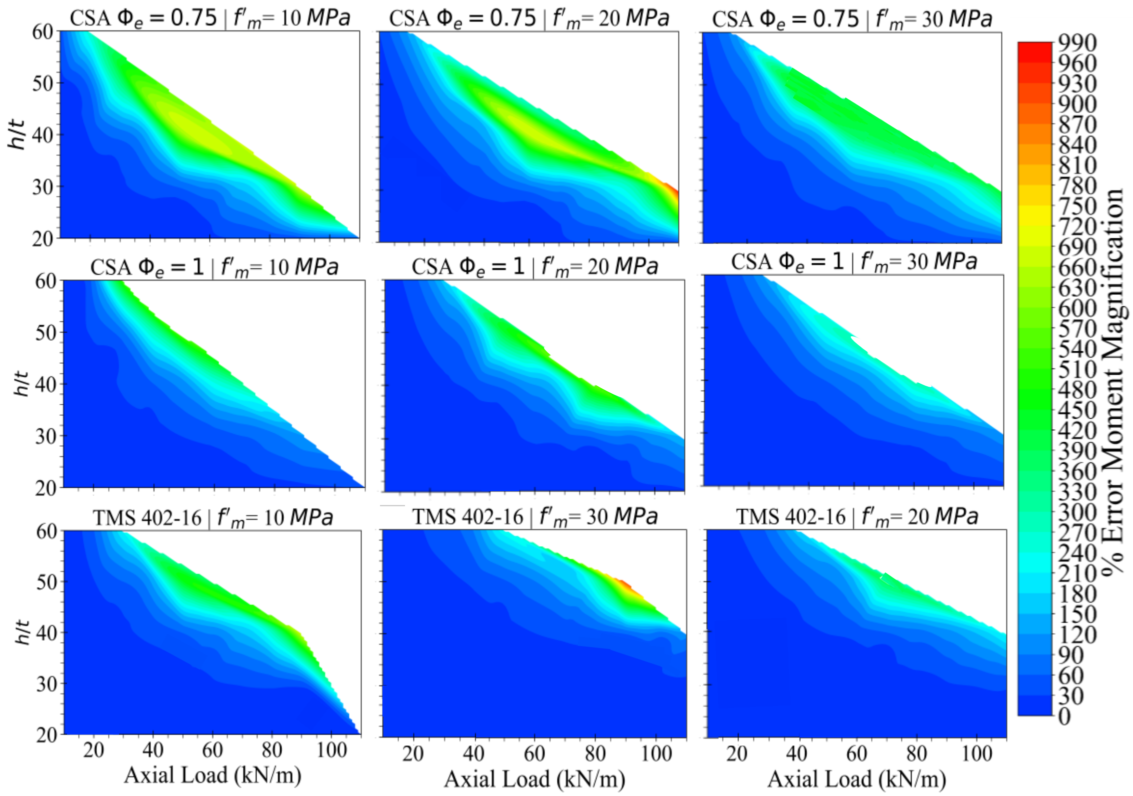

Figure 5.36 – Set A. Percentage of error in Moment Magnification factors. Partially ρ=0.52%

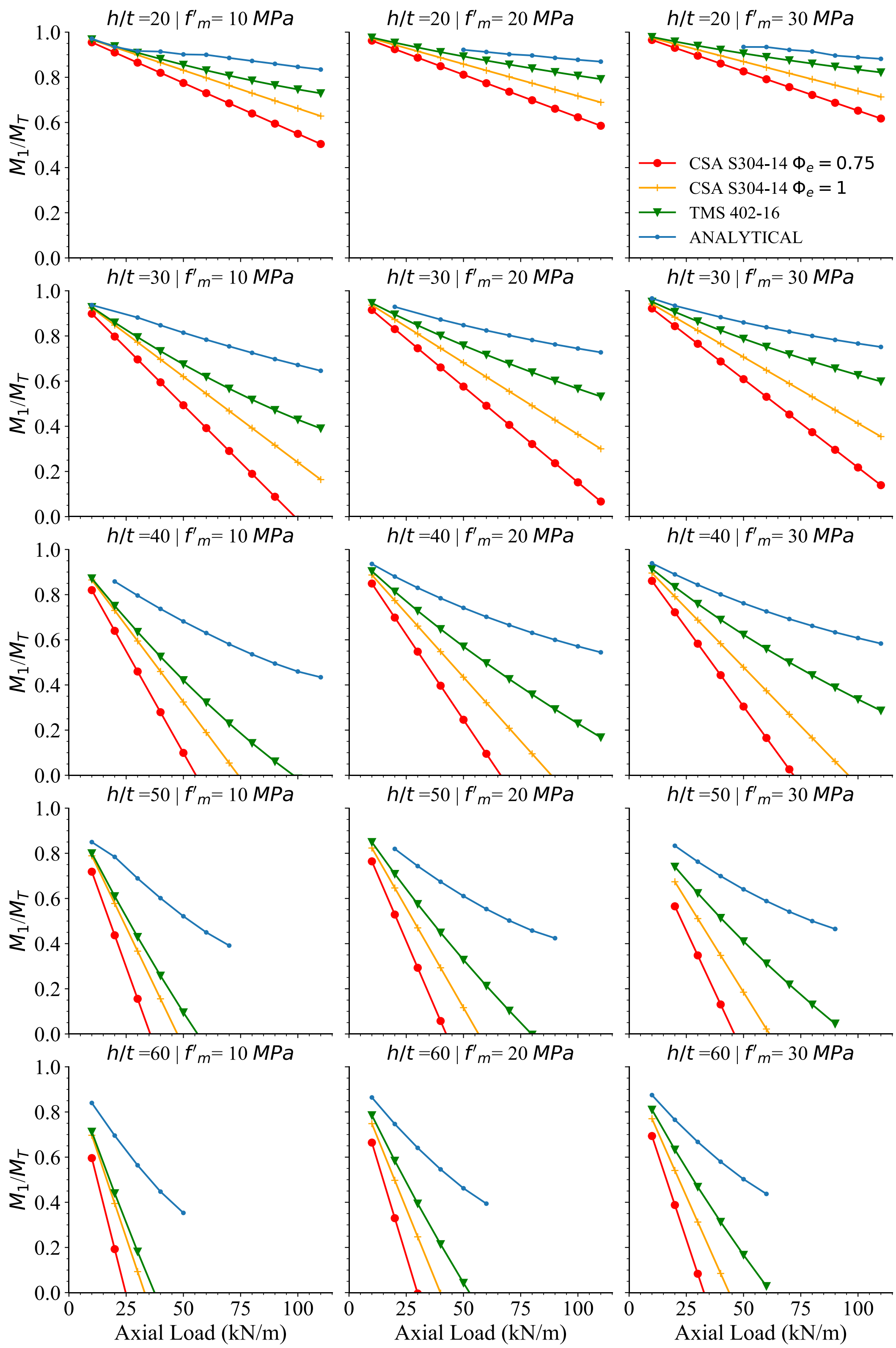

Figure 5.37 – Set B. M1/Mt vs Axial Load. Partially grouted ρ=0.52%

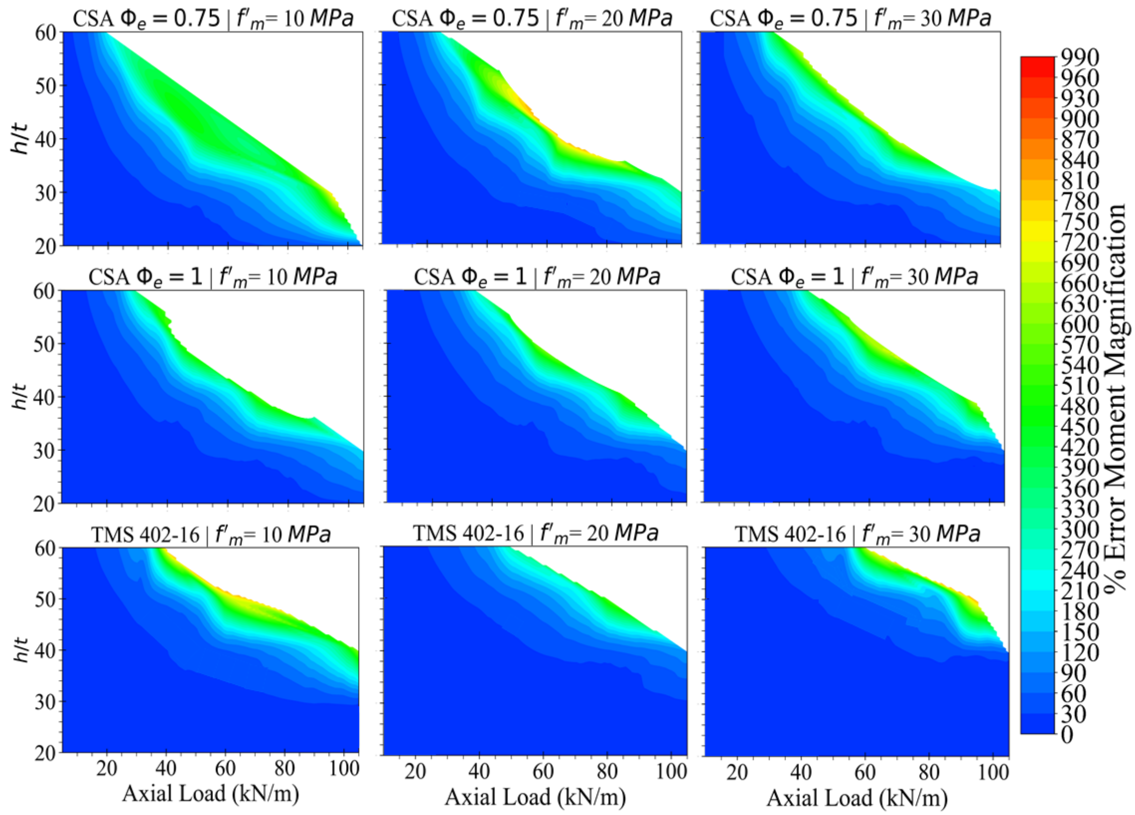

Figure 5.38 – Set A. Percentage of error in Moment Magnification factors. Fully grouted ρ=0.52%

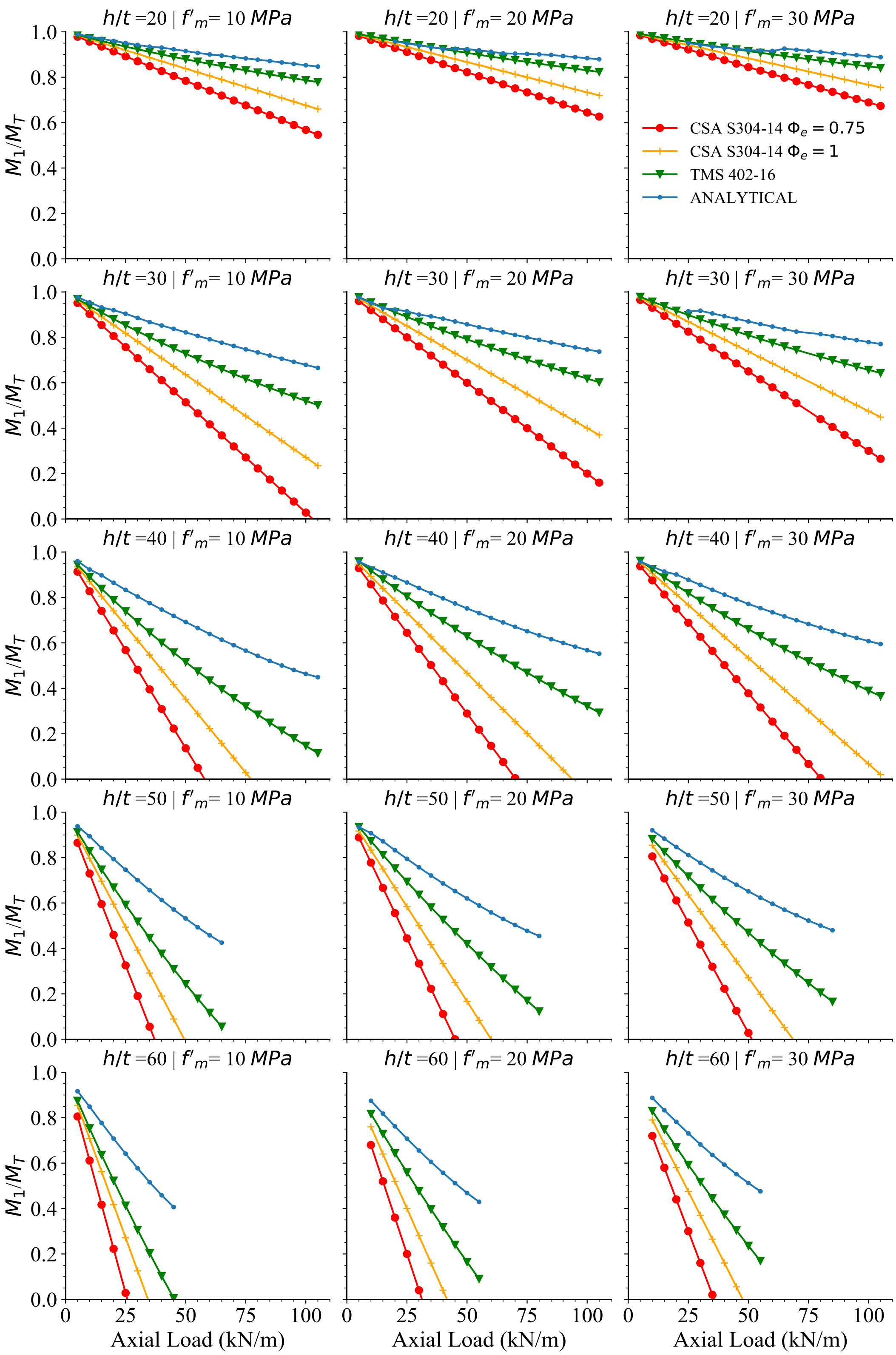

Figure 5.39 – Set B. M1/Mt vs Axial Load. Fully grouted ρ=0.52%

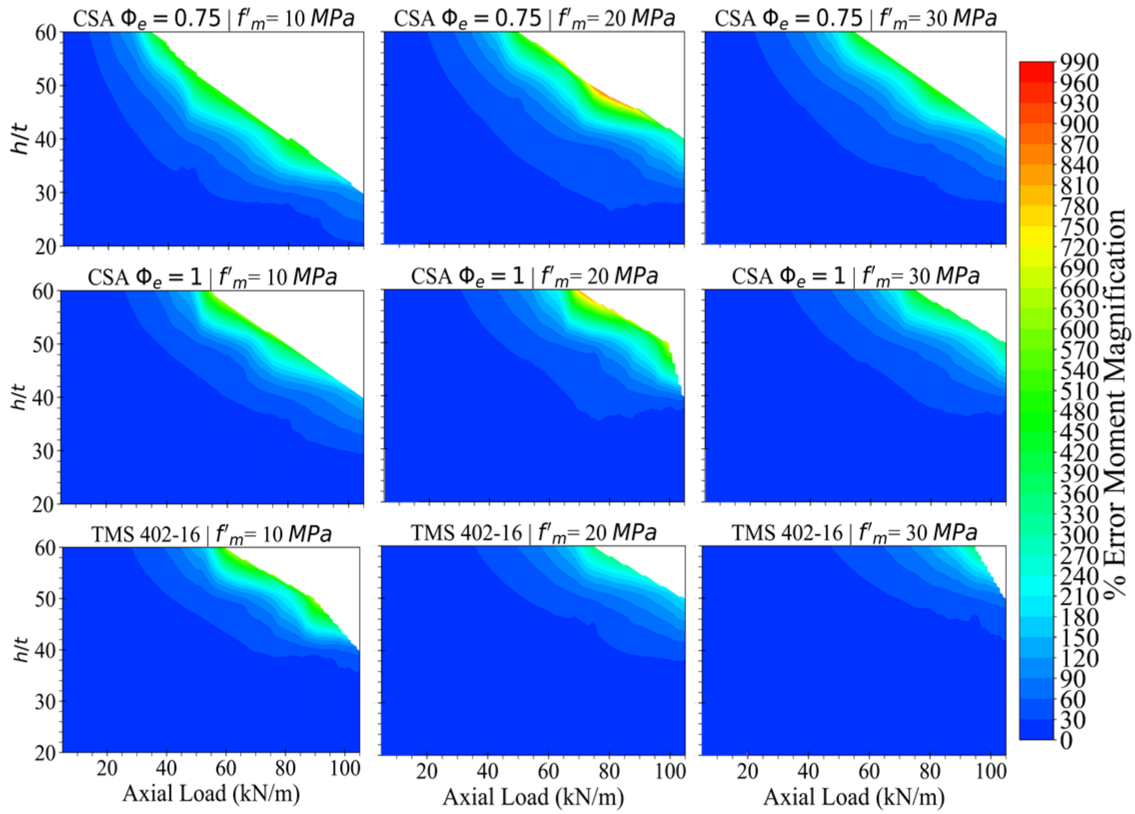

Figure 5.40 – Set A. Percentage of error in Moment Magnification factors. Fully grouted ρ =1.05%

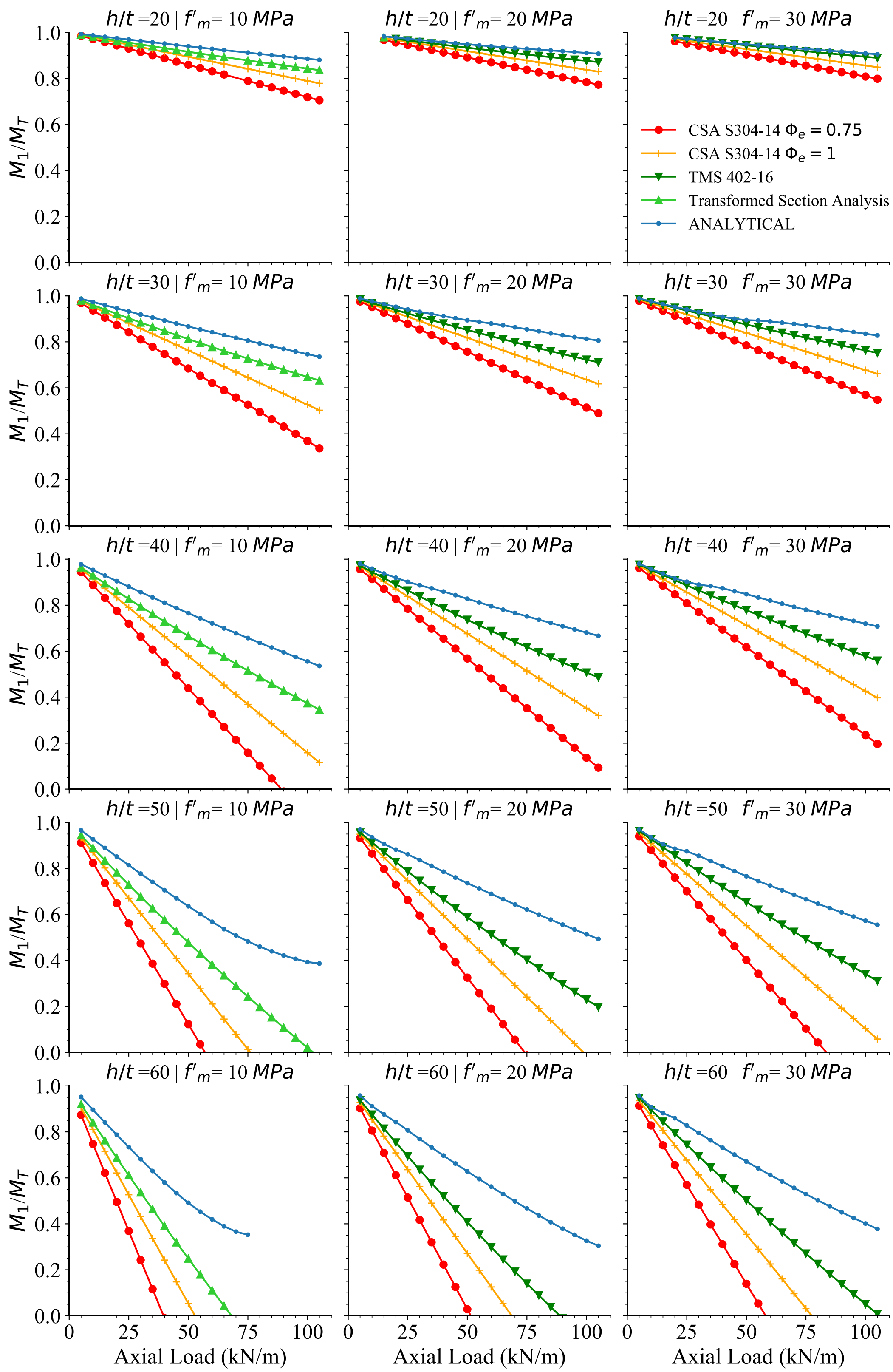

Figure 5.41 – Set B. M1/Mt vs Axial Load. Fully grouted ρ=1.05%

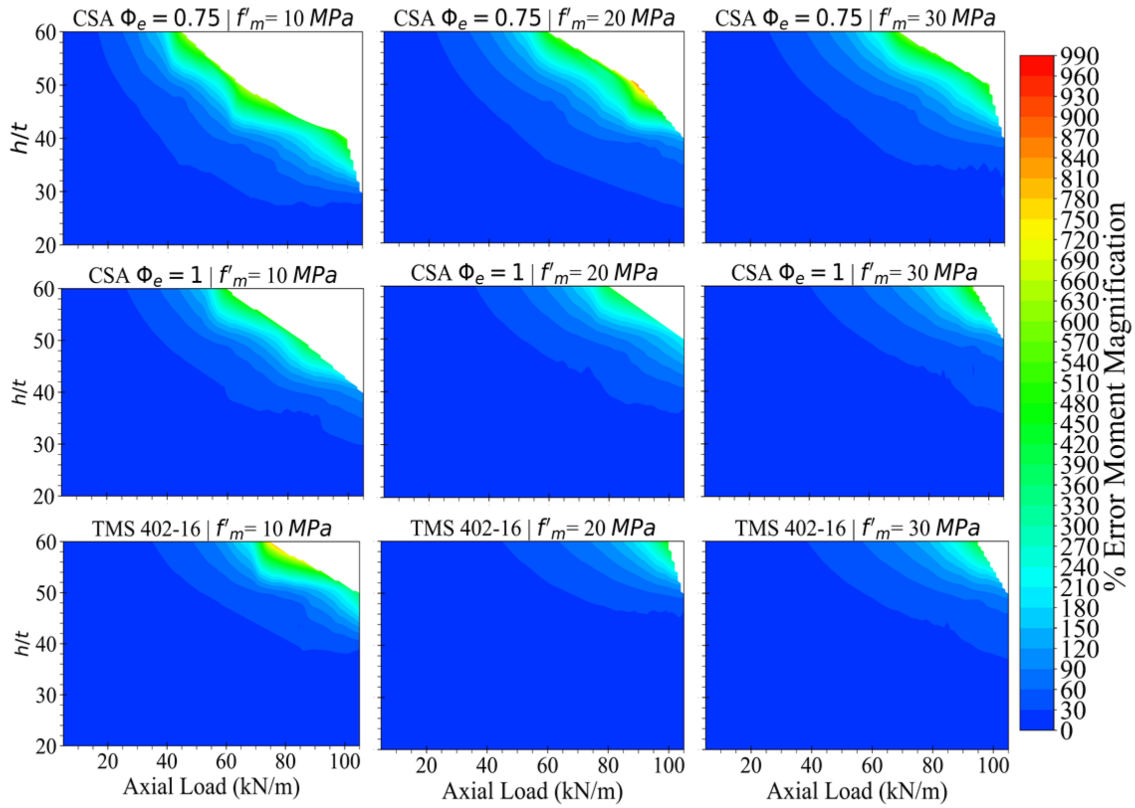

Figure 5.42 – Set A. Percentage of error in Moment Magnification factors. Fully grouted ρ =1.57%

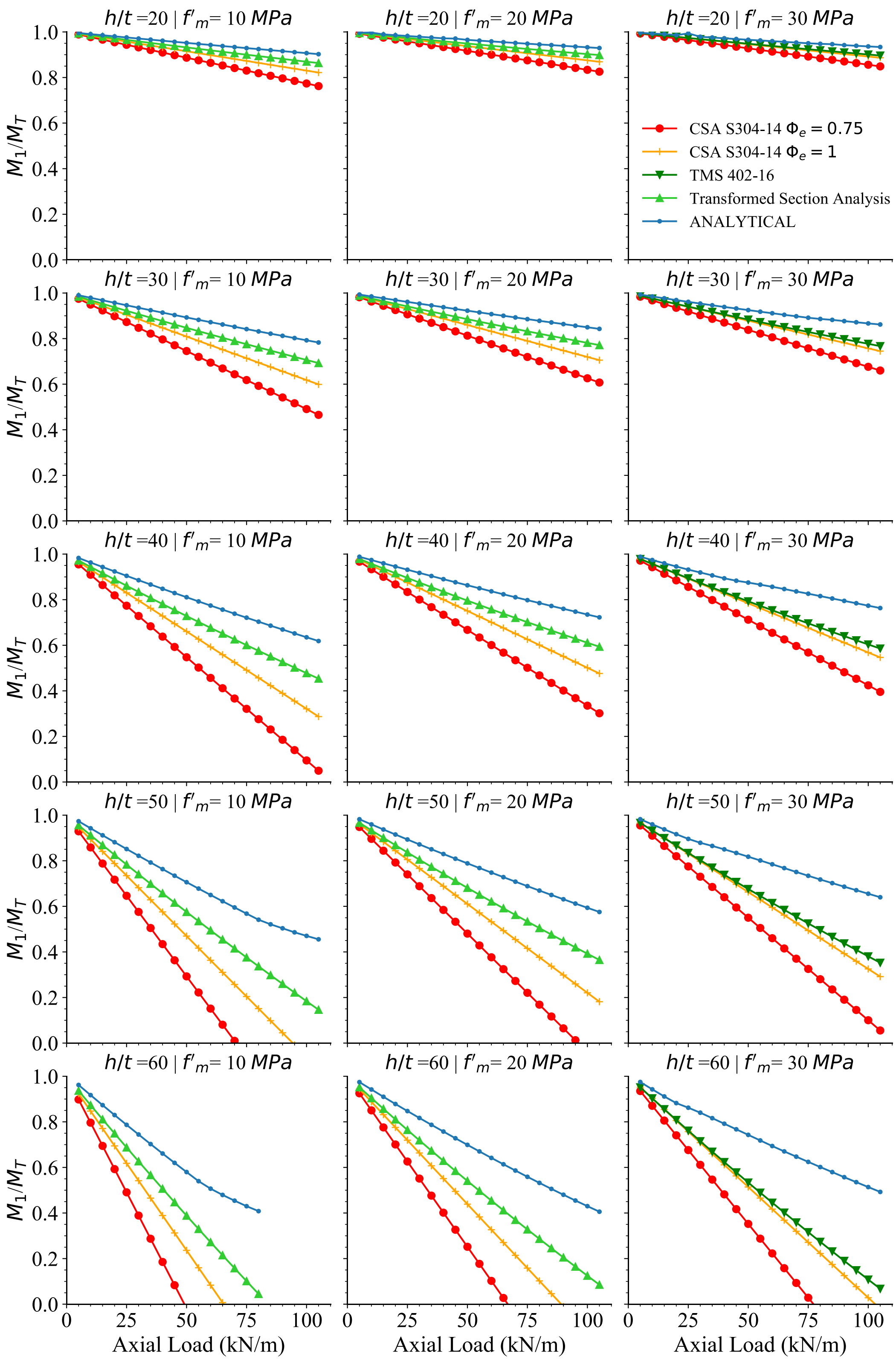

Figure 5.43 – Set B. M1/Mt vs Axial Load. Fully grouted ρ=1.57%

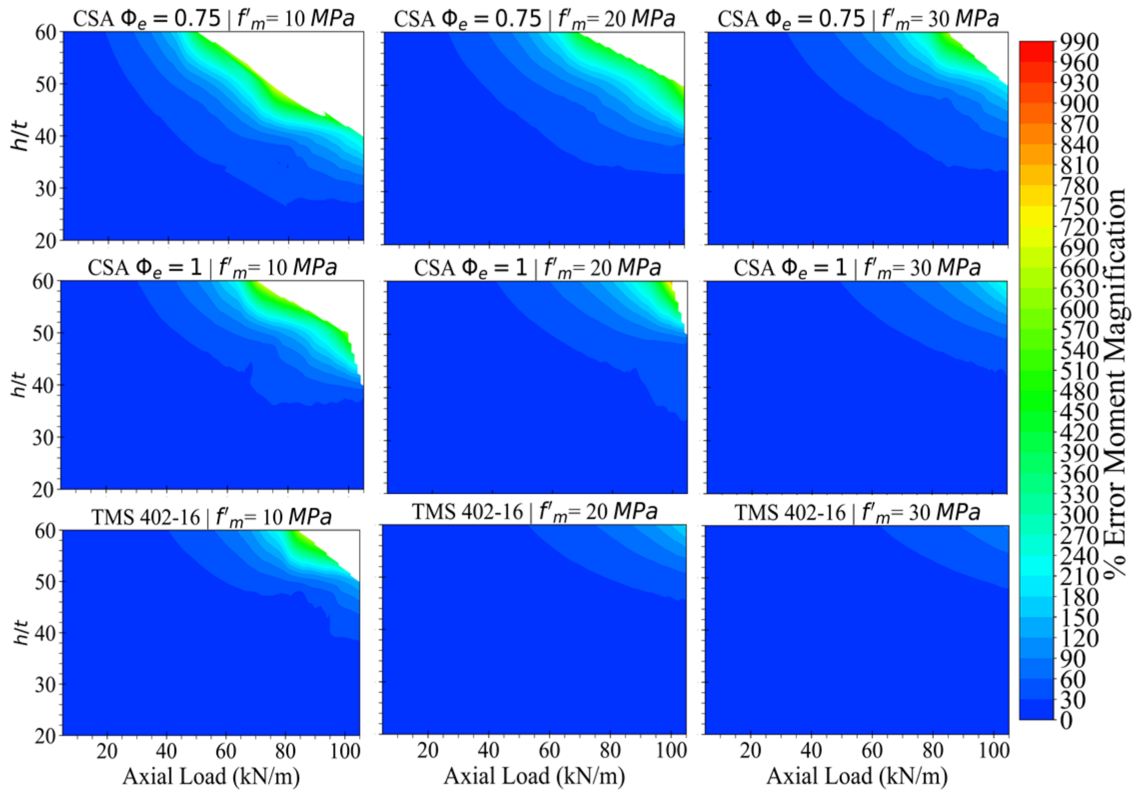

Figure 5.44 – Set A. Percentage of error in Moment Magnification factors. Fully grouted ρ =2.1%

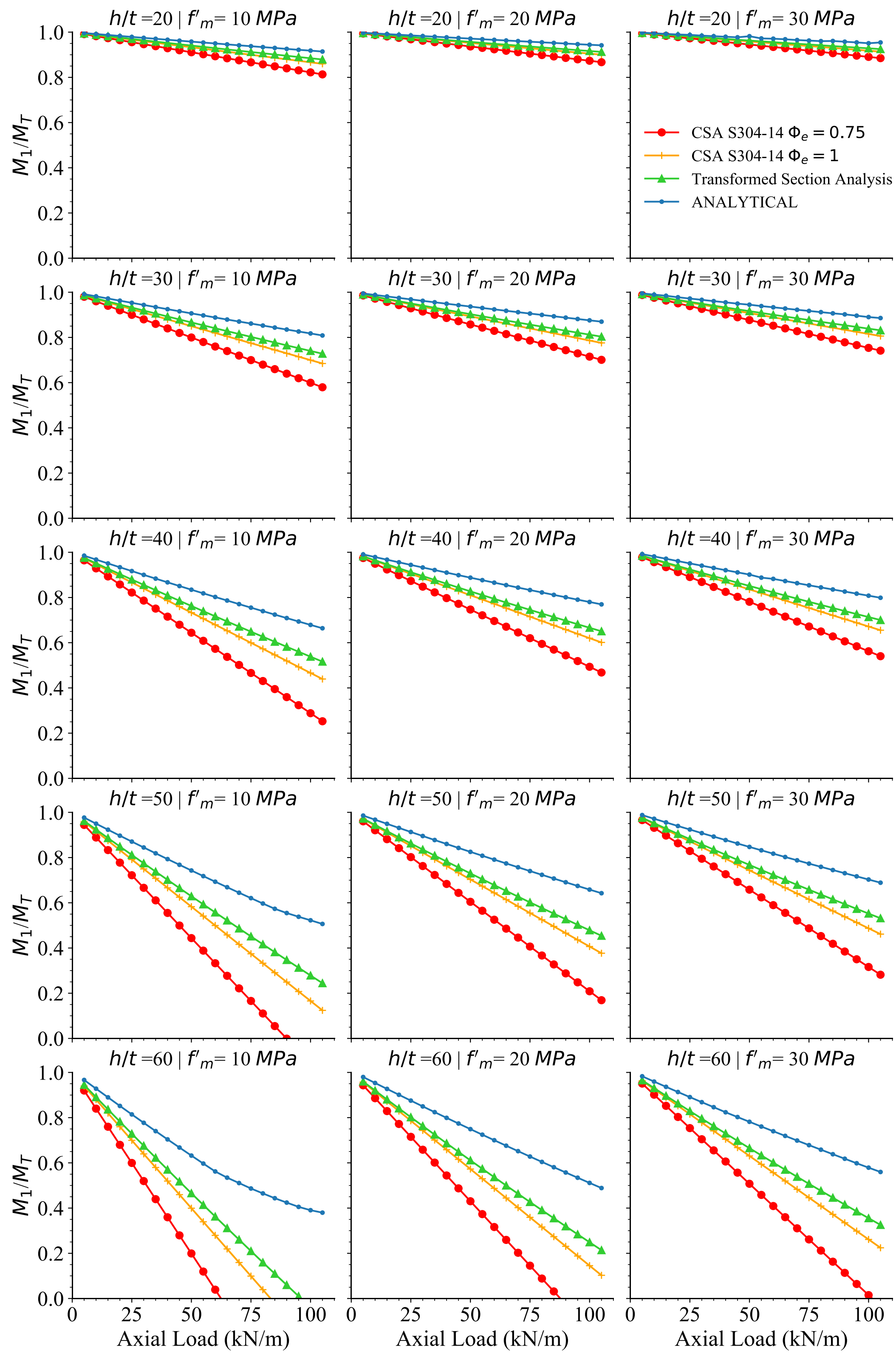

Figure 5.45 – Set B. M1/Mt vs Axial Load. Fully grouted ρ=2.1%

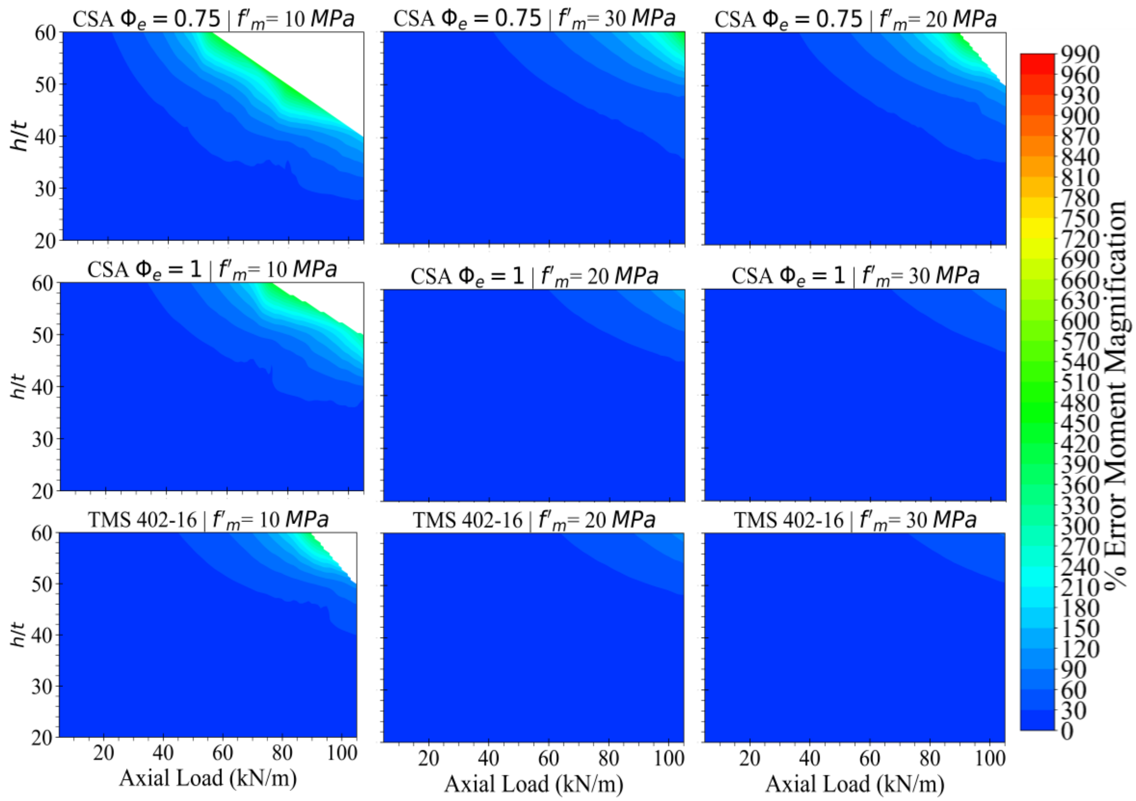

Figure 5.46 – Set A. Percentage of error in Moment Magnification factors. Fully grouted ρ =2.6%

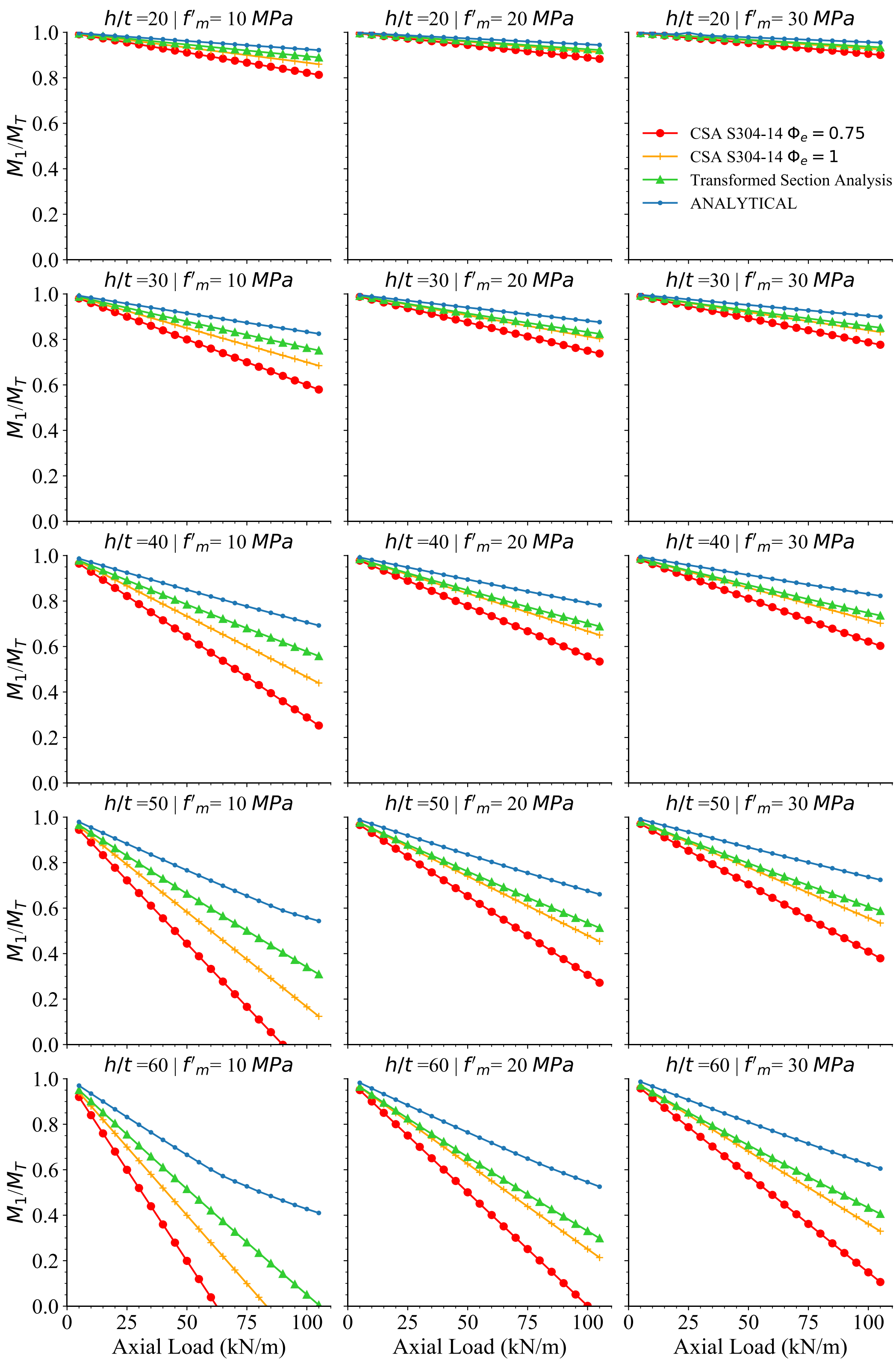

Figure 5.47 – Set B. M1/Mt vs Axial Load. Fully grouted ρ=2.6%

Throughout the discussion, it is important to consider that the percentage of error in the amplification factors should not only be attributed to inaccuracy of the standard equation in estimating the flexural rigidity of the element. This section evaluates the ability to calculate the second-order effects with the moment magnifier method using the effective stiffness expression proposed by each standard, but the method itself is not being evaluated.

From the set of figures A and B, it seems that the procedure described in CSA S304-14 is the most conservative. Neglecting the reduction factor $\emptyset_e$ has proven to improve the performance of the CSA S304-14 equation considerably. TMS 402-16 is the most viable solution within the group, however, the expression is only applicable for structures with reinforcement ratios lower than 1.8%. For higher reinforcement ratios, the percentage of error shown in the set of figure B attributed to TMS 402-16 are calculated using equations 5.2 and 5.3.

Gradual increment in the axial loading leads to an exponential rise in the percentage of error of the magnification effects computed using the North American standards. The moment magnification factor relies on the ratio between the applied axial load and the P_{cr} (P/P_{cr}). CSA S304-14 does not exhibit the influence of the axial loading in the calculation of the effective stiffness, consequently, the P_{cr} is only dependant on the mechanical properties of the cross-section, such as the amount of steel and the compressive strength (f_m'). While the axial loading is making the walls stiffer in the numerical model, the P_{cr} calculated using CSA S304-14 expression remains constant. TMS 402-16 considers a non-linear stress distribution and the interaction of the axial load in the flexural stiffness. Thus, the percentage of error is much lower compared to the CSA S304-14. While for trials under low axial forces (40 kN/m), the amplification factors from both standards are relatively similar, the difference grows exponentially for higher forces. To compare both standards, a reference point was selected. This point represents a fully grouted trial with a reinforcement ratio of 0.52%, a f_m' of 10 MPa, a slenderness ratio of 30, subjected to an axial load of 60 kN/m. Under these parameters, the magnification factor calculated using the CSA S304-14 is approximately 3.5 times higher than that of the numerical model, while the factor calculated using the TMS 402-16 is about 1.5 times bigger than that of the analytical response. This represents a relative difference of 133% between the CSA S304-14 and TMS 402-16 because of the axial load increment.

Additionally, it was found that the moment magnifier method was not applicable in some circumstances. For high axial loads, the P_{cr} calculated using CSA S304-14 exceeded the applied axial load in many circumstances where the numerical evaluation did not exhibit any instability issue. Consequently, an amplification factor cannot be calculated in cases where the failure mode is governed by material failure according to the numerical evaluation (i.g. $\frac{h}{t} = 30, \rho = 0.52\%, P = 50\ kN/m$). On the contrary, the P_{cr} calculated using TMS 402-16 was only exceeded in a few cases before the numerical model showed pronounce instability effects

In some trials, the percentage of error exceeded 900% (e.g. $\frac{h}{t} = 50, \rho = 1.26\%,\ P = 80\ kN/m$). Due to the nature of the moment magnifier method, for cases on which the P_{cr} calculated is closer to the applied load, the percentage of error tends to grow exponentially. Under these conditions, the error could be attributed to the compound effect related to the limitations of the moment magnifier method and the effectiveness of the equations to compute flexural rigidities.

The variation in slenderness ratio has a similar effect as the axial loading in the percentage of error. In both sets of figures, it was shown that the rate of error grows exponentially as the height-to-thickness ratio is increased. A higher slenderness ratio reduced the critical buckling load. Hence, the error induced in the moment amplification calculator increases. However, it appears that both standards are susceptible to the influence of slenderness by a similar margin. No significant discrepancy was found in the relative difference in the percentage of error between the standards compared to the numerical model when the height of the structure was varied.

The percentage of error in the moment amplifications are reduced when higher compressive strengths (f'_m) are used. This statement applies to both standards. TMS 402-

16 seems to be more susceptible to the influence of this parameter. Chapter 4, section 4.3.3.4.4 showed that the effective stiffness is enhanced by higher compressive strength according to the expressions proposed in the standards. However, TMS 402-16 expression was more sensitive to the variation of this parameter (Fig 4.9). In the context of the error percentage, a deviation of 10 MPa reduced the error by up to 15% for CSA S304-14 amplifications compared to the analytical results. The same variation could decrease up to 30% of error in the factors computed using TMS 402-16.

At higher reinforcement ratios, the stiffness calculations appear to be more accurate in both countries. Therefore, the percentage of error in the amplification effects are lower. In Chapter 4 section 4.3.3.4.5, it was proven that the area of steel in the cross-section enhanced the OOP stiffness of the wallets. It was also shown that the rate of increment was proportionally in both standards. Increasing the reinforcement ratio by 0.5% decreases the percentage of error by up to approximately 50%, in slender structures (i.e. 30 *h/t*) subjected to high axial forces. It should be noted that the TMS 402-16 expression was only applicable for reinforcement ratios lower than 1.8%. For walls with a higher reinforcement area, the moment amplifications were computed using 5.2 and 5.3. Using the TMS 402-16 expression to calculate the moment magnification factors for reinforcement ratios higher than 1.8% would result in unconservative moment amplification. To some extent, the cracked moment of inertia calculated under this parameter exceeded the gross inertia even for sections with minimal axial forces.

Penalizing the flexural stiffness in CSA S304-14 by a reduction factor seems unnecessary. Although the factor intends to predict any uncertainties, the degree of conservatism already inherent in the equation seems high enough so that the factor becomes unnecessary. The performance of the equation improved considerably when the factor was removed, mainly for short walls under low axial load. To some extent, amplification effects under low axial load levels were relatively close to those computed using TMS 402-16 .

All the above discussion is applicable for both partially and fully grouted elements, however, the percentage of error related with partially grouted trials appears to be more pronounced than in solid sections due to its lower gross moment of inertia and masonry area.

5.4.6.1 Range of Acceptable Results of the Moment Magnifier Method.

The previous sections showed that the error related to the moment magnification factors depends on the interaction between the axial loading, slenderness ratio, steel reinforcement, and compressive strength of the masonry. Therefore, selecting a range for which the moment magnifier method produces acceptable results is only possible if the interactions between the mentioned parameters are considered.

A threshold value of a percentage of error of 30% in the moment amplification factor is identified as an acceptable result, according to the author. This error is equivalent to amplifying the acting moment by 1.3 times more than it is required to compute the total moment of the element. The range of parameters on which the moment magnifier method would produce less than 30% of error are shown from Table 5.11 to Table 5.18. Combinations of parameters marked in the tables with an “O” represent scenarios with a lower or equal error than the threshold value selected.

Table 5.11 – Acceptable results. Partially grouted wall ρ = 0.175%

	h/t	Compressive Strength (f'_m)																	
		10 MPa						20 MPa						30 MPa					
CSA S304-14 ϕ_e=0.75	60																		
	50																		
	40																		
	30	O						O						O					
	20	O	O					O	O					O	O				
CSA S304-14 ϕ_e=1	60																		
	50																		
	40	O						O						O					
	30	O	O					O	O					O	O				
	20	O	O	O				O	O	O				O	O	O			
TMS 402-16	60																		
	50																		
	40	O						O	O					O	O				
	30	O	O					O	O					O	O				
	20	O	O	O				O	O	O	O	O		O	O	O	O		
	Axial Load kN/m	0	20	40	60	80	100	0	20	40	60	80	100	0	20	40	60	80	100

Table 5.12 – Acceptable results. Partially grouted wall ρ = 0.35%

	h/t	Compressive Strength (f'_m)																	
		10 MPa						20 MPa						30 MPa					
CSA S304-14 ϕ_e=0.75	60																		
	50							O						O					
	40	O						O						O					
	30	O	O					O	O					O	O				
	20	O	O					O	O	O				O	O	O			
CSA S304-14 ϕ_e=1	60							O						O	O				
	50	O						O						O	O				
	40	O	O					O	O					O	O				
	30	O	O	O				O	O	O				O	O	O			
	20	O	O	O	O			O	O	O	O			O	O	O	O	O	
TMS 402-16	60	O	O					O	O					O	O				
	50	O	O					O	O					O	O				
	40	O	O	O				O	O	O				O	O	O			
	30	O	O	O	O			O	O	O	O	O	O	O	O	O	O	O	O
	20	O	O	O	O	O	O	O	O	O	O	O	O	O	O	O	O	O	O
	Axial Load kN/m	0	20	40	60	80	100	0	20	40	60	80	100	0	20	40	60	80	100

Table 5.13 – Acceptable results. Partially grouted wall ρ = 0.52%

	h/t	Compressive Strength (f'_m)																	
		10 MPa						20 MPa						30 MPa					
CSA S304-14 ϕ_e=0.75	60																		
	50	O						O						O					
	40	O	O					O	O					O	O				
	30	O	O	O				O	O	O				O	O	O			
	20	O	O	O	O			O	O	O	O	O		O	O	O	O	O	
CSA S304-14 ϕ_e=1	60	O						O						O	O				
	50	O						O						O	O				
	40	O	O					O	O					O	O	O			
	30	O	O	O				O	O	O				O	O	O	O	O	
	20	O	O	O	O	O		O	O	O	O	O		O	O	O	O	O	O
TMS 402-16	60	O	O					O	O					O	O				
	50	O	O					O	O					O	O				
	40	O	O	O				O	O	O	O	O		O	O	O			
	30	O	O	O	O	O		O	O	O	O	O	O	O	O	O	O	O	O
	20	O	O	O	O	O	O	O	O	O	O	O	O	O	O	O	O	O	O
	Axial Load kN/m	0	20	40	60	80	100	0	20	40	60	80	100	0	20	40	60	80	100

Table 5.14 – Acceptable results. Fully grouted wall ρ = 0.52%

	h/t	Compressive Strength (f'_m)																	
		10 MPa						20 MPa						30 MPa					
CSA S304-14 ϕ_e=0.75	60	O						O						O					
	50	O						O						O					
	40	O	O					O	O					O	O				
	30	O	O	O				O	O	O				O	O	O			
	20	O	O	O	O			O	O	O	O			O	O	O	O		
CSA S304-14 ϕ_e=1	60	O						O						O	O				
	50	O	O					O	O					O	O				
	40	O	O					O	O					O	O				
	30	O	O	O				O	O	O	O			O	O	O	O	O	
	20	O	O	O	O	O		O	O	O	O	O	O	O	O	O	O	O	O
TMS 402-16	60	O						O	O					O	O				
	50	O	O					O	O					O	O	O			
	40	O	O					O	O	O				O	O	O	O	O	O
	30	O	O	O	O	O	O	O	O	O	O	O	O	O	O	O	O	O	O
	20	O	O	O	O	O	O	O	O	O	O	O	O	O	O	O	O	O	O
	Axial Load kN/m	0	20	40	60	80	100	0	20	40	60	80	100	0	20	40	60	80	100

Table 5.15 – Acceptable results. Fully grouted wall ρ = 1.05%

	h/t	Compressive Strength (f'_m)																	
		10 MPa						20 MPa						30 MPa					
CSA S304-14 ϕ_e=0.75	60	O						O	O					O	O				
	50	O	O					O	O					O	O				
	40	O	O					O	O	O				O	O	O			
	30	O	O	O				O	O	O	O	O		O	O	O	O	O	O
	20	O	O	O	O	O	O	O	O	O	O	O	O	O	O	O	O	O	O
CSA S304-14 ϕ_e=1	60	O	O					O	O					O	O				
	50	O	O					O	O	O				O	O	O			
	40	O	O	O				O	O	O	O			O	O	O	O		
	30	O	O	O	O	O	O	O	O	O	O	O	O	O	O	O	O	O	O
	20	O	O	O	O	O	O	O	O	O	O	O	O	O	O	O	O	O	O
TMS 402-16	60	O	O					O	O	O				O	O	O			
	50	O	O					O	O	O				O	O	O	O		
	40	O	O	O				O	O	O	O	O	O	O	O	O	O	O	O
	30	O	O	O	O	O	O	O	O	O	O	O	O	O	O	O	O	O	O
	20	O	O	O	O	O	O	O	O	O	O	O	O	O	O	O	O	O	O
	Axial Load kN/m	0	20	40	60	80	100	0	20	40	60	80	100	0	20	40	60	80	100

Table 5.16 – Acceptable results. Fully grouted wall ρ = 1.57%

	h/t	Compressive Strength (f'_m)																	
		10 MPa						20 MPa						30 MPa					
CSA S304-14 ϕ_e=0.75	60	O	O					O	O					O	O				
	50	O	O					O	O	O				O	O				
	40	O	O	O				O	O	O	O	O		O	O	O	O		
	30	O	O	O	O			O	O	O	O	O	O	O	O	O	O	O	O
	20	O	O	O	O	O	O	O	O	O	O	O	O	O	O	O	O	O	O
CSA S304-14 ϕ_e=1	60	O	O					O	O	O				O	O	O			
	50	O	O	O	O			O	O	O	O			O	O	O	O	O	
	40	O	O	O	O			O	O	O	O	O	O	O	O	O	O	O	O
	30	O	O	O	O	O	O	O	O	O	O	O	O	O	O	O	O	O	O
	20	O	O	O	O	O	O	O	O	O	O	O	O	O	O	O	O	O	O
TMS 402-16	60	O	O	O				O	O	O	O			O	O	O	O		
	50	O	O	O				O	O	O	O			O	O	O	O	O	
	40	O	O	O	O	O	O	O	O	O	O	O	O	O	O	O	O	O	O
	30	O	O	O	O	O	O	O	O	O	O	O	O	O	O	O	O	O	O
	20	O	O	O	O	O	O	O	O	O	O	O	O	O	O	O	O	O	O
	Axial Load kN/m	0	20	40	60	80	100	0	20	40	60	80	100	0	20	40	60	80	100

Table 5.17 – Acceptable results. Fully grouted wall ρ = 2.19%

	h/t	Compressive Strength (f'_m)																	
		10 MPa						20 MPa						30 MPa					
CSA S304-14 ϕ_e=0.75	60	O	O					O	O					O	O				
	50	O	O					O	O	O				O	O				
	40	O	O	O				O	O	O	O	O		O	O	O	O		
	30	O	O	O	O			O	O	O	O	O	O	O	O	O	O	O	O
	20	O	O	O	O	O	O	O	O	O	O	O	O	O	O	O	O	O	O
CSA S304-14 ϕ_e=1	60	O	O					O	O	O				O	O	O			
	50	O	O	O	O			O	O	O	O			O	O	O	O	O	
	40	O	O	O	O			O	O	O	O	O	O	O	O	O	O	O	O
	30	O	O	O	O	O	O	O	O	O	O	O	O	O	O	O	O	O	O
	20	O	O	O	O	O	O	O	O	O	O	O	O	O	O	O	O	O	O
TMS 402-16	60	O	O	O				O	O	O	O			O	O	O	O		
	50	O	O	O				O	O	O	O			O	O	O	O	O	
	40	O	O	O	O	O	O	O	O	O	O	O	O	O	O	O	O	O	O
	30	O	O	O	O	O	O	O	O	O	O	O	O	O	O	O	O	O	O
	20	O	O	O	O	O	O	O	O	O	O	O	O	O	O	O	O	O	O
	Axial Load kN/m	0	20	40	60	80	100	0	20	40	60	80	100	0	20	40	60	80	100

Table 5.18 – Acceptable results. Fully grouted wall ρ = 2.63%

	h/t	Compressive Strength (f'_m)																	
		10 MPa						20 MPa						30 MPa					
CSA S304-14 ϕ_e=0.75	60	O	O					O	O	O				O	O				
	50	O	O					O	O	O				O	O	O			
	40	O	O	O				O	O	O	O	O		O	O	O	O	O	
	30	O	O	O	O	O		O	O	O	O	O	O	O	O	O	O	O	O
	20	O	O	O	O	O	O	O	O	O	O	O	O	O	O	O	O	O	O
CSA S304-14 ϕ_e=1	60	O	O					O	O	O				O	O	O			
	50	O	O	O	O			O	O	O	O	O		O	O	O	O	O	
	40	O	O	O	O			O	O	O	O	O	O	O	O	O	O	O	O
	30	O	O	O	O	O	O	O	O	O	O	O	O	O	O	O	O	O	O
	20	O	O	O	O	O	O	O	O	O	O	O	O	O	O	O	O	O	O
TMS 402-16	60	O	O	O				O	O	O	O			O	O	O	O		
	50	O	O	O	O			O	O	O	O	O	O	O	O	O	O	O	O
	40	O	O	O	O	O	O	O	O	O	O	O	O	O	O	O	O	O	O
	30	O	O	O	O	O	O	O	O	O	O	O	O	O	O	O	O	O	O
	20	O	O	O	O	O	O	O	O	O	O	O	O	O	O	O	O	O	O
	Axial Load kN/m	0	20	40	60	80	100	0	20	40	60	80	100	0	20	40	60	80	100

5.4.7 Regression Analysis.

5.4.7.1 Regression analysis for the prediction of the effective stiffness calculated from the strain profile according to the numerical model.

This section explores the capacity of developing an equation to calculate the effective stiffness of RMWS through multilinear regression analysis. The data set was created using the numerical simulations shown in the previous sections. The effective stiffness was calculated at ultimate load, which represents the maximum lateral load that could be applied at the structure before the push-over curves started to degrade. It was calculated as $\frac{M}{\emptyset} = EI_{eff}$. The curvature was calculated from the strain profiles by dividing the masonry strain at ultimate load over the depth of the neutral axis $(\phi = \frac{\varepsilon_m}{c})$. The depth of the compressive masonry block was calculated assuming that plane sections remained plane.

Only data points from the fully grouted trials were used in this analysis. The regression analyses were conducted using the *Sklearn* library available in the computer language "Python". From multiple analyses, the three most accurate alternatives are shown and discussed in this section. The total number of walls considered for the regression analysis was 1492. The training data was set to 30% of the total number of walls.

The performance of the proposed equations is graphically shown in Fig. 5.48 and in subsequent plots of predicted effective stiffness (From the regression analysis) against the analytical effective stiffness (From the numerical evaluation). The red line is the ideal scenario, where the predicted stiffness is equal to the analytical stiffness. Both the training and the testing data are plotted. Any point above the red line overestimates the effective stiffness, while points below this line are conservative results. The closer the points to the red line, the better is the performance of the model. As performance indicators the RMSE was selected as a measure of precision and the ME as a measure of bias, while the $E_mEI_{eff\ (predicted)}/E_mEI_{eff\ (analytical)}$ ratios as a measure of accuracy.

The first linear regression model present is the simplest within the group MLR1. A single equation is proposed to estimate the flexural rigidity for all the reinforcement ratios evaluated.

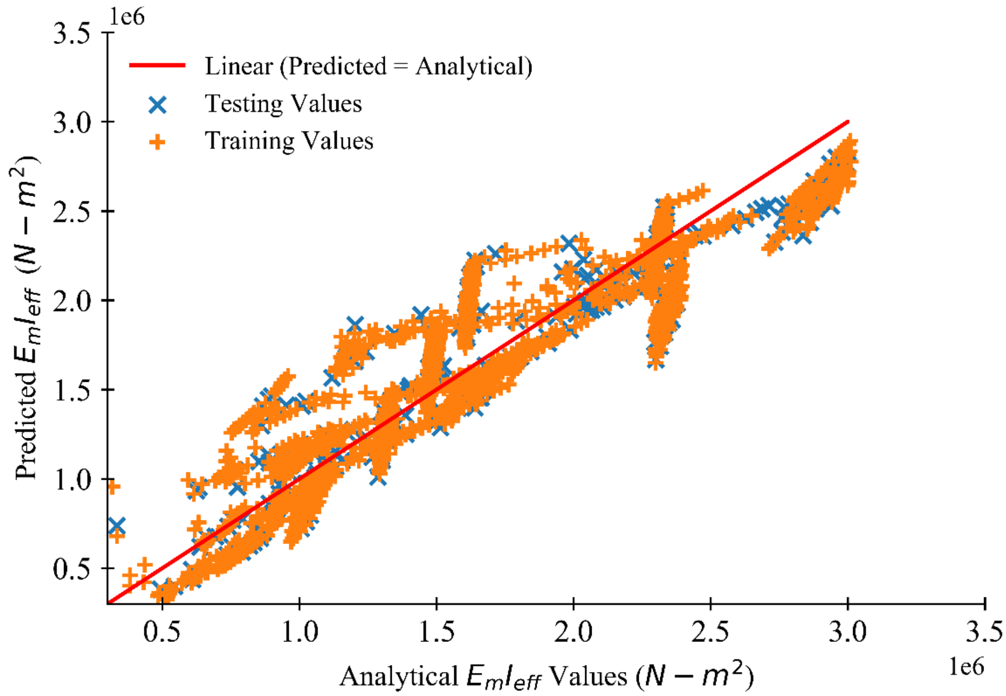

Figure 5.48 - Regression plot. Multilinear Regression 1 (MLR1).

$$E_m I_{eff} = 3505.64P + 611.717A_s + 28517.94f'_m + 5616.90\left(\frac{h}{t}\right) - 498664.35 \quad \text{MLR1}$$

Where P is the axial load in kN, As represents the total areal of steel in mm^2, f'_m is the grouted compressive prism strength in MPa, and $\frac{h}{t}$ is the height-thickness ratio. $E_m I_{eff}$ is expressed in $N - m^2$.

The performance indicator from the MLR1, is shown in Table 5.19.

Table 5.19 – Performance Indicator MLR1

	Indicator	Value
	$\mathbf{R^2}$	0.88
	RMSE $(\boldsymbol{N - m^2})$	213371.19
	ME $(\boldsymbol{N - m^2})$	42499.63
$\frac{E_m I_{eff}(Predicted)}{E_m I_{eff}(Analytical)}$	Average	1.039
	Min	0.64
	Max	1.54
	St. Dev	0.14

It was shown in section 5.4.5 that structures with lower reinforcement ratios exhibit yielding of the rebars at the ultimate load. Considering the ductility effects, a more complicated alternative is proposed as MLR2. Two equations are presented, which are conditioned by the reinforcement ratio. The regression plot is shown Fig. 5.49.

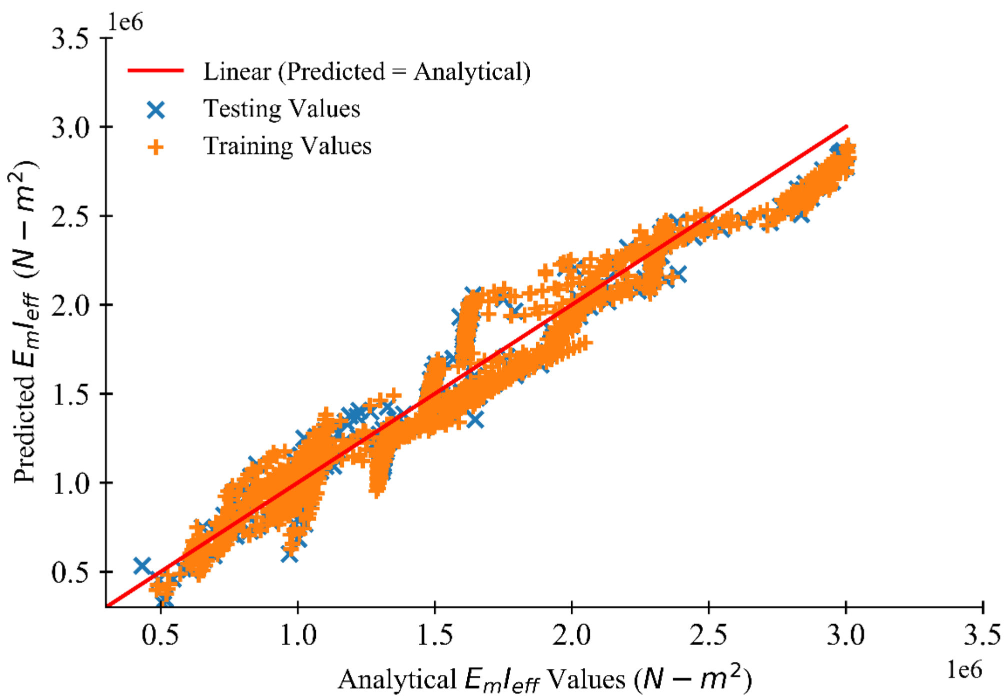

Figure 5.49 - Regression plot. Multilinear Regression 2 (MLR2)

$$E_m I_{eff} = 5607.70P + 505.93As + 10960.11f'_m + 10199.11\left(\frac{h}{t}\right) - 211274.16 \qquad For\ \rho < 1.5$$

MLR2

$$E_m I_{eff} = 2812.55P + 599.40As + 38155.99f'_m + 4456.93\left(\frac{h}{t}\right) - 582060.06 \qquad For\ \rho \geq 1.5$$

Where P is the axial load in kN, As represents the total areal of steel in mm^2, f'_m is the grouted compressive prism strength in MPa, and $\frac{h}{t}$ is the height-thickness ratio. $E_m I_{eff}$ is expressed in $N - m^2$.

The performance indicator from the MLR2, is shown in Table 5.20.

Table 5.20 – Performance Indicator MLR2

Indicator		Value
$\mathbf{R^2}$		0.91
RMSE ($N - m^2$)		182415.55
ME ($N - m^2$)		26725
$\frac{E_m I_{eff}(Predicted)}{E_m I_{eff}(Analytical)}$	Average	1.016
	Min	0.75
	Max	1.52
	St. Dev	0.11

The non-linear evolution of the effective stiffness is impossible to describe perfectly using a multi-linear regression. Therefore, the possibility of adding polynomial coefficients to the equations is explored, and the results of a polynomial regression (PR1) are shown in Fig. 5.50.

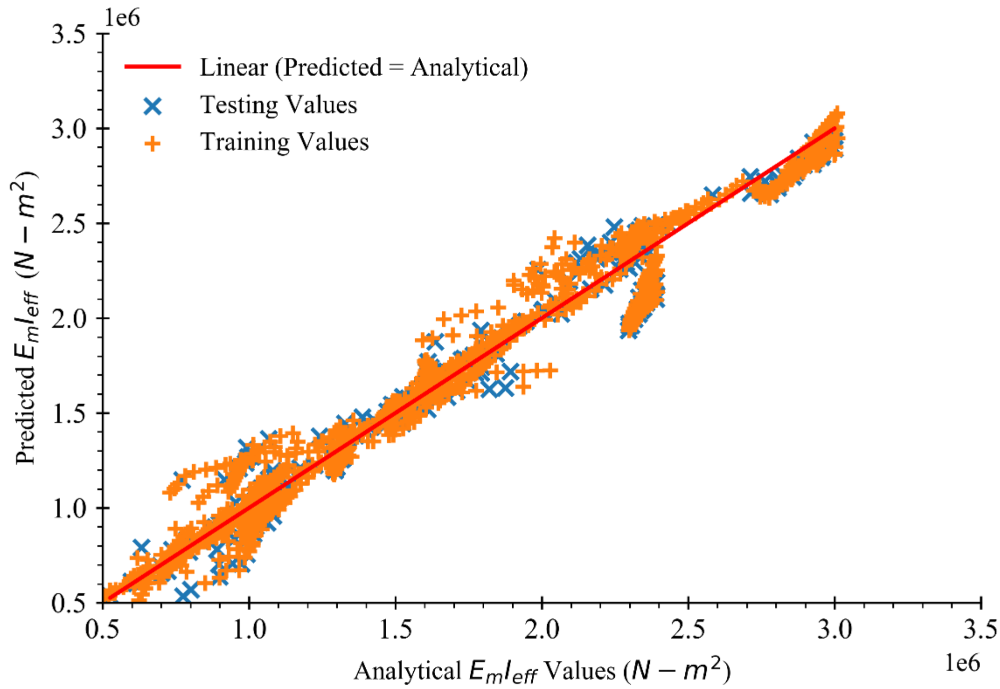

Figure 5.50 - Regression plot. Polynomial Regression (PR1).

$$\begin{aligned} E_m I_{eff} = {} & 1661.14P + 578.68As - 32785.13f'_m + 108.91\left(\frac{h}{t}\right) \\ & - 6.34Al^2 - 1.56PAs + 150.48Alf'_m + 58P\left(\frac{h}{t}\right) \\ & - 0.044As^2 + 20.61Asf'_m - 3.79As\left(\frac{h}{t}\right) - 1358.29f'_m \\ & - 5884655.41 \end{aligned} \tag{4.4}$$

Where P is the axial load in kN, As represents the total areal of steel in mm^2, f'_m is the grouted compressive prism strength in MPa, and $\frac{h}{t}$ is the slenderness ratio. $E_m I_{eff}$ is expressed in $N - m^2$

The performance indicators from the PR1, are shown in Table 5.21.

Table 5.21 – Performance Indicator PR1

Indicator		Training
$\mathbf{R^2}$		0.95
RMSE $(\boldsymbol{N-m^2})$		127912.20
RMSE $(\boldsymbol{N-m^2})$		-3726.97
$\boldsymbol{E_m I_{eff}(predicted)} / \boldsymbol{E_m I_{eff}(analyical)}$	Average	1.01
	Min	0.46
	Max	1.25
	St. Dev	0.11

5.4.7.1.1 Discussion

The three alternatives have shown a moderate level of accuracy and precision based on the interpretation of the author. MLR2 has been identified as the most optimal solution. MLR1 is the simplest expression but is highly outperformed by the other regressions. PR1 is a single and precise equation, but it requires 12 coefficients, which might not be feasible for designers.

The R^2 value from MLR2 indicates an excellent correlation, however, it is not a reliable performance indicator. The ME is relatively low, considering the units and the max and min values of the effective stiffness used for the analysis, which indicates a low bias. The average $E_m I_{eff\ (predicted)} / E_m I_{eff\ (analytical)}$ is close to 1, which is another factor that indicates high accuracy. A low standard deviation suggests a relatively small spread of the estimated values. However, it is difficult to interpret the RMSE and ME values without references to compare. Therefore, the same indicators are calculated for the North American expressions for the same range of parameters used in the regression analysis.

5.4.7.2 Performance indicator of current North American equations

Performance indicators and plots based on the same data set used in the regression analysis are provided for the North American Standards. Fig. 5.51 shows the performance plot for the equation recommended by the Canadian Standard (CSA S304-14). The reduction factor $\emptyset_e$ is included. The performance indicators are summarized in Table 5.22.

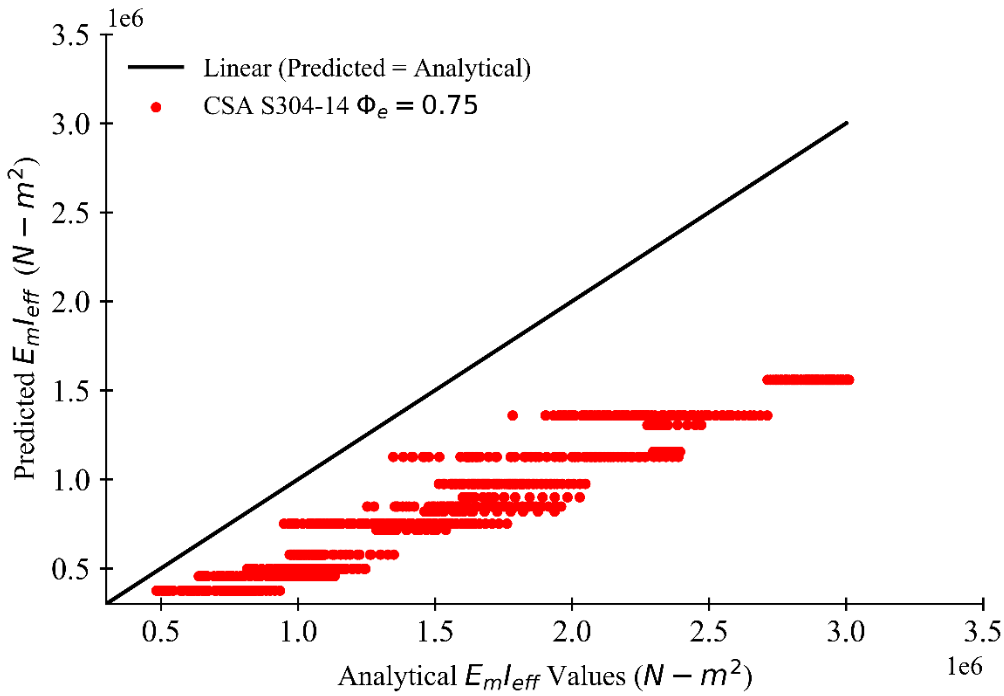

Figure 5.51 - Regression plot CSA S304-14 $\emptyset_e = 0.75$.

Table 5.22 – Performance Indicator CSA S304-14 $\emptyset_e = 0.75$.

Indicator		**Results**
R^2		0.86
RMSE $(N - m^2)$		819372.087
RMSE $(N - m^2)$		760327.57
$\frac{E_m I_{eff}(analyical)}{E_m I_{eff}(predicted)}$	Average	1.84
	Min	1.19
	Max	2.50
	St. Dev	0.20

In section 5.4.6, it was shown that the degree of conservatism added by using a reduction factor was unnecessary. The performance indicators for the Canadian expression neglecting the reduction factors are also calculated for comparison purposes. Fig. 5.52 shows the performance plot for CSA S304-14 $\emptyset_e = 1$. The indicators are summarized in Table 5.23.

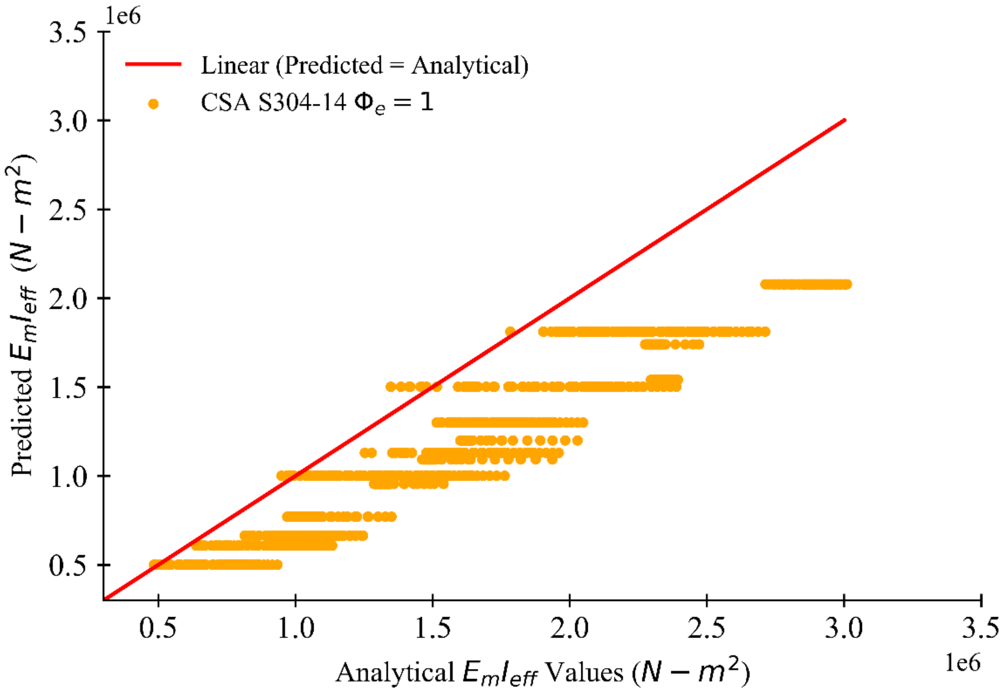

Figure 5.52 - Regression plot CSA S304-14 $\emptyset_e = 1$.

Table 5.23 – Performance Indicator CSA S304-14 $\emptyset_e = 1$.

Indicator		Results
$\mathbf{R^2}$		0.88
RMSE $(N - m^2)$		500696.82
RMSE $(N - m^2)$		452888.53
$\frac{E_m I_{eff}(analyical)}{E_m I_{eff}(predicted)}$	Average	1.3815
	Min	0.98
	Max	1.87
	St. Dev	0.15

The performance plot and indicators for the TMS 402-16 equation are shown in Fig. 5.53 and Table 5.24, respectively. These indicators were calculated using the expression from the TMS 402-16 to the applicable parameters and the transformed section analysis for cases on which the American procedure is not viable.

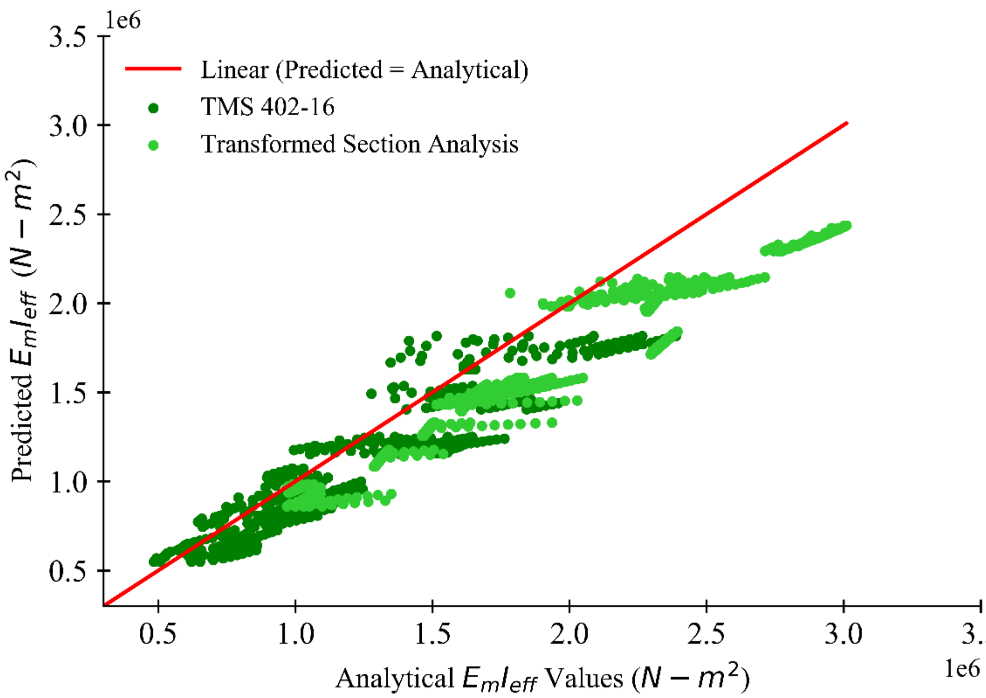

Figure 5.53 - Regression plot TMS 402-16 and Transformed Section Analysis.

Table 5.24 – Performance Indicator TMS 402-16 and Transformed Section Analysis.

Indicator		Results
R^2		0.89
RMSE $(N-m^2)$		296229.57
RMSE $(N-m^2)$		231403.76
$\frac{E_mI_{eff}(analytical)}{E_mI_{eff}(predicted)}$	Average	1.15
	Min	0.89
	Max	1.48
	St. Dev	0.11

5.4.7.2.1 Discussion and Comparison

All the indicators for the existent equations and the model developed are summarized in Table 5.25.

Table 5.25 – Comparison of performance indicators according to standards equation and regression analysis.

Equation	R^2	**RMSE** $(N-m^2)$	**ME** $(N-m^2)$	$\frac{E_m I_{eff\,analytical}}{E_m I_{eff\,predicted}}$ **Average**	**Std. Dev**
MLR1	0.88	213371.19	-42499.63	1.039	0.14
MLR2	0.91	182415.55	26725	1.016	0.11
PR1	0.95	127912.20	-3726.97	1.01	0.11
CSA S304-14 $\emptyset = 0.75$	0.86	819372.08	760327.57	1.84	0.20
CSA S304-14 $\emptyset = 1$	0.88	500696.82	452888.53	1.381	0.15
TMS 402-16	0.89	296229.57	231403.76	1.15	0.11

Of the existing equations, the TMS 402-16 alternative had the best performance. The average $E_m I_{eff\,(predicted)} / E_m I_{eff\,(analytical)}$ is close to 1, with a relatively low standard deviation, indicating low bias and a small spread of the calculated value. The RMSE value is 2.76 times lower than that of the CSA S304-14, and the ME is 3.23 times smaller, indicating a significantly lower bias and variance than its counterpart.

The CSA S304-14 equation had the worst performance within the group. The high values of RMSE and ME reflect higher bias and variance than any other equation. An average $E_m I_{eff\,(predicted)} / E_m I_{eff\,(analytical)}$ of 1.84 not only indicates deficient precision but also that the values are generally overestimated.

Neglecting the reduction factor proposed by CSA S304-14 appears to improve the performance of the equation by a significant margin. The average is closer to 1 compared to the results influenced by the $\emptyset_e$ factor. The RMSE and the ME were reduced by approximately 40%.

As illustrated in the regression plots and the min values of $E_m I_{eff_{(predicted)}} / E_m I_{eff_{(analytical)}}$ of the TMS 402-16 and CSA S304-14 expressions, there are some cases in which the effective stiffness calculated is higher than the stiffness obtained from the strain readings. Evaluating the data indicates that in these cases, the walls experienced a significant level of ductility. Thus, it is possible that calculating the rigidity of the wallets based on Euler Bernoulli's linear approximation is not the most reliable method under these circumstances.

All the regression models generated in this study vastly outperform the existing equations, as indicated by the performance indicators. The RMSE from the MLR2 is approximately 3.84 times lower than that of the CSA S304-14 equation and 1.62 times smaller than that of the TMS 402-16 equation. The ME is substantially smaller than any other existing equation. The performance plots and indicators demonstrate that the proposed equation MLR2 is an effective solution to compute effective stiffness values under the data set on which it was developed.

The M1/Mt vs Axial Load graphs shown in section 5.4.6 were repeated with the inclusion of the magnification ratios computed using MLR2. These graphs are shown in Appendix A for the fully grouted trials studied.

5.4.7.3 Limitations of the proposed equation.

The limitations of the proposed model (MLR2) to calculate the effective stiffness of RMWs are listed:

- A limited range of reinforcement ratios was explored in this study. Rebar yielding could appear at the ultimate load for higher axial forces if less reinforcement area is used. The regression analysis might fail to follow the non-linear behaviour of structures with less steel area.

- Partially-grouted walls were not included in the analysis. The accuracy of the estimated effective stiffness could be affected by the variation of the gross moment of inertia.
- No reduction factor is applied, and no reliability analysis is developed. The effective stiffness was overestimated in some cases. Design equations required a degree of conservatism, which can be implemented by including reduction factors.
- It is possible that MLR2 expression fails to estimate the flexural stiffness for walls with different parameters that are not between the selected in the study.
- Data points for high axial load where instability issues are expected were neglected. This study does not provide an alternative for those cases.

5.5 Summary

Comments of the results from the numerical simulations and the regression analyses developed in this study are as follow:

- The fibre-based model developed in this chapter showed a satisfactory correspondence with experimental results of fully and partially grouted full-scale tests.
- The effects of a series of independent parameters in the second-order effects of RMWs were evaluated. From the independent variables investigated, the axial load and the slenderness ratio were identified as the most critical parameters that amplify the second-order effects in RMWs
- The moment magnification effects are highly conditioned by the applied compressive force. Under low axial loads, the ultimate load is achieved at the crushing strain of the masonry. High compressive forces amplify the second-order effects. Consequently, the ultimate load is no longer achieved at the maximum allowed strain. Thus, less strain in the rebars is developed, and for some cases, yielded rebars never appear.

- Moment Magnification effects produced by the fibre-based model were compared to those produced by the CSA S304-14, TMS 402-16 . In all the cases examined, the standards overestimate the second-order effects. CSA S304-14 was the most conservative alternative producing amplification factors up to 11 times higher than the numerical evaluation and up to 6 times higher than the TMS 402-16.
- The percentage of error in the moment amplifications are highly influenced by the increment of the axial loading in both standards. However, this effect is more pronounced in Canadian designs, as the cracked moment of inertia expression assumes no enhancement of the flexural rigidity due to this parameter.
- Due to the nature of the MM method, the percentage of error increases exponentially the closer the acting axial load is to the critical buckling load.
- Increasing the compressive strength of the masonry and the reinforcement ratio proved to decrease the percentage of error related to the moment amplification effects calculator. A variation of 10 MPa could reduce the amplification error up to 15%. Doubling the reinforcement ratio proved to decrease the error by up to 50%.
- A range of acceptable results is presented in table form. This range considers the interaction of the independent parameters studied. A threshold value of an acceptable error of 30% is used to develop the tables.
- Three new equations to calculate the effective stiffness under the conditions evaluated are proposed. All the models developed in this study vastly outperformed the existing equations.
- The MM method has proven to be an effective method to estimate the second-order effects for RMWS with pinned supports whenever an accurate flexural stiffness is used to calculate the P_{cr}

6. CONCLUSIONS AND RECOMMENDATIONS

This chapter summarizes the steps to complete each proposed objective, describes the conclusion from this study, and establishes recommendations for future research projects.

6.1 Summary

The objectives of this study were achieved through the following process:

1. Compare the design provisions for out-of-plane walls, recommended by the CSA S304-14 and TMS 402-16 :

- The provisions related to the flexural capacity and axial capacity of out-of-plane reinforced masonry walls were theoretically compared, and the key differences were identified.
- The flexural and axial capacity as per the CSA S304-14 and the TMS 402-16 were compared using P-M interaction curves. Multiple parameters were varied, and their influences were assessed.

2. Compare the design provisions for out-of-plane walls, recommended by the CSA S304-14 and TMS 402-16 :

- The provisions related to the second-order effect of out-of-plane reinforced masonry walls were theoretically compared, and the key differences were identified.
- The methods for calculating the cracked moment of inertia (I_{cr}) and the effective stiffness (EI_{eff}) were compared through parametric analysis.

3. Evaluate the effectiveness of the provisions related to the second-order effects using a finite element model:

- A fibre-based model for fully and partially grouted reinforced masonry walls was developed using OpenSEES. The numerical model accounts for material nonlinearity with spread plasticity and geometrical nonlinearity through a corotational transformation available in the OpenSEES library.

- The numerical model was validated using previous experimental programs developed by other researchers (SEASC 1982, Mohsin 2005).
- A total of 1535 simulations of fully grouted and 403 of partially grouted RMWS subjected to out-of-plane bending moment and concentric axial loading were held. In each simulation, parameters such as axial loading, height, reinforcement ratio, and masonry compressive strength were varied. Any result that encountered convergence issues before the ultimate load was discarded. The effect of independent parameters on the second-order effects was investigated.
- From the data set created, the ratio of the primary moment (moment due to lateral loading) over the total bending moment (including second-order moments) at ultimate load was calculated. The same ratio was computed using the TMS 402-16 and the CSA S304-14. The moment amplification effects were compared against the current standard procedure.

4. Develop equations to estimate the out-of-plane stiffness of reinforced masonry walls using regression analysis.

- An analytical effective stiffness was calculated using the strain readings based on linear approximations from Euler-Bernoulli beam theory.
- Using the data set of the analytical effective stiffness, a multilinear regression analysis was held using the SKlearn library available in the Python computer language.
- Three equations were proposed to calculate the flexural rigidity of RMWs.
- The accuracy and precision of the proposed models were compared against the existing equation using performance plots and indicators.

6.2 Conclusions

Conclusions drawn from the direct comparison of the design provisions and the numerical simulations of loadbearing reinforced masonry walls are as follow:

Chapter 3:

- Major differences have been identified between the two North American standards. Overall, the CSA S304-14 produces more conservative results regarding axial and flexural capacity.
- Parametric studies of P-M interaction curves demonstrated significant differences in the compression-controlled region, while the tension-controlled region was the least affected. TMS 402-16 capacity was about 5% greater in this region.
- One of the major discrepancies between the standards is the introduction of strength reduction factors ($\emptyset_m$ and $\emptyset_s$) by CSA S304-14 , while TMS 402-16 uses behaviour-based reduction factors. The Canadians P-M interaction curves are highly affected by these factors, especially in compression-controlled regions. Parametric studies show that neglecting the $\emptyset$ factors in both standards results in relatively similar P-M interaction curves. The difference in the tension-controlled zone is negligible, while TMS 402-16 P-M capacity in the compression-zone is still 15% higher than the Canadian.
- The effective compressive width provision from CSA S304-14 is triggered at a lower rebar separation than the TMS 402-16. For a commonly used nominal block thickness of 200 mm, the compression width will be reduced at 800 mm rebar spacing according to CSA S304-14. By contrast, the TMS 402-16 provision would not be triggered until 1200 mm of rebar separation. Additionally, the Canadian limitation is more strict. Canada uses a maximum of 4 times the block thickness, while The United States uses a maximum of 6 times.
- Masonry compressive strength values prescribed in TMS 402-16 are significantly higher than those specified in CSA S304-14. Parametric analysis showed that under compression controlled regions, important dissimilarities should be expected (with TMS 402-16 having higher P-M resistances). However, under tension controlled regions, this discrepancy has a minor effect.
- The maximum reinforcement provisions related to ductility requirements in both standards are very strict. Although in theory, TMS 402-16 offers a more

conservative solution ($1.5\varepsilon_y$ vs ε_y), due to the reduction factor mandated by the CSA S304-14 , the yielding of the rebar is generally achieved at lower axial forces. Also, this limit is only mandated by the CSA S304-14 for a height-to-thickness ratio greater than 30, while TMS 402-16 requires satisfying this provision under any circumstance.

- Variation of the wall height reduces the axial capacity of the RMWs according to the TMS 402-16. The variation of this parameter does not affect the CSA S304-14 P-M curves for elements with slenderness ratio lower than 30. For slender structures (i.e. h/t = 30), both committees introduce new axial limits based on the gross axial capacity. TMS 402-16 offers a stricter limit for these conditions (5% vs. 10% of the gross axial capacity).

Chapter 4:

- The moment magnifier methods proposed by each standard are relatively similar. CSA S304-14 introduces a C_m factor to relate moment diagrams to an equivalent moment distribution. However, in most cases (e.g. $\frac{M_1}{M_2} = 1$), this factor is considered to be 1. The differences in the second-order effects provisions are related to the calculation of the effective stiffness.
- The CSA S304-14 relies on an equation with an upper and lower bound limit to calculate the effective stiffness. The TMS 402-16 committee proposes an expression for uncracked walls and another for cracked structures. One of the major differences is the inclusion of the axial loading in the TMS 402-16 formulation, whereas the expression used in Canada typically does not consider its effects directly. A gradual increment of the axial loading leads to an enhancement of the flexural stiffness if the TMS 402-16 equation is used. However, the CSA S304-14 expression would usually be unaffected.
- A major difference in the flexural stiffness calculation is the inclusion of the rigidity coefficient by the CSA S304-14. This coefficient mandates affecting the stiffness by a reduction factor $\emptyset_e = 0.75$ and includes the effect of additional deformation due to sustained load over a period of time, using a creep factor (β_d).

Parametric studies have shown a reduction in the flexural stiffness by up to 60% due to the (β_d) factor. The American committee considers it unnecessary to include any reduction factor and neglects the effect of creep in masonry walls.

- Variation of the reinforcement ratio enhanced the flexural rigidity of both standards by a similar margin. Doubling the reinforcement ratio proved to increase the stiffness of the wall by approximately 60%.
- The equations proposed in TMS 402-16 are only applicable for cases in which the neutral axis lies within the faceshell of the block. Parametric analysis showed that under a compressive strength of 15 to 25 MPa, the equations would only be applicable for reinforcement ratios lower than 1.5%.
- Variation of the compressive strength of the masonry has a minor effect on the flexural rigidity, according to both committees. Increasing the compressive strength from 10 MPa to 25 MPa proved to enhance the effective stiffness by 25%.

Chapter 5:

- The second-order effects are highly influenced by the axial loading. Increasing the axial load has proven to enhance the flexural stiffness of the cross-section (EI), but it decreases the global stiffness (k). Thus, the crushing strain of the masonry (0.003) is achieved at ultimate load for walls subjected to low axial forces. A higher compressive load amplifies second-order moment; consequently, the ultimate load is achieved before the crushing strain of the masonry. Therefore, less strain is developed in the rebars, and for some circumstances, the yield strength is never reached.
- The critical buckling load was not exceeded in any of the simulations held in this analysis. However, high axial forces led to instability conditions where a slight lateral pressure produced a sudden failure in many circumstances (e.g., Axial load = 80 kN/m).
- Structures with higher reinforcement ratios are less susceptible to second-order effects, but the ductility is sacrificed. For reinforcement ratios greater than 1.8%, the ultimate load was reached before yielding of the rebar appeared.

- The development of yielding strain in the rebar affects the effective stiffness considerably. The more yield strain developed at ultimate load, the higher the degradation of the effective stiffness. Increasing the compressive strength (f'_m) increases the structure's ductility, and the yield strain could be achieved with higher axial forces before the ultimate load is reached. Nevertheless, higher f'_m could lead to stiffer structures if the ultimate load is reached before the yielding of the rebar appears.
- Comparison of the moment amplification factors from the numerical analysis to those from the CSA S304-14 demonstrated that the current provisions for estimating second-order effects are vastly conservative. Even for 50 kN/m of axial loading and $\frac{h}{t} = 20$, the amplification factors double those produced by the fibre-based model. For a higher axial loading and slenderness ratio, the percentage of error exceeded 800%. After a slenderness ratio of 40, axial loading higher than 50 kN/m exceeded the P_{cr} calculated using the CSA S304-14 equation. Consequently, the amplification factors could not be calculated for cases where the FE model did not exhibit instability effects.
- The reduction factor $\emptyset_e$ mandated by CSA S304-14 was found unnecessary, as, in most of the circumstances, the second-order effects were highly underestimated.
- Second-order effects calculated following TMS 402-16 provisions showed an acceptable percentage of error up to a slenderness ratio of 30. For higher $\frac{h}{t}$, the percentage of error grew gradually, and vastly conservative amplifications are expected. For reinforcement ratios greater than 1.8%, the TMS 402-16 equations were not applicable to computing amplification factors. Only in a few cases was the P_{cr} exceeded before the numerical model demonstrated pronounced instability effects.
- The percentage of error related to the calculation of the moment amplification factors grew exponentially as the axial loading was increased. This effect seems to be more pronounced for factors calculated using CSA S304-14, as the standard

does not include the effect of the axial loading in the cracked moment of inertia calculation.

- Increasing the compressive strength and the reinforcement ratio proved to decrease the percentage of error in the moment amplification calculations. The rate of decrement was similar in both standards.
- From the three regression analyses presented in this study, the author identifies MRL2 as the most optimal solution. MLR1 is a simple equation but the least accurate within the group. PLR1 is the most precise and accurate but the most complicated. MRL2 has the best combination of precision, accuracy, and simplicity.
- The proposed MLR2 equation vastly outperformed the existing equations for calculating the effective stiffness based on the performance indicators calculated. However, the expression proved to be unconservative in some cases, and a reliability analysis is recommended before implementing it in future standards.
- The moment magnifier method has proven to be a viable method to estimate the second-order effects for RMWs subjected to concentric axial loading and out-of-plane bending under pinned-pinned condition, when a more accurate alternative for computing the flexural stiffness was used (MLR2)

6.3 Recommendations

The following recommendations are suggested for future research projects.

- The maximum crushing strain recommended by the TMS 402-16 is 0.0025, while the CSA S304-14 recommends 0.003. Future research should identify an ideal strain limit. Both standards could benefit from an increase in the maximum allowed strain.
- Future research program should revise the strength reduction factor $\emptyset_m$ and $\emptyset_s$ proposed by the CSA S304-14. Canadian designers could benefit from using a single behaviour-based factor as recommended by TMS 402-16
- New limitations for the compressive width limits, backed by an experimental program, could be proposed. The CSA S304-14 alternative is the most

conservative. However, even the limit proposed by the TMS 402-16 could be extended.

- An intensive research program, either experimental or analytical, should revise the maximum reinforcement limit provisions for walls with a slenderness ratio equal or greater than 30. Parametric studies proved that this limit could be applied for higher slenderness ratios. Also, a similar program could explore the creep effect, which is included in the Canadian standard but neglected in the TMS 402-16.
- Second-order effects could be calculated using a more refined procedure based on the effective stiffness to quantify the percentage of error more accurately.
- Future research should focus on creating a more complete data set of numerical evaluations. A bigger data set would not only be beneficial for understanding the flexural behaviour of RMWs under a wider range of parameters, but it would also provide more data points for further regression analyses. The following recommendations to improve the data set are listed:
    a. Include simulations of partially grouted specimens and cross-sections with different moments of inertia.
    b. Evaluate eccentric axial loading. The minimum eccentricity to consider could be the accidental eccentricity (0.1t) recommended by the CSA S304-14.
    c. Include the effect of the creep in the finite element model.
    d. Explore the behaviour of walls with a lower reinforcement ratio for which the ductility effect would be more pronounced.
    e. Include a wider range of axial loading to understand the behaviour of reinforced masonry walls under higher compressive forces.
    f. Modify the boundary conditions and include base rigidity as done by previous researchers (Mohsin 2003 and Clayton 2020).

REFERENCES

ACI-SEASC Task Committee on Slender Walls, “Test Report on Slender Walls”, American Concrete Institute and the Structural Engineers Association of Southern California, February 1980 - September 1982, Los Angeles.

Aguilar, V., Sandoval, C., Adam, J. M., Garzón-Roca, J., and Valdebenito, G. (2016). Prediction of the shear strength of reinforced masonry walls using a large experimental database and artificial neural networks. *Structure and Infrastructure Engineering*, *12*(12), 1661–1674. https://doi.org/10.1080/15732479.2016.1157824

Ali, S., Page, A. ., and Kleeman, P. W. (1986). “Non-Linear Finite Element Model for Concrete Masonry with Particular Reference to Concentrated Loads.” *4th Canadian Masonry Symposium*, New Brunswick, CA, 137–148.

Bean Popehn, J. R., Schultz, A. E., and Tanner, J. E. (2009). “Influence of Second Order Effects on Slender, Unrienforced Masonry Walls.” *Proceedings of the 11th Canadian Masonry Symposium*, Toronto, ON, Canada.

Cranston, W. B., and Roberts, J. J. (1976). “Structural Behaviour of Concrete Masonry - Reinforced and Unreinforced.” *Structural Engineer*, 54(11), 423–436.

Creazza, G., Matteazzi, R., Saetta, A., and Vitaliani, R. (2002). “Analyses of masonry vaults: A macro approach based on three-dimensional damage model.” *Journal of Structural Engineering*, 128(5), 646–654.

CSA S304-14 . (2014). *Design of masonry structures.* Canadian Standards Association.

Entz, J., Cruz-Noguez, C., Guzman Sanchez, O., and Banting, B. (2017). “Tall Masonry Walls with In-Line Boundary Elements.” *Effect of boundary elements confinement level on the behaviour of reinforced masonry structural walls with boundary elements*, 4–14.

Hatzinikolas, M., Longworth, J., and Warwaruk, J. (1978a). *Concrete Masonry Walls. University of Alberta - Structural Engineering Report No. 70*.

Hatzinikolas, M., Longworth, J., and Warwaruk, J. (1978b). *Experimental Data for Concrete Masonry Walls. University of Alberta - Structural Engineering Report No. 71*.

Isfeld, A. C., Müller, A. L., Hagel, M., and Shrive, N. G. (2019). "Analysis of safety of slender concrete masonry walls in relation to CSA S304-14 ." *Canadian Journal of Civil Engineering*, 46(5), 424–438.

Kent, D.C., and Park, R. (1971) "Flexural members with confined concrete", *Journal of the Structural Division*, ASCE, 97(7), pp. 1969-1990.

Karsan, I.D., and Jirsa, J.O. (1969), "Behavior of concrete under compressive loads", *Journal of the Structural Division,* ASCE, 95(ST12), pp. 2543-2563.

Liu, Y., and Dawe, J. L. (2001). "Experimental determination of masonry beam-column behaviour." *Canadian Journal of Civil Engineering*, 28(5), 794–803.

Liu, Y., and Dawe, J. L. (2003). "Analytical modeling of masonry loadbearing walls." *Canadian Journal of Civil Engineering*, 30(5), 795–806.

Liu, Y., and Hu, K. (2007). "Experimental study of reinforced masonry walls subjected to combined axial load and out-of-plane bending." *Canadian Journal of Civil Engineering*, 34(11), 1486–1494.

Lopez, J., Oller, S., Oñate, E., and Lubliner, J. (1999). "A homogeneous constitutive model for masonry." *International Journal for Numerical Methods in Engineering*, 46(10), 1651–1671.

Lotfi, H. R., and Shing, P. B. (1994). "Interface Model Applied to Fracture of Masonry Structures." *Journal of Structural Engineering, ASCE*, 120(1), 63–80.

Ma, G., Hao, H., and Lu, Y. (2001). "Homogenization of Masonry Using Numerical Simulations." *Journal of Engineering Mechanics*, 9399(July), 646–652.

MacGregor, J. G., Breen, J., and Pfrang, E. (1970). "Design of Slender Concrete

Columns." *ACI Structural Journal*, 67(1), 6–28.

Mohsin, E. (2005). "Support Stiffness Effect on Tall Load Bearing Masonry Walls." University of Alberta.

Muqtadir, M. A. (1991). "Slenderness Effects in Eccentrically Loaded Masonry Walls." University of Alberta.

Page, A. (1978). "Finite Element Model for Masonry." *Journal of the Structural Devision*, 104(8), 1267–1285.

Pettit, C. (2019). "Effect of Rotational Base Stiffness on the Behaviour of Loadbearing Masonry Walls" University of Alberta.

Sayed-Ahmed, E. Y., and Shrive, N. G. (1994). "Numerical Modelling of Face-Shell Bedded Hollow Masonry." *10th International Brick and Block Masonry Conference*, Calgary, AB, 117–126.

Sayed-Ahmed, E. Y., and Shrive, N. G. (1996). "Nonlinear finite-element model of hollow masonry." *Journal of Structural Engineering*, 122(6), 683–690.

Simpson, W., Adham, S., Amrhein, J., Coil, J., Dobrowolski, J., Foth, U., Johnson, J., Lai, J., Lee, D., McLean, R., Selna, L., and Tobin, R. (1982). *Test Report on Slender Walls*. Los Angeles.

TMS 402-16 402/602-16. (2016). *Building code requirements and specifications for masonry structures*. The Masonry Society.

Wang, R., Elwi, A. E., Hatzinikolas, M. A., and Warwaruk, J. (1997). "Tests of Tall Cavity Walls Subjected to Eccentric Loading." *Journal of Structural Engineering, ASCE*, 123(7), 912–919.

Yokel, F., Mathey, R., and Dikkers, R. (1970). "Compressive Strength of Slender Concrete Masonry Walls." *National Bureau of Standards*, (Building Science Series 33).

Yokel, F., Mathey, R., and Dikkers, R. (1971). "Strength of Masonry Walls Under Compressive and Transverse Loads." *National Bureau of Standards*, (Building Science Series 34).

APPENDIX A: MOMENT MAGNIFICATION FACTORS CALCULATED USING MLR2

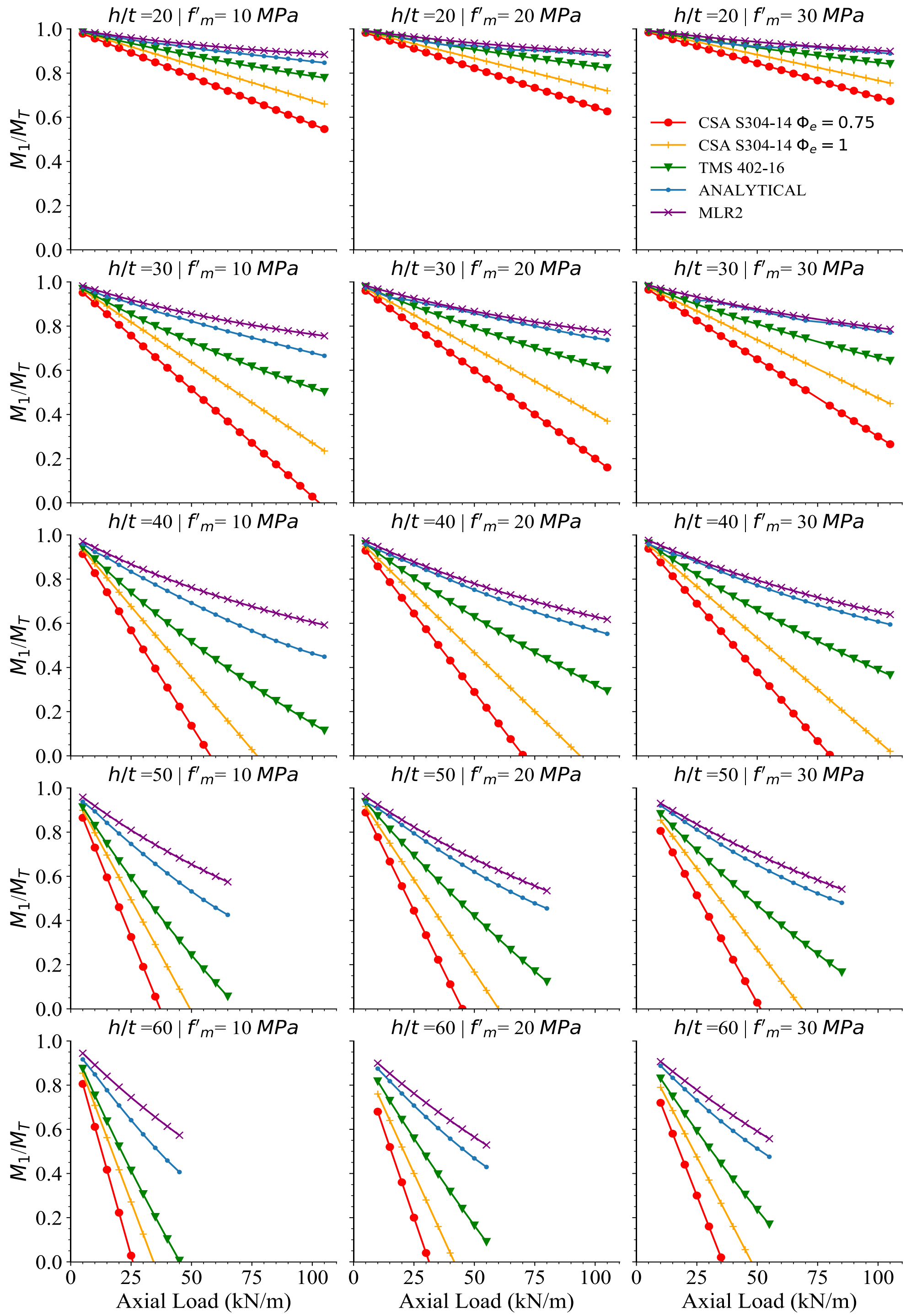

Figure A.1 – M1/Mt vs Axial Load. Fully grouted ρ=0.52%

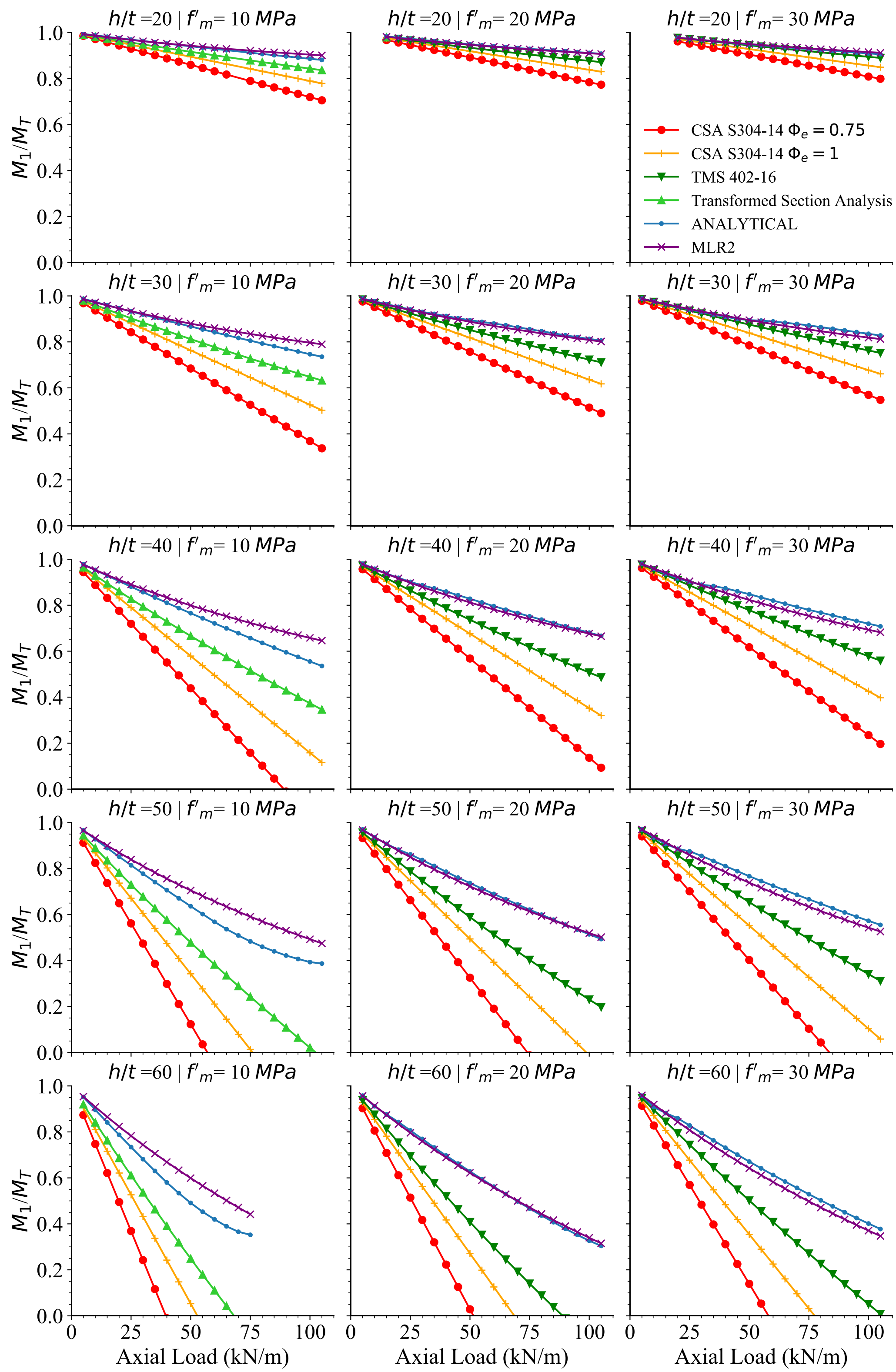

Figure A.2 – M1/Mt vs Axial Load. Fully grouted ρ=1.05%

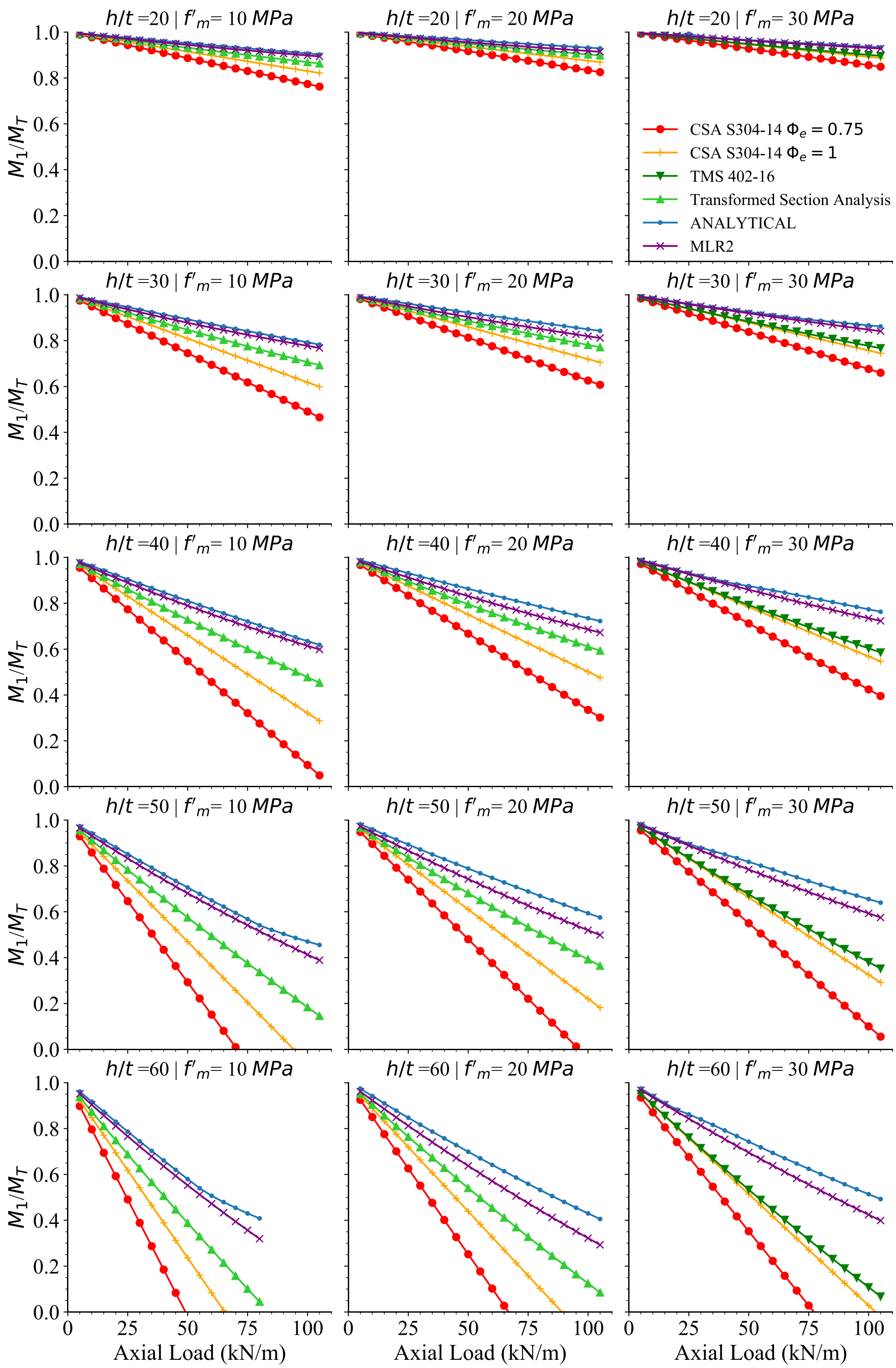

Figure A.3 – M1/Mt vs Axial Load. Fully grouted ρ=1.57%

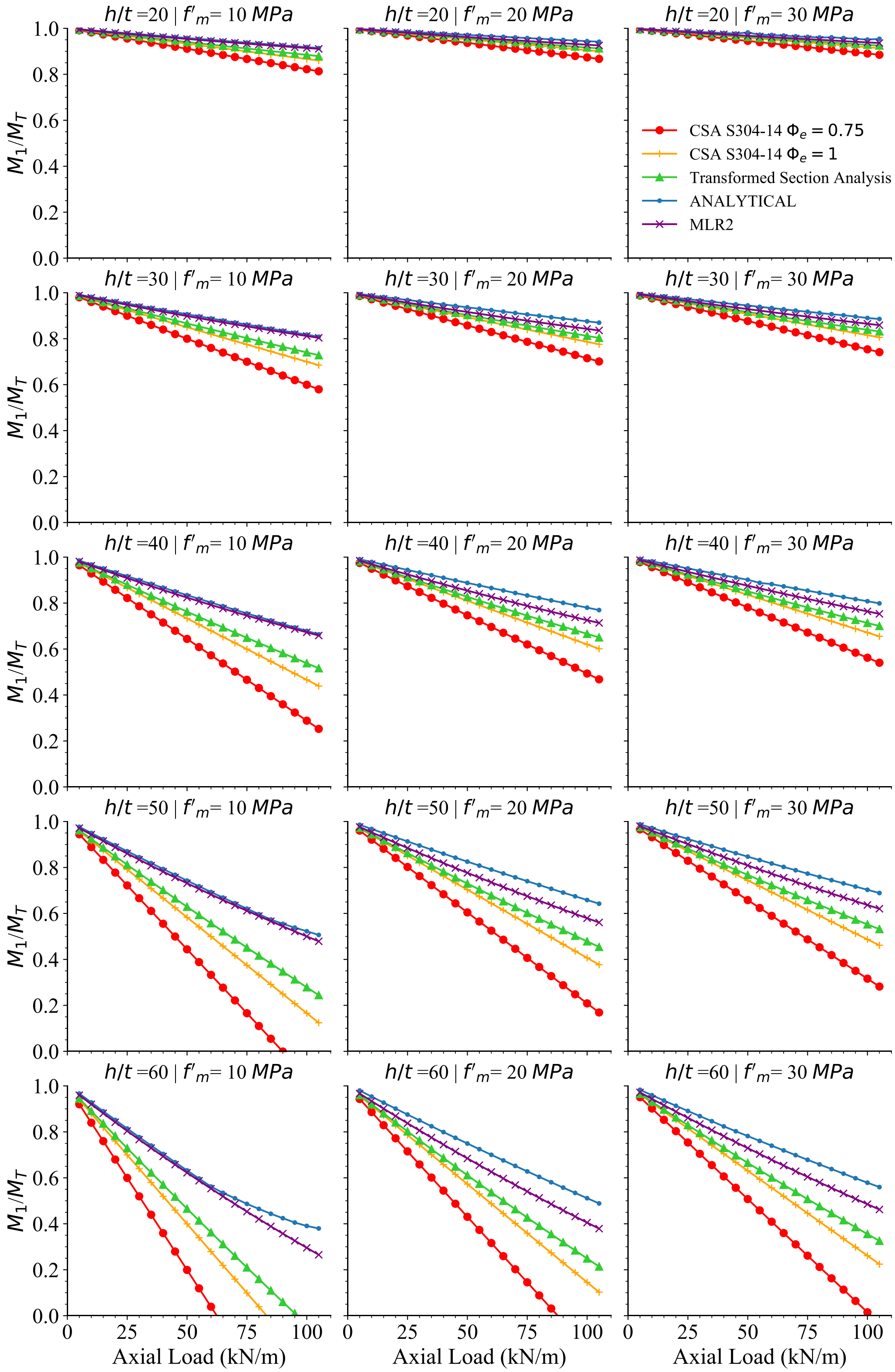

Figure A.4 – M1/Mt vs Axial Load. Fully grouted ρ=2.19%

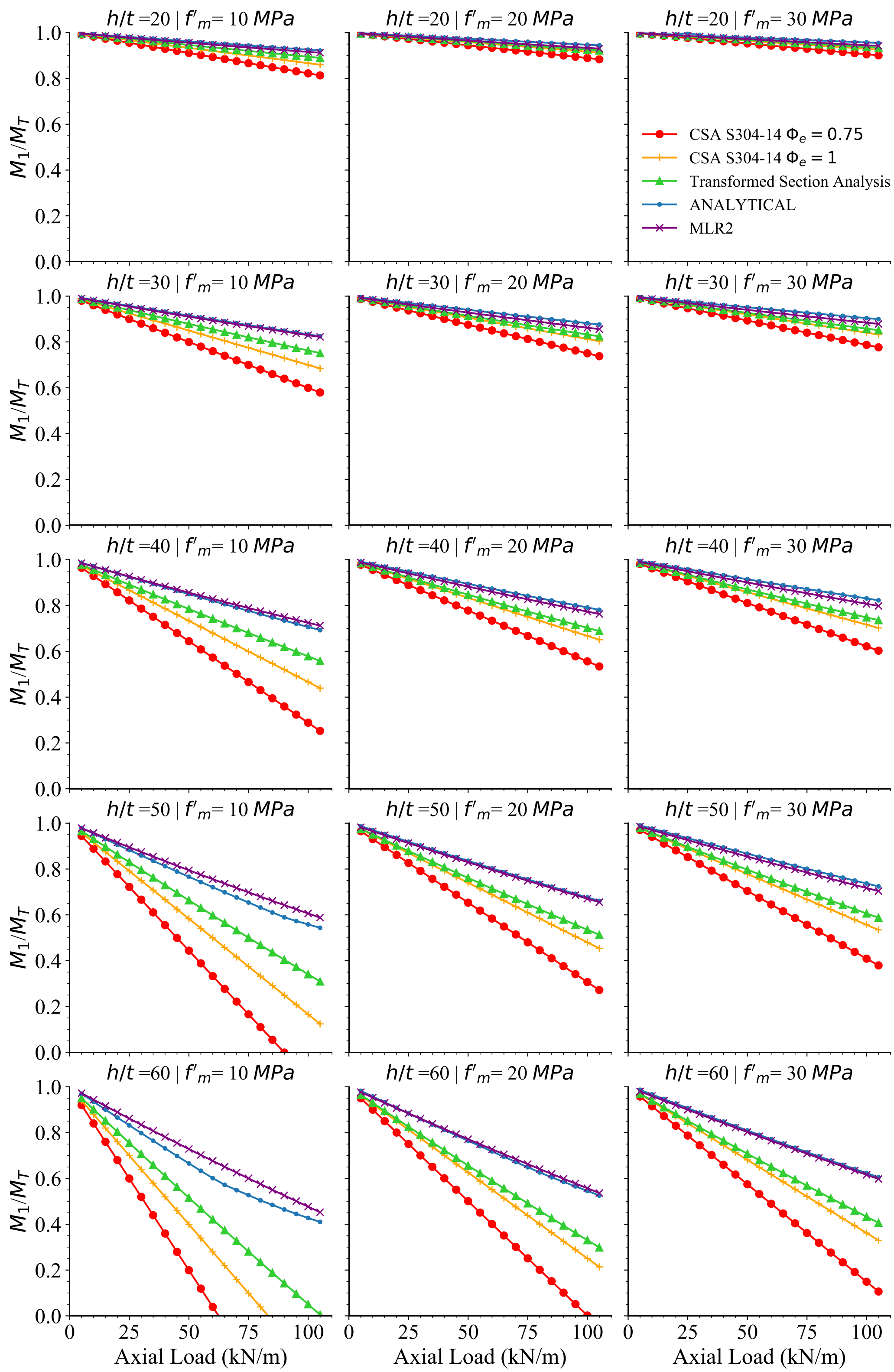

Figure A.554 – M1/Mt vs Axial Load. Fully grouted ρ=2.63%.